The structural evolution of transtensional basins and rifted margins

Nicola De Paola

THE STRUCTURAL EVOLUTION OF TRANSTENSIONAL BASINS AND RIFTED MARGINS

by
Nicola De Paola

A thesis submitted for the degree of Doctor of Philosophy at the Department of Earth Sciences, University of Durham.
2004

COPYRIGHT

ABSTRACT

The geometry, kinematics and structural evolution of homogeneous and partitioned transtensional deformations arising from oblique divergence have been studied in this thesis. 3-D faulting patterns ranging from outcrop- to reservoir- to plate-margin-scales have been described and analysed using examples from NE England (Northumberland basin) and NE Africa (Dead Sea transform).

During transtensional deformation events, markedly different strain responses can reflect pronounced lithologically-controlled variations in the value of Poisson's ratio in adjacent rock units. An outcrop- to reservoir-scale case study from the post-Carboniferous (Permo-Trias?) 90-Fathom Fault, NE England, is presented as an example preserving micro- to meso-scale faulting patterns that are strongly influenced by lithological control, strain partitioning and reactivation during oblique divergence. This study shows that 3-D strain analysis is the proper tool with which to study complex 3-dimensionally arranged fault patterns developed under partitioned transtension conditions.

In a second study, the strain analysis is applied to the Carboniferous Northumberland Basin, traditionally considered as a classic example of a Variscan inverted basin. Our findings reduce the deformation history to a single kinematically partitioned phase of dextral transtension during the late Carboniferous-early Permian. These findings have profound implications for the routine interpretation of inversion structures in any rift basin where the direction of extension may be significantly oblique to the basin margins and where basement reactivation plays an important role during basin development.

Finally, an example of strain partitioning in a modern oblique margin is studied and discussed from the present-day Dead Sea Transform (DST), NE Africa. The choice of an active area means that earthquakes focal mechanisms can be used to infer stress/strain fields during 3-D strain analysis, and there is little ambiguity concerning the timing of deformation. 3-D strain analysis here suggests slightly sinistral oblique (α = 5° - 10°) regional plate motions. A transtensional model is proposed for the DST based on the integration of published geodetic and geological data, together with a new analysis of seismological datasets. Key controlling variables are the angular relationships between plate motion vectors, plate boundaries and pre-existing intraplate margin faults.

These studies have significant relevance and potential applicability in the field of oil exploration as they deal with fractured reservoirs behaviour and potential trap development in basins undergoing transtensional deformation.

ACKNOWLEDGEMENTS

When my experience in Durham started three years ago, I never thought I could reach the point where I am now. I have to thank many people who helped and supported me during the last three years.

First of all I have to thank my supervisors Bob Holdsworth, Ken McCaffrey and Massimiliano Barchi that believed in me from the first moment and gave me the chance to do a PhD. Being a self funded postgraduate student I have to gratefully thank the University of Perugia (Italy) for partial financial support during the three years of my studies. In particular, I feel I have to personally thank Massimiliano Barchi who was so enthusiastic to support a student who wanted to broaden his horizons with an experience abroad. A particular thank you goes to Bob who "looked after" me over the last three years and was always able to stimulate and encourage my research interests. A big thank you goes to all RRG group members and particularly to Woody, Sharon, Jonny, Phil, Jones, that represented "my family" in the department.

Many thanks go to Sharon and Woody who have been my best friends in Durham where we shared almost everything inside an outside the department. Other friends in the department that I like to thank are Gary, Dougal, Rich, Darren, James, Karen, Janice, Phil, Tom and Sophie, that made my social life in Durham more enjoyable and introduced me to the joy of the "pints" and "kebabs".

In the department I like to say thank you to Karen and Janice for being always nice and patient toward my incapacity to understand bureaucracy, to Dave and Carol for being always available and finally a big thank you goes to Gary that has been one of the most friendly and genuine person I met.

Special thanks must go to the GSG group in Perugia for welcoming me during the short periods I spent in Italy. In particular I want to say thank you to Cristiano Collettini firstly, for being always a honest and good friend and, secondly, for the useful advice he gave me during my studies, and for the fruitful discussions we had.

I feel I have to say thank you to Bob's family as well, to the children (Christopher, Thomas, Callam and new boy Daniel), and particularly to Michelle who has always been nice and friendly toward me as a person and as a student having to share Bob's time.

A big thank you goes to my family, mum, dad, Michele and Rosy, for encouraging my choices in all circumstances and for supporting me in the most difficult moments I had during this three years.

Finally, I have to thank you Donatella for accepting my choice to study abroad and staying away for long periods of time. She has been always positive about my choice and we both believed that our feelings would have been stronger than the distance. This gave me the strength to continue and complete my work.

CONTENTS

PLATES ENCLOSED

PLATE 1: Geological map of the Northumberland Basin (after Johnson, 1995)

PLATE 2: Detailed structural map of Grey Mares Rock (SS6), scale 1: 200, Northumberland Basin.

PLATE 3: Detailed structural map of Cullernose Point (SS5), scale 1: 300, Northumberland Basin.

LIST OF TABLES AND ILLUSTRATIONS

CHAPTER 2

CHAPTER 3

CHAPTER 4

CHAPTER 5

1. INTRODUCTION

This thesis is primarily concerned with a study of the geometry, kinematics, and structural styles of homogeneous and partitioned transtensional deformations arising from obliquely divergent crustal displacements operating on various different scales. Obliquely divergent (and convergent) displacements are an inevitable consequence of plate motions on a sphere (Dewey, 1975). In addition, oblique deformations also arise in situations where plate margins are irregular along-strike and/or contain obliquely-oriented pre-existing structures such as old faults or fabrics that undergo reactivation during lithosphere deformation episodes (Dewey et al., 1998).

Geological, geophysical and geodetic datasets in modern settings show that deformation patterns in regions of oblique deformation are typically diffuse and complex either at regional (lithosphere) or local (basin/sub-basin) scales (Tikoff and Teyssier, 1994; Teyssier et al., 1995; Dewey, 2002; Oldow, 2003). Similar geometric and kinematic complexities are also observed in ancient regions of oblique divergence (e.g. Dewey, 2002; Dewey and Strachan, 2003). Oblique displacements inevitably lead to 3-D rotational strains known as transtension or transpression, even in the simplest case where the deformation is homogeneous. In most documented examples (e.g. Jones and Tanner, 1995; Holdsworth et al., 2002a; Clegg and Holdsworth, 2005) the deformation patterns are highly partitioned and heterogeneous, with faulting patterns often being domainal in character. In recent years, geologists have begun to study and unravel the geometric and kinematic complexities of transpression zones using combinations of strain modelling, analogue and numerical modelling studies and field-based investigations of natural examples in both ancient and modern settings (for example see Holdsworth et al., 1998 and references therein). Strain modelling (e.g. Fossen and Tikoff, 1998; Dewey, 2002) and analogue experimental studies (e.g. Withjack and Jamison, 1986; Schreurs and Colletta, 1998; Ramani and Tikoff, 2002) have begun to shed new light on the deformation patterns of transtension zones, but – compared to transpression zones – there are rather fewer detailed studies of natural examples (although see Dewey, 2002). As a result, our understanding of the geometric and kinematic character and evolution of transtensional deformation zones is incomplete. This is

not a trivial problem: something like half of the worlds' present day divergent deformation zones are significantly oblique – and a similar percentage is likely to have existed throughout Earth history (Woodcock, 1986). Yet almost all our existing models of plate boundary deformations and basin structural evolution are based on the assumption of 2-D plane strain. We can only begin to assess whether or not this assumption is reasonable once we have obtained a clearer understanding of the deformation patterns in natural transtension zones.

The topics studied and discussed in this thesis are also extremely relevant to the fields of applied geology, specifically hydrocarbon production, and seismic hazard. From experimental studies (Oertel, 1965; Reches and Dieterich, 1983) and field-based investigations of natural examples (Krantz, 1988 and 1989; Kirschner and Teyssier, 1994; Sagy et al., 2003), it is already well known that 3D strain fields should be associated with polymodal patterns of faulting. These are significantly more complex than the bimodal Andersonian conjugate faults that characterise 2D strain fields, yet a majority of hydrocarbon reservoir and seismological models assume Andersonian faulting patterns. Is this a reasonable assumption? If not, it means that the development of transtensional strains at different scales will have a strong influence upon features such as: 1) the internal structure and geometry of fractured reservoirs, influencing fluid migration paths and degree of compartmentalization; 2) the internal structure and evolution of sedimentary basins in terms of localization and development of potential trap geometry; 3) plate boundary deformation patterns and the associated distribution and character of seismicity.

1.1 AIM AND CONTENTS

The main aim of this thesis is to apply the existing theoretical studies of transtensional deformation to real geological examples, spanning from outcrop/reservoir-scales up to the plate boundary scale. In addition, the existing theory of transtensional deformations is further developed and expanded where necessary to incorporate the effects of variations in lithology, magma intrusion and strain partitioning in both space and time.

The theoretical principles of transtensional deformation and strain are presented and discussed in Chapter 2, together with some of the most significant analogue modelling results investigating deformation patterns associated with oblique divergence.

In Chapter 3, the role played by lithology during transtensional deformations is theoretically modelled and the results are tested against a real, reservoir-scale, fault pattern studied in detail and located at Cullercoats, NE-England.

Chapter 4 deals with the regional, basin-scale implications of strain partitioning during transtensional deformation and how this may be influenced by pre-existing basement structures at depth using as a field-based case study the Northumberland Basin in NE England..

Chapter 5 expands the study of deformation associated with oblique divergence to the plate-boundary scale of observation. A seismically active, slightly transtensional plate boundary, the Dead Sea Transform, NE Africa, is investigated by using existing available geological, geodetic and seismological datasets.

Chapter 6 summarises and discusses the main implications of the thesis in a broader context and a comparison between the structural style exhibited by the active example (Dead Sea Transform) and the ancient case (Northumberland Basin) is attempted.

1.2 METHODS

The datasets used in this work have either been collected in the field, e.g. Northumberland basin study area, or utilise different data sources available in literature, e.g. geological, seismological and geodetic, datasets related to the Dead Sea transform boundary. Structural analysis techniques, particularly strain analysis and stress inversion techniques have been applied to the collected datasets.

1.2.1 Dataset collection

FIELD DATA

A preliminary review of the existing published papers and unpublished datasets was carried out to identify the regional deformation patterns and the key-areas for

further detailed field studies. In particular, the BGS geology map of the Northumberland area and the PhD thesis of Bower (1990) were consulted.

The best exposures of rocks in the Northumberland Basin lie along the coastline running from SSE to NNW (see the enclosed Plate 1). The structural axis and the main fault zones of the Northumberland Basin trend roughly E-W, so a series of structural stations were selected along an approximately N-S transect across the basin. The key localities where measurements have been taken are identified with the code SSx (i.e. structural station), where x is the locality number of each site from south to north. The whole dataset collected in the Northumberland Basin is summarised in the Appendices at the end of the thesis.

Since the geological information reported in the geological maps consulted are of good quality, field work mainly involved making detailed measurements and observations of minor structures, together with their distribution and relative age relationships. Detailed structural mapping was carried out in two key outcrops (SS5 and SS6, see the enclosed Plate 1 and Plate 2).

The main structures studied during fieldwork have been faults and their associated kinematic indicators, and secondary structures such as folds, shear planes and associated veins and stylolites. Secondary structures orientation, as pinnate or en-echelon vein geometry, and kinematic indicators, such as calcite slickenfibers, slickensides and grooves, have been used to deduce the kinematics of the fault and shear planes. Particular attention has been paid to studying the associations of minor structures and to the reconstruction of their kinematic link with the major structures.

SEISMOLOGICAL DATA

Seismological data from major events along the Dead Sea transform boundary have been selected from available studied focal mechanisms associated with events that occurred in the last 30 years. Major events ($m_b > 5$) are considered where they are unambiguously associated with the main faults that accommodate most of the deformation along the boundary. Available geological datasets and aftershock sequences are used to discriminate the orientation of the likely rupture planes from the nodal planes of the focal mechanisms solutions. Slip vectors and focal mechanism nature discriminate the kinematics of the single events. The stress tensor

reconstructed from focal mechanisms provides the orientation and nature of the stress/infinitesimal strain axes.

The information obtained from the earthquake focal mechanisms allow the discriminated fault planes to be treated, during the stress/strain analysis, as major faults accommodating most of the deformation associated with the boundary activity. The advantage of using earthquakes for stress/strain analysis is fundamental when testing the nature of 3-dimensional fault patterns since these events are unequivocally contemporaneous. Seismically active areas are also especially useful as plate boundary geometries are well constrained and plate kinematics can be independently measured using patterns of sea-floor magnetic stripes or in real time measurements made using geodetic techniques.

1.2.2 Dataset analysis

Field data and earthquakes focal mechanisms have been plotted on stereonets using the free-stereoplotting software Daisy 2 (Salvini, 2001). This software can be used to obtain contoured diagrams which are very useful when discriminating different sets of structures in each dataset, and stress axes after running the stress inversion option Mohr-Coloumb multiple faulting (rotax) for faults and slickenlines datasets (Salvini, 2001).

The whole fault and slickenline dataset is analysed by the stress inversion program which automatically identifies the groups of structures and associated stress fields. No preliminary/manual selection was made on the fault and slickenline datasets before the stress inversion was run. The only inevitable interpretation about faults is the identification of the kinematics and sense of movements made in the field.

In some localities, X/Y diagrams, where the possible kinematic fields are shown (see next chapter), have been plotted for the faults vs veins orientations to discriminate the nature of the displacements accommodated by the numerous minor faults and shear planes.

The plotted data have been statistically analysed for each lithology (Chapter 3), structural station (Chapter 4) and homogeneous earthquake events (Chapter 5). Sets of structures have been grouped to form a consistent deformation pattern on the basis of age, crosscutting and kinematic consistency. The analysed data are then plotted

together, for each case study, and analysed again applying the techniques of 3-D strain analysis to the whole dataset.

These data are then compared with stress inversion results from fault and slickenline datasets to test the consistency of the reconstructed association of structures and also the reliability of the stress inversion methodology. The comparison between strain axes, reconstructed from structures measured in the field, and stress axes, derived from stress inversion, is approximately valid only if we assume: 1) low strain intensity (i.e. the finite strain observed $\approx$ infintessimal strain) and 2) that significant rotations during progressive deformation are absent. Under these conditions, stress axes can be considered to approximately correspond to the strain axes as follows: $\sigma_1 \equiv \lambda_3$; $\sigma_2 \equiv \lambda_2$ $\sigma_3 \equiv \lambda_1$.

In this thesis a strain approach to the investigated problem is used, but at the same time I refer a lot to stress axes, that are considered in the examples studied to coincide with the infinitesimal strain axes. It is important to note, however, that the results of the stress inversions are *never* used in isolation: they are always verified using deductions concerning strain that are based on structural observations made in the field. The only exception to this occurs when stress inversions are applied to earthquakes, when the stress axes deduced are clearly related to instantaneous deformation released during the seismic events. In this case, stress axes can be reasonably considered to correspond to infinitesimal strain axes.

2. TRANSTENSION: THEORY AND EXPERIMENTAL OBSERVATIONS

Transtension is the state of strain resulting from a divergent displacement applied oblique to the boundaries of a deformation zone (Harland, 1971; Dewey, 1998). Transtensional deformations occur at various scales ranging from regional, plate-scale to local, small-scale. On the largest scale, transtensional deformations are normally induced by the obliquity between the far-field plate displacement vectors and plate boundaries, and are an inevitable consequence of relative plate motion on a spherical surface (Dewey, 1975 and 1998). Regional scale transtensional deformations are a common feature for two reasons: i) it has been estimated that about 50% of the modern plate boundaries are significantly oblique (Woodcock, 1986); ii) transtensional strains may arise as the consequence of the obliquity between regional (or local) strain fields and pre-existing rock anisotropies as layering, foliations, old fractures and faults, etc. (Holdsworth et al., 1997).

In this chapter, the mathematical principles of transtensional strain are presented, followed by a discussion on the consistency of the theory with experimental results derived from analogue modeling and faulting tests in 3-D strain fields.

2.1 STRAIN REVIEW

2.1.1 Strain parameters

The state of strain of an object, in our case a volume of rock, refers to changes in its shape, volume and rotation with respect to an oriented, initial reference state. We choose a unit cube ($l_0 = 1$) as the reference state, oriented relative to a Cartesian coordinate system defined by three orthogonal axes, respectively labelled a, b, c parallel to its edges (Fig. 2.1). Changes of size (volume) and shape of the unit cube can be described by the change in length of the body along the coordinate system axes a, b, c. The strain parameters commonly used to quantify relative changes of length are the stretch λ_i

$$\lambda_i = \frac{l_i}{l_0} \tag{2.1}$$

and the extension e_i

$$e_i = \frac{l_i - l_0}{l_0} \tag{2.2}$$

where the index i refers to the axis of the particular coordinate system used, l_i is the length of a material line in the deformed state measured along the i axis and $l_0 = 1$ is the original length of the line in the unit volume reference state. The relationship between the stretch λ_i and the extension e_i is

$$\lambda_i = e_i + 1 \tag{2.3}.$$

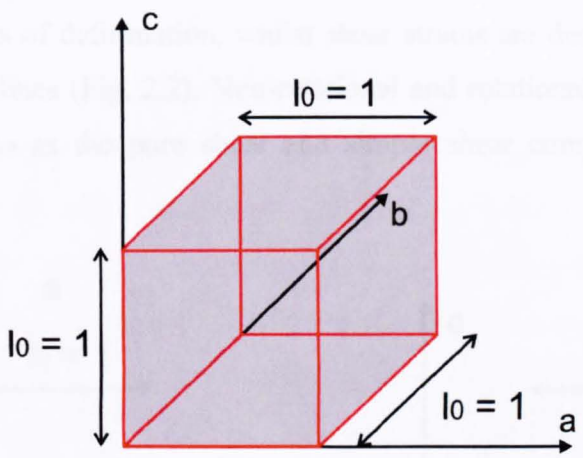

Figure 2.1: The reference state of undeformed material is a unit volume cube, $l_0 = 1$, oriented with respect to the orthogonal a, b, c coordinate axes.

Any homogeneous strain applied to the unit cube will change its shape and/or its volume resulting in a new state of strain. A strain ellipsoid is often used to describe the new deformation state. The state of strain of an object in three dimensions is defined by a second-rank tensor that has 9 strain components. The strain tensor is mathematically equivalent to the square matrix

$$\begin{bmatrix} \lambda_{aa} & \lambda_{ab} & \lambda_{ac} \\ \lambda_{ba} & \lambda_{bb} & \lambda_{bc} \\ \lambda_{ca} & \lambda_{cb} & \lambda_{cc} \end{bmatrix} \tag{2.4}$$

where the first subscript of each term (i.e. a strain component) refers to the plane orthogonal to that axis, whilst the second refers to the direction in which the strain is measured. For example, λ_{aa} is the strain measured in the plane orthogonal to the axis a and along the axis a, λ_{ab} is the strain measured in the plane orthogonal to the axis a and along the axis b. The strain tensor is symmetric about the principal diagonal of the strain matrix (Eq. 2.4), thus the conditions

$$\lambda_{ab} = \lambda_{ba} \; ; \quad \lambda_{ac} = \lambda_{ca} \; ; \quad \lambda_{bc} = \lambda_{cb} \; . \tag{2.5}$$

reduce the 9 components of the 3-D strain tensor to only 6 independent parameters.

The principal diagonal of the strain tensor (Eq. 2.4) is made of orthogonal strains (i.e. strains measured orthogonal to a plane, Fig. 2.2a) whilst the other components are all shear strains (i.e. strain measured parallel to a plane, Fig. 2.2b). Orthogonal strains are fully described by change in length of material lines implying non-rotational components of deformation, whilst shear strains are described by angular rotations of material lines (Fig. 2.2). Non-rotational and rotational deformations are commonly referred to as the pure shear and simple shear components of strain, respectively.

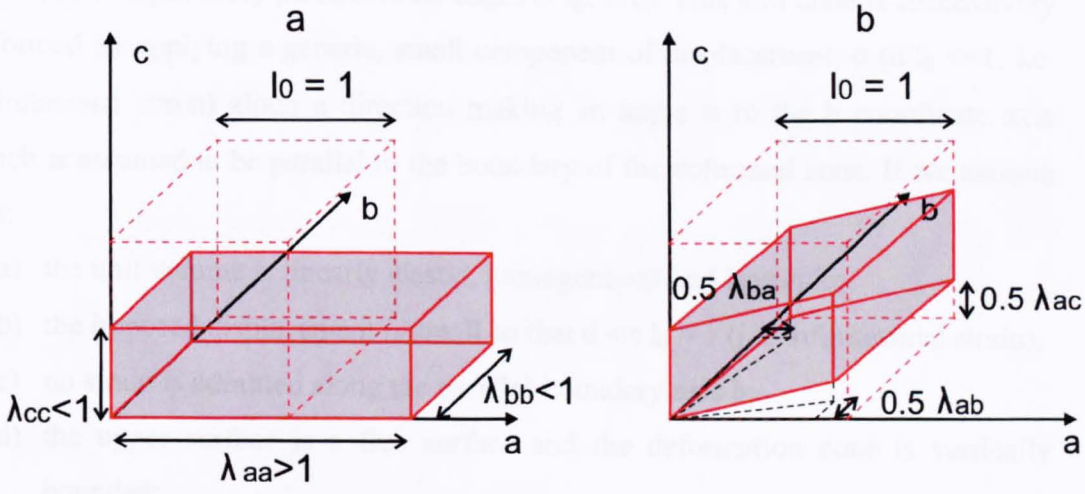

Figure 2.2: a) Orthogonal strains are expressed by the strain parameter stretch λ_{ii}, when both the subscripts are equal (e.g. λ_{aa}, λ_{bb}, λ_{cc}). Stretch is defined as the ratio between the deformed length and the initial length along a fixed direction (i.e. a,b,c). $\lambda_{ii} < 1$ implies shortening, $\lambda_{ii} > 1$ implies extension and $\lambda_{ii} = 1$ implies no-strain along that particular direction. b) Shear strains are expressed by the symbol λ_{ii}, when both the subscripts are different (e.g. λ_{ac}, λ_{ab}, λ_{bc}, etc.).

A general coordinate system a, b, c, does not represent the best option to study deformations. In fact, a coordinate system parallel to the principal strain axes, i.e. the maximum (λ_1 or e_1), intermediate (λ_2 or e_2) and minimum (λ_3 or e_3) strain axes simplifies the strain tensor to

$$\begin{bmatrix} \lambda_1 & 0 & 0 \\ 0 & \lambda_2 & 0 \\ 0 & 0 & \lambda_3 \end{bmatrix} \tag{2.6}$$

with $\lambda_1 \geq \lambda_2 \geq \lambda_3$. In the principal strain reference system, the shear strains are zero on the three mutually perpendicular principal planes. The independent parameters of the strain tensor are always six since the three transformation equations from a generic coordinate system to the principal coordinate system need to be known in order to define the strain tensor.

2.1.2 Extension: generic state of strain

In order to describe the different state of strains discussed in this chapter, we consider a unit cube with initial length $l_0 = 1$, in a reference coordinate system with axes a, b, c respectively parallel to its edges (Fig. 2.1). This unit cube is successively deformed by applying a generic, small component of displacement, d ($d/l_0 \ll 1$, i.e. infinitesimal strain) along a direction making an angle α to the b coordinate axis which is assumed to be parallel to the boundary of the deformed zone. If we assume that:

a) the unit volume is linearly elastic, homogeneous and isotropic;
b) the imposed displacement is small so that $d \ll l_0 = 1$ (i.e. infinitesimal strain);
c) no strain is admitted along the parallel-boundary axis b;
d) the upper surface is a free surface and the deformation zone is vertically bounded;
e) the system is basally confined;

then the equations of the infinitesimal strain components are (Figs. 2.3a-b, Withjack and Jamison, 1986)

$$\lambda_{aa} = d\sin\alpha + 1 \tag{2.7}$$

$$\lambda_{bb} = 1 \tag{2.8}$$

$$\lambda_{cc} = 1 - \left(\frac{\nu}{1-\nu}\right) d \sin\alpha \tag{2.9}$$

$$\lambda_{ab} \approx d \cos\alpha \tag{2.10}$$

$$\lambda_{ba} = \lambda_{ac} = \lambda_{ca} = \lambda_{bc} = \lambda_{cb} = 0 \tag{2.11}$$

where ν is the Poisson's ratio coefficient and equation 2.10 is valid for $d << l_0$ when $\lambda_{ab} = \tan\psi \approx d \cos\alpha$ (Fig. 2.3b).

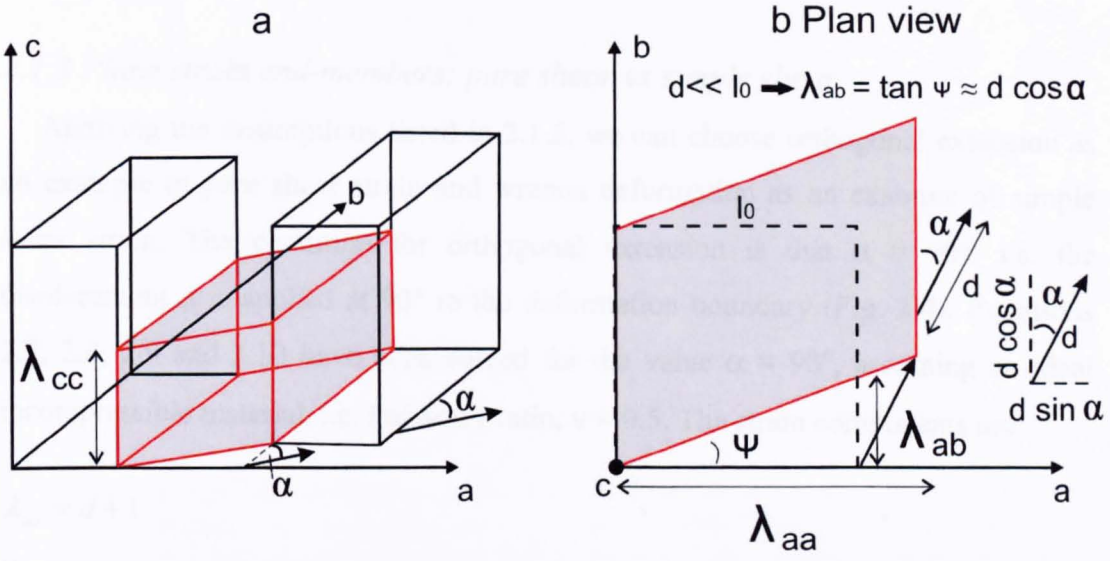

Figure 2.3: a) Three-dimensional view of a generic deformation caused by an oblique displacement applied at an angle α to the b-axis. b) Plan view of the deformation represented in figure 2.3a where the parameters used to calculate equations 2.7, 2.8, 2.9, 2.10 and 2.11 are also shown.

Because of the vertical orientation of the deformation zone, $\lambda_H = \lambda_1$; $\lambda_h = \lambda_2$ or λ_3; $\lambda_V = \lambda_3$ or λ_2. The corresponding equations of these strains are (Withjack and Jamison, 1986)

$$\lambda_H = [0.5d(\sin\alpha + 1)] + 1 \tag{2.12}$$

$$\lambda_h = [0.5d(\sin\alpha - 1)] + 1 \tag{2.13}$$

$$\lambda_V = 1 - \left[\left(\frac{\nu}{1-\nu}\right) d \sin\alpha\right] \tag{2.14}$$

where λ_H and λ_h are the maximum and minimum horizontal infinitesimal principal strain axes, respectively, and λ_V is the vertical infinitesimal principal strain axis. The maximum principal strain axis λ_H makes an angle

$$\beta = 90° - 0.5 \tan^{-1}(\cot \alpha) \tag{2.15}$$

with respect to the b axis, measured clockwise from the deformation zone boundary (Withjack and Jamison, 1986).

2.1.3 Plane strain end-members: pure shear vs simple shear

Applying the assumptions listed in 2.1.2, we can choose orthogonal extension as an example of pure shear strain and wrench deformation as an example of simple shear strain. The condition for orthogonal extension is that $\alpha = 90°$, i.e. the displacement d is applied at 90° to the deformation boundary (Fig. 2.4). Equations 2.7, 2.8, 2.9 and 2.10 have been solved for the value $\alpha = 90°$, assuming an ideal incompressible material, i.e. Poisson'r ratio, $\nu = 0.5$. The strain components are:

$$\lambda_{aa} = d + 1$$
$$\lambda_{bb} = 1$$
$$\lambda_{cc} = 1 - d$$
$$\lambda_{ab} = 0.$$

Solving equations 2.12, 2.13, 2.14 and 2.15 gives principal infinitesimal strain axes as follows:

$$\lambda_H = d + 1$$
$$\lambda_h = 1$$
$$\lambda_V = 1 - d$$
$$\beta = 90°$$

In our case, they are parallel and equal to the coordinate system axes a, b, c (Fig. 2.4). If we introduce the former values into eq. 2.6, we obtain:

$$\begin{bmatrix} \lambda_H & 0 & 0 \\ 0 & 1 & 0 \\ 0 & 0 & \lambda_V \end{bmatrix} \tag{2.16}$$

the strain tensor for orthogonal extension.

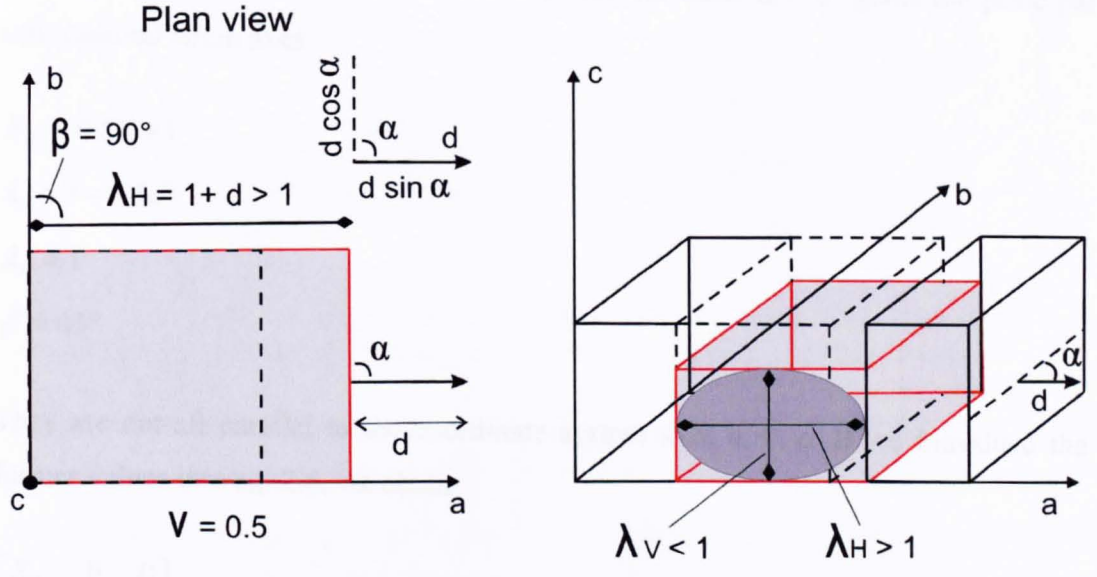

Figure 2.4: Extensional infinitesimal pure shear along the axis a ($\alpha = 90°$) generates plane strain deformation in the plane a-c which can be described by a strain ellipse. The absence of rotational components of deformation leads to the coincidence between the principal infinitesimal strain axes and the chosen coordinate system ($\beta = 90°$).

Thus orthogonal extension is a 2-D plane strain ($k = 1$) with no components of shear strain, i.e. a pure shear, and can be conveniently represented by a strain ellipse (Fig. 2.4), with a maximum horizontal stretch $\lambda_H > 1$ (λ_1), a vertical stretch $\lambda_V < 1$ (λ_3) and a minimum horizontal stretch $\lambda_h = 1$ (λ_2) which is neutral. The principal maximum stretch λ_H is orthogonal to the boundary ($\beta = 90°$, Fig. 2.4). In the particular case of orthogonal extension both finite and infinitesimal strain axes are parallel to stress axes.

The condition for wrench deformation is that $\alpha = 0°$, i.e. the displacement d is applied parallel to the deformation boundary (Fig. 2.5). Equations 2.7, 2.8, 2.9 and 2.10 have been solved for the value $\alpha = 0°$, assuming an ideal incompressible material, i.e. $\nu = 0.5$. The strain components are:

$$\lambda_{aa} = 1$$

$$\lambda_{bb} = 1$$

$$\lambda_{cc} = 1$$

$$\lambda_{ab} = d\,.$$

Solving equations 2.12, 2.13, 2.14 and 2.15 for the value $\alpha = 0°$ gives the principal infinitesimal strain axes

$$\lambda_H = 0.5d + 1$$

$$\lambda_h = 1 - 0.5d$$

$$\lambda_V = 1$$

$$\beta = 45°$$

They are not all parallel to the coordinate system axes a, b, c. If we introduce the former values into eq. 2.6, we obtain

$$\begin{bmatrix} \lambda_H & 0 & 0 \\ 0 & \lambda_h & 0 \\ 0 & 0 & 1 \end{bmatrix} \qquad (2.17)$$

the strain tensor for wrench deformation. Thus wrench deformation is a 2-D plane strain (k = 1) with components of shear strain, i.e. simple shear, expressed by solution to eq. 2.10 where $\lambda_{ab} = d$ is commonly expressed as $\lambda_{ab} = \gamma = \tan \psi$ where γ is the shear strain and ψ is the angular shear (Fig. 2.5). Simple shear deformation can be represented by a strain ellipse (Fig. 2.5) with a maximum horizontal stretch $\lambda_H > 1$ (λ_1), a minimum horizontal stretch $\lambda_h < 1$ (λ_3) and a principal vertical stretch λ_V (λ_2) which is neutral (= 1). The principal horizontal maximum stretch λ_H is oblique to the boundary at an angle $\beta = 45°$ (Fig. 2.5). In the particular case of wrench simple shear finite and infinitesimal strain axes do not coincide. Infinitesimal strain axes are parallel to stress axes with λ_H (λ_1) $\equiv \sigma_3$; λ_h (λ_2) $\equiv \sigma_2$ and λ_V (λ_3) $\equiv \sigma_1$.

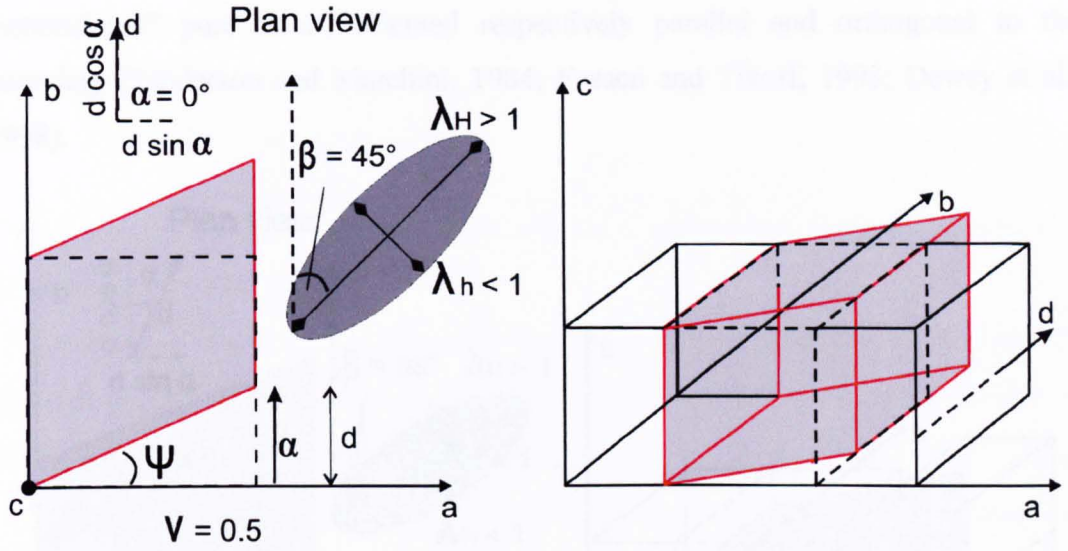

Figure 2.5: Wrench infinitesimal simple shear, applied along the b-axis, results in a rotational plane strain deformation accommodated within the horizontal plane.

The absence of rotational components of strain (e.g. during orthogonal extension; see solutions to eq. 2.7, 2.8, 2.9, 2.10) during pure shear strains, leads to "*coaxial*" deformations with coincidence between finite and infinitesimal strain axes during progressive deformation. The presence of rotational components of strain during simple shear strains (e.g. during wrenching; see solutions to eq. 2.7, 2.8, 2.9, 2.10) leads to "*non-coaxial*" deformations with a significant mismatch between infinitesimal and finite strain axes. This mismatch increases with rising strain intensity as finite strain rotate relative to the deformation zone boundaries. In particular, λ_H rotates towards parallelism with the boundary, while λ_h rotates toward parallelism with a direction orthogonal to the boundary.

Parallelism of stress and strain axes can only be assumed if intensity of strain and amounts of displacement are small (i.e. $d << l_0 = 1$).

2.2 TRANSTENSIONAL DEFORMATIONS

2.2.1 Oblique extension: 2-D vs 3-D strain

Oblique divergence, respect to a fixed boundary (b-axis in Fig. 2.3), can be qualitatively described as the simultaneous and combined action of boundary-parallel wrenching and boundary-orthogonal extensional movements (Fig. 2.6). This can be seen as equivalent to the contemporaneous action of a "wrench" simple shear and an

"extensional" pure shear, oriented respectively parallel and orthogonal to the boundary (Sanderson and Marchini, 1984; Fossen and Tikoff, 1993; Dewey et al., 1998).

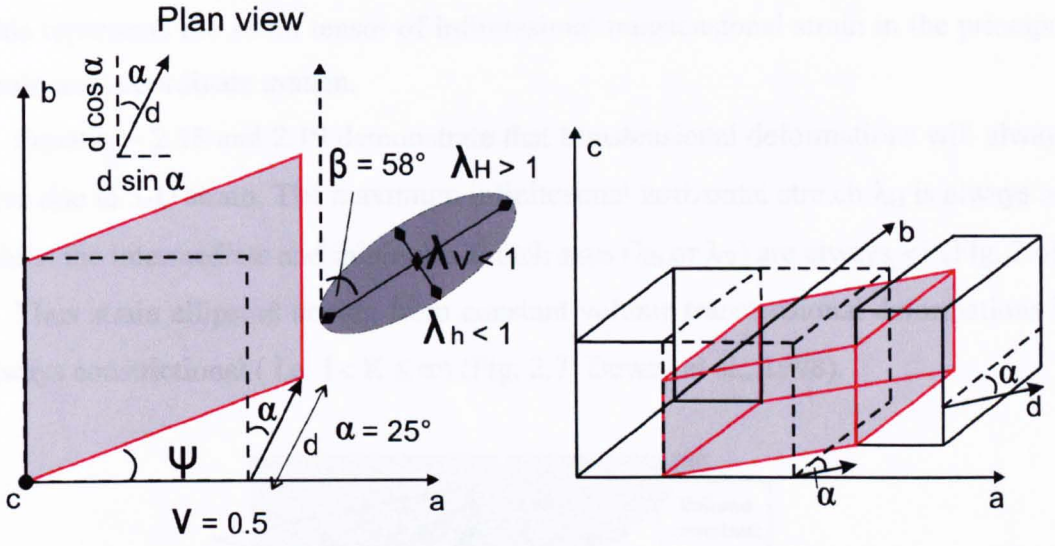

Figure 2.6: Transtensional strains arising from oblique displacement applied at $\alpha = 25°$ to the b-axis. The state of strain is three-dimensional since all the three principal axes λ_H, λ_h and λ_V are $\neq 1$. Note how there is no-coincidence between the angle α, between the imposed displacement d and the b-axis, and either the angular shear ψ or the angle β between the b-axis and the infinitesimal horizontal maximum axis.

The conditions of oblique extension are realized when $0° < \alpha < 90°$. Thus the wrench and extensional plane strains discussed in the preceding section can be considered as the two end-members of transtensional deformation. Equations 2.7, 2.8, 2.9, 2.10 and 2.11 define the components of transtensional strain in the coordinate system a, b, c and they can be arranged into the matrix:

$$\begin{bmatrix} d\sin\alpha + 1 & 0 & 0 \\ d\cos\alpha = \gamma(d\sin\alpha + 1) & 1 & 0 \\ 0 & 0 & 1 - d\sin\alpha \end{bmatrix} \qquad (2.18).$$

This represents the strain tensor for infinitesimal transtensional deformations, assuming an ideal incompressible material, i.e. $\nu = 0.5$. The same transtensional strain can be described in terms of principal infinitesimal strain components rearranging eq. 2.12, 2.13 and 2.14 into the matrix

$$\begin{bmatrix} \lambda_H & 0 & 0 \\ 0 & \lambda_h & 0 \\ 0 & 0 & \lambda_V \end{bmatrix} \qquad (2.19).$$

This represents the strain tensor of infinitesimal transtensional strain in the principal strain axes coordinate system.

Equations 2.18 and 2.19 demonstrate that transtensional deformations will always give rise to 3-D strain. The maximum infinitesimal horizontal stretch λ_H is always >1 whilst the intermediate and minimum stretch axes (λ_h or λ_V) are always <1 (Fig. 2.6).

Thus strain ellipsoid arising from constant volume transtensional deformations is always constrictional (i.e. $1 < K \leq \infty$) (Fig. 2.7; Dewey et al., 1998).

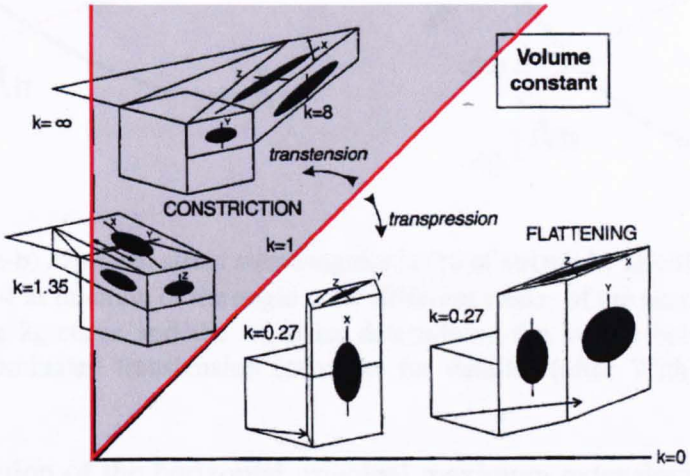

Fig. 2.7: Flinn plot to illustrate the constrictional field for transtensional deformations (grey sector delimited by the lines K = 1 and K = ∞, respectively (after Dewey et al., 1998).

2.2.2 *Infinitesimal strain: wrench-dominated vs extension-dominated transtension*

If we plot the solutions of equations 2.12, 2.13 and 2.14 for all values $0° < \alpha < 90°$ on a diagram, assuming fixed small values of the ratio d/l_0 (0.33 and 0.67 in Fig. 2.8a-b, respectively) and an ideal incompressible material, i.e. $\nu = 0.5$, we observe the following (Withjack and Jamison, 1986):

a) λ_1 is always equal to λ_H, independent of the value of angle α.

b) For $0° < \alpha < 20°$, $\lambda_h < \lambda_V$, i.e. λ_2 is vertical and λ_3 is horizontal

c) For $\alpha = 20°$ $\lambda_h = \lambda_V$, i.e. $\lambda_2 = \lambda_3$

d) For $20° < \alpha < 90°$ $\lambda_h > \lambda_V$, i.e. λ_2 is horizontal and λ_3 is vertical.

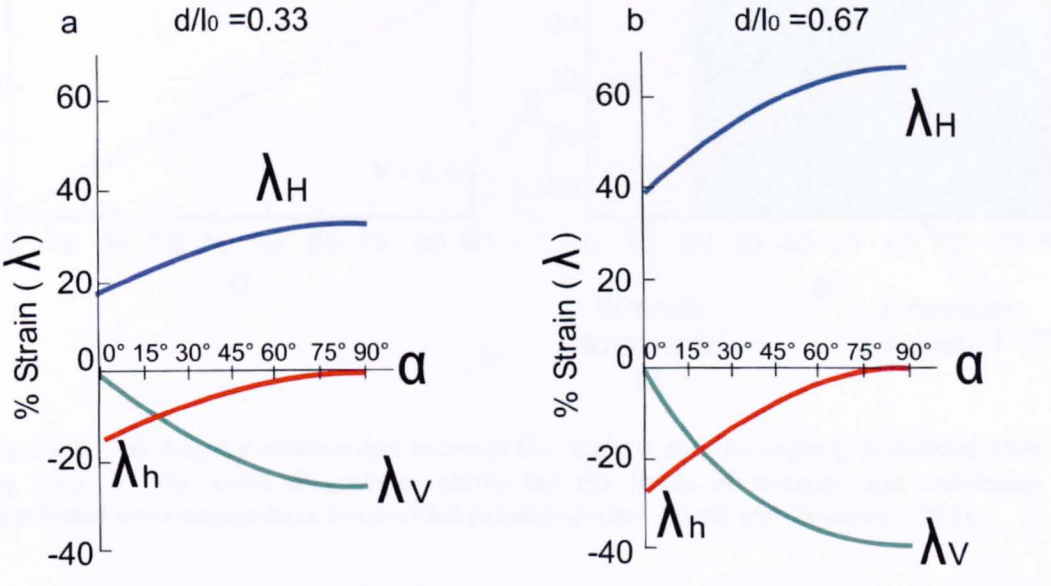

Figure 2.8: a-b) Principal strain axes magnitude (% of stretch λ) calculated from eq. 2.12, 2.13 and 2.14 in function of the angle α for different values of the ratio d/l_0. Note how for $\alpha = 20°$ the λ_h curve and the λ_V cross determining the switch between wrench- and extension-dominated transtension (see text for details) (after Withjack and Jamison, 1986).

The orientation of the horizontal principal maximum extensional axis relative to the deformation zone boundary is expressed by the angle β which is related to the value of the angle α by equation 2.15 (Fig. 2.9a). The value $\alpha = 20°$ represents a critical value during infinitesimal transtensional deformations because it corresponds to point at which the intermediate and the minimum shortening principal strain axes switch orientation. For $\alpha < 20°$, $\lambda_H > \lambda_V > \lambda_h$. This corresponds to a *wrench-dominated transtensional strain* where the intermediate strain axis is *vertical* but not neutral (Fig. 2.8, cf eq. 2.14). For $20° < \alpha < 90°$, $\lambda_H > \lambda_h > \lambda_v$. This corresponds to an *extension-dominated transtensional strain* where the maximum shortening axis is vertical and the intermediate axis is *horizontal* but not neutral (Fig. 2.8, cf eq. 2.13).

Figure 2.9b shows the plots of angles α vs β to which the fields of wrench-dominated and extension-dominated transtension, calculated for volume constant deformation and ideal incompressible material where ν = 0.5, have been added.

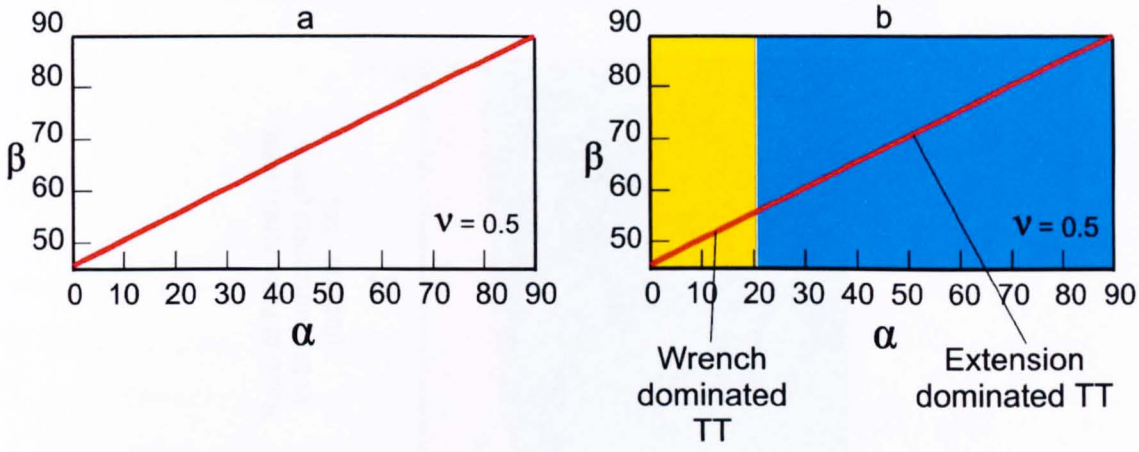

Figure 2.9: a) Angular relationship between the angle α and the angle β calculated after eq. 2.15. b) The same diagram as above but the fields of wrench- and extension-dominated transtension have been added (modified after Tikoff and Teyssier, 1994).

2.2.3 Finite strain and stable deformation fields

The corresponding finite strain axes for oblique divergence are given by the following equations (Withjack and Jamison, 1986; Jaeger, 1964):

$$\lambda_H{}^f = \left(\sqrt{1 + d\sin\alpha + 0.25d^2} + 0.5d - 1\right) + 1 \qquad (2.20)$$

$$\lambda_h{}^f = \left(\sqrt{1 + d\sin\alpha + 0.5d^2} - 0.5d - 1\right) + 1 \qquad (2.21)$$

$$\lambda_V{}^f = \left(\frac{1}{1 + d\sin\alpha} - 1\right) + 1 \qquad (2.22).$$

Where λ^f_i, with i = H, h, V, are the finite strain (stretch) axes.

For a given value of the angle α, it is possible to calculate the corresponding value of the imposed displacement d at which the condition $\lambda^f_h = \lambda^f_V$ is satisfied. This condition, for a given value of the angle α, corresponds to the switch between wrench- and extension-dominated transtensional deformation as a function of the progressive displacement d. The boundary between wrench-dominated transtension and extension dominated transtension is plotted on the diagram of figure 2.10, as a function of the angle α and of finite strain intensity, expressed as the ratio between

the horizontal finite strains λ^f_H / λ^f_h (Tikoff and Greene, 1997). This illustrates that wrench-dominated transtension is not a stable state of strain during progressive oblique divergence and that for high values of finite strain, extension dominated transtension is the expected state of strain (Fig. 2.10).

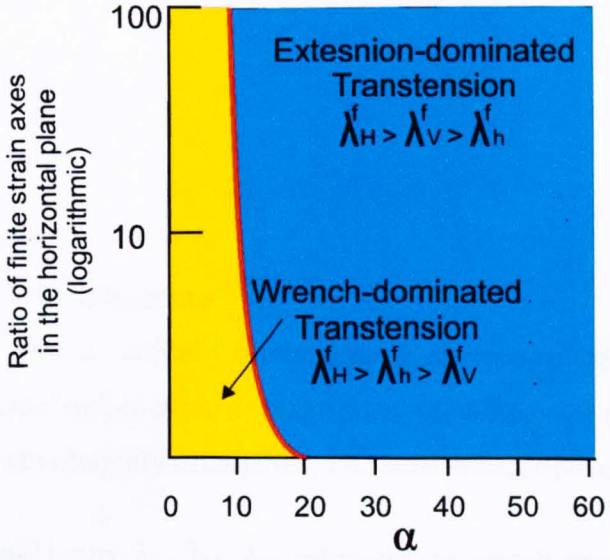

Figure 2.10: Plot of the angle of the boundary between wrench- and extension-dominated transtension as a function of the divergence angle α and the ratio of the finite strain axes of the horizontal strain ellipse. Note how for high strain intensity extension-dominated trantension is the stable state of strain (Slightly modified after Tikoff and Greene, 1997).

2.2.4 Homogeneous transtension: extended models

The generally adopted transtensional model used to illustrate the main features of oblique deformations is based on the basic model presented by Sanderson and Marchini (1984). The main boundary conditions and assumptions are as follows:

a) Deformation is homogeneous.
b) Deformation zone is vertically oriented and is bounded by faults.
c) No lateral extrusion allowed, i.e. no strain along the parallel-boundary direction, i.e. the b axis.
d) The model is basally confined.
e) Volume is constant during deformation.
f) The upper surface is a free surface, i.e. extension across the boundary results in an area change which must be compensated by vertical thinning.

Fossen and Tikoff (1993) noted that the boundary conditions imposed by the Sanderson and Marchini (1984) model were too strict for most of the deformations occurring in the crust. They proposed a more generic model for transpressional/transtensional deformations mathematically expressed as

$$\begin{bmatrix} \lambda_{aa} & \Gamma_{ab} & \Gamma_{ac} \\ 0 & \lambda_{bb} & \Gamma_{bc} \\ 0 & 0 & \lambda_{cc} \end{bmatrix} \tag{2.23}$$

whose restrictions are:

a) Deformation is homogeneous
b) Deformation zone is vertically oriented and is bounded by faults.
c) Coaxial principal deformation axes are perpendicular to the shear planes
d) Shear planes are mutually orthogonal, i.e. wrench shear or vertical shear

The principal diagonal terms, λ_{aa}, λ_{bb}, λ_{cc}, represent the stretch components along the a,b,c axes (Fig. 2.11a) whilst the off-diagonal terms Γ_{ab}, Γ_{ac}, Γ_{bc} represent elements of shear deformation, respectively (Figs. 2.11b-c-d).

The terms Γ_{ab}, Γ_{ac}, Γ_{bc} differ from the terms λ_{ab}, λ_{ac}, λ_{bc} since they account for simultaneous pure and simple shear (Fossen and Tikoff, 1993). Thus equation 2.23 is the combination of different deformation components that can be changed according to the boundary conditions of the system studied.

For example, relaxing the constant volume condition

$$\lambda_{aa} * \lambda_{bb} * \lambda_{cc} = 1 \qquad \text{equivalent to} \qquad e_{aa} + e_{bb} + e_{cc} = 0 \tag{2.24}$$

to the volume change allowed conditions

$$\lambda_{aa} * \lambda_{bb} * \lambda_{cc} \neq 1 \qquad \text{equivalent to} \qquad e_{aa} + e_{bb} + e_{cc} \neq 0 \tag{2.25}$$

we can account for volume change deformations (e.g. Fossen and Tikoff, 1993; Teyssier and Tikoff, 1999).

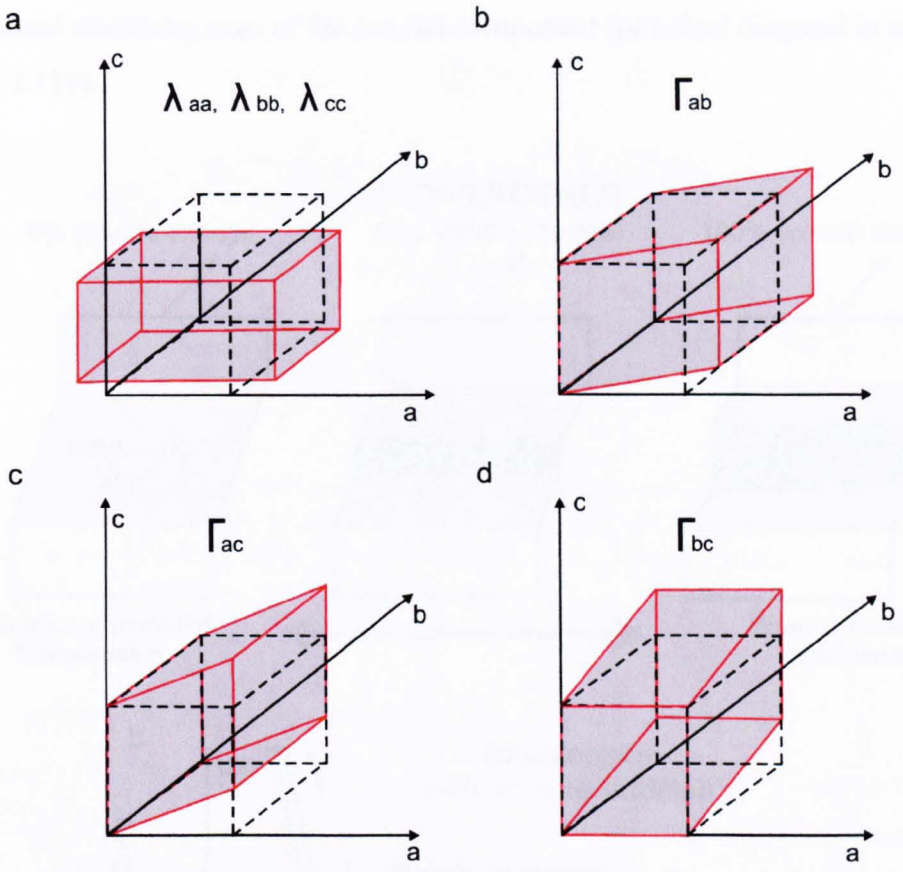

Figure 2.11: a-b-c-d) Components of strain accounted for in the three-dimensional deformation matrix (eq. 2.24) (slightly modified after Fossen and Tikoff, 1993).

Teyssier and Tikoff (1999) model transtensional deformation with volume increase, where the added volume is due to emplacement of vertical tabular bodies in an orientation that increases the width of the deformation zone (Fig. 2.12a). The geological analogue of such deformation is the intrusion of vertical dykes during oblique rifting. In their model the added volume takes up a component of extension normal to the shear zone boundaries leaving a residual component of simple shear in the country rocks. The results of transtensional deformation with volume addition are plotted on Figure 2.12b. Positive volume change generally increases the size of the wrench-dominated transtension field, meaning that this type of deformation can occur at higher angles of divergence than would be possible during a constant volume transtensional strain (Fig.2.12b). Another example of relaxed boundary conditions is given in Fossen and Tikoff (1998) where constant volume transtensional deformations under a single, constant, simple shear component (Γ_{ab}) are modelled against all possible variations in the relative magnitudes of the

infinitesimal stretching axes of the coaxial component (principal diagonal in eq. 2.23, see Fig. 2.11a).

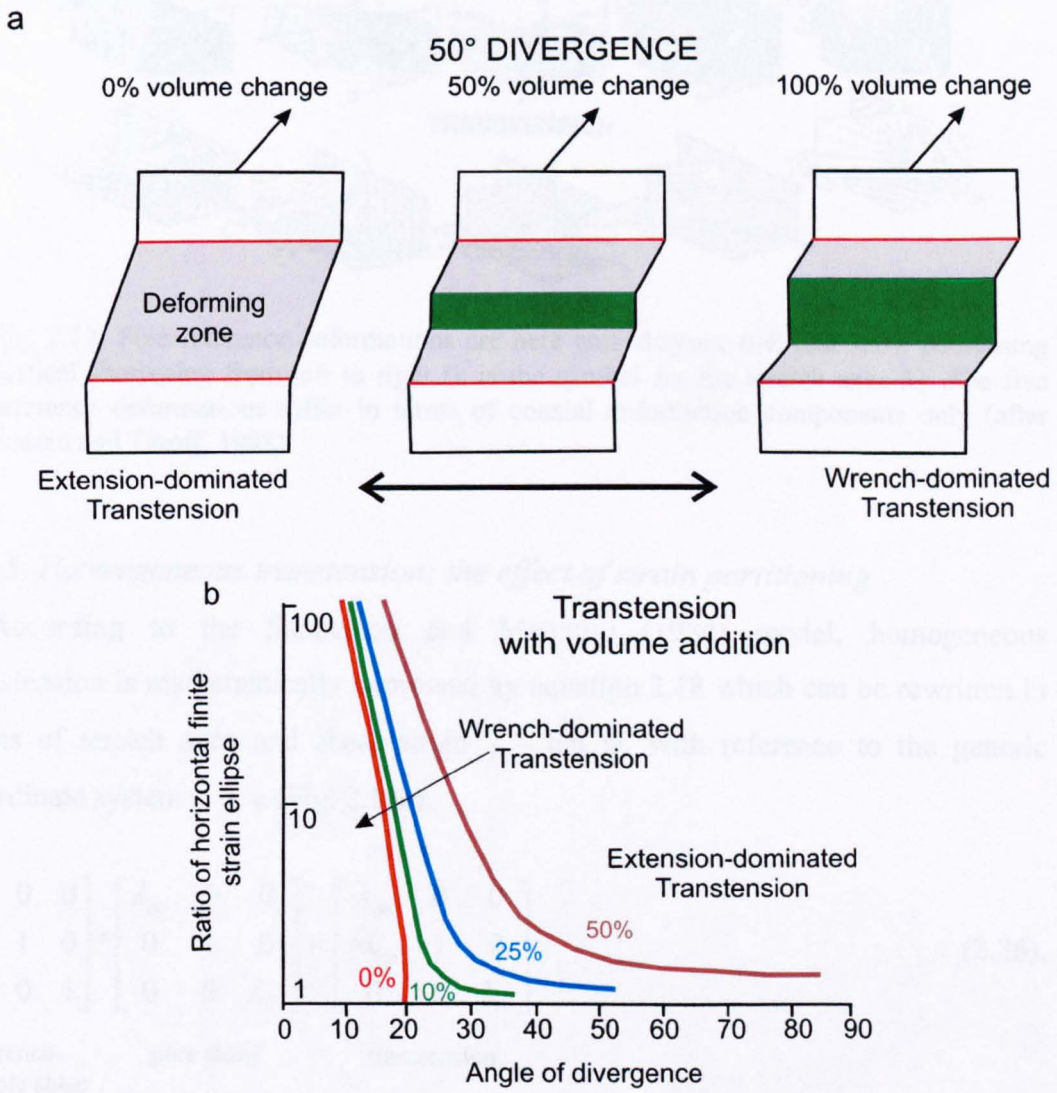

Fig. 2.12: a) Transtensional deformation with anistropic volume addition (green zones are tabular magmatic intrusions). In the latter case (100% volume change) only simple shear occurs in the non-intrusive units (gray area). b) Angle of divergence plotted against horizontal finite strain ellipse ratio for transtension and volume addition. Each line separates stability fields between wrench- and extension-dominated transtension that have been calculated for different amounts of volume addition (after Teyssier and Tikoff, 1999).

Figure 2.13 shows the entire spectrum of transtensional deformations possible. Type B is the type of transtension modelled by Sanderson and Marchini (1984); other transtensional models with additional components of strain could arise, for example, due to irregularities such as a curved plate boundaries (see also Dewey et al., 1998).

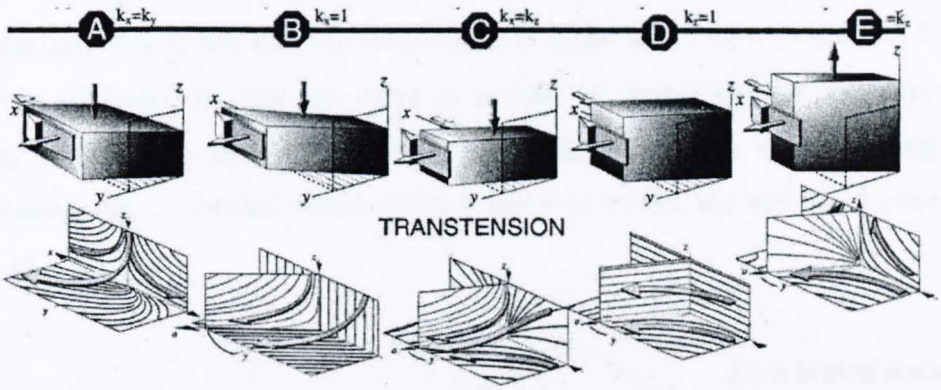

Fig. 2.13: Five reference deformations are here named types A-E and show decreasing vertical shortening from left to right (k is the symbol for the stretch axes λ). The five reference deformations differ in terms of coaxial deformation components only (after Fossen and Tikoff, 1998).

2.2.5 Heteregeneous transtension: the effect of strain partitioning

According to the Sanderson and Marchini (1984) model, homogeneous transtension is mathematically expressed by equation 2.18 which can be rewritten in terms of stretch axes and shear strain $\gamma = \tan \psi$, with reference to the generic coordinate system a, b, c (Fig. 2.14a):

$$\begin{bmatrix} 1 & 0 & 0 \\ \gamma & 1 & 0 \\ 0 & 0 & 1 \end{bmatrix} * \begin{bmatrix} \lambda_{aa} & 0 & 0 \\ 0 & 1 & 0 \\ 0 & 0 & \lambda_{cc} \end{bmatrix} = \begin{bmatrix} \lambda_{aa} & 0 & 0 \\ \gamma\lambda_{aa} & 1 & 0 \\ 0 & 0 & \lambda_{cc} \end{bmatrix}. \qquad (2.26).$$

wrench-simple shear | pure shear | transtension

This is equivalent to the factorization of transtension into wrench-simple shear and pure shear plane strains.

The homogeneous strain assumption implies that both components are uniformly distributed across the deformation zone. However, homogeneous transtension appears to be rare during real deformations. Heterogeneous 3-D deformations, which lead to strain partitioning have been described as an almost inevitable consequence of progressive 3-D deformations (Tikoff and Teyssier, 1994; Teyssier et al., 1995; Jones and Tanner, 1995). Although these authors mostly refer to transpressional settings, their general findings can be applied to transtensional deformations as such strains are the exact numerical inverse of transpressional strain. Figures 2.14 b-c

illustrate examples of strain partitioning where one of the plane strain components of deformation, usually the wrench-component, is taken up along well defined faults or networks of faults, leaving the other as a residual component in the surrounding country rocks. The fault planes accommodating strike-slip and inducing strain partitioning can be located either at the margin or within the deformed zone (Figs. 2.14b-c).

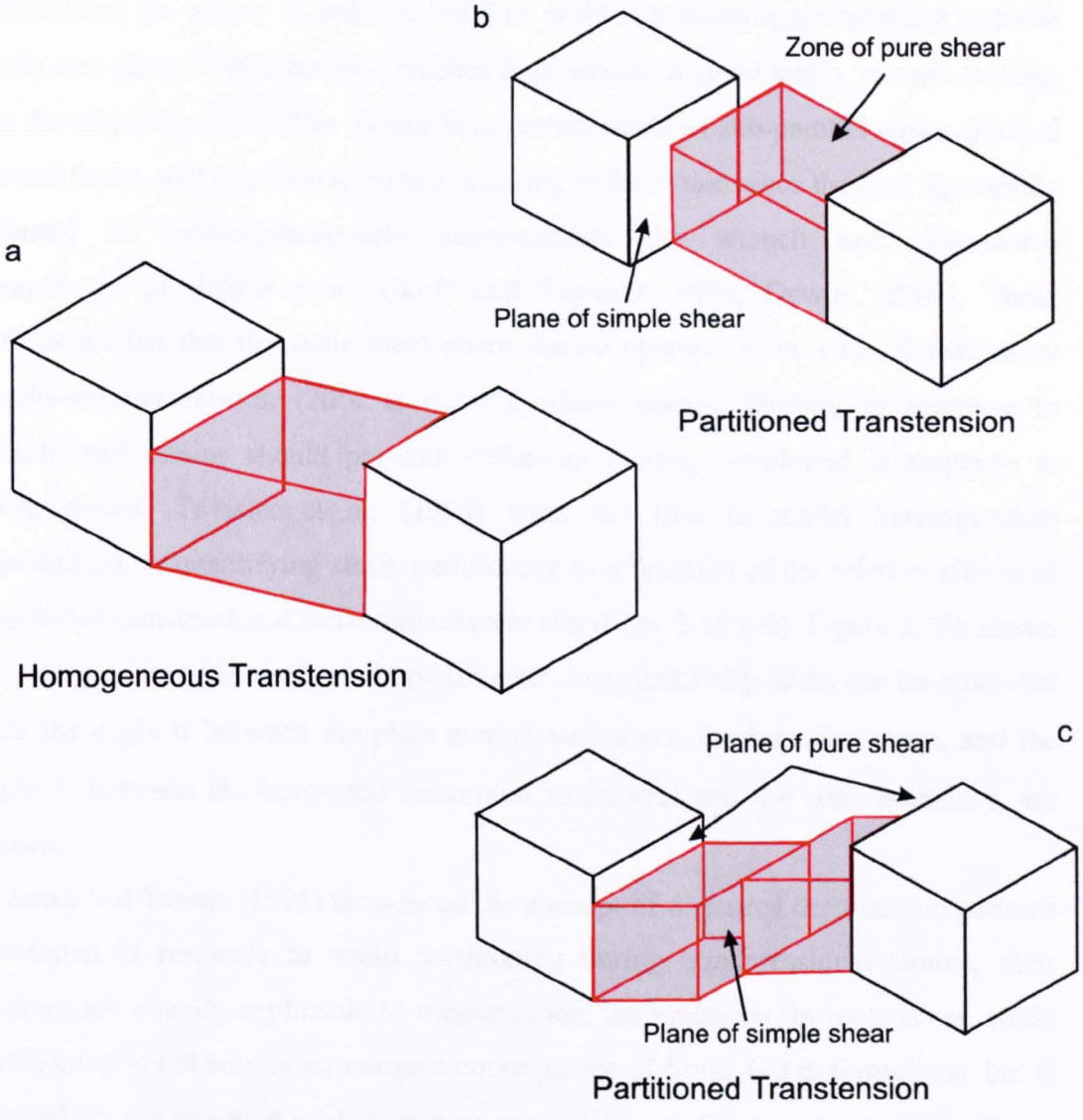

Figure 2.14: a) Homogeneous transtension (Sanderson and Marchini, 1984). b) Partitioned transtension with simple shear localized along the boundary and extensional pure shear diffuse across the zone boundary (Jones and Tanner, 1995). c) Partitioned transtension with simple shear localized along discrete vertical shear zones and extensional pure shear along the boundary of the deforming zone (Tikoff and Teyssier, 1994).

Strain partitioning has been described by Tikoff and Teyssier (1994) as an inevitable consequence during 3-D deformations, reflecting the complex relationships that exist between infinitesimal and finite strains. During wrench-dominated transtension ($\alpha < 20°$, Figs. 2.8-2.9) the infinitesimal strain axes have an orientation consistent with strike-slip faulting, e.g. $\lambda_H > \lambda_V > \lambda_h$, but at the same time, the component of extensional pure shear intrinsic in the bulk transtensional deformation ($\lambda_V \equiv \lambda_2 < 1$), tends to build up and to be increasingly recorded as finite strain cumulates. If deformation reaches high values of finite strain, normal faulting can develop (Fig. 2.10). The former fault pattern made of sub-parallel strike-slip and normal faults, will continue to be active during deformation since they are favourably oriented to contemporaneously accommodate the wrench and extensional components of deformation (Tikoff and Teyssier, 1994, Dewey, 2002). These authors predict that the same mechanism should operate in the case of extension-dominated transtension ($20° < \alpha < 90°$), where normal faulting in response to infinitesimal strains should pre-date strike-slip faulting developed in response to finite strains. Teyssier et al. (1995) were the first to model heterogeneous transtension by quantifying strain partitioning as a function of the relative effects of distributed transtensional strain and discrete slip (Figs. 2.15 a-b). Figure 2.15b shows how the amount of the bulk strain partitioned along strike-slip faults can be estimated once the angle α between the plate motion vector and the boundary zone, and the angle β, between the horizontal maximum strain axis and the zone boundary, are known.

Jones and Tanner (1995) introduced the concept of domainal deformation patterns developed in response to strain partitioning during transpressional strains; their findings are equally applicable to transtensional deformations. In most cases, strain partitioning is not simply an intrinsic consequence of finite 3-D deformations, but is induced by the presence of one or more pre-existing surfaces or zones of weakness along which a component of wrench simple shear can be preferentially accommodated. Such pre-existing weaknesses might include faults, shear zones, lithological boundaries and/or rheological anisotropies, that can either define the transtensional zone boundary or be situated entirely within the deforming zone (Figs. 2.14b-c).

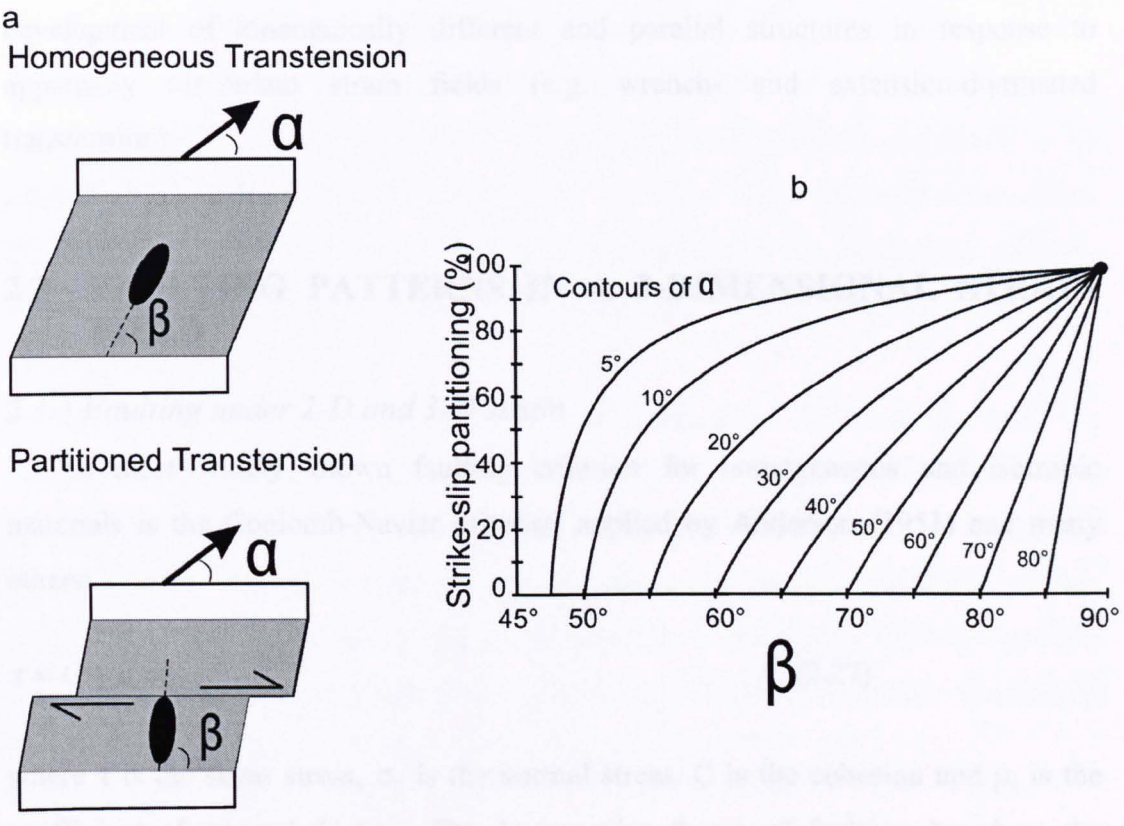

Figure 2.15: a) Map view of deforming zone (grey) between obliquely divergent plates (white) for both non-partitioned and partitioned transtension. The angle β, between the maximum horizontal infinitesimal strain axis and the deforming zone boundary, is also shown in both cases. b) The relationship between angle of relative displacement (contours of α), orientation of maximum horizontal instantaneous axis (β) and degree of strike-slip partitioning (After Teyssier et al., 1995).

Kinematically different, sub-parallel and contemporaneously active, adjacent structural domains form when bulk transtensional strain is partitioned. Figures 2.14b-c and 2.15a show how one domain (wrench-dominated domain) is deforming dominantly by homogeneous simple shear whilst the other, adjacent domain (extension-dominated domain) is deforming dominantly by extensional pure shear. These two partitioned strains are fully described by the matrix of equation 2.26. Jones and Tanner (1995) recognised that partitioning is unlikely in most geological situations to be perfect, i.e. not all of the simple shear strain is accommodated along pre-existing discontinuities (see Fig. 2.15b).

Thus, strain partitioning during transtensional (and transpressional) deformations can be induced by progressive deformation and/or by reactivation of pre-existing structures at the margin and/or within the deformed zone. The main consequence of strain partitioning during transtensional deformations is the contemporaneous

development of kinematically different and parallel structures in response to apparently discordant strain fields (e.g. wrench- and extension-dominated transtension).

2.3 FAULTING PATTERNS IN A 3-DIMENSIONAL STRAIN FIELD

2.3.1 Faulting under 2-D and 3-D strain

The most widely known faulting criterion for homogeneous and isotropic materials is the Coulomb-Navier criterion applied by Anderson (1951) and many others:

$$\tau = C + \mu_i \sigma_n \qquad (2.27)$$

where τ is the shear stress, σ_n is the normal stress, C is the cohesion and μ_i is the coefficient of internal friction. The Andersonian theory of faulting, based on the Coulomb criterion, predicts the development of a conjugate set of faults, which intersect parallel to the intermediate stress axis and have no slip component in the direction of this axis (Anderson, 1951). The symmetry of the system reflects the symmetry of the stress/infinitesimal strain tensor and the angle between the conjugate sets is a function of the internal friction coefficient μ_i (Fig. 2.16).

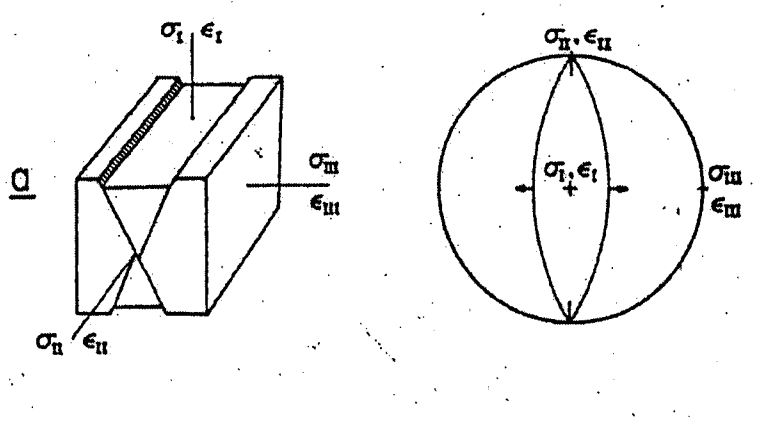

Figure 2.16: Andersonian fault system and relative symmetry of the associated stress and strain tensor (after Reches, 1983). ε_1, ε_2 and ε_3 are the infinitesimal strain axes.

The Andersonian faulting model is associated with plane strain deformations since it implies no strain along the intermediate axis and does not allow oblique-slip during faulting (Fig. 2.16) since one of the three principal stresses is constrained to be normal to the earth surface, a surface where $\tau = 0$, i.e. it is a principal stress plane. Bott (1959) suggests therefore that oblique faulting occurs in cases where oblique-slip on reactivated pre-existing planes is realized under the influence of a reoriented stress system.

The Andersonian model cannot explain transtensional deformations since the latter is associated with a 3-dimensional strain field. The slip model proposed by Reches (1978, 1983b) demonstrated that three sets of faults are necessary and sufficient to accommodate three-dimensional strain. If however, a specified rotation field is applied to the model in addition to a specified strain field, four sets of faults are necessary and are sufficient to accommodate the eight independent components of both tensors (Fig. 2.17; Reches, 1978).

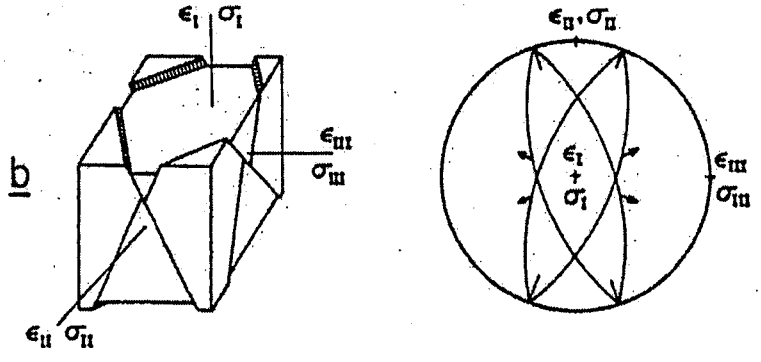

Figure 2.17: Orthorhombic fault systems composed by four fault sets and four sets of slickenlines (black arrows in the stereonet to the right). Four sets of faults are necessary to accommodate three-dimensional strain (after Reches, 1983). The symmetry of the fault patterns reflects the symmetry of the stress/infinitesimal strain tensor.

The three or four sets of faults required to accommodate the deformation may have arbitrary orientations with respect to the principal strain axes. Reches (1983) demonstrated how faults with certain orientations are more efficient (energetically speaking) than faults with other orientations. As the strain field has orthorhombic symmetry, every efficient fault has three additional faults, generated by the orthorhombic symmetry operations, which carry the same contributions to the principal strains e_1, e_2, e_3 (Fig. 2.17). In this way, Reches (1978, 1983) has shown by

symmetry arguments that the four sets required to accommodate the deformation, are arranged in orthorhombic symmetry with respect to the principal strain axes.

Krantz (1988 and 1989) proposed the odd axis model, basically an application of the slip model elaborated by Reches (1978 and 1983), to predict the expected kinematics of the fault sets and the nature of the strain tensor, once the symmetry of a deformation pattern is known. In the odd axis model, the general strain tensor comprises an odd axis with a sign different from the other two, and of an intermediate and a similar axis sharing the same sign, but opposite to the odd axis. For transtensional deformations the odd axis is $\lambda_H = \lambda_1$, the intermediate axis is λ_V (λ_h) = λ_2 and the similar axis is λ_h (λ_V) = (λ_3) for wrench- (extensional-) dominated transtension. The odd axis model has been successfully tested against real orthorhombic fault patterns and it is also valid for plane strain deformations that are seen as a particular case of more general 3-dimensional fault patterns (Krantz, 1988 and 1989). Figure 2.18 shows how the slip vector rake expected on a fault plane is related to the nature of the transtensional strain tensor and to the ratio between the intermediate and the similar strain axes.

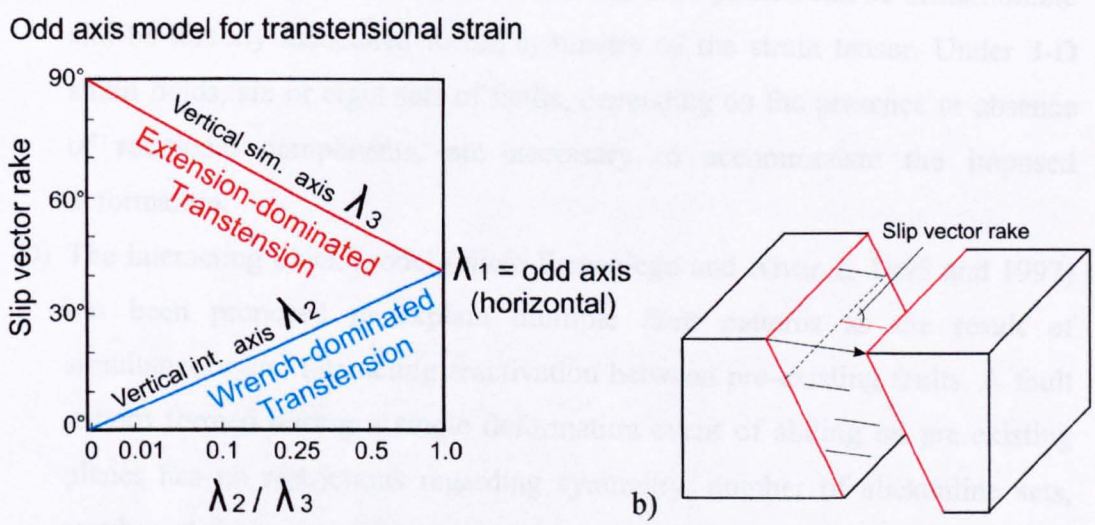

Figure 2.18: a) Graph showing the relationship of slip vector rake to the ratio of intermediate (λ_2) to similar (λ_3) strain for orthorhombic fault patterns developed under three-dimensional transtensional deformations, i.e. odd axis (λ_1) always horizontal. The plot assumes a uniform coefficient of internal friction $\mu_i = 30°$ (modified after Krantz, 1989). b) Block diagram displaying the slip vector rake as the angle between the strike of a fault plane and the slip direction on the fault plane.

2.3.2 Multiple fault patterns: polyphase deformations or 3-D strain?

Multiple fault patterns are common in many geological settings (e.g. Krantz, 1988 and 1989; Kirschner and Teyssier, 1994; Nieto-Samaniego and Alvarez, 1997; Sagy et al., 2003). There are 4 known mechanisms to develop such patterns:

A) There are more than two sets of faults, because there have been two or more deformation events, separated in time, each with differently oriented stress axes, i.e. polyphase deformation. This explanation is linked to the Anderson's application of the Coulomb-Navier behaviour (eq. 2.27) that precludes the simultaneous development of more than two conjugate sets of fault under a fixed stress field. We have seen that strain fields associated with this faulting criterion are inevitably plane strain.

B) Reactivation of non-interacting faults according to the Bott (1959) model can account for different faults orientation. This model can also explain the mechanics of oblique-slip faulting, not allowed by the Anderson's model.

C) Multiple fault patterns are simultaneously developed as the response to applied 3-dimensional strain field (Reches, 1978 and 1983). In this case it has been demonstrated that the symmetry of the fault pattern can be orthorhombic and be directly associated to the symmetry of the strain tensor. Under 3-D strain fields, six or eight sets of faults, depending on the presence or absence of rotational components, are necessary to accommodate the imposed deformation.

D) The interacting block model (Nieto-Samaniego and Alvarez, 1995 and 1997) has been proposed to explain multiple fault patterns as the result of simultaneous and interacting reactivation between pre-existing faults. A fault pattern formed during a single deformation event of sliding on pre-existing planes has no restrictions regarding symmetry, number of slickenline sets, number of faults, or orientation of the faults (Nieto-Samaniego and Alvarez, 1997). As the number of phases of faulting increases, lower symmetry is expected. In this last case, a quantitative analysis of stress/strain axes direction is difficult since the pattern of deformation does not necessarily reflect the symmetry of the stress/strain tensor (Nieto-Samaniego, 1999).

During a bulk homogeneous transtensional deformation, case C seems to be the most likely kinematic solution which will govern the development of faulting patterns under infinitesimal strain fields. As finite strains accumulate, however, case B and particularly case D could increasingly become important. The Andersonian faulting patterns predicted by case A, in theory, should not develop. However, this observation seems to be at odds with worldwide evidence that both Andersonian faulting patterns and oblique displacements, are often associated, although they must operate at different scales. This apparent paradox is most easily explained by heterogeneous transtension. Most crustal deformation zones contain numerous pre-existing anisotropies on varies scales, i.e. layering, foliation, shear zones, etc., which may undergo reactivation when subjected to renewed episodes of stress/strain (Holdsworth et al., 1997). This could easily lead to strain partitioning where the regional transport direction lies at an oblique angle to pre-existing structures, that are in an orientation favourable to the accommodation of strike-slip shearing, for example. We have seen how strain partitioning, in the simplest case, is the simultaneous action of two plane strain deformations (eq. 2.26), often acting into adjacent, kinematically distinct structural domains. If strain partitioning is total, case A provides the most likely kinematic solution which will control local faulting in each structural domain. If strain partitioning is not total, then we could have the development and juxtaposition of local fault patterns into the different domains controlled by cases A-B-C-D. The latter situation leads to rather complicated fault patterns.

2.3.3 Wrench- vs extension-dominated transtensional deformation patterns

Dewey (2002) studied in detail the patterns of structures associated with the different states of transtensional deformation that are here discussed. Figure 2.8 shows how for $0° < \alpha < 20°$, assuming a basic transtensional deformation model (e.g. Sanderson and Marchini, 1984), the state of infinitesimal strain is $\lambda_H > \lambda_V > \lambda_h$ (Fig. 2.8). The orientation of the maximum horizontal strain axis λ_H (angle β) is a function of the angle α (Fig. 2.9). Dewey (2002), following the geometric analysis of McCoss (1986), proposed a rapid and easy way to calculate the angle β, once the angle α is known. Specifically, β will be the angle between the bisector of the angle $(90-\alpha)$ and the deformation zone boundary. Thus, if we assume an idealized case of

homogeneous transtensional deformation with a divergence angle $\alpha = 15°$ between the deformation zone boundary and the imposed displacement, then the maximum horizontal strain axis λ_H makes an angle $\beta = 52.5°$ to the deformation zone boundary (Fig. 2.19a). The intermediate axis λ_V is vertical and the minimum shortening axis λ_h is horizontal and lies at 90° to λ_H (Figs. 2.8 and 2.19b). The patterns of structures that develop from this state of triaxial strain reflect the symmetry of the strain tensor. Four sets of wrench, to slightly oblique-extensional, faults should form. As these faults have to accommodate a 3-D strain, they must have an orthorhombic symmetry (Reches, 1978 and 1983; Fig. 2.19b). Shortening structures such as minor folds, thrusts, stylolites and cleavage, will develop at high angles to the deformation zone boundary, whilst minor extensional structures such as tensile veins, dykes, etc, will develop at low angles to the deformation zone boundary (see also Sanderson and Marchini, 1984; Dewey, 2002) (Fig. 2.19b). The end-member plane strain deformation during wrenching is the Riedel/antiRiedel type structures developed under simple shear strain applied to the boundary (Fig. 2.19c).

Similarly, when $20° < \alpha < 90°$ the deformation is an extension-dominated transtension (Fig. 2.9) where $\lambda_H > \lambda_h > \lambda_V$ (Fig. 2.8). Assuming an idealized case of transtensional deformation with $\alpha = 50°$, then the maximum horizontal strain axis λ_H makes an angle $\beta = 70°$ to the deforming boundary (Fig. 2.19a). The intermediate shortening axis λ_2 is horizontal (λ_h) and the maximum shortening axis λ_3 is vertical (λ_V) (Fig. 2.8 and Fig. 2.19d). The pattern of deformation reflects the symmetry of the strain tensor and orthorhombic sets of normal faults with oblique-extensional kinematics develop. Minor structures developed during this stage are less complicated than for the previous case and are mostly represented by vertical veins and horizontal stylolites. For high values of the angle α, the angle between the two families of faults reduces to simulate a plane strain state, i.e. the orthorhombic symmetry is less evident (Withjack and Jamison, 1986). The correspondent plane strain deformation is pure shear extensional strain accommodated by bimodal conjugate sets of normal faults (Fig. 2.19e).

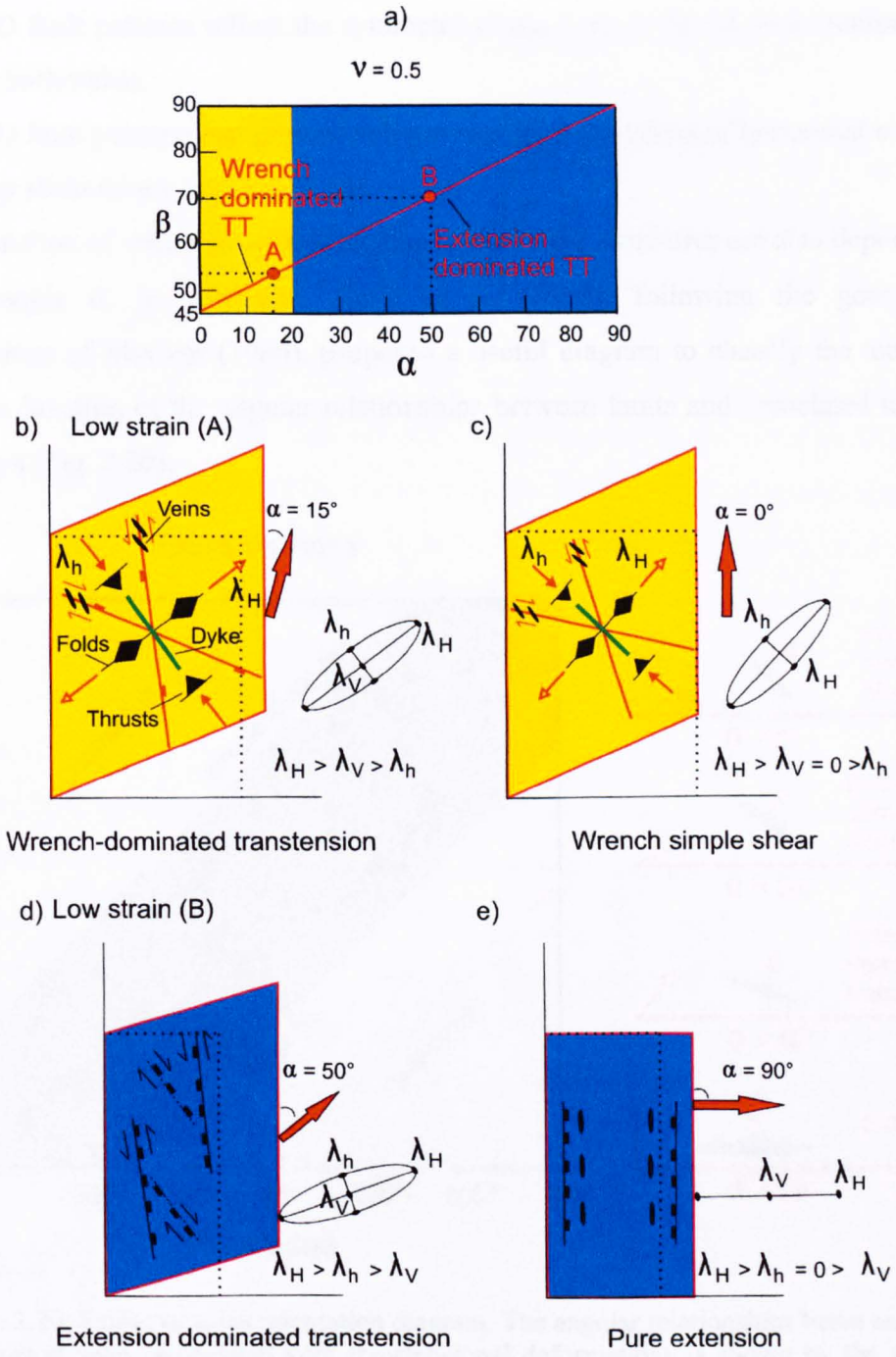

Figure 2.19: a) α vs β diagram. b-c) Mesoscale faulting pattern developed under extension-dominated transtensional strain (α = 15°) and wrench simple shear (α = 0°). d-e) Mesoscale faulting pattern developed under extension-dominated transtension (α = 50°) and pure extension (α = 90°).

The fault patterns associated with 3-D transtensional infinitesimal strain (Figs. 2.19b-d) differ from the fault patterns associated with plane strain deformations (Figs. 2.19c-e), in the following ways:

a) 3-D fault patterns are oblique to margins so that $45° < \beta < 90°$,

b) 3-D fault patterns reflect the symmetry of the 3-dimensional strain tensor, i.e. orthorhombic.

c) 3-D fault patterns can present oblique-extensional instead of horizontal or dip-slip slickenlines (e.g. Fig. 2.18).

The orientation of minor structures relative to the major structures are also dependent on the angle α. In particular, Kelly et al. (1998), following the geometric constructions of McCoss (1986), proposed a useful diagram to classify the tectonic regime in function of the angular relationships between faults and associated tensile vein arrays (Fig. 2.20).

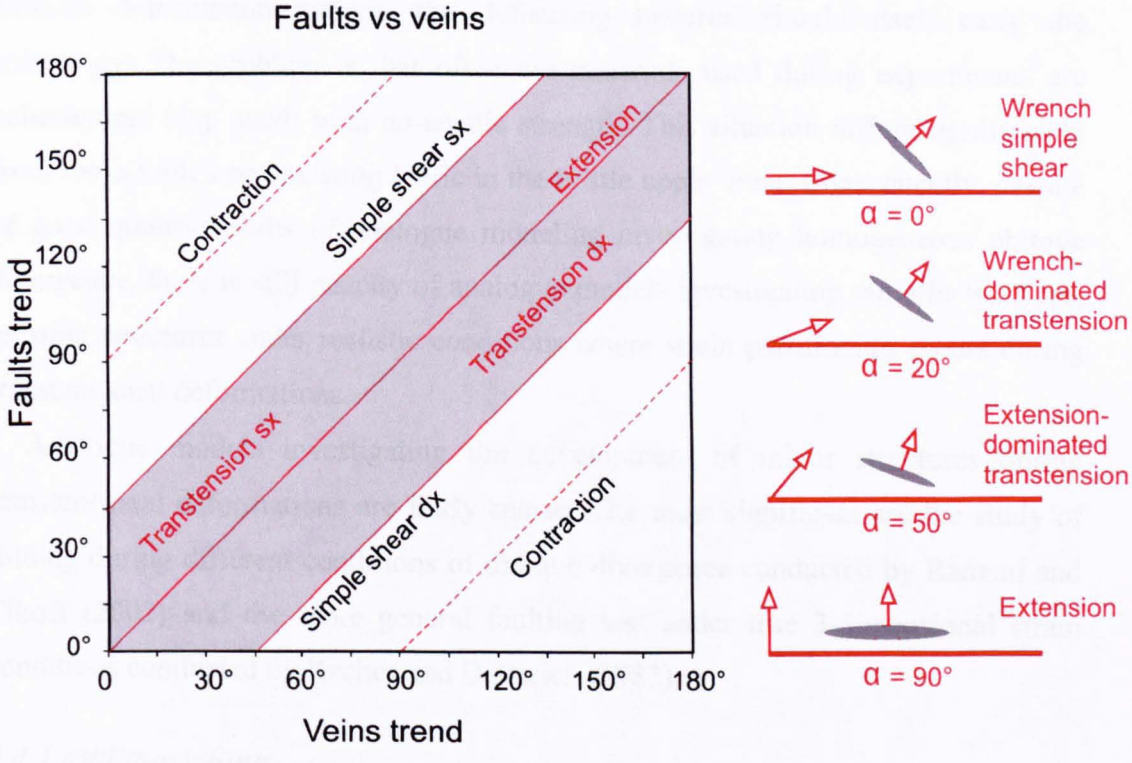

Figure 2.20: Faults vs veins orientation diagram. The angular relationships between faults and related veins, associated with transtensional deformations is shown by the shaded area on the diagram. The orientation of the veins with respect to the faults during transtensional deformations (i.e. between the end members deformations extension and wrench simple shear), is shown in the cartoons to the right (modified after Kelly et al., 1998).

The transtensional field (including both wrench- and extension-dominated transtension) lies between extensional deformations, where tensile veins are vertical and parallel to the fault boundary, and wrench deformations, where the vein-fault angle is 45° (Fig. 2.20).

2.4 ANALOGUE MODELING OF TRANSTENSIONAL DEFORMATIONS

The influence of pre-existing fabrics and different angles of obliquity on the evolution and geometry of fault patterns associated with rift zones, has been one of the main topics investigated during analogue modeling (e.g. Withjack and Jamison, 1986; Serra and Nelson, 1988; Tron and Brun, 1991; Smith and Durney, 1992; McClay and White, 1995; Bonini et al., 1997; Schreurs and Colletta, 1998). Morley (1999) points out that most models use pre-cut geometries in underlying plates to impose pre-existing fabrics on the developing fault pattern. However, to reproduce a realistic deformation pattern, the deforming material should itself carry the anisotropy. The problem is that often the materials used during experiments are cohesionless (e.g. sand) with no-tensile strength. This situation differs significantly from rocks with a pre-existing fabric in the brittle upper crust. Consequently, despite of good quality results of analogue modeling investigating homogeneous oblique divergence, there is still paucity of analogue models investigating the effects of pre-existing structures under realistic conditions where strain partitioning occurs during transtensional deformations.

Analogue models investigating the development of minor structures during transtensional deformations are fairly sparse. The most significant are the study of folding during different conditions of oblique divergence conducted by Ramani and Tikoff (2002) and the more general faulting test under true 3-dimensional strain conditions conducted by Reches and Dieterich (1983).

2.4.1 Oblique rifting

The experimental study of Withjack and Jamison (1986) is here illustrated in detail, since it reproduced geometries of significant relevance for the topic of this thesis. The aim of their work was to describe the strain states and fault patterns produced during oblique rifting by integrating analytical and experimental (clay) models.

Soft clay has been used as the experimental material during a series of combined extension and shear tests. The clay consists predominantly of quartz and kaolinite. The experimental apparatus has a horizontal metal base and three parallel, vertical metal walls connected by threaded rods (Fig. 2.21). The outer walls are stationary,

whilst the middle wall can move toward either outer wall by rotating the threaded rods. The acute angle α between the edge of the metal sheet (representing the rift trend) and the displacement direction of the movable wall is either 0°, 15°, 30°, 45°, 60°, 75° or 90°. A thin, rectangular rubber strip covers part of the metal base and metal sheet. A rectangular layer of soft clay 2.5 cm thick covers the metal base, metal sheet and rubber strip. The metal base, the metal sheet and the rubber strip provide displacement boundary conditions on the lower clay surface, all other clay surfaces are free. With $\alpha = 0°$ shear parallel to the rift trend deforms the rubber strip, with $\alpha = 90°$ extension perpendicular to the rift trend deforms the rubber strip and with $0° < \alpha < 90°$ both extension perpendicular to and shear parallel to the rift trend deform the rubber strip.

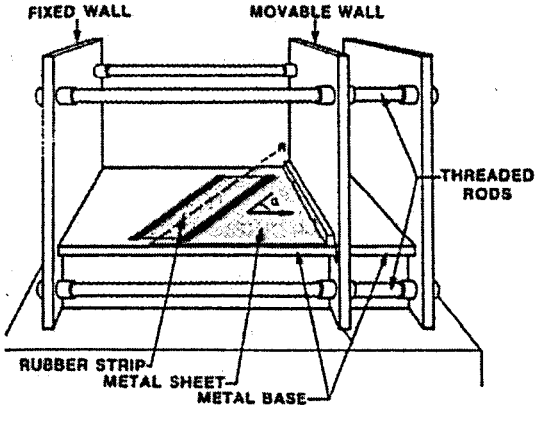

Figure 2.21: Sketch of the experimental apparatus without clay. α is the acute angle between the edge of the metal sheet that represents the rift trend, R, and the displacement direction of the movable wall (arrow) (after Withjack and Jamison, 1986).

Circular markings, applied to the upper clay surface before each experiment, indicate the strain state in the clay for each experiment. During an experiment the circles become ellipses. The long axis of each ellipse represents λ_H, the short axis of each ellipse represents λ_h, whilst the third vertical axis is λ_V. λ_V magnitude is calculated, when required, using the values of the two horizontal components assuming that no volume change occurs during the experiment.

The experimental results show that for all values of the angle α and d/u ratios (u is the original width of the plate and d is the displacement applied along the direction

expressed by α) one horizontal principal strain is the greatest extensional strain λ_H. For $\alpha < 30°$, the other horizontal strain axis, λ_h, is always the maximum shortening axis λ_3, whilst for $\alpha > 30°$ (45°), the vertical strain axis λ_V is always the maximum shortening axis λ_3 (Fig. 2.22).

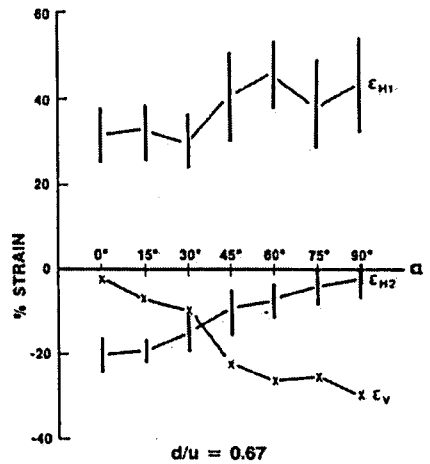

Figure 2.22: Magnitude of the principal strains in the clay models for a certain value of the d/u ratio (ratio of displacement to original rift width). The vertical bars show the range of measured values in the clay for the horizontal principal strains, the X's show the calculated values of the vertical principal strain, assuming no volume change (after Withjack and Jamison, 1986).

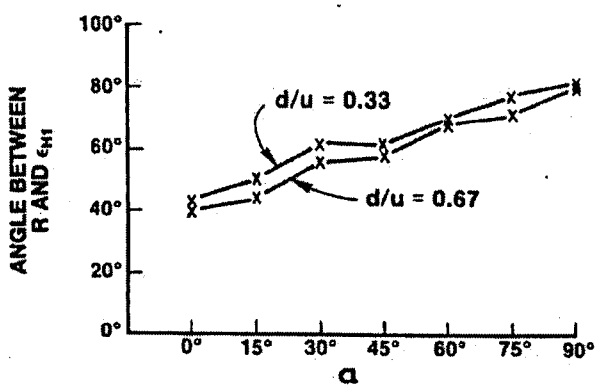

Figure 2.23: Orientation (expressed by the angle β) of the greatest extensional strain (ε_{H1}) relative to the rift trend, R, in the clay models for different values of the ratio d/u (after Withjack and Jamison, 1986).

The direction of the maximum horizontal strain axis, λ_H (expressed by the previously defined angle β), increases from about 40° to 90° as α increases from 0° to 90° (Fig. 2.23, cf Fig. 2.9a).

The direction of λ_H is approximately halfway between the normal to the rift trend and the displacement direction. The fault patterns, associated with the strain state described, are strongly influenced by the value of the angle α. The following patterns form:

a) $\alpha < 30°$: conjugate sets of steeply dipping strike-slip faults form. The Riedel-type strike-slip faults tend to strike parallel to the rift trend with increasing values of the angle α (Figs. 2.24a-b).

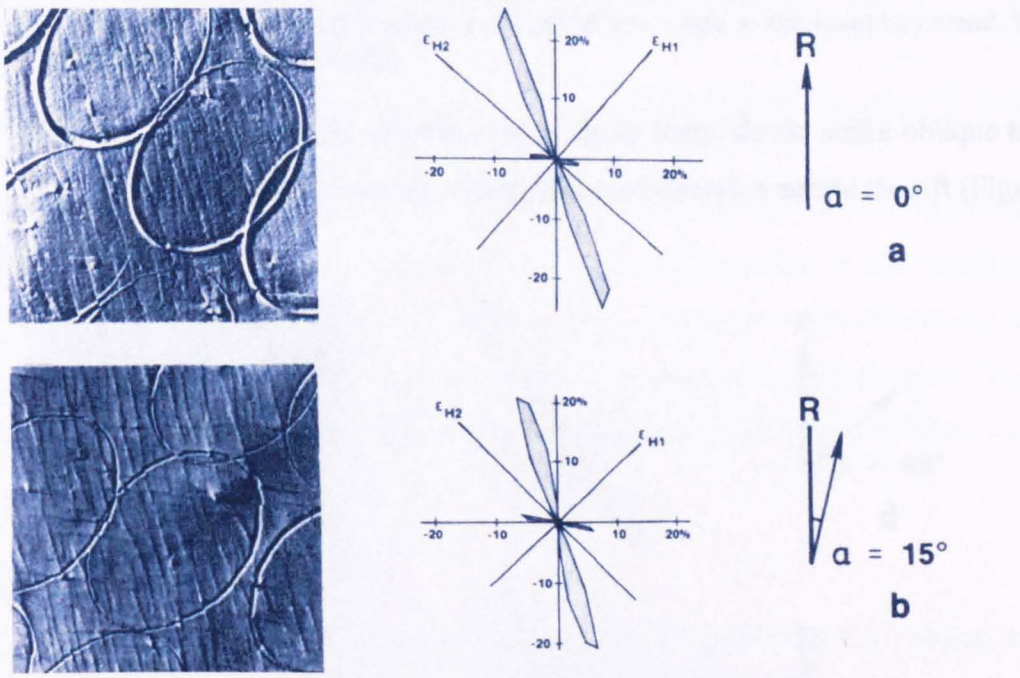

Figure 2.24: (a-b) Photograph of the clay surface and corresponding rose diagrams of fault trends for different values of α. The axes of the ellipses on the clay surface parallel the directions of the greatest horizontal extensional strain, (ε_{H1}), and the greatest horizontal contractional strain, (ε_{H2}). For both cases the strain axis display symmetry with respect to the faults formed and to the boundary conditions (i.e. for increasing values of the angle α, the axes (ε_{H1} and ε_{H2}) tend to rotate clockwise, relative to the trend of the boundary R (after Withjack and Jamison, 1986).

b) $\alpha \approx 30°$: strike-slip, combined strike-slip/normal, and/or normal faults form. Riedel –type strike-slip faults strike sub-parallel to the rift trend. Normal faults strike about 30° counterclockwise from the rift trend (Fig. 2.24c).

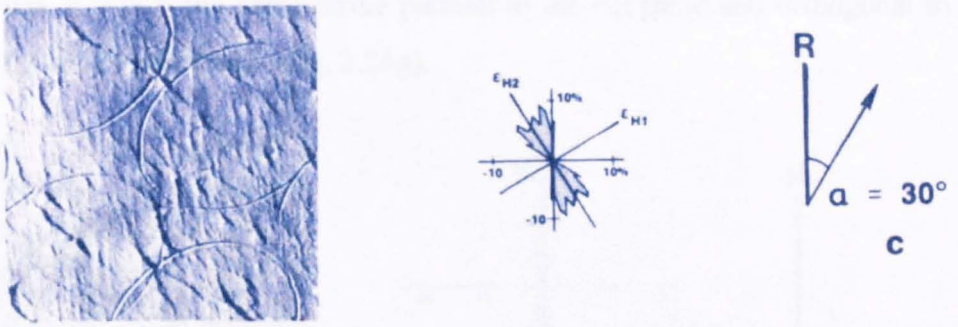

Figure 2.24: c) Photograph of the clay surface and corresponding rose diagrams of fault trends for $\alpha = 30°$. The synthetic faults trend are at low angle to the boundary trend, R (after Withjack and Jamison, 1986).

c) $30° < \alpha \leq 90°$: moderately dipping normal faults form. Faults strike oblique to both the rift trend and the imposed displacement direction across the rift (Figs. 2.24d-e-f).

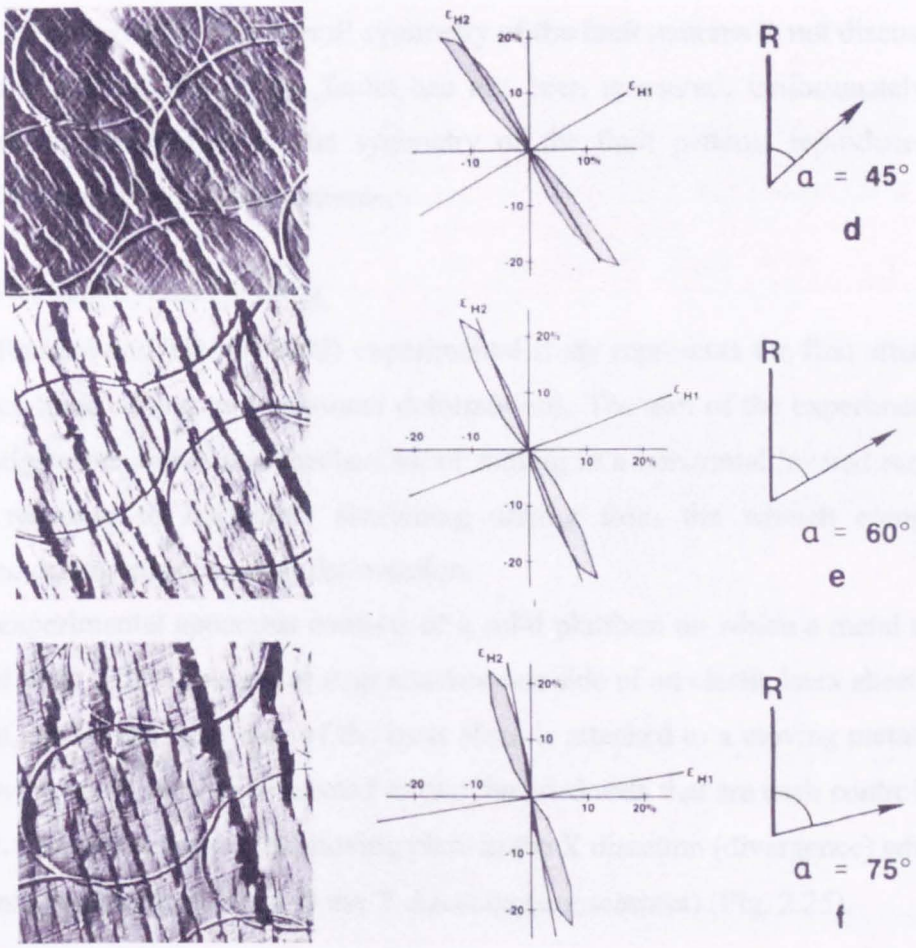

Figure 2.24: d-e-f) Photograph of the clay surface and corresponding rose diagrams of fault trends for the extension-dominated transtension, $30° < \alpha < 90°$ (after Withjack and Jamison, 1986).

d) When $\alpha = 90°$: the faults strike parallel to the rift trend and orthogonal to the imposed displacement (Fig. 2.24g).

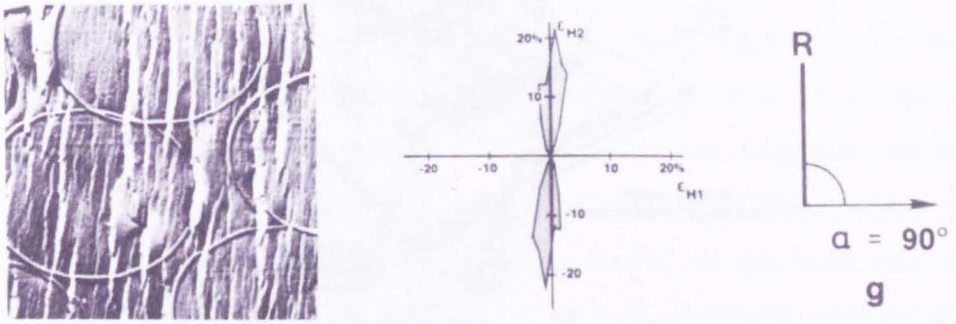

Figure 2.24: g) Photograph of the clay surface and corresponding rose diagrams of fault trends for pure extension ($\alpha = 90°$) (after Withjack and Jamison, 1986).

The results of this experiment are in close agreement with the theory of transtensional deformations and associated fault patterns presented in the previous 2.2 and 2.3 paragraphs. The overall symmetry of the fault patterns is not discussed in their work and the dip of the faults has not been measured. Unfortunately, this precludes the recognition of the symmetry of the fault patterns reproduced, i.e. bimodal vs quadrimodal fault patterns.

2.4.2 Transtension and folding

The Ramani and Tikoff (2002) experimental study represents the first attempt to reproduce folds during transtensional deformations. The aim of the experiment was to investigate the nature and mechanism of folding in a horizontal layered sequence as the response to horizontal shortening arising from the wrench component generated during transtensional deformation.

The experimental apparatus consists of a solid platform on which a metal strip is mounted (Fig. 2.25). This metal strip attaches one side of an elastic latex sheet to the platform, whilst the other side of the latex sheet is attached to a moving metal plate. The moving metal plate is connected to two threaded rods that are each controlled by a motor. One motor moves the moving plate in the X direction (divergence) while the other simultaneously moves it in the Y direction (transcurrent) (Fig. 2.25).

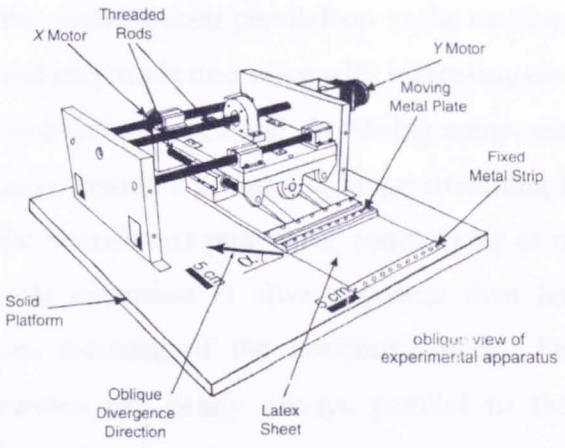

Figure 2.25: Line drawing of experimental apparatus used to create transtensional folds. Motors operate simultaneously to create sinistral oblique divergence of moving plate (after Ramani and Tikoff, 2002).

The experiments were run at $\alpha = 15°$, 22°, 30° and 45°. Transtensional folds were observed for three different angles: 15°, 22° and 30° but not for $\alpha = 45°$ (Fig. 2.26 for $\alpha = 15°$)

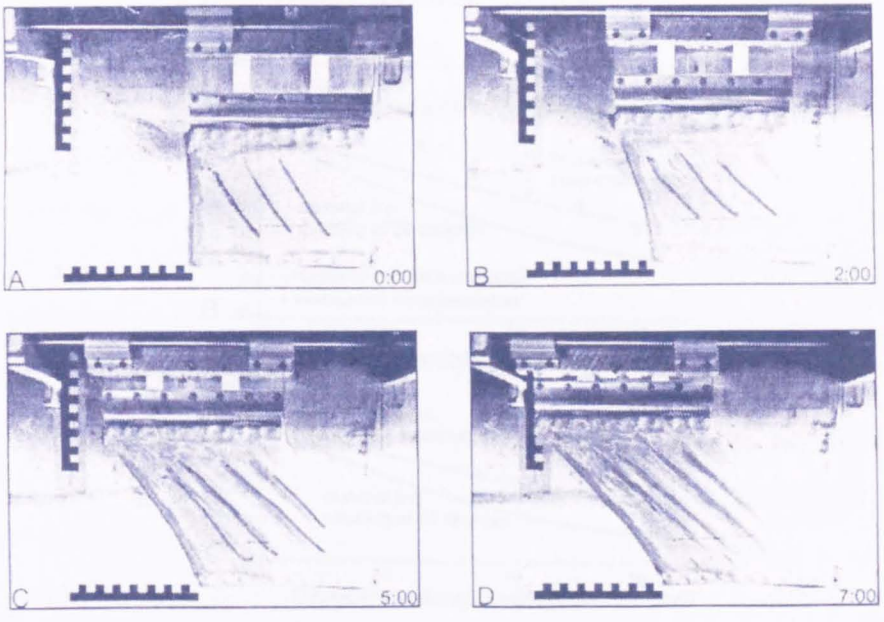

Figure 2.26: Results of $\alpha = 15°$ experimental deformation (after Ramani and Tikoff, 2002).

The fold hinges tend to form at a slightly higher angle to the shear-zone boundary than predicted for the calculated orientation of the horizontal finite strain axes (Fig. 2.27). Fold hinges begin to rotate toward the calculated finite strain orientation during progressive deformation (Fig. 2.27). The experimentally created fold hinges initiate parallel to the long axis of the infinitesimal strain ellipse with vertical axial

planes, and subsequently rotate toward parallelism to the maximum horizontal finite stretching direction. Fold amplitude decreases with increasing divergence angle. This is consistent with the decreasing horizontal shortening component with increasingly oblique divergence. Large amounts of parallel hinge stretching have been observed as the result of both the wrench and pure shear components of transtensional strain. Consequently, horizontal extension is always greater than horizontal shortening resulting in a net area increase of the horizontal plane. Folds formed during transtensional deformations are nearly always parallel to the long axis of the infinitesimal strain ellipsoid and tend to rotate toward parallelism with the oblique divergence direction that corresponds to the stable orientation of the maximum finite strain axis at high strains.

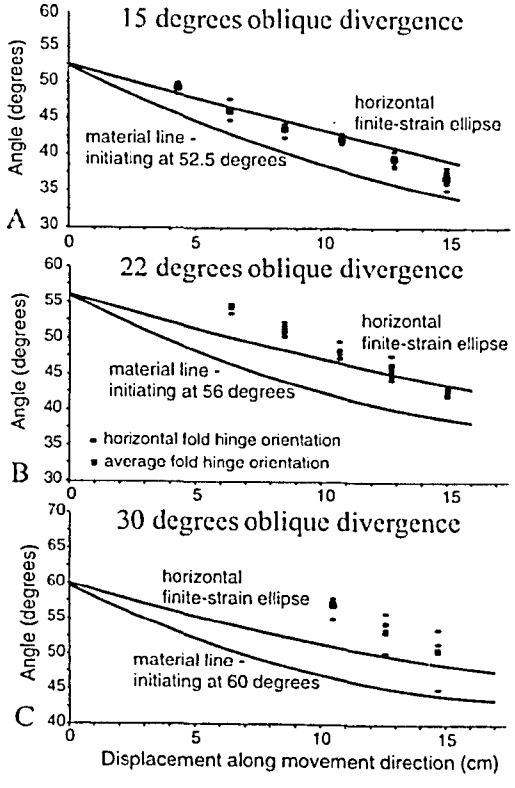

Figure 2.27: Orientation of fold hinges plotted against oblique-divergent displacement for $\alpha = 15°$, $\alpha = 22°$ and $\alpha = 30°$ experiments. Reference orientation is shear-zone boundary defined by edges of plates. Tick marks indicate all measured fold hinge orientations. These experiment results are compared with orientations of long axis of horizontal finite strain ellipse, calculated using kinematic models for transtension (after Ramani and Tikoff, 2002).

The results of this experiment are in accord with the theoretical assumptions that predicted the development of minor shortening structures in the field of wrench-dominated transtensional deformations.

2.4.3 Faulting tests under 3-D strain conditions

Traditional faulting experiments are carried out under axis-symmetric test condition in which cylindrical samples are axially loaded by moving pistons and laterally loaded by pressure applied by a fluid or solid (e.g. Brace, 1964; Friedman and Logan, 1973). This geometry means that, the dependence of fault orientation on the magnitude and sense of the intermediate stress cannot be determined. Reches and Dieterich (1983) conducted an experiment under a 3-dimensional strain field (polyaxial or "truly" triaxial tests) during which loads are applied on three opposite pairs of faces of cubic samples. Previous polyaxial tests dealt primarily with the yielding stresses, and the orientation of faults were not considered (Hojem and Cook, 1968; Mogi, 1971; Atkinson and Ko, 1973; Paterson, 1978). The experiment was stimulated by the observation that fault patterns developed in a 3-dimensional strain field cannot be explained by Anderson's theory (1951) or by the theory of plasticity (Oertel, 1965).

The deformation apparatus consists of three mutually perpendicular hydraulic presses, which independently load a cubic specimen. The servo system significantly increases the stiffness of the presses so that it is possible to continue deformation of a specimen after yielding without complete disintegration (Fig. 2.28).

The controlled displacements applied were always compressional in the x axis and either compressional or extensional in the y axis (Fig. 2.28). The pressure in the z axis was kept constant during a single experiment. The loads of x and y axes were modified by the servo control system during the experiment. The ratio of the strain rate $k = e^t_y / e^t_x$ ranged from 4.0 to –0.4, where $k = 0$ for plane strain. All experiments were run to a total strain of a few percent, leading to the development of several small faults and fractures in the sample. The rock types used were the Berea sandstone, the Sierra-White granite and the Candoro limestone, since their mechanic parameters are well known as they are all commonly used in rock experiments.

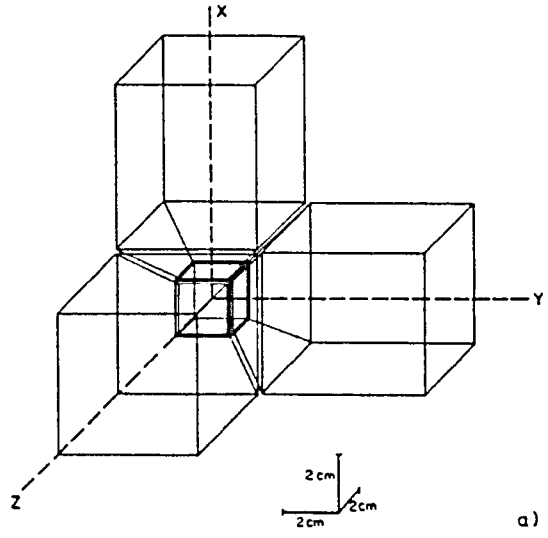

Figure 2.28: The cube sample and the loading anvils used in the Reches and Dieterich (1983) experiment.

The six faces of the samples exhibited several faults and numerous small fractures. In many cases, several faults ran through the complete sample, whereas in others the faults terminated within the sample. In general, the fault patterns within samples of three-dimensional (non-plane strain) deformation, (where $k \neq 0$), tended to be orthorhombic with three or four fault sets (Fig. 2.29).

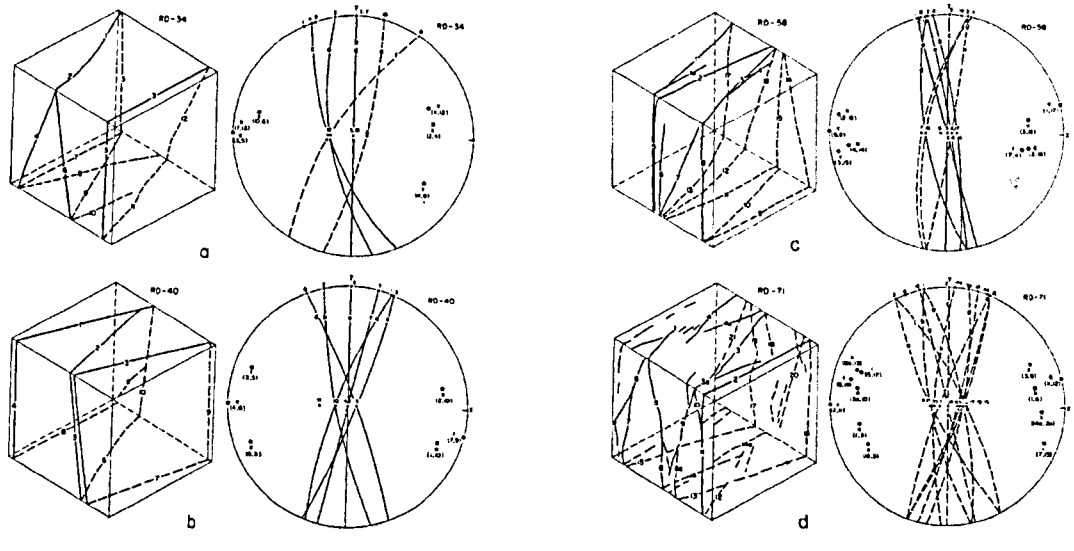

Figure 2.29: On the left side block diagrams of the faulted samples with the fault traces marked in solid line. The traces are numbered and marked on both the block diagrams and the stereonet projections (Wulff net, lower hemisphere). A dashed great circle indicates an inferred fault (after Reches and Dieterich, 1983).

The case of three fault sets is seen similar to the formation of a single set of faults, instead of a conjugate pair, during plane strain experiments. The poles to the formed faults do not lie on the principal strain planes as predicted by the theory of faulting under 3-D strain conditions (Reches, 1978 and 1983). On the other hand, the faults within samples which underwent plane strain, k = 0, tend to be arranged in a conjugate set with two faults sets. In this case, the poles to the fault tend to cluster into the xz principal strain plane. Furthermore, many samples show systematic variations of the orientation of the fault sets in function of the applied strain ratio. The stresses in the two servo-controlled axes, x and y, vary during the experiment, leading to three recognizable stages in most experiments (Fig. 2.30). In fact, during the first stage the stresses increase monotonously until a yielding event, then, during the second stage, several yielding events occur and the two principal stresses, σ_x and σ_y, vary somewhat irregularly and finally, the third stage is characterized by a slow decrease of σ_x and σ_y (Fig. 2.30).

The Reches and Dieterich (1983) experiment indicates that, under three-dimensional strain, four sets of faults develop, rather than the two sets observed in axisymmetric, triaxial tests. It further indicates that the stress history during yielding of rocks may be relatively complicated even under a simple strain history.

Fault patterns displaying similar geometries and symmetry to those reproduced by Reches and Dieterich (1983) experimental tests have been recognised and documented by several authors in diffrent parts of the world. The first to recognize field evidence for multiple fault patterns developed contemporaneously were Donath (1962) and Thompson and Burke (1974) in the Basin and Range. Other evidence for mutually cross-cutting and penecontemporaneously developed orthorhombic fault patterns have been reported from the sandstones of southeastern Utah (Aydin, 1977), from San Rafael Swell of Utah (Krantz, 1988 and 1989), from Central Australia (Kirschner and Teyssier, 1994), from African rifts, the Rhine graben, the Oslo graben and the Triassic Basins of eastern North America (Reches, 1978 and references therein), from the Dead Sea transform (Sagy et al., 2003), from Arran, Scotland, in the New Red Sandstone (Underhill and Woodcock, 1987; Woodcock and Underhill, 1987) and from brittle faults in the metamorphic gneisses of the Lewisian Complex of NW Scotland (Beamon et al., 1999). In all these cases, the geometry of the

multimodal fault patterns has been interpreted as the result of general triaxial strain, as an alternative to bimodal patterns that reflect plane strain conditions.

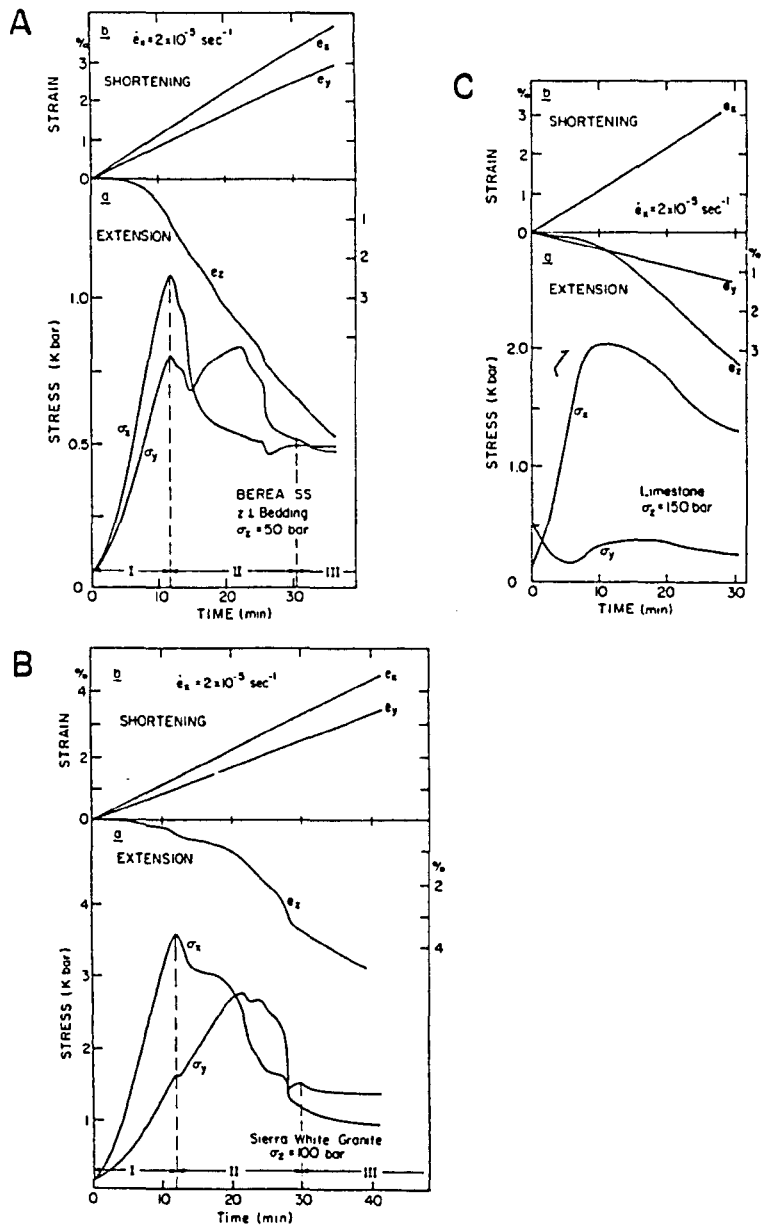

Figure 2.30: The complete stress-time and strain-time curves for three experiments. a) Berea sandstone, b) Sierra-White granite and c) Candoro limestone. Note the division into three stages I, II and III of the stress curves in a and b (after Reches and Dieterich, 1983).

3. THE INFLUENCE OF LITHOLOGY AND PRE-EXISTING STRUCTURES ON RESERVOIR-SCALE FAULTING PATTERNS: THEORY AND FIELD APPLICATION FROM THE 90-FATHOM FAULT, NORTHUMBERLAND BASIN, NE ENGLAND

ABSTRACT

In transtensional and transpressional deformation zones, the bulk 3-D strains are often kinematically partitioned into regions of wrench- and extension- or shortening-dominated faulting. Most strain models assume ideal incompressible materials with a Poisson's ratio (ν) of 0.5. It is well known from experimental and geophysical data, however, that natural rocks have values of $\nu < 0.5$ and that significant variations in the values of ν occur for different lithologies. We demonstrate that for non-coaxial, 3-D transtension and transpression, this should lead to an expansion of the wrench-dominated strain field. The effect is especially marked in lithologies with very low Poisson's ratios ($\nu \leq 0.15$), where wrench-dominated deformation can occur even where the regional direction of divergence or convergence is only modestly oblique (e.g. 52°). The Carboniferous basin-bounding 90 Fathom Fault, NE England was reactivated as a dextral transtensional structure during NE-SW regional stretching in post-Carboniferous times. The preferential dip-slip reactivation of pre-existing E-W structures in the underlying Carboniferous basement led to kinematic partitioning of the transtensional bulk strain. In addition, however, the geometric, spatial and kinematic patterns of minor faulting in Permian rocks located in the fault hangingwall are markedly influenced by the host lithology. Quartz-rich sandstones ($\nu = 0.12$) preserve complex faulting patterns consistent with a wrench-dominated transtension while immediately overlying dolostones ($\nu = 0.29$) preserve simpler patterns of Andersonian conjugate faults consistent with a more extension-dominated regime. We propose that the markedly different strain response during the same deformation reflects pronounced lithologically-controlled variations in the value of Poisson's ratio in the adjacent rock units. Our findings illustrate that micro- to meso-scale faulting patterns are likely to be substantially influenced by lithology in all regions of oblique divergence or convergence.

3.1 INTRODUCTION

In the last 30 years, geologists have increasingly realised that the three classic tectonic regimes predicted by the Andersonian model of faulting - extension, shortening, strike-slip - (Anderson, 1951), do not fully describe the three dimensional strain patterns that characterise crustal deformation zones where convergence or divergence is significantly oblique. There are two main reasons why oblique displacements are commonplace: 1) Oblique convergence or divergence is inevitable during motion of plates on a sphere (Dewey, 1975; Dewey et al., 1998). Woodcock

(1986) has shown, for example, that the relative plate motions at well over 50% of modern plate boundaries are significantly oblique. A similar percentage is likely in ancient settings. 2) Most crustal deformation zones contain pre-existing structures, such as layering, foliation, faults, fractures and shear zones, which may undergo reactivation when subjected to renewed stress (Holdsworth et al., 1997). Many of these pre-existing structures are likely to lie significantly oblique to the new regional transport direction. The Andersonian tectonic regimes have therefore been extended to include transtension and transpression which can be defined as: *strike-slip deformations that deviate from a simple shear due to a component of extension (or shortening) orthogonal to the deformation zone boundary* (Fig. 3.1a; Dewey et al., 1998).

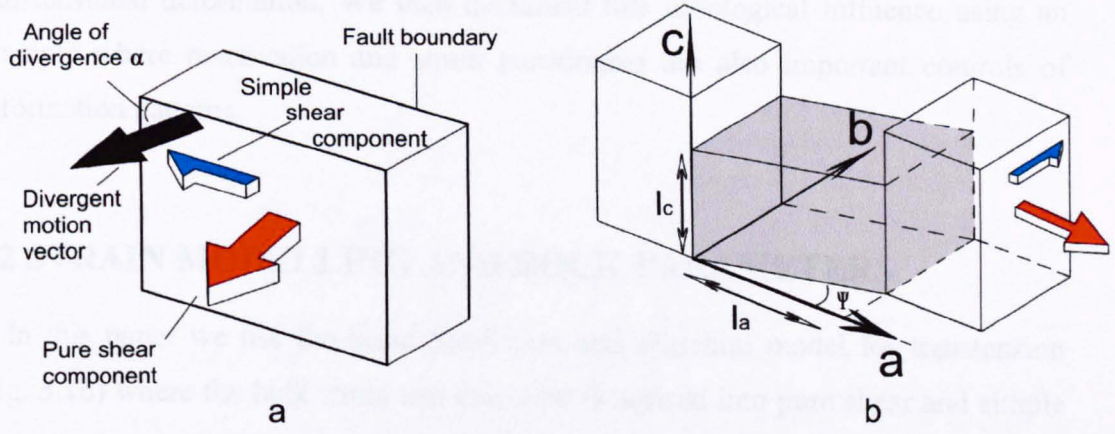

Figure 3.1: a) A transtension can be viewed as the combined action of extensional pure and wrench simple shear resulting from an oblique direction of extension relative to the deformation zone boundaries. b) Sanderson and Marchini (1984) transtensional model: a unit cube ($l_0 = 1$) is deformed assuming that the fault boundaries are vertical and parallel, with no stretch along the zone ($l_b = 1$). Horizontal extension across the zone is totally balanced by vertical shortening. Constant volume is assumed ($\Delta V = 0 + e_c + e_a = 0$), fault zone is basally confined and deformation is homogeneous. Deformation parameters are: extension $e_i = (l_i - l_0)/l_0$ where i = a,b,c and $l_0 = 1$ and shear strain $\gamma = \tan \Psi$ where Ψ is the angular shear.

Sanderson and Marchini (1984) provided a basic vertically-oriented, constant volume, homogeneous strain model that can be used for analysing regions of transpression and transtension. Many authors have further investigated and modelled 3-D transtensional and transpressional strains, often by changing the boundary conditions of the original model. These include: using a strain matrix for simultaneous simple shear, pure shear and volume change (e.g. Fossen and Tikoff, 1993); investigating the effects of strain partitioning (e.g. Tikoff & Teyssier, 1994;

Jones and Tanner, 1995); modelling heterogeneous strain (e.g. Robin and Cruden, 1994); including basal and lateral extrusion (Jones et al., 1997; Fossen and Tikoff, 1998); investigating the effects of oblique simple shear (Lin et al., 1998; Jones and Holdsworth, 1998) and incorporating inclined deformation zone boundaries (Jones et al., 2004). In transtensional settings, there have also been a number of field- and laboratory-based studies of deformation styles (e.g. Withjack and Jamison, 1986; Dewey, 2002; Ramani and Tikoff, 2002), although these are less extensive compared to the equivalent literature for transpression zones (e.g. see Dewey et al., 1998 and references therein)

In this paper we begin by investigating how changes in Poisson's ratio (ν) related to host-rock lithology may influence the development of brittle structures during transtensional deformation. We then document this lithological influence using an example where reactivation and strain partitioning are also important controls of deformation patterns.

3.2 STRAIN MODELLING AND ROCK PARAMETERS

In this paper we use the basic Sanderson and Marchini model for transtension (Fig. 3.1b) where the bulk strain can easily be factorised into pure shear and simple shear components. In all transtension (and transpression) zones, the relative displacement direction across the deformation zone, infinitesimal strain (or stress) and finite strain axes are all oblique to one another. However, predictable geometric relationships exist between the orientations of the deformation zone boundaries, the axes of infinitesimal strain (stress) and the relative displacement direction across the deformation zone. In many cases, therefore, it is useful to apply an analysis using infinitesimal strain, which is equivalent to the more conventional, widely-used stress-inversion techniques (e.g. Angelier, 1979 and 1984; Michael, 1984). Note, however, that this approach is only reasonable in regions where bulk finite strain – or more correctly, finite *non-coaxial* strains – are reasonably low, so that the misorientation between finite and infinitesimal strain axes is limited.

Transtensional infinitesimal strain will occur when the bulk displacement is at an oblique angle α to the deformation zone boundary faults (i.e. $0° < \alpha < 90°$) (Figs. 3.1a and 3.2a). When the divergence angle α is perpendicular ($\alpha = 90°$) or parallel (α

= 0°) to the boundary fault, we have pure shear coaxial extension (Fig. 3.2b) and non-coaxial wrench simple shear (Fig. 3.2c), respectively. These represent end-member strain states for transtension and both are considered in the present analysis to lead to plane strain (2-D) deformation (Figs. 3.2b-c). When the divergence vector is at an oblique angle, non-coaxial 3-D strain is always developed (Fig. 3.2a).

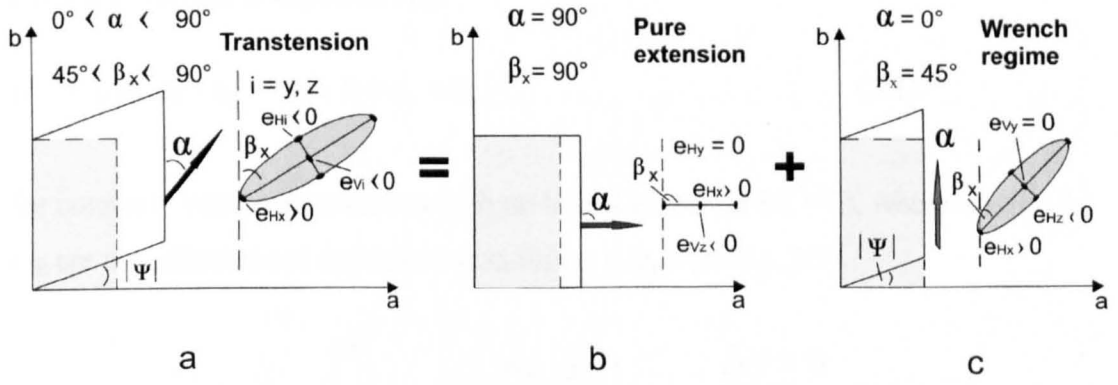

Figure 3.2: a) 3-D constrictional non-coaxial transtensional strain ($0° < \alpha < 90°$). Note that $e_{Hi} = e_{Hz}$ and e_{Hy} for wrench- and extension-dominated transtension, respectively. b) Plane strain pure shear coaxial extension ($\alpha = 90°$). c) Plane strain simple shear wrench deformation ($\alpha = 0°$). Parameters shown in the figure: β_x is the angle between the maximum horizontal extension axis and the boundary fault; $|\psi|$ is the infinitesimal angular shear; α is the divergence angle between the displacement and the boundary fault; x, y, z are the maximum, intermediate and minimum infinitesimal extension axes; e_{Hi} is the horizontal infinitesimal principal extension axis with i = x, y or z; e_{Vi} is the vertical infinitesimal principal extension axis with i = z or y. Note that the plane of plane strain is vertical for pure extension (i.e. parallel to Cartesian plane ac) and horizontal for wrench regime (i.e. parallel to Cartesian plane ab).

In this case, the infinitesimal strain ellipsoid lies in the constrictional field ($1 < k \leq \infty$, with $k = [(1+e_x)/(1+e_y) - 1] / [(1+e_y)/(1+e_z) - 1]$) and the (horizontal) maximum principal extension axis (e_{Hx}) always lies in the horizontal plane during progressive deformation. The other horizontal infinitesimal principal extension axis can be either e_{Hz} (minimum principal extension axis) or e_{Hy} (intermediate principal extension axis), depending on the value of α. The switch of the minimum principal extension axis from a horizontal to a vertical orientation marks the transition between wrench- and extension-dominated transtension, respectively. The threshold angle α between wrench- and extension-dominated transtension has been termed the critical angle of displacement α_{crit} (Smith and Durney, 1992). It has a value of 20° if one assumes no volume change during deformation and following the other assumptions of the Sanderson and Marchini model (McCoss, 1986). The isovolumetric assumption

implies that an ideal incompressible material (i.e. a liquid phase) is involved in the deformation, with a Poisson's ratio $\nu = 0.5$. Following Withjack and Jamison (1986), we propose a more general transtensional model in which the constant volume condition of the Sanderson and Marchini model (3.1) has been relaxed to allow volume change at fault initiation (3.2) due to the Poisson's effect (Fig. 3.3). The change in volume is expressed by:

$$\Delta V = e_a + e_b + e_c = e_a + 0 + e_c = 0 \qquad (3.1)$$

for constant volume transtension with no lateral extrusion ($e_b = 0$), where $e_i = (l_i - l_0) / l_0$ are the infinitesimal extension axes for i = a, b, c (cf Fig. 3.3).

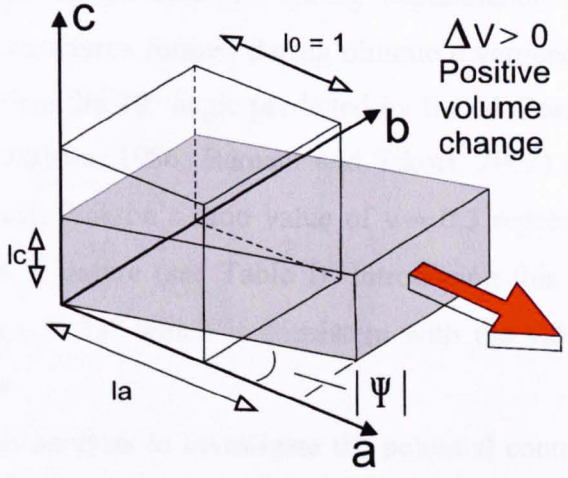

Figure 3.3: Volume change induced by the Poisson's effect in the case of uniaxial tension. The Sanderson & Marchini model assumes a volume constant condition ($\Delta V = 0$) with $\nu = 0.5$ (ideal incompressible material) and the parameter $C = (\nu / (1 - \nu)) = 1$. For all the other cases (i.e. real rocks), $0 < \nu < 0.5$ and thus the parameter $C = (\nu / (1 - \nu)) \neq 1$, allowing positive volume change ($\Delta V > 0$), but not lateral extrusion ($e_b = 0$). The general condition of volume change is given by equation $\Delta V = e_a + e_b + Ce_c$ (see text).

If the effect of Poisson's ratio is included, equation 3.1 becomes:

$$\Delta V = e_a + 0 + Ce_c \neq 0 \qquad (3.2)$$

where the parameter $C = (\nu / (1-\nu)) \neq 1$ for $\nu \neq 0.5$ (cf Fig. 3.3). The incorporation of Poisson's effect will in general lead to positive volume change ($\Delta V > 0$) at fault initiation during transtensional deformation (Jaeger, 1964), because most rocks have values of $\nu < 0.5$ (Table I).

Thus the calculated angle α_{crit} is now additionally controlled by the parameter C which is related to the Poisson's ratio value as follows:

$$0.5\ (w / l_0)\ (\sin \alpha_{crit} - 1) = - C\ (w / l_0) \sin \alpha_{crit} \qquad (3.3)$$

This represents the situation where $e_{Hz} = e_{Vy}$ (i.e. the transition strain-state when $\alpha = \alpha_{crit}$, equation 2 and 4 in Appendix 1, Withjack and Jamison, 1986). w is the infinitesimal displacement in a direction at an angle α to the fault boundary and e_{Hz} and e_{Vy} are the horizontal and vertical infinitesimal minimum and intermediate principal extension axes, respectively.

The likely importance of Poisson's ratio in determining deformation patterns is illustrated by the α_{crit} values obtained during experimental analogue modelling studies investigating structures formed during oblique divergence. These values are significantly greater than the 20° angle predicted by the McCoss (1986) model, e.g. 30° (Withjack and Jamison, 1986; Ramani and Tikoff, 2002) and 45° (Smith and Durney, 1992). A mean Poisson's ratio value of $\nu \approx 0.3$ represents a typical mean value for most rocks in nature (see Table I). Introducing this value into equation (3.3), we obtain a $\alpha_{crit} = 33°$ which is consistent with the values observed in the analogue experiments.

We can extend this analysis to investigate the potential control that variations in lithology (e.g. variations in Poisson's ratio) might exert upon faults forming in a compositionally heterogeneous bedded rock sequence. Following Christensen (1996) we calculated dynamic Poisson's ratio values (see Table I) using compressional (V_p) and shear (V_s) wave velocities for a range of typical igneous, metamorphic and sedimentary rocks (Christensen, 1996 (igneous and metamorphic rocks); Johnston and Christensen, 1992 (sedimentary rocks)). This is achieved using the following equation:

$$\nu = 0.5\left[1 - \frac{1}{\left(\frac{Vp}{Vs}\right)^2 - 1}\right] \qquad (3.4)$$

Magmatic rocks with Vp/Vs obtained between 200-1000 Mpa

Rock type	ν	α_{crit}
Andesite	0.29	33°
Basalt	0.29	33°
Diabase	0.28	34°
Granite	0.24	38°
Diorite	0.26	35°
Gabbro	0.29	33°

Sedimentary rocks with Vp/Vs obtained at the average pressure of 200 Mpa

Rock type	ν	α_{crit}
Limestone	0.32	31°
Dolostone	0.29	34°
Silty limestone	0.29	34°
Shale	0.25	37°
Sandstone	0.23	38°
Quartz-rich Sandstone (90%)	0.12	52°
Mean lowest static Value measured	0.15	48°

Table I: Poisson's ratio ν and the α_{crit} angle calculated for a variety of lithologies using equations 5 and 3. See text for details.

The solutions of equation (3.3) have been plotted on a ν vs α_{crit} graph (Fig. 3.4a)

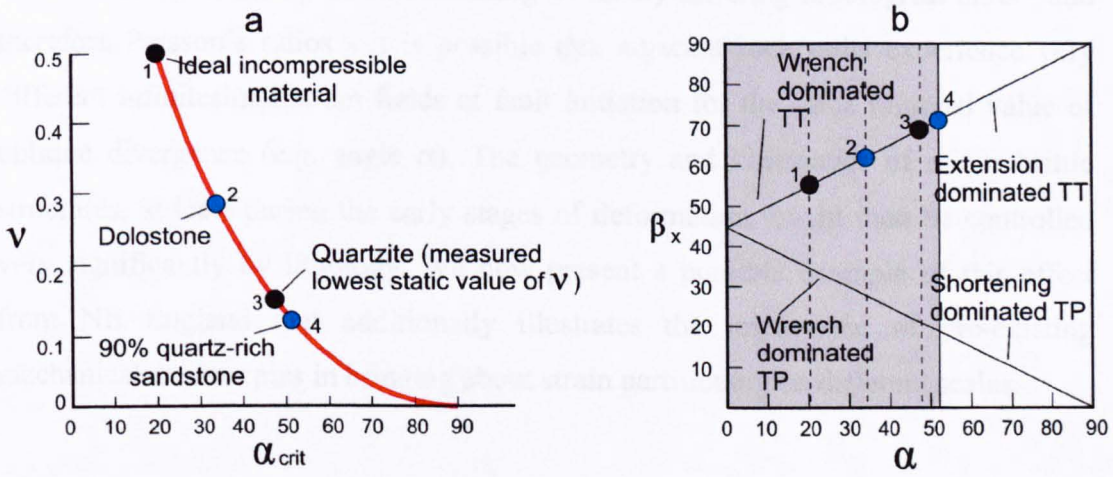

Figure 3.4: a) ν vs α_{crit} graph plotting solutions of equation (3.3). Data for: 1) an ideal incompressible material; 2) dolostones; 3) quartzite, the lowest static value measured for real rocks; and 4) quartz-rich sandstones ($\approx$ 90%) have been plotted as dots. b) α vs β_x diagram plotted with the field of wrench-dominated transtension highlighted (grey area and dashed lines) for the points 1-4 displayed on figure 3.4a and listed in Table I. The abbreviations TT and TP in the graph are transtension and transpression, respectively.

to show the influence of different lithologies on strain regime during transtensional (and transpressional) deformations.

A further equation (equivalent to equation 3 in Appendix 1 of Withjack and Jamison, 1986) relates α to β_x, the angle between the infinitesimal horizontal maximum extension strain axis and the b-axis of the Cartesian co-ordinate frame, which corresponds to the deformation zone boundary (Fig. 3.2a):

$$\beta_x = 90° - 0.5 \tan^{-1} (\cot \alpha) \qquad (3.5)$$

The solutions to equations (3.5) and (3.3) are plotted on an α vs β_x diagram (Fig. 3.4b) for four representative Poisson's ratio values (≡ lithologies) listed in Table I and also shown in figure 3.4a (incompressible material, dolostones, the lowest static value measured for real rocks and quartz-rich sandstones where quartz content ≈90%). In all cases, compared to the ideal incompressible material, the reduced value of the Poisson's ratio leads to an expansion of the wrench dominated field at the point of fault initiation (Figs. 3.4a-b). This suggests that in quartz-rich sandstones, for example, faulting could initiate in a wrench-dominated transtensional regime even where displacements are only modestly oblique (e.g. α values up to 52°; Fig. 4b). Furthermore, in any basin containing markedly differing lithological units - and therefore Poisson's ratios - it is possible that adjacent rock units experience very different infinitesimal strain fields at fault initiation for the same regional value of oblique divergence (e.g. angle α). The geometry and kinematics of minor brittle structures, at least during the early stages of deformation, might then be controlled very significantly by lithology. We now present a possible example of this effect from NE England that additionally illustrates the importance of pre-existing mechanical anisotropies in bringing about strain partitioning on different scales.

3.3 CASE STUDY: THE 90-FATHOM FAULT, NE ENGLAND

3.3.1 Regional geological setting

The early Carboniferous Northumberland Basin, NE England forms one of the northernmost basins that developed in the foreland of the Variscan orogenic belt (Fig. 3.5a). The basin has an asymmetric shape and can be described as a half-

graben. It is bounded to the south by the Stublick - 90-Fathom normal fault system which dips to the N and trends ENE-WSW to E-W (Figs. 3.5b-c; Kimbell et al., 1989; Leeder et al., 1989; Collier, 1989).

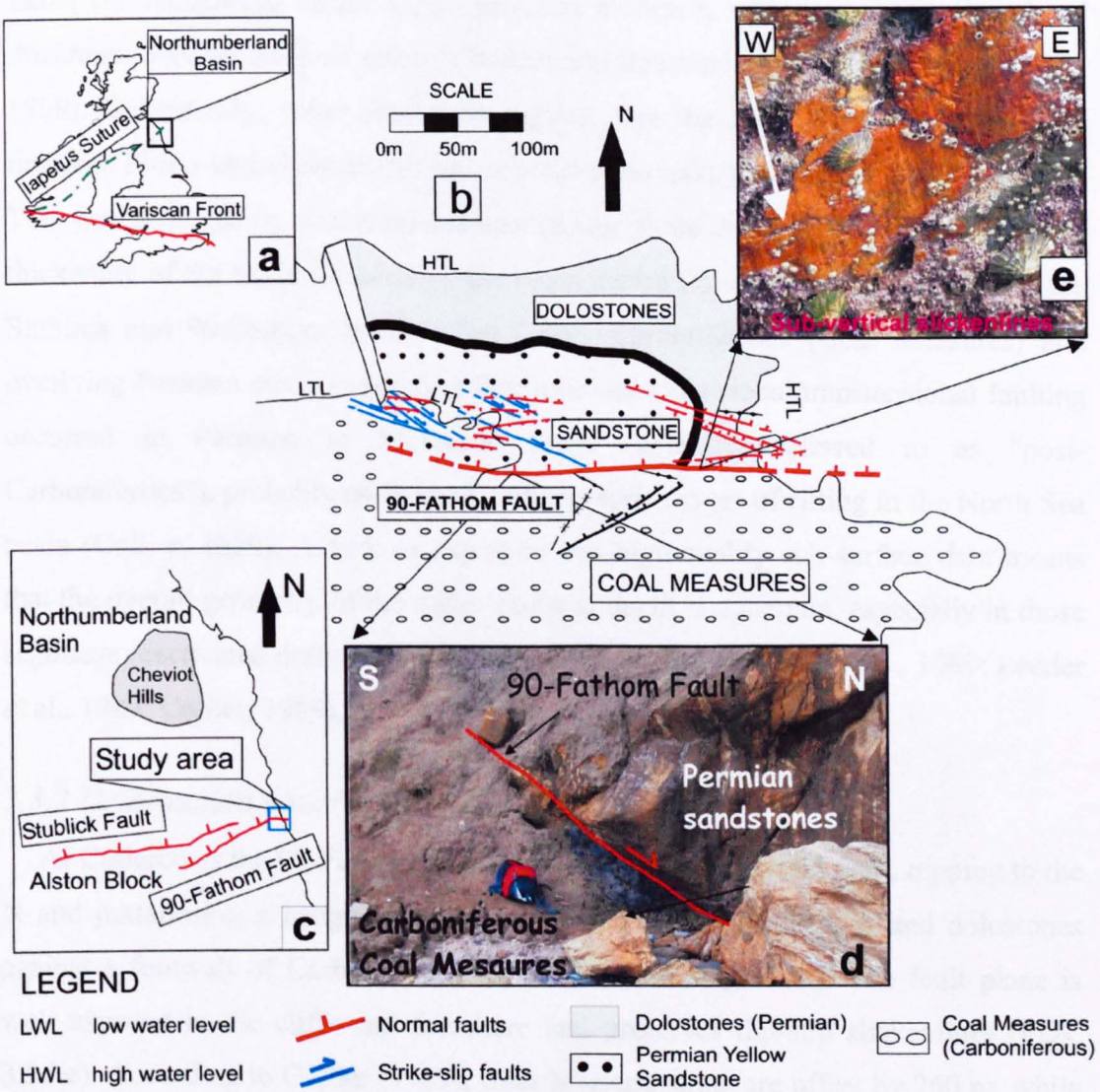

Figure 3.5: a) Location map of Northumberland Basin. b) Detailed structural map of the 90-Fathom Fault at Cullercoats showing mesoscale structures (i.e. normal and strike-slip faults) in the hangingwall. c) Simplified structural map of Northumberland Basin, showing main bounding faults and location of Cullercoats study area. Note change in trend of 90-Fathom Fault. d) Exposure of 90-Fathom Fault shear plane in cliff. e) Dip-slip slickenlines preserved on main fault plane exposed on foreshore.

The fault system appears to be segmented, with the main movement transferred S and E along-strike from the western Stublick Fault to the easternmost 90-Fathom Fault (Fig. 3.5c). Thickness changes in the early Carboniferous strata (Dinantian) are recorded across the fault system, with more than 4.2 km of Dinantian sedimentary

rocks in the hangingwall, compared to a few hundred metres overlying the Alston block, the structural high in the footwall (Kimbell et al., 1989). This is taken as evidence of syn-depositional fault activity (Kimbell et al., 1989). Other intrabasinal faults are recognized based on geophysical evidence, variations in stratigraphical thickness, concentration of channel bodies and dewatering structures (Leeder et al., 1989). Collectively, these structures suggest that the early Carboniferous rifting involved N-S oriented extension that is believed to have ended during the Namurian. This was followed by a thermal subsidence sag phase during the Westpahlian, with thickening of the basin fill towards the basin centre (Kimbell et al., 1989). Both the Stublick and 90-Fathom faults offset Upper Carboniferous (Coal Measures) and overlying Permian strata suggesting that renewed extensional/transtensional faulting occurred in Permian to Mesozoic times (hereafter referred to as "post-Carboniferous"), probably associated with the early stages of rifting in the North Sea basin (Collier, 1989). A lack of exposure and high-quality sub-surface data means that the overall geometry of the major faults at depth is uncertain, especially in those segments reactivated during the post-Carboniferous (e.g. Kimbell et al., 1989; Leeder *et* al., 1989; Collier, 1989).

3.3.2 Deformation patterns

At Cullercoats the 90-Fathom Fault is an E-W striking normal fault, dipping to the N and juxtaposing a hangingwall sequence of Permian sandstones and dolostones against a footwall of Carboniferous Coal Measures (Fig. 3.5b). The fault plane is well exposed in the cliffs and foreshore and preserves dip-slip slickenlines (Figs. 3.5d-e). According to Collier (1989), Coal Measure strata are offset by 260 m, while the base of the Permian is estimated to exhibit 90 m of dip-slip normal displacement on the basis of cross sections constructed from British Coal mine plans and borehole data.

Kinematically the overall pattern of deformation associated with the 90 Fathom Fault at Cullercoats has previously been interpreted to be consistent with a dextral transtensional deformation due to post-Carboniferous reactivation of a pre-existing E-W trending Dinantian normal fault at depth (Collier, 1989). However, in the aeolian sandstones of the immediate hangingwall region, ascribed to the mid-

Permian (Collier, 1989), the faulting patterns appear much more complex compared to the immediately overlying dolostones (Figs. 3.6a-b).

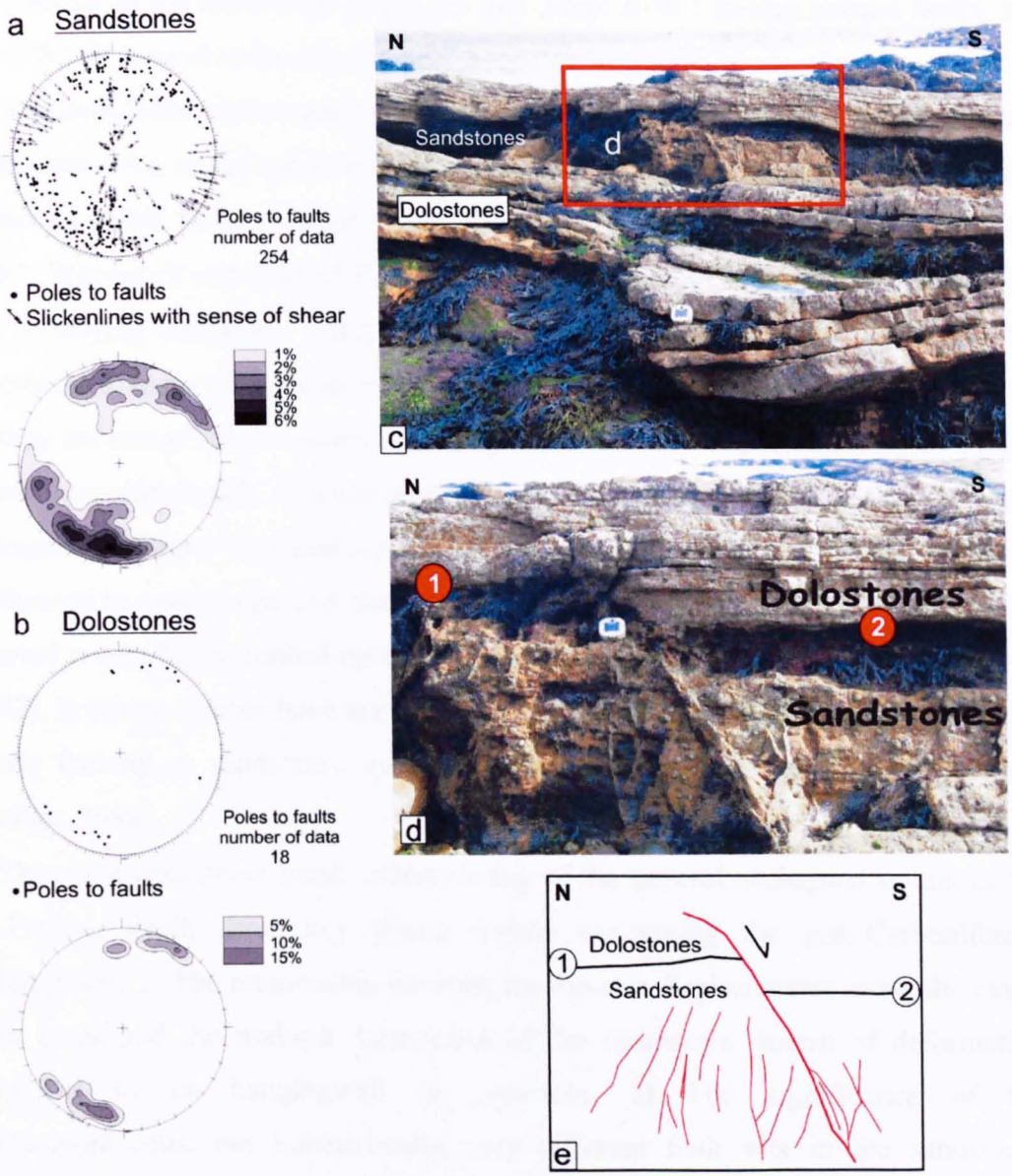

Figure 3.6: a-b) Fault data plotted on an equal area lower hemisphere projection for both lithologies show that normal (E-W trending) and dextral (ESE-WNW) strike-slip faults are present in the sandstone units, whilst less abundant, discrete normal/oblique faults, occur in the dolostone units. Contouring intervals refer to percent data per one percent of the net. c-d) Contrasts in the patterns of faulting in the sandstones + dolostones where they are interbedded adjacent to their mapped boundary in the field. e) Line drawing showing how the small faults in the sandstones terminate against the lithological boundary with the dolostones. Compared to the sandstones, the dolostones present a simpler fault pattern since only the main faults propagate into the dolostones.

The sandstones contain: a) significantly higher numbers of closely-spaced faults (i.e. higher fault densities); and b) geometrically different patterns of conjugate fault

sets, e.g. quadrimodal (Fig. 3.6a) vs bimodal (Fig. 3.6b). Two distinct sets of mutually cross-cutting, and therefore broadly contemporaneous, cataclastic faults are recognized in the sandstones (Figs. 3.5 and 3.6a): E-W trending normal faults; and ESE-WNW dextral strike-slip faults.

The cataclastic, deformation-band style of faulting in the sandstones is generally consistent with strain hardening behaviour and intense grain size reduction along localized brittle faults (Collier, 1989; Knott et al., 1996, Underhill and Woodcock, 1987; Woodcock and Underhill, 1987). At the concordant sedimentary contact with the overlying dolostone units, in a zone where sandstone and dolostone are interbedded, many of the smaller faults observed in the sandstones appear to die out as they are traced into the dolostones (Figs. 3.6c-d-e). In the latter lithologies a much more straightforward, low-density pattern of conjugate ESE-WNW trending extensional/oblique displacement faults occurs (Figs. 3.6b, d-e). The observed difference in complexity and density of faulting clearly suggests that lithology has exerted a significant control on the faulting pattern (e.g. Woodcock and Underhill, 1987). Previous authors have attributed these differences to changes in rheology, i.e. brittle faulting in sandstones vs more ductile folding and faulting in dolostones (Collier, 1989).

Despite a reasonably good understanding of the general geological setting of the 90-Fathom Fault, three key issues remain concerning the post-Carboniferous deformation. 1) The relationship between the dip-slip displacements along the major fault plane and the multiple kinematics of the mesoscale pattern of deformation exhibited in its hangingwall is uncertain. 2) The significance of the contemporaneous, but kinematically very different fault sets in the sandstones requires explanation. 3) Does lithology account for the very different patterns of faulting in the Permian sandstones and dolostones? A detailed 3-D strain analysis has been carried out in the attempt to address these issues and give some new insights into the development of complex fault patterns in transtensional settings. Our findings illustrate the importance of strain partitioning acting simultaneously and on different scales during transtensional deformation.

3.3.3 Strain analysis: strain partitioning, reactivation and lithological control

In both sandstones and dolostones, individual fault displacements are small, rarely exceeding a few tens of centimetres, suggesting low finite strain intensities. This observation, together with a lack of evidence for significant bulk shear-induced rotations (i.e. no sigmoidal vein arrays observed), means that an approximate coincidence between the stress and infinitesimal strain axes may reasonably be assumed, i.e. $\sigma 1 = e_z$; $\sigma 2 = e_y$; $\sigma 3 = e_x$.

Stress inversion has been applied to the fault-slickenline dataset from all faults in the sandstones (Fig. 3.7).

The software package used (Daisy 2 of Salvini, 2001) automatically separated the faults into two groups, each associated with very different stress fields: respectively, extensional (vertical $\sigma 1$, horizontal N-S trending $\sigma 3$) (Figs. 3.7a-b-c) and dextral strike-slip (horizontal NW-SE-trending $\sigma 1$ and NE-SW-trending $\sigma 3$) (Figs. 3.7d-e-f). These two groups correspond exactly to the two-fold sub-division of faults recognised in the field on kinematic grounds, i.e. the stress inversion results and the field observations suggesting strain partitioning are consistent.

The quartz content of sandstones at Cullercoats has been estimated at about 80% (T. Needham pers. com., 2004) and lies close to the quartz-content of the sandstone shown in Table I. Assuming that the Poisson's ratio of this sandstone ($\nu = 0.12$) is representative of those at Cullercoats, we use an appropriate version of the α vs βx diagram in the following strain analysis (Fig. 3.8a).

The preferential accommodation of N-S extension by E-W-trending dip-slip normal faults could be related to reactivation of the suitably oriented pre-existing structures associated with the 90-Fathom Fault in the Carboniferous rocks immediately below the Permian strata (Fig. 3.8b). This is consistent with the dip-slip slickenlines preserved on the present-day exposed fault plane (Fig. 3.5e). This condition is fixed by the relation $\alpha_1 = \beta_x = 90°$ which express the partitioned extensional component of displacement, α_1 (Figs. 3.8a,b).

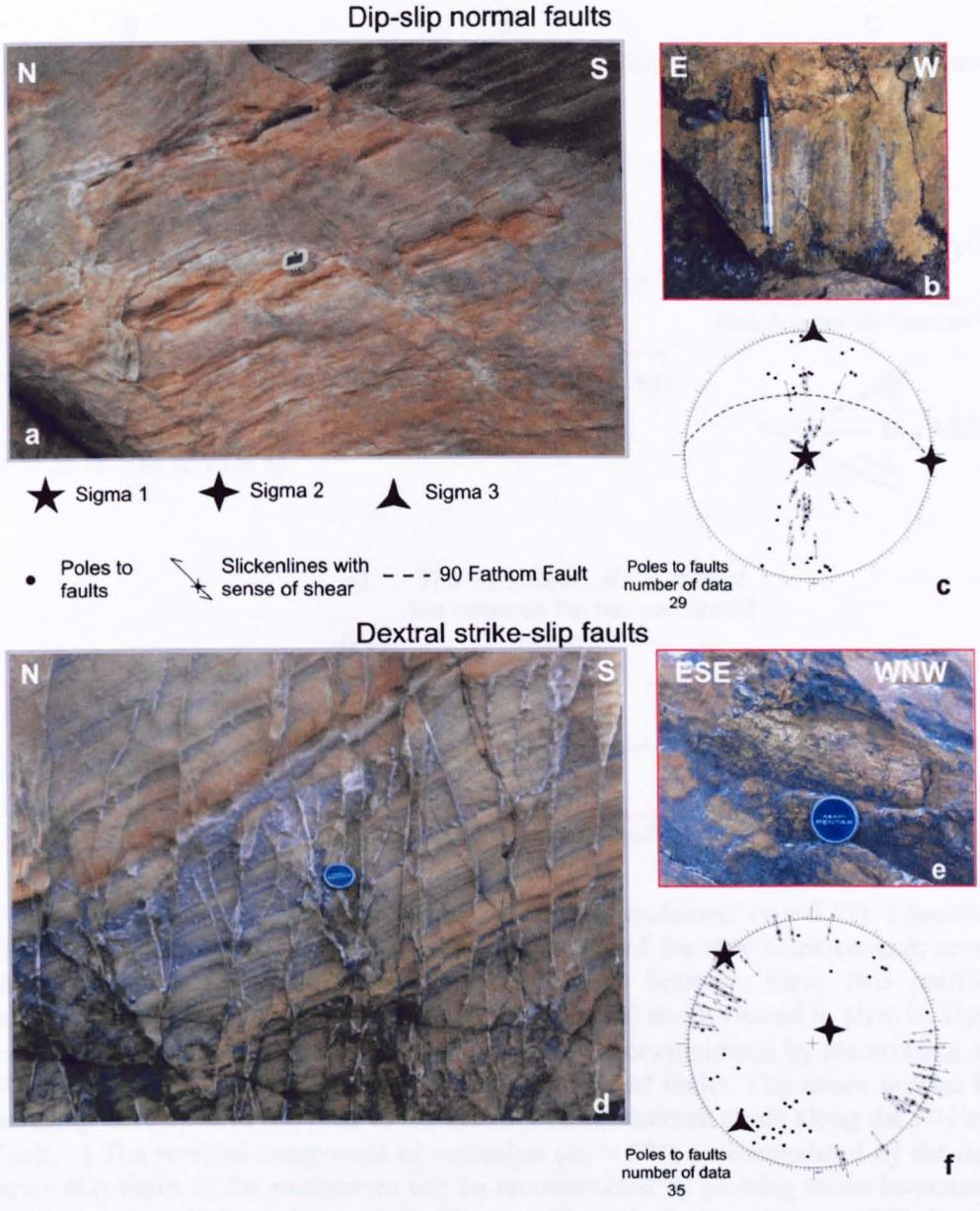

Figure 3.7: a-b) Typical dip-slip normal faults and slickenlines in the sandstones which trend parallel to the main 90-Fathom Fault and form an approximately Andersonian conjugate system. c) Stress inversion applied to these faults (equal area lower hemisphere projection) yields a vertical σ1 and a N-S trending σ3. d-e) Typical dextral strike-slip faults and slickenlines which have an ESE-WNW trend. f) Stress inversion applied to these faults (equal area lower hemisphere projection) yields a NW-SE oriented σ1 and a NE-SW oriented σ3.

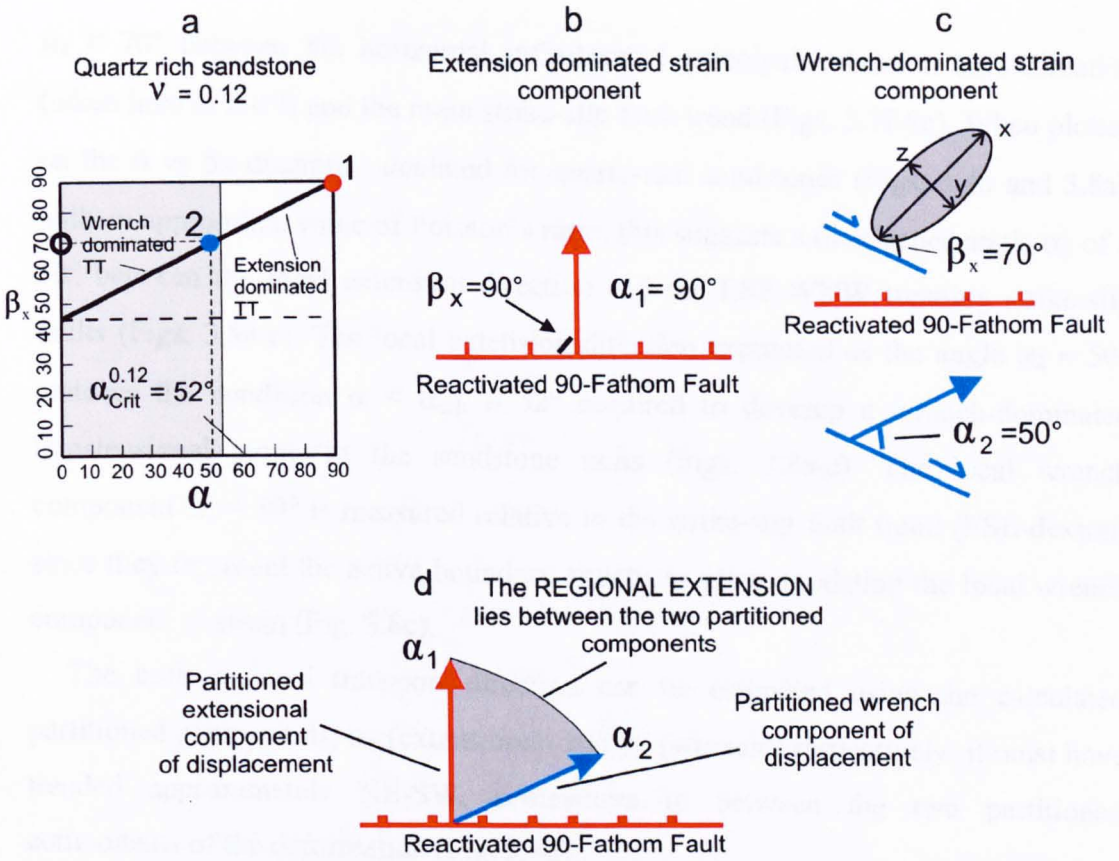

Figure 3.8. a) α vs β_x diagram plotted for quartz rich sandstones (ν = 0.12). 1 (extension) and 2 (wrench) represent the partitioned components of the total displacement; note that the regional displacement vector lies somewhere between these two partitioned components. b-d) Analysis of faulting and infinitesimal strain viewed in plan. b) The N-S extension component of strain (α_1 = 90°) has been accommodated by reactivation of the 90-Fathom Fault and by adjacent E-W-trending normal faults. The minor normal faults probably developed in response to the partitioned extensional strain along the 90-Fathom Fault. c) The residual component of extension (α_2 = 50°) accommodated by the dextral strike-slip faults in the sandstones can be reconstructed by plotting stress inversion and field data (β_x = 70°) on the α vs β_x diagram. The calculated angle α_2 = 50° lies in the wrench-dominated field and is therefore consistent with the development of dextral strike-slip faults. d) The regional displacement vector must lie somewhere between the two partitioned end-member directions (α_1 = 90° and α_2 = 50°), i.e. NE-SW trending. Note that its precise orientation cannot be determined in the absence of information concerning strain magnitude.

We suggest that the dextral ESE-WNW faults in the hangingwall region are the product of a residual wrench-dominated strain (with a displacement component α_2) left over after the extensional component (α_1) of the bulk regional strain was taken up by fault reactivation (Figs. 3.8a-c). Repeated cycles of reactivation and strain partitioning led to the observed mutually crosscutting relationships exhibited by the kinematically different sets of structures in the sandstones. The stress inversion applied to the ESE-WNW dextral strike-slip faults in the sandstones yields an angle

β_x = 70° between the horizontal infinitesimal principal extension axis direction (taken here as ≡ σ3) and the main strike-slip fault trend (Figs. 3.7f-8c). When plotted on the α vs βx diagram calculated for quartz-rich sandstones (Figs. 3.4b and 3.8a), with an appropriate value of Poisson's ratio, this suggests a divergence angle α_2 of ≈ 50° between the local extension direction and the ESE-WNW trending strike-slip faults (Figs. 3.8a-c). The local extension direction expressed as the angle $\alpha_2 \approx 50°$ matches the condition $\alpha < \alpha_{crit} \approx 52°$ required to develop a wrench-dominated transtensional strain in the sandstone units (Figs. 3.8a-c). The local wrench component $\alpha_2 = 50°$ is measured relative to the strike-slip fault trend (ESE-dextral) since they represent the active boundary structures accommodating the local wrench component of strain (Fig. 3.8c).

The bulk regional transport direction can be estimated using the calculated partitioned components, α_1 (extensional) and α_2 (wrench), respectively; it must have trended approximately NE-SW, somewhere in between the two partitioned components of the deformation (Fig. 3.8d).

Compared to the sandstones, the dolostones preserve a much simpler pattern of deformation (Figs. 3.6a-b) with main faults having a similar orientation to the main dextral strike-slip faults in the sandstones. Unfortunately, no slickenlines are preserved on these fault planes, but the bimodal conjugate style of faulting and the extensional stratigraphic offsets, seem to suggest an extension with a small component of dextral shear. Significantly, this is consistent with what is predicted if we plot the previously calculated value α_2 for the partitioned wrench direction on an α vs β_x diagram for a material with a Poisson's ratio appropriate for a dolostone (Figs. 3.9a-b-c). In this case, an angle $\alpha_2 \approx 50°$ matches the condition $\alpha_2 > \alpha_{crit} \approx 34°$ required to develop an extension-dominated transtension (Fig. 3.9a).

Thus for the same value of α_2, the dolostone will experience a markedly less non-coaxial deformation compared to that experienced by the adjacent sandstones undergoing wrench-dominated transtension (Figs. 3.9d-e-f). Inclusion of the Poisson's effect mainly results in a change in the simple shear-pure shear ratio, i.e. the kinematic vorticity. For a fixed regional displacement direction, this should lead to changes in the orientation and shape of the infinitesimal strain ellipsoid in different lithologies. Unfortunately we cannot quantitatively analyse this further in

the present case study due to the lack of exposed kinematic indicators in the limited outcrops of dolostones.

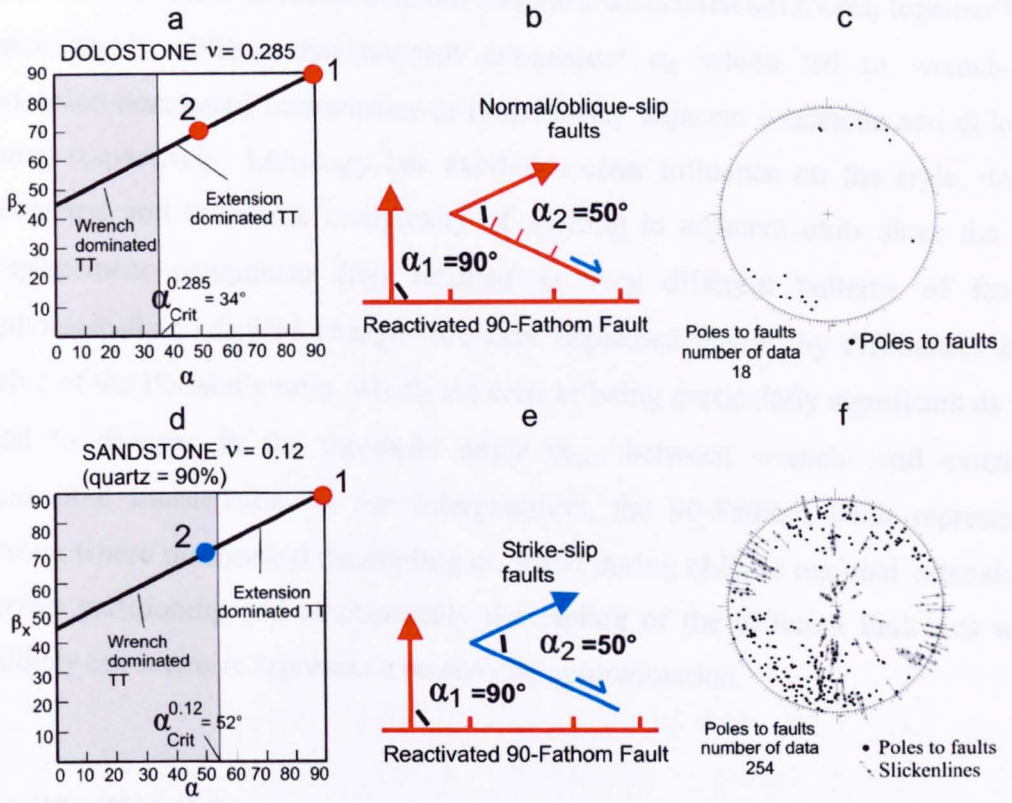

Figure 3.9: The lithological control on style and geometry of faulting is evident when α vs β_x diagrams are plotted for each lithology. a-b) The calculated angle $\alpha_2 = 50°$ for the oblique partitioned component of displacement, accommodated in the hangingwall of the 90-Fathom Fault, plots in the extension-dominated field for dolostone rocks. c) The deformation in the dolostones is accommodated by extensional/oblique slip normal faults (equal area lower hemisphere projection). d-e) The same component of displacement ($\alpha_2 = 50°$) plots in the wrench dominated field for quartz-rich sandstones. f) The pattern of deformation observed in the sandstone units is consistent with what predicted by the strain modelling (equal area lower hemisphere projection). Note that b) and e) are in plan view.

Independent validation of the NE-SW direction of bulk regional extension derived from our analysis (Fig. 3.8d) is provided by the patterns of offshore normal faulting in the immediately adjacent Mesozoic rocks of the southern North Sea (Structural framework of the North Sea and Atlantic Margin, 2000).

In summary, we have demonstrated that the mesoscale pattern of deformation in the Permian hangingwall of the 90-Fathom Fault can be interpreted as resulting from partitioning of a bulk transtensional strain, induced by the obliquity between the pre-existing E-W striking, basin-bounding fault and the NE-SW regional direction of post-Carboniferous extension. This transtension has been partitioned into an

extensional strain with a displacement component α_1, manifested by the dip-slip normal reactivation of the 90-Fathom Fault and associated structures, together with a more highly oblique displacement component α_2 which led to wrench- and extension-dominated transtension in immediately adjacent sandstone and dolostone units, respectively. Lithology has exerted a clear influence on the style, density, geometric and kinematic complexity of faulting in adjacent units since the same displacement component (α_2) resulted in very different patterns of faulting. Lithologically-controlled changes are here explained mainly by differences in the value of the Poisson's ratio, which are seen as being particularly significant as these lead to changes in the threshold angle α_{crit}, between wrench- and extension-dominated transtension. In our interpretation, the 90-Fathom Fault represents a system where mechanical decoupling occurred during oblique regional extension. A perfect partitioning and mechanically decoupling of the different fault sets seems unlikely but seems to represent a reasonable approximation.

3.4 DISCUSSION

Our interpretation of the complex faulting patterns associated with the 90-Fathom Fault is relevant to the ongoing debate concerning whether it is stress or the imposed displacement (strain) that controls the faulting process (e.g. Tikoff and Wojtal, 1999). The 90-Fathom Fault illustrates that the only parameter not affected by the orientation of structures accommodating local deformation is the regional imposed displacement, i.e. the NE-SW opening direction during post-Carboniferous times. The stress (≡ infinitesimal strain) distribution in the hanging wall of the 90-Fathom Fault appears to be highly partitioned (Figs. 3.7a-d) and depends on local controls such as lithology and reactivation of pre-existing zones of mechanical weakness in the sub-adjacent basement (see also Woodcock and Underhill, 1987). In an ancient structure of this kind we have no independent evidence to constrain the orientation of the regional stress. Traditionally, the observed heterogeneities in apparent stress patterns encountered here might be interpreted as being due to polyphase deformation. This is at odds with the field observations.

More generally, our findings illustrate that kinematic partitioning is particularly likely to occur during the deformation of heterogeneous anisotropic crust where pre-

existing structures are often significantly oblique to regional tectonic transport directions (e.g. Dewey et al., 1998; Jones et al., 2004). It is important to note that the direction of the infinitesimal principal extension axes (β_x) does not correspond to the bulk extension direction accommodated by the overall fault system; this is a consequence of strain partitioning and non-coaxial strain component present during 3-D transtensional strain (Dewey et al., 1998).

Our findings further illustrate that the use of two-dimensional strain ellipse models to describe faulting patterns (Wilcox et al., 1973; Harding, 1974) is inappropriate when dealing with complex deformation patterns arising from 3-D strain. Such 2-D methods are still used widely in the interpretation of faulting patterns in sedimentary basins, including the 90-Fathom Fault (e.g. Collier, 1989). Given the marked differences between faulting patterns that arise during 2-D and 3-D finite strain, this practice is unwise in any areas where there is evidence for obliquely divergent plate motions or rifting oblique to reactivated basement faults.

Our findings also have significant implications for structural models of fracture interconnectivity and fluid flow in hydrocarbon reservoirs. For example, the association of contemporaneous normal and strike-slip faults produces a potential mixture of preferential structural permeability patterns. In 2-D (plane strain) extensional or wrench regimes, the horizontal or vertical σ_2 directions, are generally thought to form preferential flow paths for migrating fluids (e.g. Sibson, 2000). Fracture interconnectivity models, based on simple Andersonian faults are not sufficient to predict the structural permeability pattern in the hangingwall of the 90-Fathom Fault. A 3-D model of fault pattern that incorporates the intersections between the various conjugate fault sets will reproduce a more reliable structural permeability model, with multiple flow directions likely to develop. If the faults act as effective pressure seals, as seems likely, this will result in a highly compartmentalized reservoir with a low chance of being economically productive, since each fault-bounded sector will not communicate with the others (Underhill and Woodcock, 1987). A similar case has been recently presented by Olsson et al. (2004) for progressive deformation in sandstone units showing different, almost simultaneously developed, fault patterns.

Thus in cases where there is evidence for transtensional (or transpressional) strain, 3-D strain modelling should be used as a tool to investigate and predict faulting and

structural permeability patterns. It is very likely that many offshore basins have experienced transtensional deformation and have been influenced by reactivation of pre-existing structures oblique to direction of extension.

3.5 CONCLUSIONS

Traditional transtensional strain modelling assumes a Poisson's ratio $\nu = 0.5$ (ideal incompressible material) and predicts that the threshold angle α_{crit} between faults and transport direction is 20° for wrench-dominated ($\alpha < 20°$) and extension-dominated ($\alpha < 20°$) transtension (Fig. 3.4). α_{crit} angles recalculated for dynamic ν values from a range of real rocks show a general expansion of the wrench dominated field for most rock types ($\alpha_{crit} \approx 30°$), except in quartz-rich rocks which display a substantial increase (α_{crit} up to 52°).

The 90-Fathom Fault, NE England, has been used as a field example to test this model and to discuss the significance of geometrically and kinematically complex fault patterns as well as the influence of lithology on faulting. Regional post-Carboniferous NE-SW extensional strain has been partitioned into an extensional component accommodated along the reactivated 90-Fathom Fault and with a residual oblique component accommodated in the hangingwall of the fault. 3-D strain analysis suggests that the calculated divergence angle $\alpha_2 = 50°$, for the residual oblique component of extension has led to wrench-dominated transtension for quartz-rich (≈ 90%) sandstones ($\nu \approx 0.12$) where the threshold angle $\alpha_{crit} \approx 52°$ (Figs. 3.8 and 3.9). In immediately adjacent dolostone units ($\nu \approx 0.29$), however, the same analysis suggests that extension-dominated transtension has occurred, where the threshold angle $\alpha_{crit} \approx 34°$ (Fig. 3.9). Field data match the assumptions of the strain modelling and seem to explain well both the kinematically complicated patterns of deformation and the lithological control on style of faulting.

4. PARTITIONED TRANSTENSION AND BASEMENT REACTIVATION IN THE LATE CARBONIFEROUS OF NORTHERN BRITAIN – AN ALTERNATIVE TO BASIN INVERSION MODELS

ABSTRACT

"Inversion structures" (e.g. folds, reverse faults) spatially associated with basin-bounding faults are very widely recognised in rift basins in both onshore and offshore settings worldwide. The great majority of such structures are attributed to local or regional crustal shortening events. There is, however, an alternative, which is investigated in this paper: inversion could reflect a horizontal shortening component of deformation formed during progressive and partitioned transtension. A case study from the Carboniferous Northumberland Basin shows that shortening structures can also form in obliquely divergent rifts if the bulk strain undergoes kinematic partitioning into distinct regions of wrench- and extension-dominated transtension. Such strain partitioning appears to be particularly favoured in basins where fault localisation is strongly influenced by pre-existing basement structures. This may occur because the pre-existing anisotropies are zones of long-lived weakness that lie in an orientation particularly favourable to the preferential accommodation of either strike-slip or dip-slip displacements. Our strain analysis applied to the Northumberland Basin, traditionally considered as a classic example of a Variscan inverted basin, reduces the deformation history to a single kinematically partitioned phase of dextral transtension during the late Carboniferous-early Permian. Our findings have profound implications for the routine interpretation of inversion structures in any rift basin where the direction of extension may be significantly oblique to the basin margins.

4.1 INTRODUCTION

It has long been recognised that many regions of rift-related deformation will experience directions of divergence that are significantly oblique to the main basin-bounding faults, i.e. bulk transtensional strain (Fig. 4.1; Harland, 1971; Woodcock, 1986; Withjack and Jamison, 1986; Smith and Durney, 1992; Dewey et al., 1998; Dewey, 2002). Such 3-D (non-plane strain) non-coaxial strains can arise when the causative plate separation is oblique to the plate boundary and/or when basin-bounding or intrabasinal faults reactivate pre-existing structures that lie at an oblique angle to the regional direction of extension. The first case is adequately described using a homogeneous transtension model (Sanderson and Marchini, 1984; Dewey et al., 1998) (Fig. 4.1a). In contrast, the second scenario can give rise to a partitioned transtension where the bulk strain is split-up into kinematically distinct and subparallel structural domains, whose location and orientation is controlled by pre-

existing anisotropies in the crustal basement such as lithological contacts, faults and shear zones (Tikoff and Teyssier, 1994; Jones and Tanner, 1995; Jones et al., 2004) (Fig. 4.1b). Thus, components of wrench simple shear (Jones & Tanner 1995) or dip-slip extension (De Paola et al., 2005a) may be preferentially taken up along pre-existing planar structures, or within narrow zones, leaving a residual components of strain to be accommodated within the adjacent country rock domains (e.g. Fig. 4.1b).

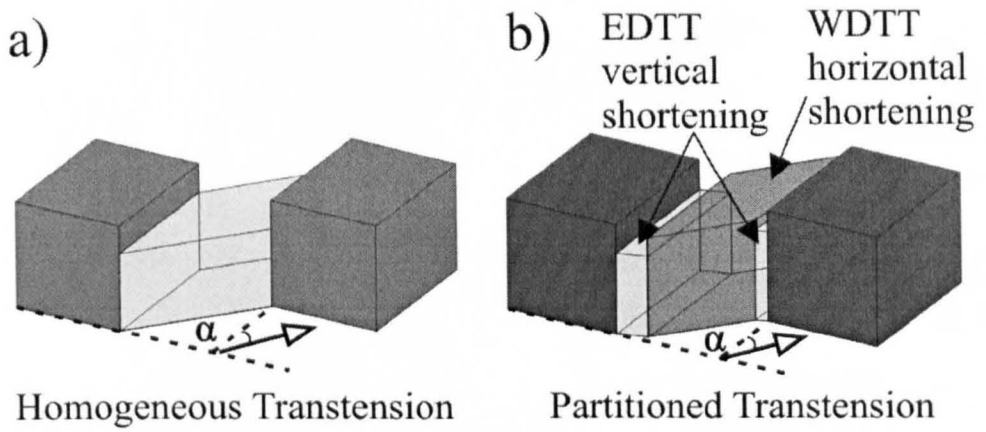

Figure 4.1: a) Homogeneous transtension. b) Partitioned transtension, with a central wrench-dominated domain (WDTT; horizontal infinitesimal shortening) and adjacent extension-dominated domains (EDTT; vertical infinitesimal maximum shortening). Note that other domain configurations are possible, but that, in general, their boundaries are normally parallel to the regional boundaries of the deformation zone.

Transtensional (and transpressional) strains are characterised by complex relationships between finite and infinitesimal strain (≡ stress) axes. In transtensional zones with low to high angles of divergence ($20° < \alpha < 90°$), where α is the angle between regional displacement and boundary faults (assuming an ideal incompressible material with a Poisson's ratio $\nu = 0.5$; McCoss, 1986; Dewey et al., 1998; De Paola et al., 2005a), the axes of infinitesimal (z) and finite shortening (Z') should always be coincident and vertical; this is identical to the case of orthogonal extension ($\alpha = 90°$) ('extension-dominated transtension' (EDTT); Figs. 4.1b, 4.2a-b-c). However, at low angles of divergence ($\alpha < 20°$), the infinitesimal axis z is horizontal, with the finite axis (Z') eventually swapping orientation with the vertical intermediate finite axis Y' with increasing amounts of finite strain ('wrench-dominated transtension' (WDTT); Figs. 4.1b, 4.2a-b-d). It has been demonstrated, both theoretically (McCoss, 1986; Teyssier and Tikoff, 1999; Dewey, 2002) and in analogue modelling studies (Withjack and Jamison, 1986; Smith and Durney, 1992;

Ramani and Tikoff, 2002), that the horizontal shortening arising from wrench-dominated transtension should be sufficient to generate structures such as thrusts, conjugate strike-slip faults and folds (Fig. 4.2d). The development of such structures could easily be incorrectly attributed to localised or regional-scale episodes of crustal shortening due to basin inversion.

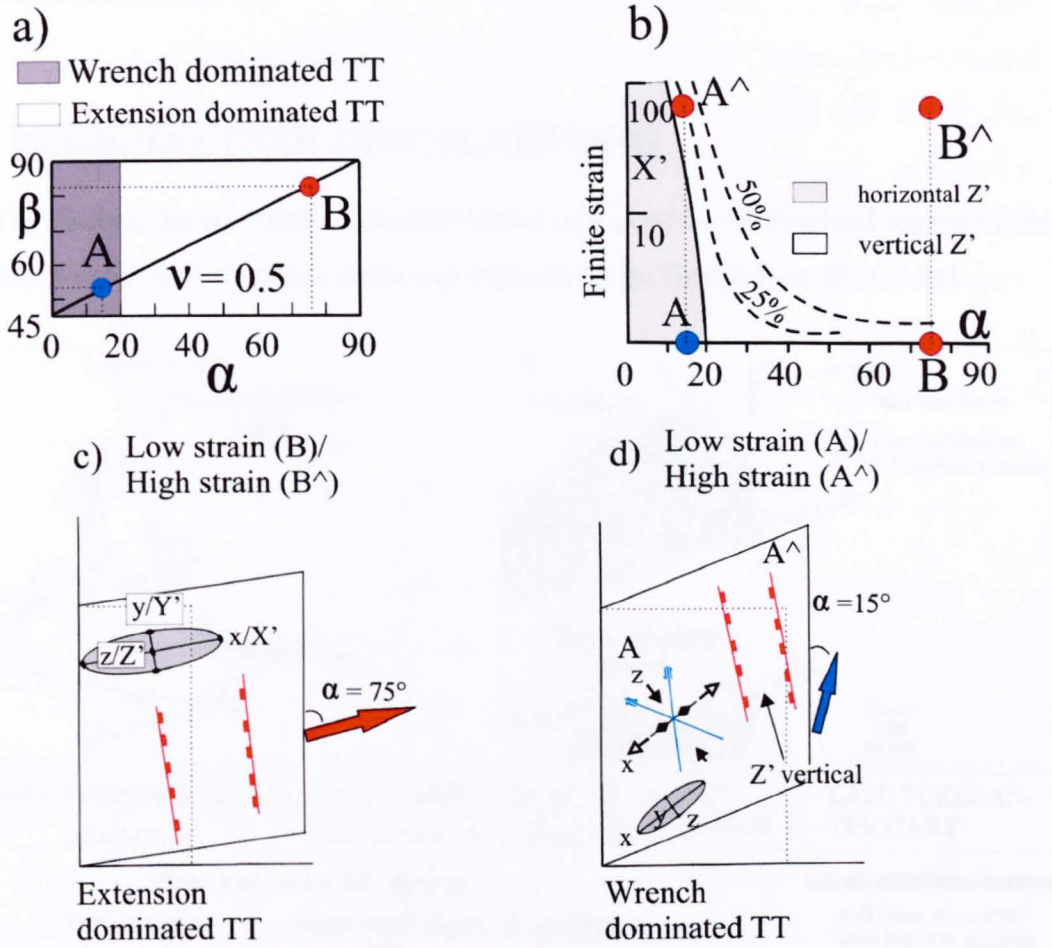

Figure 4.2. a) The fields of wrench-dominated transtension (horizontal infinitesimal maximum shortening) and extension-dominated transtension (vertical infinitesimal maximum shortening) represented on an α vs β diagram. β and α are the angle between the boundary fault and the infinitesimal maximum extension axis and the transport direction, respectively. b) α vs X' (here expressed as finite strain intensity) diagram illustrating that the swap from wrench- to extension-dominated transtension is a function of the angle α and of the amount of finite strain. Note that X' is always in the horizontal plane for transtensional deformation. The dashed curves show how the boundary between wrench- and extension-dominated TT changes with different amounts of volume increase during transtensional deformation (Teyssier & Tikoff 1999). The field of stability of wrench-dominated transtension is expanded when volume increase occurs. c-d) Plan views of structural styles and geometries of associated minor structures are shown for homogeneous transtension zones with divergence angles of α = 75° (EDTT, c) and α = 15° (WDTT, d).

In this paper, we illustrate this problem using observations and data collected from late-Carboniferous-early Permian structures developed across the Upper Palaeozoic Northumberland Basin of NE England. We demonstrate that structures previously interpreted as resulting from successive phases of extension and compression are more readily explained using a single protracted phase of partitioned dextral transtension.

4.2 REGIONAL GEOLOGICAL SETTING

The Carboniferous Northumberland Basin is located in the foreland region of the Variscan orogenic belt which crops out in the southern British Isles (Fig. 4.3a).

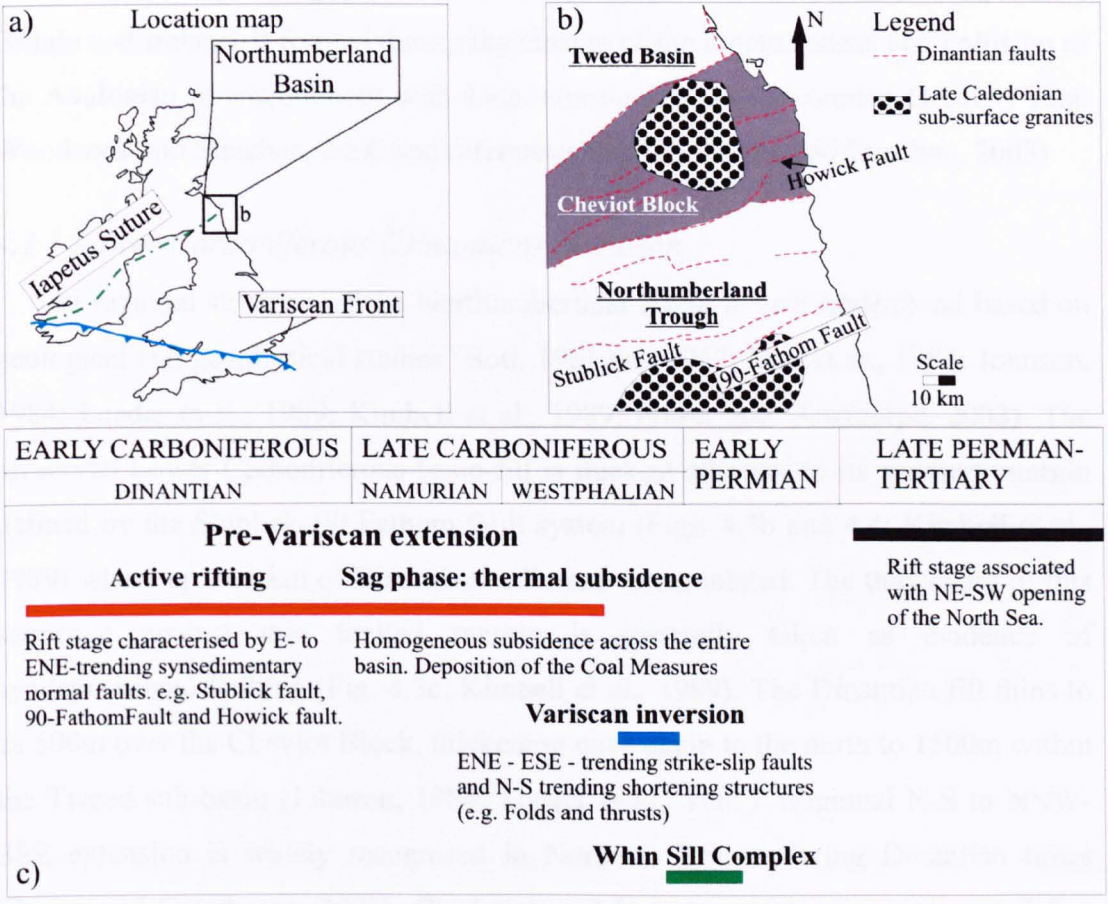

Figure 4.3: a) Location of Northumberland Basin relative to Iapetus Suture and Variscan Front. b) Internal sub-basin of the Northumberland Basin showing main Dinantian bounding faults and locations of Caledonian plutons at depth. c) The currently accepted regional tectonic history of the Northumberland Basin.

The foreland region of Northern Britain is characterised by a system of Lower Carboniferous-age fault-bounded structural highs, cored by relatively buoyant Late Caledonian granites and overlain by a thin cover of Carboniferous sediments (Fig. 4.3b). These are separated by intervening subsided basinal regions with much thicker Carboniferous infills. In the present paper, the term 'Northumberland Basin' is used to refer to two deeper basins, the Tweed sub-basin to the north and the Northumberland Trough to the south which are separated by a fault-bounded central high with a relatively thin Lower Carboniferous cover – the Cheviot Block (Fig. 4.3b, Fraser et al., 1990). Importantly, the Northumberland Trough overlies the northward dipping Iapetus Suture zone buried at depth (Figs. 4.3a-b) (Bott et al., 1985; Chadwick and Holliday, 1991; Soper et al., 1992). This suture zone represents one of the most important structures in the Palaeozoic lithospheric template of Britain and Ireland. It formed during the closure of the Iapetus ocean and collision of the Avalonian microcontinent with Laurentia during the Caledonian Orogeny (e.g. Woodcock and Strachan, 2000 and references therein; Dewey and Strachan, 2003).

4.2.1 Lower Carboniferous (Dinantian) extension

The regional structure of the Northumberland Basin is well understood based on geological and geophysical studies (Bott, 1961 and 1967; Bott et al., 1984; Johnson, 1984; Leeder et al., 1989; Kimbell et al., 1989; Fraser and Gawthorpe, 2003). The preserved Lower Carboniferous basin-fill is thickest adjacent to its southern margin defined by the Stublick–90 Fathom fault system (Figs. 4.3b and 4.4; Kimbell et al., 1989) where up to 4 km of Dinantian sediments accumulated. The thickening of this sequence against this faulted margin is generally taken as evidence of syndepositional faulting (Fig. 4.3c; Kimbell et al., 1989). The Dinantian fill thins to ca 500m over the Cheviot Block, thickening once again to the north to 1500m within the Tweed sub-basin (Johnson, 1984; Leeder et al., 1989). Regional N-S to NNW-SSE extension is widely recognised in Northern Britain during Dinantian times (Fraser and Gawthorpe, 2003). Chadwick and Holliday (1991) have suggested that the brittle E-W to ENE-WSW-trending normal faults recognised by Bott et al. (1984) and Kimbell et al. (1989) detach directly at depth onto the NW-dipping Iapetus suture, which is therefore considered to have been reactivated as an extensional shear zone.

Leeder and McMahon (1988) suggest that the Dinantian rifting was superseded by a regional phase of thermal subsidence in which fault-bounded blocks and basins subsided at uniform rates during the Upper Carboniferous (Westphalian) (Bott et al., 1984; Kimbell et al., 1989) (Fig. 4.3c).

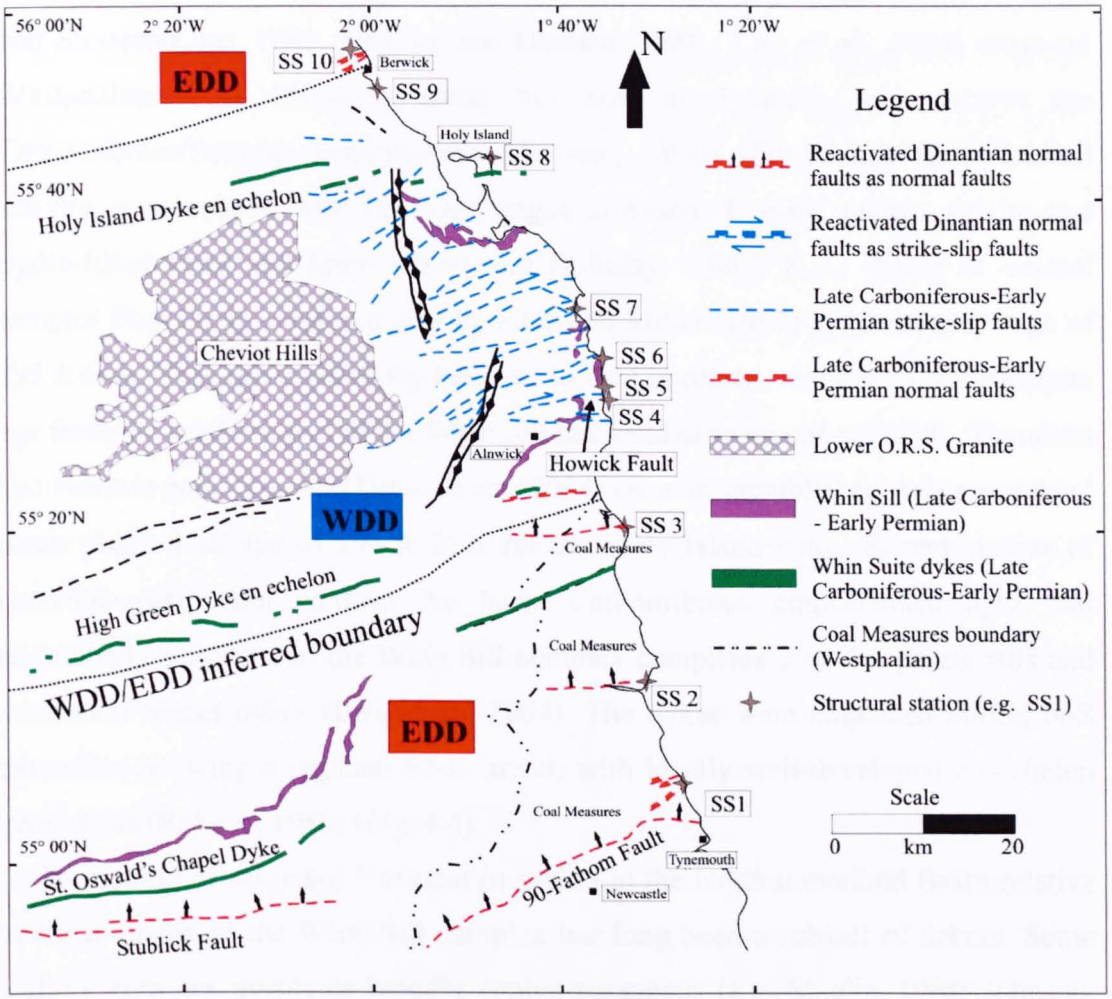

Figure 4.4. Structural map of the Northumberland Basin, NE England showing location of key localities (SS1-10), and late Carboniferous extension-dominated domains (EDD) and wrench-dominated domain (WDD).

4.2.2 Late Carboniferous shortening ('Variscan inversion')

The Northumberland Basin is considered a classic example of an inverted basin (Leeder et al., 1989; Collier, 1989) (Fig. 4.3c). Shiells (1964) and Bower (1990) present detailed accounts of the mesoscale shortening structures in the basin. They identified a characteristic association of three main types of structures: N-to NE-trending folds, reverse faults (thrusts) and conjugate strike-slip faults trending ENE-WSW (dextral) and ESE-WNW (sinistral). This pattern of deformation suggests ~E-

W shortening that all authors relate to the far-field effects of the Variscan Orogeny in Southern Britain in late Carboniferous-early Permian times.

4.2.3 Late Carboniferous-early Permian magmatism: the Whin Sill complex

The Whin Sill complex intrusions in Northumberland (Francis, 1982; Dunham and Strasser-King, 1982; Jonhson and Dunham, 2001; Liss et al., 2004) cross-cut Westphalian Coal Measures strata but not the Permian rocks above the Carboniferous/Permian unconformity (Robson, 1980) (Fig. 4.3c). Hydrothermal activity is associated with the later stages intrusion, forming quartz, calcite and pyrite-filled veins and joints (Frost and Holliday, 1980). K-Ar dating of several samples from the igneous complex by Fitch and Miller (1967) yielded a mean age of 295 ± 6Ma. This age is generally believed to date intrusion, while a U-Pb baddelyite age from the southern part of the Whin Sill has yielded an age of ca297Ma (Hamilton and Pearson pers. comm.). Timmerman (2004) cites an unpublished Ar/Ar weighted mean plagioclase age of 294 ± 2Ma for the Holy Island dyke. Recent studies of palaeomagnetic data confirm the latest Carboniferous emplacement ages, but additionally suggest that the Whin Sill complex comprises 3 or 4 separate sills and associated feeder dykes (Liss et al., 2004). The dykes were emplaced during N-S extension, showing a regional ENE- trend, with locally well-developed en-echelon geometries (Robson, 1980) (Fig. 4.4).

The timing of supposed Variscan inversion in the Northumberland Basin relative to the intrusion of the Whin Sill complex has long been a subject of debate. Some authors view the events as broadly contemporaneous (e.g. Shiells, 1964; Johnson, 1995), whilst others (e.g. Leeder et al., 1989; Collier, 1989; Bower, 1990) have argued that the Whin Sill intrusions post-date inversion. In the latter view, the timing of inversion is confined to a 14 Ma period between the deposition of the youngest preserved Carboniferous sediments in NE Northumberland (ca 311 Ma) and intrusion of the Whin Sill Complex (ca 297 Ma) (Collier, 1989). On a regional scale, the Whin Sill complex is thought to be associated with a major suite of magmatic intrusions recognised across NW Europe and formed during lithospheric extension (Neumann, 1994; Sundvoll and Larsen, 1994; Smythe et al., 1995; Ernst and Buchan, 1997 and 2001; Timmerman, 2004).

4.2.4 Post-basal Permian deformation

Late-stage, mostly minor fault arrays have long been recognised in the Northumberland Basin cross-cutting the Whin Sill complex intrusions (e.g. Shiells, 1964). On a larger scale, structures such as the 90-Fathom fault offset Upper Carboniferous (Coal Measures) and overlying Permian strata suggesting that reactivation of pre-existing faults occurred during Permian to Mesozoic times, probably associated with NE-SW extension during the early stages of rifting in the North Sea basin (Collier, 1989; De Paola et al., 2005a).

4.2.5 Summary of existing models and key problems

The accepted model for the late Carboniferous - early Permian evolution of the Northumberland Basin (Fig. 4.3c) suggests that an early phase of Dinantian N-S extension is post-dated by Varisacn inversion, the effects of which partially overlapped with the thermal subsidence phase that followed rifting. These events are then supposedly post-dated – or perhaps overlapped - by renewed N-S extension related to emplacement of the Whin Sill complex ca 294-7Ma. Finally, the region was subjected to NE-SW extension during Permian Mesozoic times, with significant reactivation of pre-existing Carboniferous faults. Two significant problems exist with the current model: 1) the approximately E-W shortening direction in the Northumberland Basin is markedly non-parallel to the NNW direction of Variscan convergence in Southern Britain (e.g. Sanderson, 1984); and 2) there is uncertainty concerning the timing of E-W shortening relative to the emplacement of the Whin Sill complex. The emplacement of a tholeiitic suite of intrusions of a type more generally associated with lithospheric extension (e.g. Timmerman, 2004) seems to be at odds with the occurrence of a crustal shortening episode in this part of Northern Britain.

4.3 REGIONAL STRUCTURAL PATTERNS

In Carboniferous outcrops, post-Dinantian, pre-Permian (hereafter referred to as 'late Carboniferous') ages of movement can be inferred based on four criteria: i) the structures cross-cut Westphalian Coal Measures sedimentary sequences deposited during post-Dinantian thermal subsidence; ii) the faults are not associated with

features indicative of syn-sedimentary activity; iii) faulting is synchronous with quartz-calcite-pyrite mineralization similar to the hydrothermal activity broadly associated with intrusion of the Whin Sill complex (Frost and Holliday, 1980); iv) the structures pre-date geometrically and kinematically distinct sets of faults inferred to be Permian-Mesozoic (see below).

Late Carboniferous extensional movements dominate south of Alnwick and in a smaller region immediately N of Berwick (labelled 'extension-dominated domain' (EDD) in Fig 4.4. This domain is characterised by a simple bimodal pattern of E-W to ENE-WSW-trending conjugate normal faults with dip-slip kinematics (Fig. 4.5a), i.e. the classical Andersonian geometry.

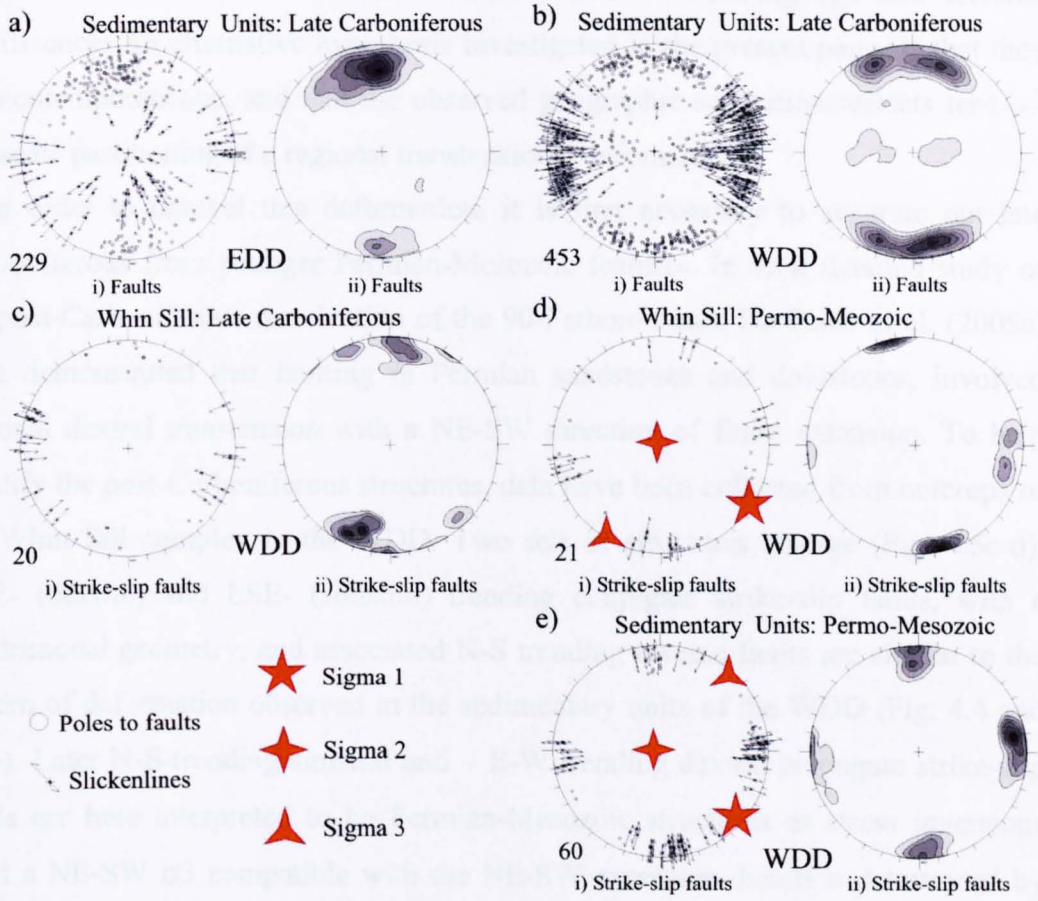

Figure 4.5. Summary equal-area stereoplots of structures measured within the Northumberland Basin. In each case, (i) shows poles to planes and slickenlines, while (ii) shows contoured plot of poles to planes. a) Late Carboniferous structures, EDD Carboniferous; b) late Carboniferous structures, WDD Carboniferous; c) late Carboniferous structures, WDD Whin Sill dolerites; d) Permian-Mesozoic strucutres, Whin Sill Dolerites, with stress axes; e) Permian-Mesozoic structures, Carboniferous country rocks, with stress axes.

A contrasting pattern of late Carboniferous deformation is seen in the region to the north of Alnwick, E of the Cheviot Hills along the coast to Berwick (labelled 'wrench-dominated domain' (WDD) in Fig. 4.4). Here, a more complicated pattern of deformation consistent with E-W shortening occurs, with the dominant structures being quadrimodal, conjugate strike-slip faults, with dextral and sinistral sets trending ENE and ESE, respectively (Fig. 4.5b).

The E-W shortening domain is located within the Carboniferous rocks that overlie the Cheviot block and its boundaries appear to broadly coincide with the locations of major ENE-WSW dykes related to the Whin Sill complex (Figs. 4.3b and 4.4). All previous workers have assumed that the distinct structural assemblages found in the EDD and WDD result from deformation events of differing age and tectonic significance. An alternative hypothesis investigated in the present paper is that they are contemporaneous, and that the observed geographic separation reflects tens-of-km-scale partitioning of a regional transtensional deformation.

In order to unravel this deformation, it is first necessary to separate out late Carboniferous from younger Permian-Mesozoic features. In their detailed study of the post-Carboniferous reactivation of the 90-Fathom Fault, De Paola et al. (2005a) have demonstrated that faulting in Permian sandstones and dolostones, involved regional dextral transtension with a NE-SW direction of finite extension. To help identify the post-Carboniferous structures, data have been collected from outcrops of the Whin Sill complex in the WDD. Two sets of structures emerge (Fig. 4.5c-d). ENE- (dextral) and ESE- (sinistral) trending conjugate strike-slip faults, with a quadrimodal geometry, and associated N-S trending reverse faults are similar to the pattern of deformation observed in the sedimentary units of the WDD (Fig. 4.4 and 4.5b). Later N-S-trending sinistral and ~ E-W trending dextral conjugate strike-slip faults are here interpreted to be Permian-Mesozoic structures as stress inversions yield a NE-SW $\sigma 3$ compatible with the NE-SW extension direction determined by De Paola et al. (2005a) (Fig. 4.5d). Geometrically and kinematically identical structures are found in the Carboniferous sedimentary rock exposures (Fig. 4.5e) where they consistently cross-cut or reactivate late Carboniferous fractures (e.g. N-S stylolites are often reopened as veins).

4.4 DETAILED KINEMATIC ANALYSIS OF LATE CARBONIFEROUS STRUCTURES

Detailed measurements of the geometries, kinematics and relative overprinting relationships have been made for late Carboniferous structures at a number of well-exposed localities across the Northumberland Basin (labelled SS1 to SS10 in Fig. 4.4). These localities exhibit the key structural relationships and were selected based on the detailed field descriptions given by Shiells (1964) and Bower (1990), together with additional regional reconnaissance work by the authors.

4.4.1 The extension-dominated domains (EDD)

Late Carboniferous extension-dominated domains occur in the region south of a line coincident with the High Green Echelon Dyke - Hauxley Fault (i.e. the Northumberland Trough of Kimbell et al., 1989) and in a smaller region immediately north of Berwick in the coastal outcrops of the east-central Tweed sub-basin. Here we present details of structural patterns typical of the southern and northern EDD (using SS1 and SS10, respectively, Fig. 4.4).

SS1: S. MARY'S LIGHTHOUSE-HARTLEY SECTION

This locality is located about 4 km north of the faulted southern margin of the basin, in coastal exposures near Hartley (Figs. 4.4 and 4.6a). The lithological units are the Coal Measures (Westphalian), comprising interbedded sandstones, silty-sandstones, shales and thin coal seams which provide useful markers to estimate the sense and magnitude of displacements.

The dominant structures are conjugate Andersonian normal faults on cm- to tens-of-metre-scales, with E-W to ENE-WSW trends, exhibiting dip-slip slickenlines and associated subvertical veins (Figs. 4.6a-h). The veins are mostly filled with calcite, but a conspicuous number show pyrite mineralisation (Fig. 4.6e). Pyrite mineralization also occurs on all the main fault planes shown on Figure 4.6a.

A narrow belt of dextral faults, with slightly oblique-extensional displacement, is present in one fault system west of St Mary's Lighthouse (Figs. 4.6a and h). These faults are steeply dipping, displaying small (cm-scale) extensional offsets of the sub-horizontal bedding. The trend of these structures is E-W to ENE-WSW, subparallel to the adjacent normal faults (Figs. 4.6a and h). These dextral strike-slip faults carry

syn-shearing calcite, hematite and pyrite mineralisation identical to that associated with the normal faults.

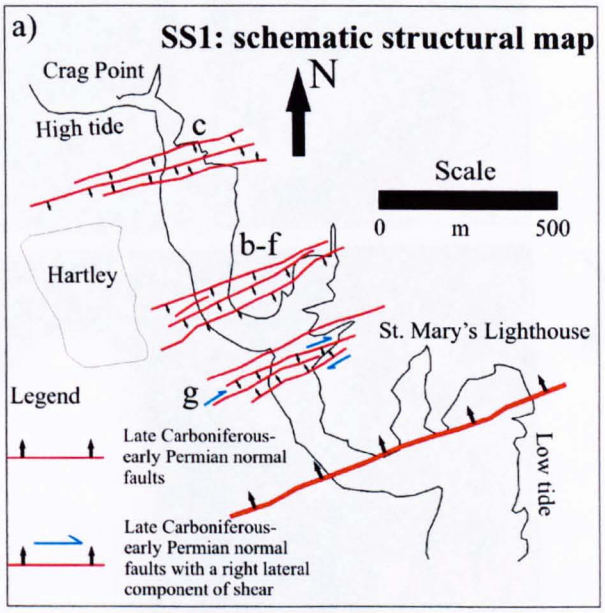

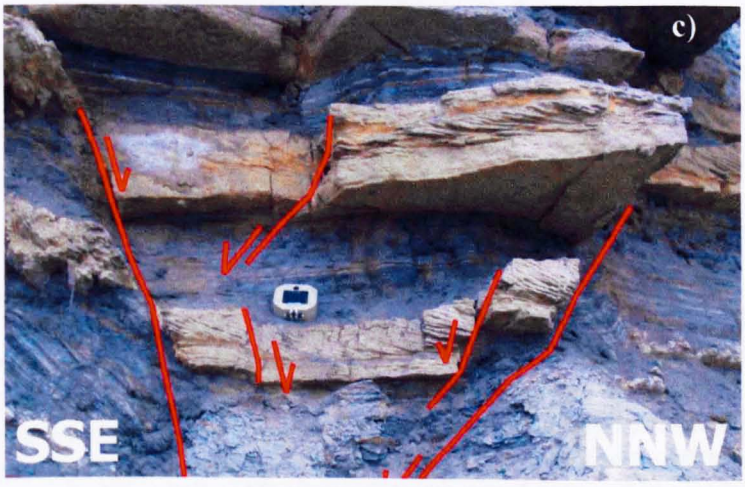

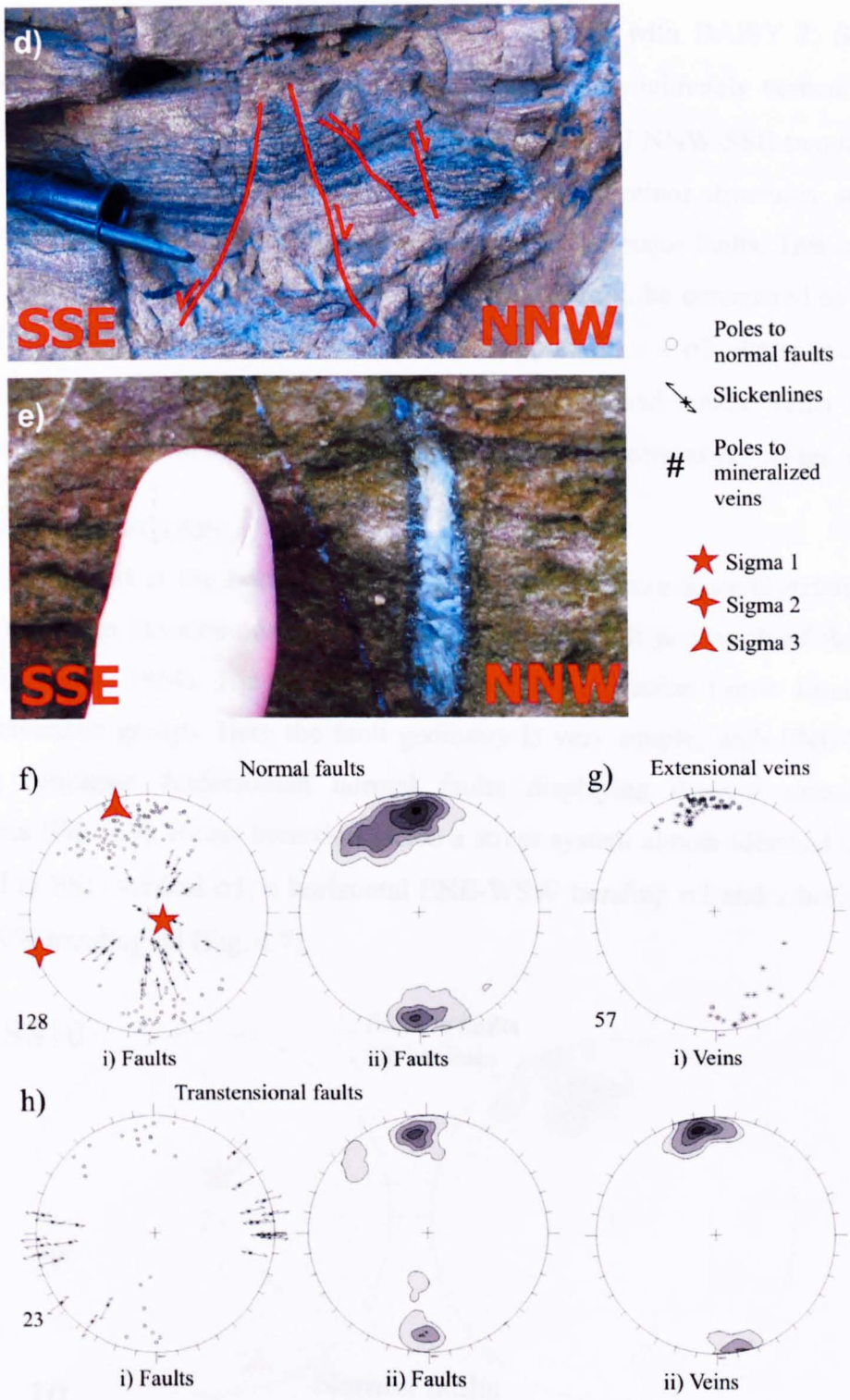

Figure 4.6: a) Schematic structural map of SS1 at St. Mary's Lighthouse – Hartley (for location see Fig. 4.4). b-c-d) Large- to meso-scale dip-slip normal faults at SS1 showing classic Andersonian conjugate geometry. e) Subvertical extensional vein, associated with normal faulting at SS1, with calcite-pyrite mineralization. f) Stereoplots of normal faults and associated slickenlines measured at SS1, with calculated stress axes. g) Stereoplots of tensile mineralised veins at SS1. h) Stereoplots of strike-slip-oblique extensional faults and associated slickenlines. All stereoplots are equal area and in similar format to those in Figure 4.5.

Stress inversion (using the inversion routine supplied with DAISY 2; Salvini, 2001), applied to the dip-slip normal faults, yields an approximately vertical σ1, a sub-horizontal ENE-WSW trending σ2, and a subhorizontal NNW-SSE trending σ3 (Fig. 4.6f). There is no evidence of substantial rotation of minor structures, such as veins or synthetic and antithetic shears associated with the major faults. This implies that the calculated stress axes can, to a first approximation, be considered as direct equivalents to infinitesimal strain axes, i.e. $z \equiv \sigma 1$, $y \equiv \sigma 2$, $x \equiv \sigma 3$. Stress inversion data are in good accord with the orientation of mineralised tensile veins for an Andersonian extensional system, i.e. σ3 corresponds to the poles to vein (Figs. 6f-g).

SS10: BERWICK SECTION

SS10 is located at the northern margin of the basin where a small extensional domain occurs in the area north of the Greens Haven Fault just north of Berwick (Fig. 4.4; Shiells, 1964). The lithological units are the Dinantian Lower Limestone and Scremertson groups. Here the fault geometry is very simple, with ENE-WSW trending conjugate Andersonian normal faults displaying dip-slip extensional kinematics (Fig. 4.7). Stress inversion yields a stress system almost identical to that observed at SS1: vertical σ1, a horizontal ENE-WSW trending σ2 and a horizontal SSE-WNW trending σ3 (Fig. 4.7).

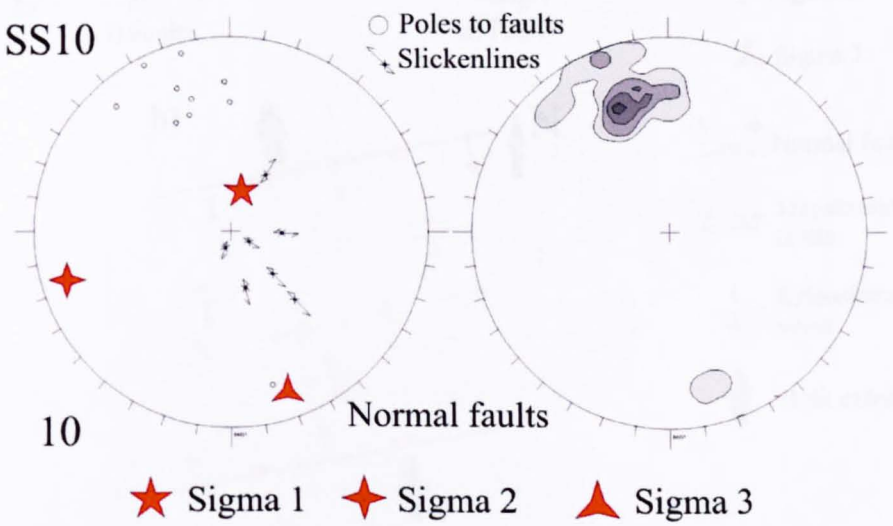

Figure 4.7. Stereoplots of normal faults, associated slickenlines and calculated stress axes at SS10 (for location see Fig. 4.4). Stereoplots are equal area and in similar format to those in Figure 4.5.

4.4.2 EDD: summary and structural model

The EDDs display a uniform and straightforward pattern of late Carboniferous deformation (Figs. 4.8a-b). The dominant structures are E-W to ENE-WSW trending normal faults arranged in conjugate Andersonian sets with dip-slip kinematics (Fig. 4.8a). Sub-vertical tensile veins have the same trend as the faults (Fig. 4.8b). Stress inversions suggest NNW-SSE extension ($\sigma 3$) and subvertical shortening ($\sigma 1$). Minor, subordinate sets of faults displaying wrench-transtensional kinematics occur locally, separate from, but parallel to the adjacent major normal faults within the EDD. If the faults cutting the Coal Measures strata reactivate pre-existing Dinantian structures at depth, the zones of wrench faulting could represent reactivated structures that preferentially accommodate residual wrench components following dip-slip extensional reactivation of the major faults in the section, cf. the model presented by De Paola et al. (2005a) for the Permian-Mesozoic faulting along the 90Fathom Fault.

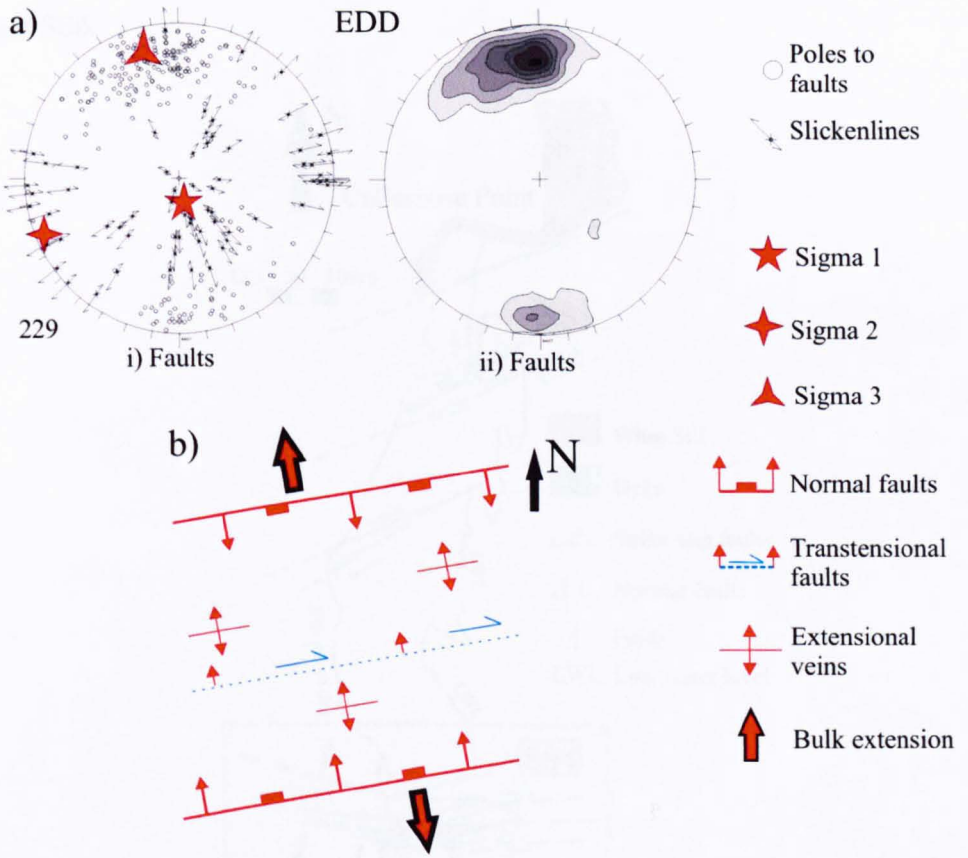

Figure 4.8: a) Stereoplots of all faults and associated slickenlines in the EDD, with calculated stress axes. All stereoplots are equal area and in similar format to those in Figure 4.5. b) Summary plan-view structural model for the extension dominated domains.

4.4.3 The wrench-dominated domain (WDD)

The dominant structures in the WDD are ENE-trending dextral and ESE-trending sinistral shear zones (Fig. 4.4). Two N-S- to NNE-SSW-trending regional-scale folds also occur, bounded to the west by east-dipping thrusts. Mesoscale dextral fault zones trending ENE-WSW define the regional shear zones across the WDD (Fig. 4.4) and are associated with a characteristic assemblage of minor structures comprising: a) ENE-trending dextral Riedel and ESE-trending sinistral anti-Riedel type faults; b) ~N-S trending folds and associated subparallel thrusts; c) en-echelon shear arrays; d) tension gashes; and e) stylolites. Detailed data from some key localities are now discussed.

SS4-SS5-SS6: THE HOWICK SECTION

The ~5 km long Howick section lies on the coast east of Howick northwards to Grey Mares Rocks (Figs. 4.4, 4.9-4.11) and includes three structural stations, SS4, SS5 and SS6.

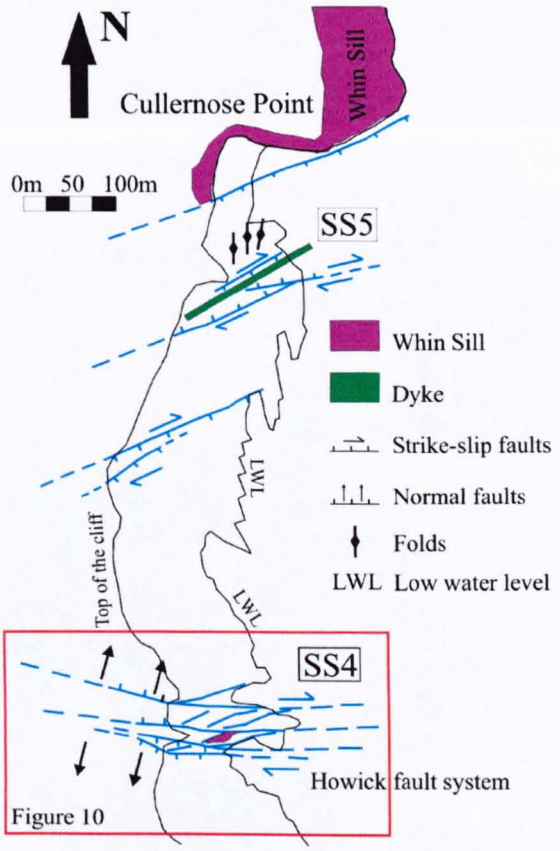

Figure 4.9. Simplified structural map of the Howick-Cullernose Point area (SS4-SS5, for location see Fig. 4.4). The box shows location of Figure 4.10.

The coastal exposure from Howick (SS4) to Cullernose Point (SS5) (Figs. 4.4 and 4.9) is particularly important as it illustrates the relative age relationships between Dinantian and late Carboniferous faulting and intrusion of the Whin Sill complex.Rocks belonging to the Middle Limestone Group (Visean) and Upper Limestone Group (Namurian) are juxtaposed by the south-dipping Howick normal fault (Fig. 4.4 and Fig. 4.9). The Howick fault system is well exposed on the cliff at SS4, where a series of ~ E-W trending Andersonian conjugate normal faults, displaying dip-slip slickenlines, are present (Figs. 4.10a and d).

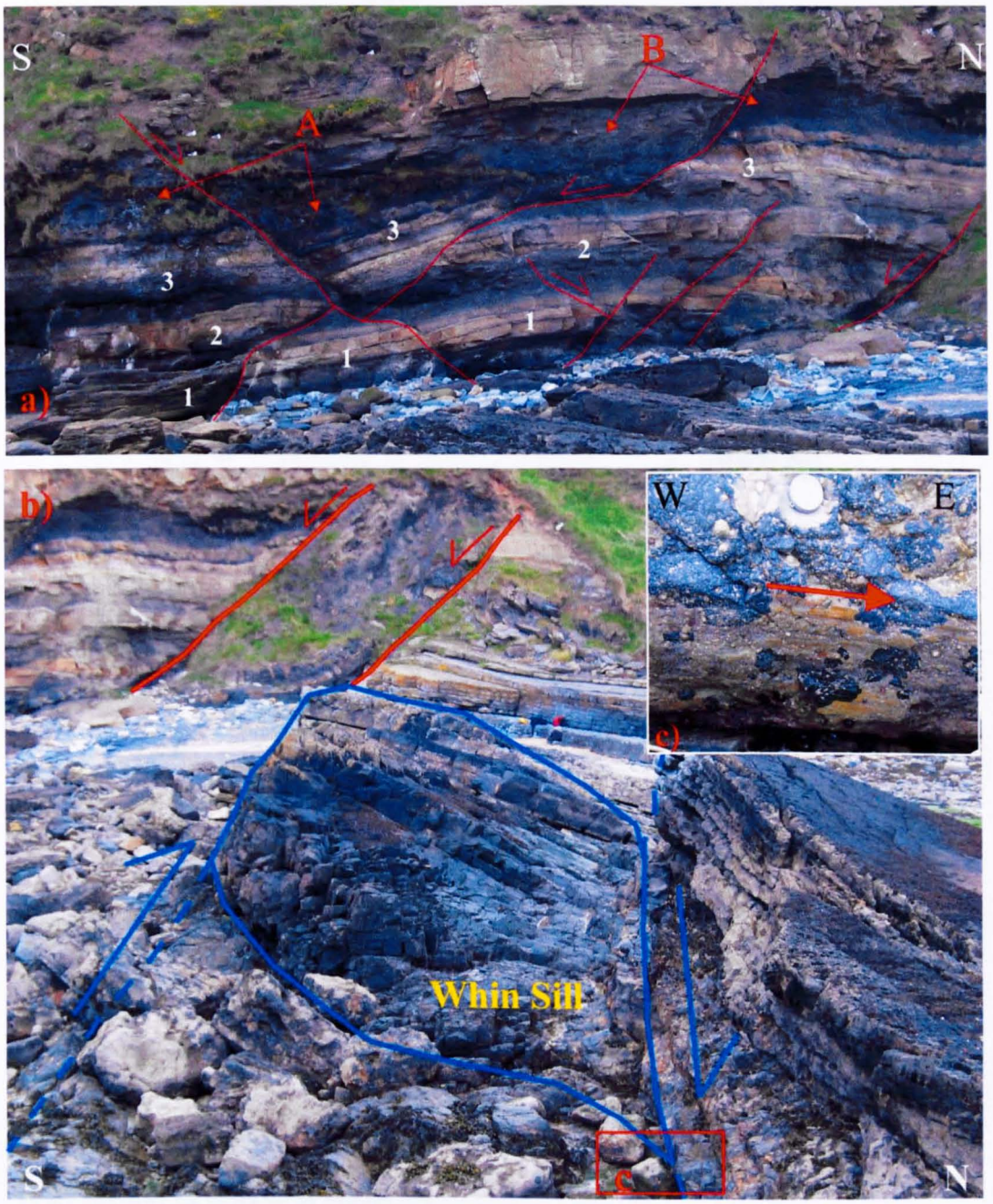

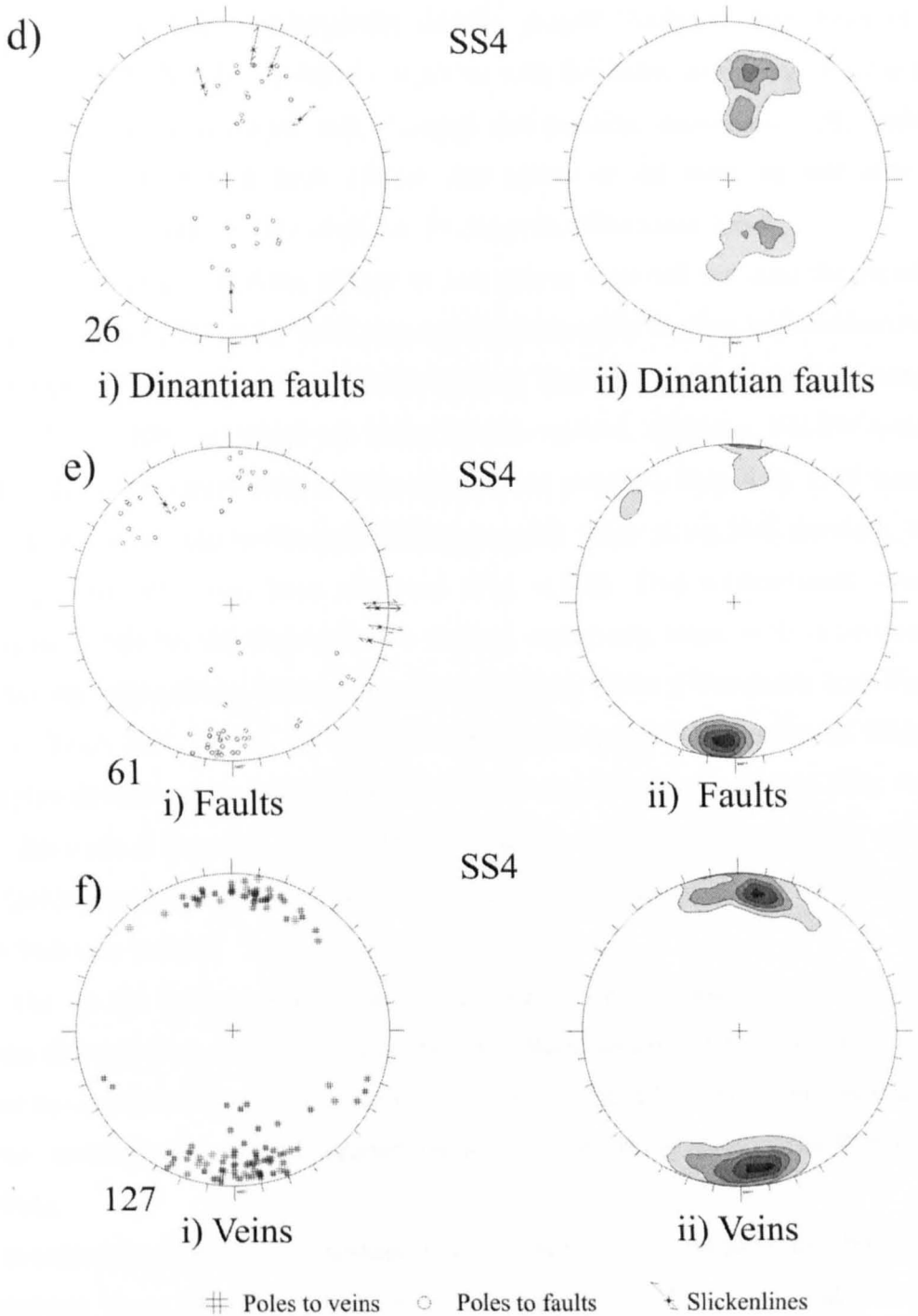

Figure 4.10: a) The Howick fault system (SS4, for location see Fig. 4.9) exposed on the cliff just east of the town of Howick. Syn-sedimentary (Dinantian/Namurian) normal faults displaying hangingwall thickening (points A-B), listric geometry and soft sediment deformation. b) Stereoplots of the syn-sedimentary normal faults. c) Whin Sill intrusion between two segments of strike-slip reactivated normal faults (in background cliff) as dextral strike-slip faults. d) Subhorizontal slickenlines observed on early Carboniferous (Dinantian/Namurian?) normal fault planes reactivated as strike slip faults during the Whin Sill intrusion (late Carboniferous-early Permian). e) Stereoplots of strike-slip faults. f) Stereoplots of tensile veins in Howick Fault duplex. All stereoplots are equal area and in similar format to those in Figure 4.5.

Locally, beds in fault hangingwalls display greater thickness than beds in the footwall (Fig. 4.10a). This evidence, together with the listric geometry of some fault planes and locally-observed soft-sediment deformation associated with faulting, suggest that the Howick fault system was active at the time, or just after the deposition of the sedimentary units, i.e. in Dinantian-Namurian times.

The geometries of faulting change as one moves eastward out onto the foreshore along the strike of the faults; fault planes are more steeply dipping with subhorizontal slickenlines (Figs. 4.10b and c). Dextral offsets occur along the main E-W trending faults (Figs. 4.10b-c-e) which are linked by sub-vertical, synthetic, NE-SW-trending dextral faults consistent with a strike-slip duplex structure (Fig. 4.9). E-W trending vertical veins and top-to-the-east bedding-parallel shear along N-S trending, west-dipping beds have also been observed (Fig. 4.10f). This contractional strain is consistent with the development of a dextral restraining bend, with extension and shortening respectively orthogonal and parallel to faults (Woodcock and Fischer, 1986; Walsh et al., 1999). An approximately bedding-parallel intrusion of Whin Sill complex dolerite up to 3m thick occurs within the Howick fault zone (Fig. 4.10b). The intrusion is bounded by two strike-slip faults, but is not brecciated or cross-cut by faulting suggesting that emplacement may be contemporaneous with the strike-slip fault movements.

The change in the geometry and kinematics of faulting observed along the strike of the Howick fault system suggests that the Dinantian synsedimentary normal faults have been reactivated as dextral strike-slip faults (Fig. 4.9). The latter event appears to be contemporaneous with emplacement of at least some parts of the Whin Sill ca 297Ma.

North of the Howick fault system, E-W to ENE-WSW dextral strike-slip faults are dominant (e.g. SS5-SS6, Figs. 4.4, 4.9 and 4.11). The mesoscale structures associated with these faults include: strike-slip faults, shear arrays and associated veins, parallel-bedding thrusts, folds and stylolites (Fig. 4.11a). The mesoscale strike-slip faults can be divided into four groups based on their orientation representing two conjugate sets with opposed dips (i.e. quadrimodal faults; Figs. 4.11a-b-c); faults trending E-W to ENE-WSW and E-W to ESE are dextral and sinistral, respectively. The angle between the two sets of conjugate faults is between

40° and 50°. All faults display shallowly-plunging slickenlines and horizontal offsets of bedding (Figs. 4.11b-c).

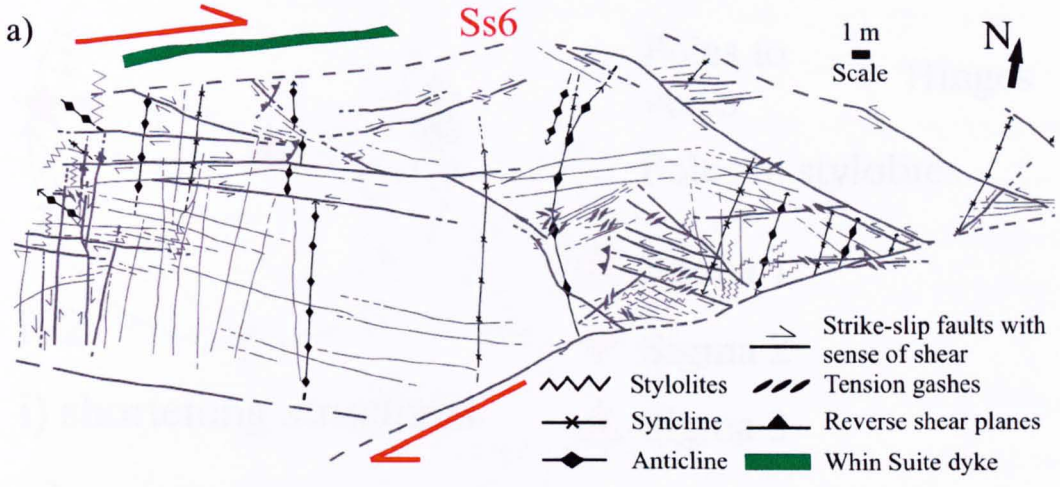

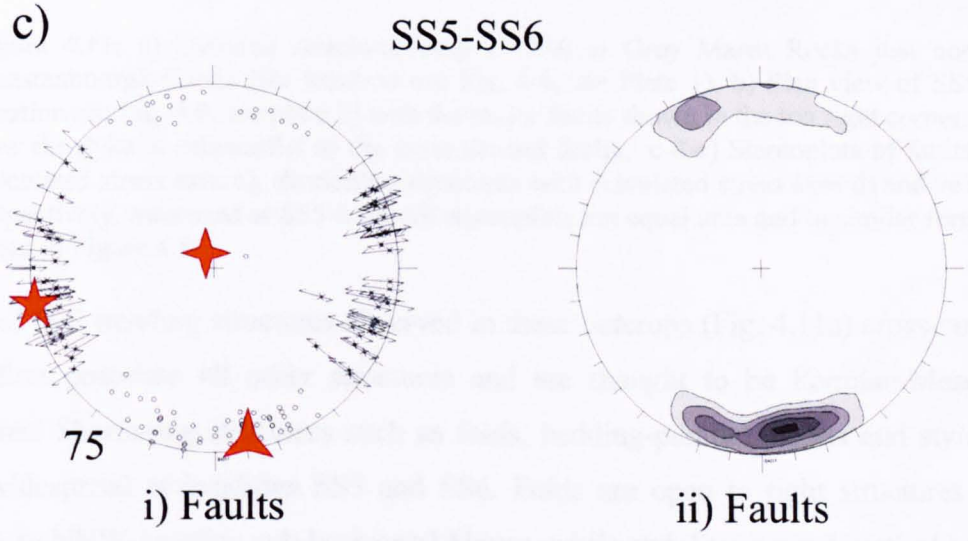

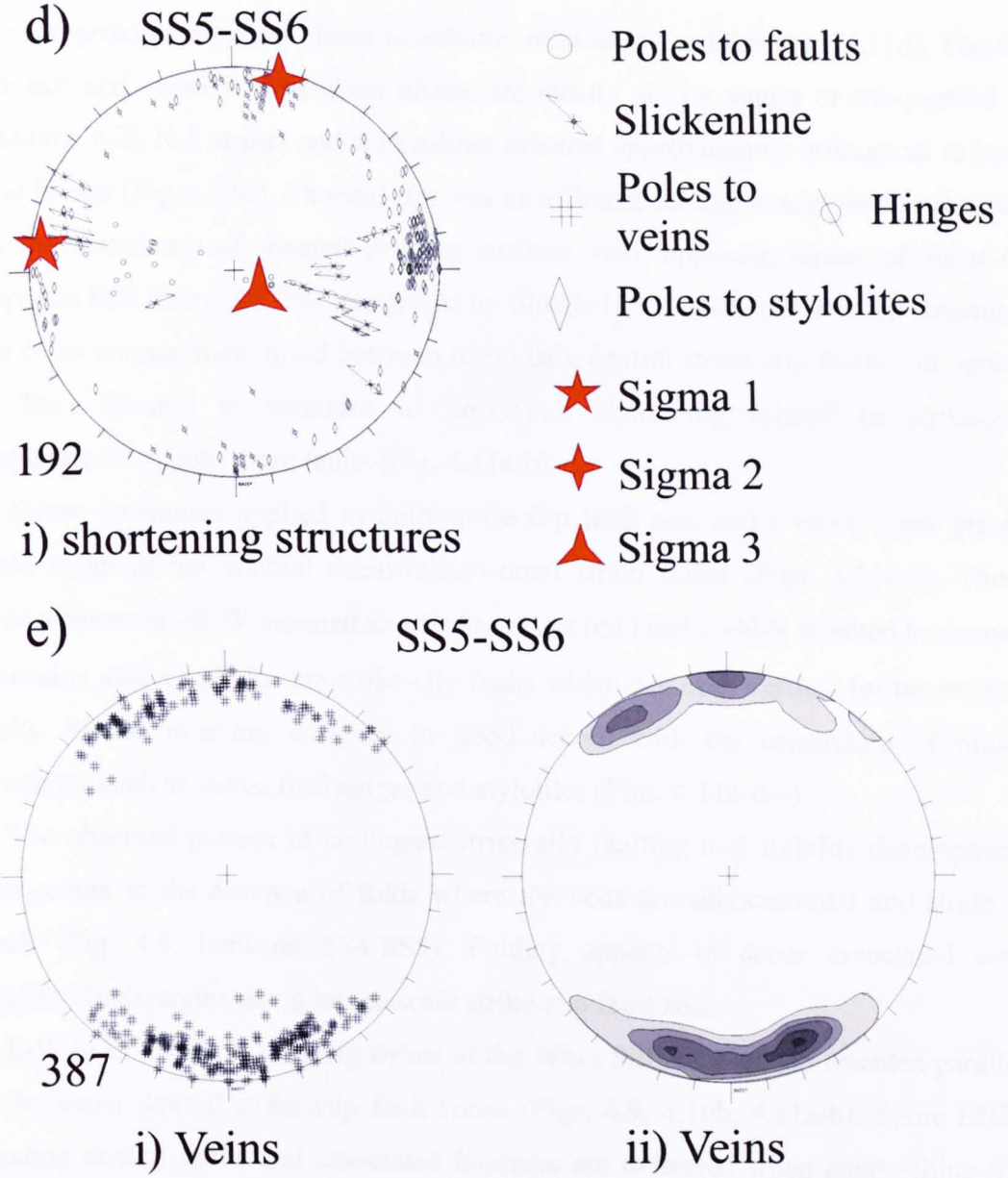

Figure 4.11: a) Detailed structural map of SS6 at Grey Mares Rocks just north of Dunstanbourgh Castle (for location see Fig. 4.4, see Plate 1). b) Plan view of SS5 (for location see Fig. 4.9, see plate 2) with the major faults shown in the top right corner. Note how the dyke is subparallel to the main dextral faults. c-d-e) Stereoplots of faults with calculated stress axes c), shortening structures with calculated stress axes d) and veins e), respectively, measured at SS5-SS6. All stereoplots are equal area and in similar format to those in Figure 4.5.

Sets of N-S trending structures observed in these outcrops (Fig. 4.11a) cross-cut and therefore post-date all other structures and are thought to be Permian-Mesozoic features. Shortening structures such as folds, bedding-parallel thrusts and stylolites are widespread at localities SS5 and SS6. Folds are open to tight structures with NNE- to NNW-trending sub-horizontal hinges, while stylolites are subvertical and lie

in an approximately axial planar orientation relative to the folds (Fig. 4.11d). Top-to-the-east and –west reverse shear planes are mostly at low angles or sub-parallel to bedding, with N-S strikes and slickenlines oriented approximately orthogonal to local fold hinges (Fig. 4.11d). Flexural slip was an efficient folding mechanism as testified by the abundance of sheared bedding surfaces with opposing senses of shear on opposite fold limbs. As first recognised by Shiells (1964), these shortening structures are often compartmentalised between mesoscale dextral strike-slip faults and appear to have formed in response to horizontal shortening related to strike-slip displacements along these faults (Fig. 4.11a-b).

Stress inversions applied to both strike-slip fault sets and reverse shear planes yield different but coaxial stress/infinitesimal strain fields (Figs. 4.11c-d). These have a common ~E-W oriented shortening axis z (σ1) and a ~N-S oriented horizontal extension axis x (σ3) for the strike-slip faults which becomes vertical for the reverse faults. Stress inversion data are in good accord with the orientation of minor structures such as veins, fold hinges and stylolites (Figs. 4.11c-d-e).

The observed pattern of conjugate strike-slip faulting and stylolite development also occurs in the absence of folds where the beds are subhorizontal and strain is small (Fig. 4.9, between SS4-SS5). Folding appears to occur associated with localised high strains along larger-scale strike-slip fault zones.

E-W to ENE-WSW trending dykes of the Whin Sill complex are oriented parallel to the major dextral strike-slip fault zones (Figs. 4.9, 4.10b, 4.11a-b). Some ENE-trending dextral faults and associated fractures are deflected when approaching the dyke (Figs. 4.9 and 4.11b, SS5), suggesting that the dyke had been already intruded at the time of faulting or that intrusion and faulting were synchronous. The intensity of brecciation and quartz-carbonate mineralization of the country rocks in the fault zones seems to correlate with the local thickness of the dykes. Once again, this may suggest a link between faulting and emplacement of the Whin Sill complex.

A characteristic association occurs between the strike-slip faults and tensile veins (Figs. 12a-b) which are typically arranged in en-echelon arrays adjacent to faults and fault tip zones. Most veins are tabular in shape, with sigmoidal forms rarely preserved (Figs. 4.12a-b). ENE and ESE sub-vertical vein orientations are dominant (Fig. 4.11e). The trends of individual veins and of each tension gash can be plotted

versus faults and shear-array trends on the x and y axes of a Cartesian diagram, respectively (Fig. 4.12c, McCoss, 1986; Kelly et al., 1998).

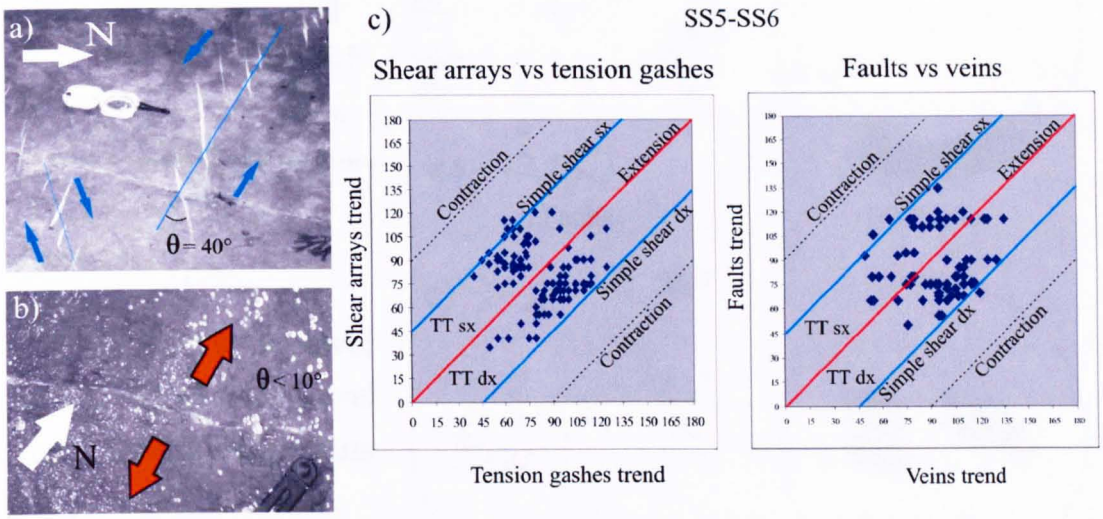

Figure 4.12. a) Shear arrays (thin dark line) and associated tension gashes (white veins) displaying dextral and sinistral senses of shear. Note the angle $\theta \approx 40°$ between the inferred arrays and the tension gashes. b) Extension array and associated tension gashes display ~ NNE extension with an angle $\theta < 10°$. c) Cartesian diagrams, displaying the fields of all tectonic regimes (McCoss, 1986), where shear arrays vs tension gashes trends and faults vs vein trends (Kelly et al., 1998), measured at SS5-SS6, are plotted. Note how most of the data plot in the transtensional strain field (i.e. $0° < \theta < 45°$), dextral (TTdx) and sinistral (TTsx), respectively.

The geometric relationship between the shear arrays and the associated tension gashes is expressed by the angle θ. This angle can be used to characterise the bulk strain field operating at the time when they formed (e.g. extension $\theta = 0°$, transtension $0° < \theta < 45°$, wrench simple shear $\theta = 45°$, transpression $45° < \theta < 90°$, shortening $\theta = 90°$). Tension gash arrays and veins associated with shear arrays and faults from SS5-SS6 (and other localities in the WDD), mostly cluster in the fields of transtensional strain with sinistral and dextral kinematics (Fig. 4.12c).

SS7: BEADNELL

The SS7 is located on the coast (Fig. 4.4) where the Middle Limestone Group (Visean) crops out close to the small town of Beadnell. The outcrop is characterised by a 5m thick, E-W trending vertical dyke, belonging to the Whin Sill complex and by conjugate strike-slip faults trending ENE (dextral) and ESE (sinistral) (Fig. 4.13a).

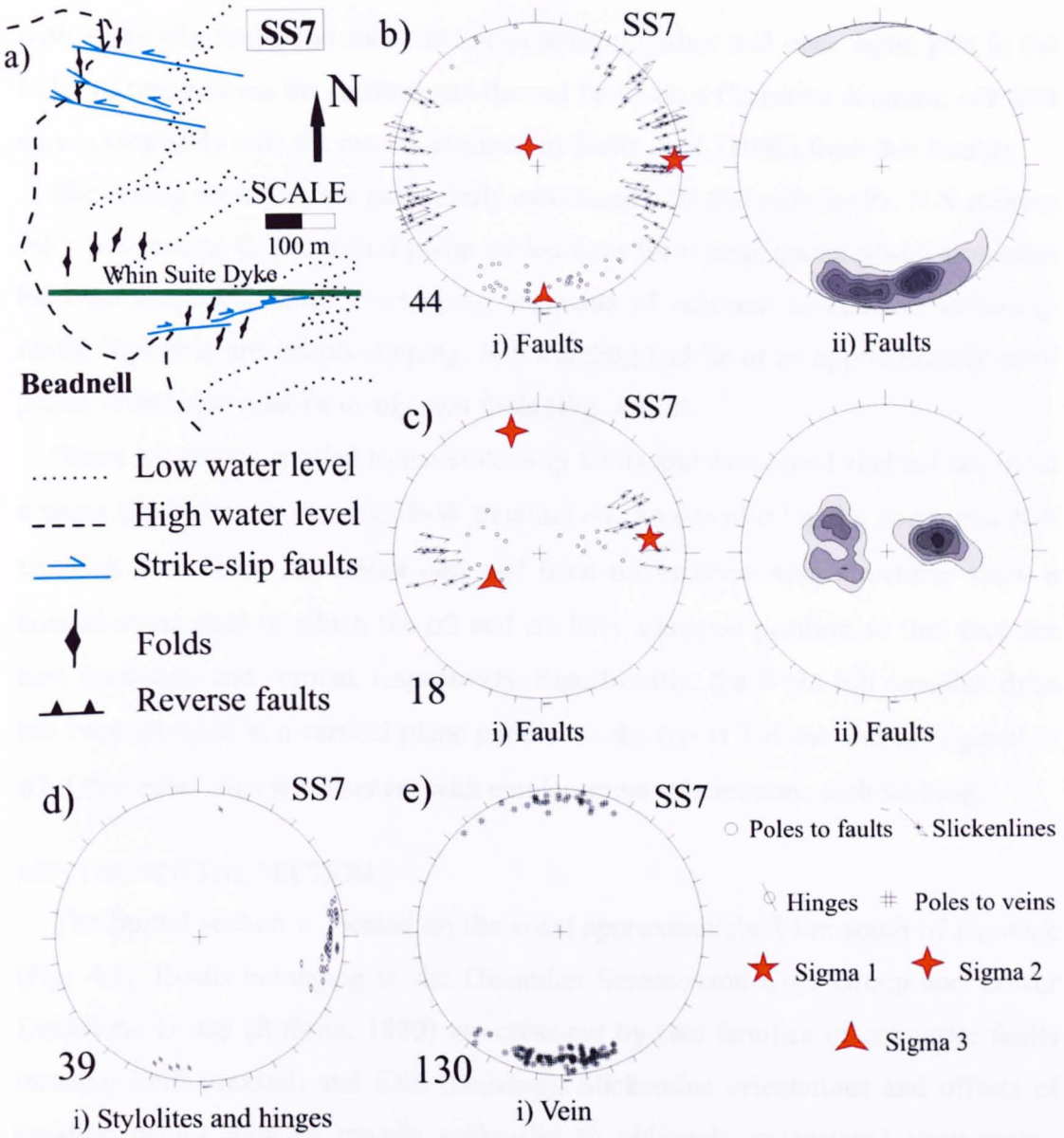

Figure 4.13: a) Schematic structural map of SS7 at Beadnell (for location see Fig. 4.4). b-c) Stereoplots of strike-slip faults with calculated stress axes (b) and reverse faults with calculated stress axes (c). d-e) Stereoplots of minor structures as stylolites and hinges (d) and veins (e) measured at SS7. All stereoplots are equal area and in similar format to those in Figure 4.5.

The deformation is heterogeneous and is localised within the country rocks adjacent to the dyke. The dominant structures are ENE-trending dextral strike-slip faults and ESE trending sinistral strike-slip faults, both with sub-horizontal slickenlines (Fig. 4.13b). Minor structures associated with the major fault zones include tensile veins and shortening structures such as reverse faults, folds and stylolites (Figs. 4.13c-e). The tensile veins are vertical, E-W trending and calcite-filled, with orientations similar to the dyke (Figs. 4.13a and e). They are associated

with strike-slip faults and shear arrays as tension gashes and once again plot in the fields of transtension for sinistral and dextral faults on a Cartesian diagram; our data agree completely with the results obtained by Kelly et al. (1998) from this locality.

Shortening structures are particularly associated with the main faults. N-S striking folds and reverse faults, with dip-slip slickenlines form conjugate push-up structures between compressionally overlapping segments of adjacent en-echelon strike-slip faults. Stylolites are steeply-dipping, N-S trending and lie in an approximately axial planar orientation relative to adjacent folds (Fig. 4.13d).

Stress inversions applied to the strike-slip faults and associated slickenlines yield a stress field with a horizontal, E-W trending $\sigma 1$, a vertical $\sigma 2$ and a horizontal N-S trending $\sigma 3$. Stress inversions obtained from minor shortening structures show a coaxial stress field in which the $\sigma 2$ and $\sigma 3$ have swapped position so that they are now horizontal and vertical, respectively. Significantly, the Whin Sill complex dyke has been intruded in a vertical plane parallel to the $\sigma 1$- σ 2 plane and orthogonal to $\sigma 3$. Once again, this is consistent with emplacement synchronous with faulting.

SS9: THE SPITTAL SECTION

The Spittal section is located on the coast approximately 2 km south of Berwick (Fig. 4.4). Rocks belonging to the Dinantian Scremerston Coal Group and Lower Limestone Group (Robson, 1980) are cross-cut by two families of conjugate faults trending ENE (dextral) and ESE (sinistral). Slickenline orientations and offsets of bedding planes indicate mainly strike-slip to obliquely extensional stratigraphic displacements (Figs. 4.14a-b-c).

Minor structures such as veins, folds and thrust faults are once again closely associated with the major strike-slip faults (Fig. 4.12c). Veins are less abundant compared to other sections, often occurring at the tips of fault as tension gash arrays; they are subvertical and NNE-trending (Fig. 4.14c). Folds are restricted mainly to the limestone beds with generally NNE-trending subhorizontal hinges. They are gently periclinal in form and are mainly open to tight disharmonic buckles (Figs. 4.14c-d). Top-to-the-east and top-to-the–west thrusts lie at low angles or subparallel to bedding planes, with dip-slip slickenlines oriented orthogonal to local fold hinges (see also Shiells, 1964). Stress inversion of the fault data sets yields a stress field

with a horizontal ~E-W trending σ1, a horizontal ~N-S trending σ3 and a vertical σ2 (Fig. 4.14c).

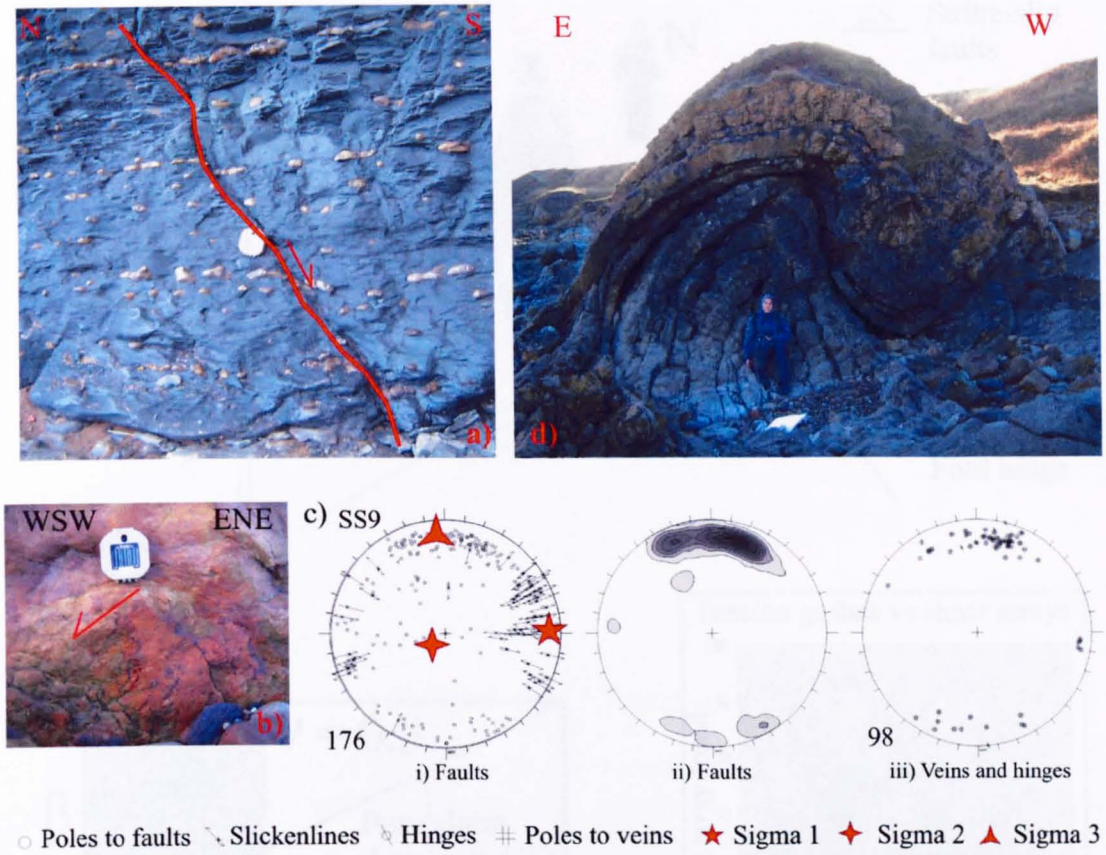

Figure 4.14: a) Oblique-slip extensional fault at SS9 (for location see Fig 4.4). b) Oblique shallow dipping sickenlines on slightly oblique extensional faults. c) Stereoplots of structures, faults and veins respectively, measured at SS9 with calculated stress axes. All stereoplots are equal area and in similar format to those in Figure 4.5. d) Spectacular folds displaying a western overturned limb at SS9.

4.4.4 WDD: structural model

The dominant structures are ENE-trending dextral faults, with a subordinate set of associated ESE-trending sinistral faults. The geometry and kinematics of associated small-scale structures are strictly related to the deformation accommodated along these major strike-slip faults (Figs. 4.15a-b). The stress-infinitesimal strain analyses carried out using the small-scale structures allow us to reconstruct the orientation of the bulk (infinitesimal) strain ellipsoid in the areas between the mesoscale faults (Figs. 4.15a-b). In all cases, we are able to assume that stress and infinitesimal strain axes are *approximately* parallel as finite strains are generally low (e.g. shortening

strains <5%, very locally rising to 25%); there is also little evidence to suggest that substantial fault block rotations have occurred.

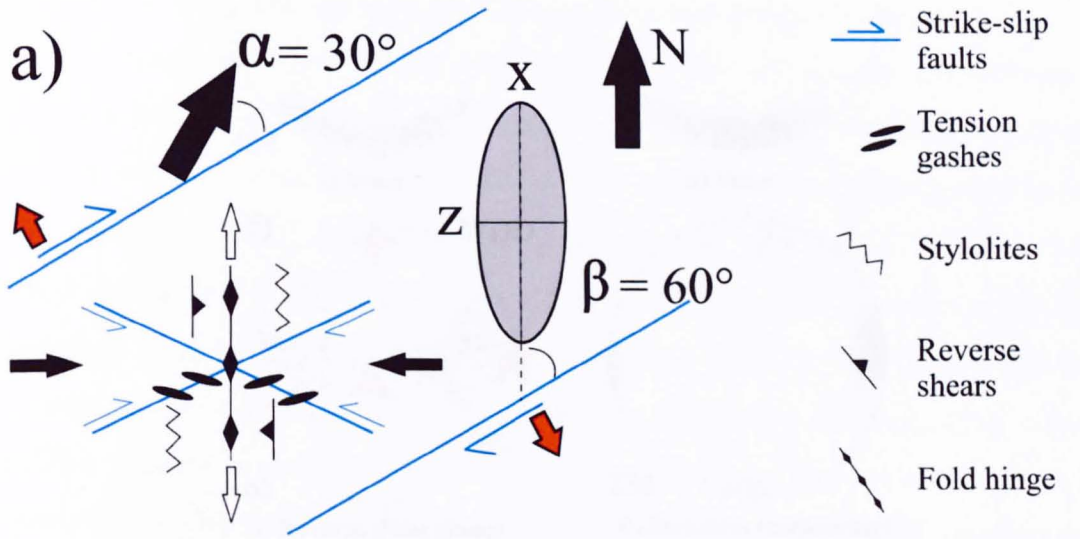

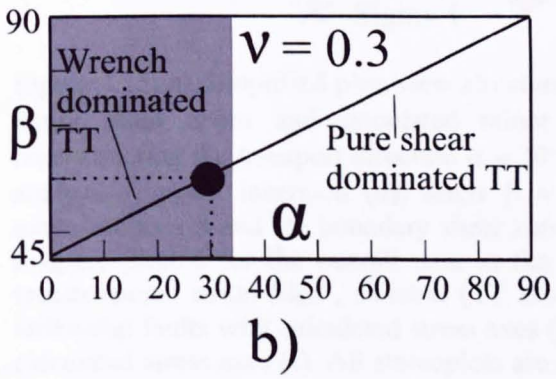

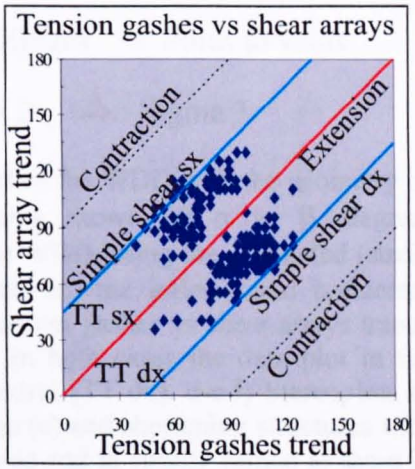

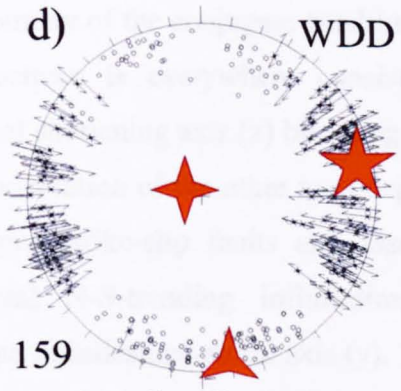

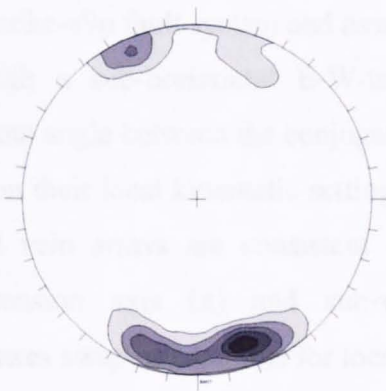

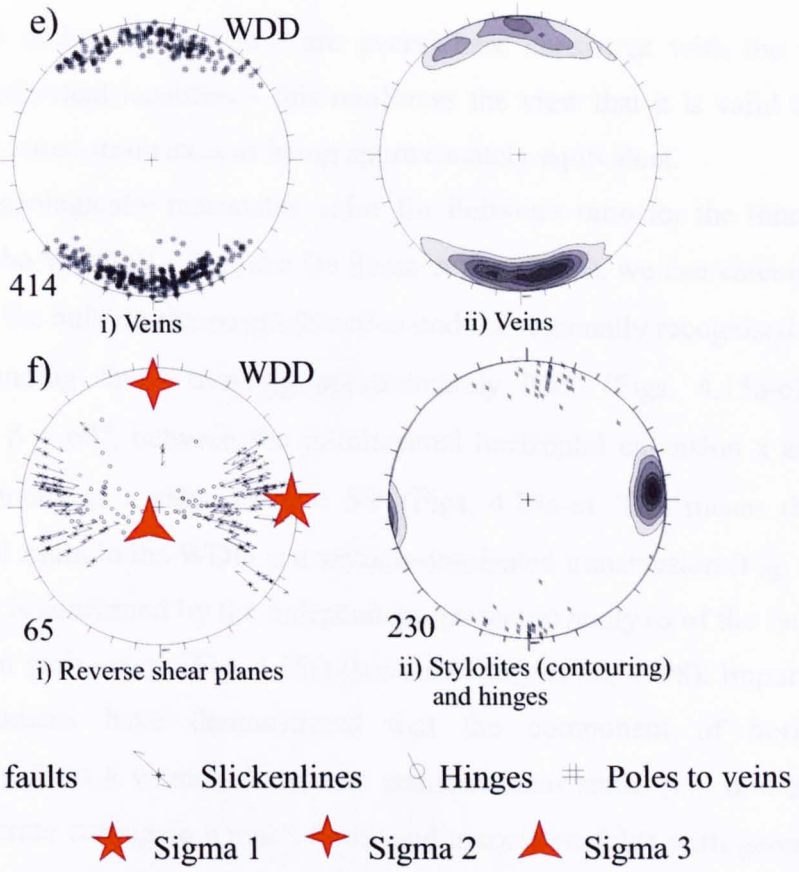

Figure 4.15: a) Simplified plan-view structural model of the WDD with the geometry of major shear zones and associated minor structures shown. b) α vs β diagram reconstructing the transport direction $\alpha \approx 30°$, for the WDD, using the calculated (strain analysis + stress inversion (d)) angle $\beta \approx 60°$ between the infinitesimal horizontal extension axis x and the boundary shear zone. c) Tension gashes vs shear arrays trends diagram plotted for the overall data in the WDD. In both cases the data plot in the transtensional strain filed , sinistral (TT sx) and dextral (TT dx). d-e-f) Stereoplots of strike-slip faults with calculated stress axes (d), veins (e) and shortening structures with calculated stress axes (f). All stereoplots are equal area and in similar format to those in Figure 4.5.

The geometry of the conjugate quadrimodal strike-slip fault system and associated minor structures is everywhere consistent with a sub-horizontal E-W-trending infinitesimal shortening axis (z) bisecting the acute angle between the conjugate fault sets. The orientation of the other axes depends on their local kinematic setting. Thus the conjugate strike-slip faults and associated vein arrays are consistent with a subhorizontal N-S-trending infinitesimal extension axis (x) and sub-vertical intermediate infinitesimal strain axis (y). These axes swap orientations for local folds and associated shortening structures. Stress inversions applied to fault and sickenline data sets yield stress fields consistent with the infinitesimal strain fields inferred from the geometry of the structures observed in the field (Figs. 4.15a-b-c-d). The results

obtained for the entire WDD region are everywhere consistent with the results obtained from individual localities – this reinforces the view that it is valid to treat stress and infinitesimal strain axes as being approximately equivalent.

Assuming a geologically reasonable value for Poisson's ratio for the lithologies cropping out in the WDD ($\nu = 0.3$; see De Paola et al., 2005a), we can calculate the angle α between the bulk displacement direction and the regionally recognised basin- and domain-bounding faults trending approximately 060° (Figs. 4.15a-e). The calculated angle $\beta = 60°$, between the infinitesimal horizontal extension x and the boundary zone, indicates a value for $\alpha \approx 30°$ (Figs. 4.15a-e). This means that the bulk infinitesimal strain in the WDD is a wrench-dominated transtension (Fig. 4.15a-e). This proposal is confirmed by the independent geometric analysis of the fault and associated tension gash arrays (Fig. 4.15f) (see also Kelly et al., 1998). Importantly, analogue experiments have demonstrated that the component of horizontal shortening arising from a wrench-dominated transtensional strain (i.e. $\alpha < 30°$) is sufficient to generate conjugate wrench faults and associated folds with geometries identical to those observed in the Northumberland Basin WDD (Withjack and Jamison, 1986; Ramani and Tikoff, 2002).

4.4.5 Summary & synthesis of strain data

The late Carboniferous deformation patterns of the EDD and WDD in the Northumberland Basin are significantly different. Reconstructions of palaeostress/infinitesimal strain axes suggest that both domains are associated with regional sub-horizontal extensional displacements, which are NNW- and NNE-directed in the EDD and WDD, respectively (Fig. 4.16). We can find no compelling evidence to suggest that the late Carboniferous structural assemblages are different ages and we therefore propose that the structures are contemporaneous and that they result from partitioning of a regional bulk strain. The mismatch in extension directions suggests an approximately N-S-trending, sub-horizontal regional bulk extension (Fig. 4.16).

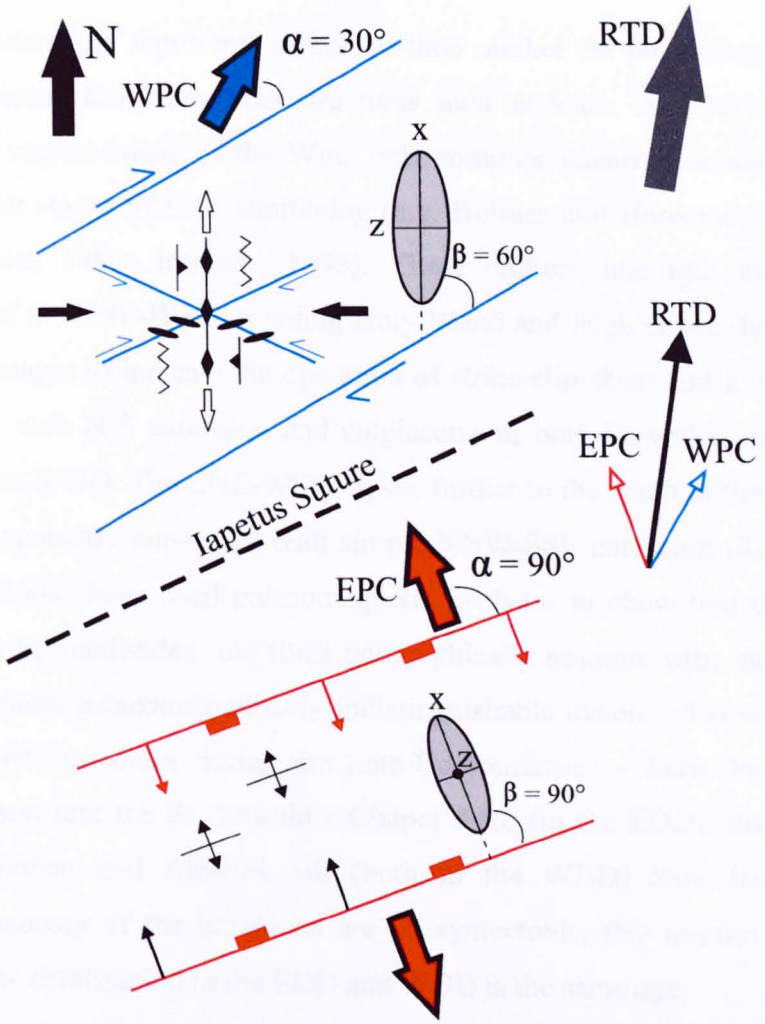

RTD = regional transport direction

EPC = extension partitioned component

WPC = wrench partitioned component

Figure 4.16: Structural plan-view model of Northumberland Basin during the late Carboniferous - early Permian deformation. It is proposed that the wrench (WPC) and extension (EPC) components of deformation in the EDD and WDD arise from partitioning of a NNE-directed regional transport direction (RTD). Strain partitioning occurred because the regional transport direction was at an oblique angle to pre-existing structures in the Laurentian Caledonian basement.

4.5 DISCUSSION

4.5.1 Relative age of structures: the emplacement of the Whin Sill complex

No clear examples of overprinting relationships between the late Carboniferous structures recognised in the EDD and WDD have been recognised in the Northumberland Basin. The timing of emplacement of the Whin Sill complex

intrusions potentially represents a relative time marker for the deformation events. Some intrusions clearly cross-cut structures such as folds, but many authors have argued that emplacement of the Whin Sill complex occurred contemporaneously with the latter stages of E-W shortening (e.g. Holmes and Harwood, 1928; Shiells, 1964; Robson, 1980; Johnson, 1995). These authors highlight the en-echelon geometries of the ENE-WSW-trending Holy Island and High Green dykes (Fig. 4.4) which are thought to indicate the operation of strike-slip shear and E-W shortening, synchronous with N-S extension and emplacement; both lie within or close to the margins of the WDD. The ENE-WSW dykes further to the south in the EDD show a more linear geometry consistent with simple NNW-SSE extension (Robson, 1980). Liss et al. (2004) have used palaeomagnetic analyses to show that the Whin Sill complex can be subdivided into three geographically separate sills, each associated with one or more palaeomagnetically indistinguishable dyke(s), that were emplaced at slightly different times during the Late Carboniferous – Early Permian. These authors suggest that the St. Oswald's Chapel dyke (in the EDD), the High Green Dyke en echelon and Alnwick sill (both in the WDD) have been emplaced contemporaneously. If the intrusions are all syntectonic, this implies that the late Carboniferous deformation in the EDD and WDD is the same age.

The regional patterns seem to be confirmed by outcrop-scale observations. Quartz-calcite-pyrite mineralisation broadly contemporaneous with Whin Sill complex emplacement is also synchronous with late Carboniferous fault movements in the EDD and WDD. Local intrusions such as the small lensoid sill in the Howick Fault zone (Fig. 4.10) appear to be bounded, but not cut by strike-slip fault movements and in some locations (e.g. SS7 Beadnell, Fig. 4.13), Whin Sill complex dykes trend E-W in the correct orientation relative to the local dextrally transtensional stress/strain field. Finally, the earlier set of quadrimodal conjugate ENE dextral and ESE sinistral strike slip faults cutting Whin Sill dolerites in the WDD is very similar to the late Carboniferous faulting patterns observed in the adjacent sedimentary units (compare Figs. 4.5b and c).

One puzzling association occurs repeatedly in many locations. Zones of N-S-trending minor folds and strike-slip faults are often localised in regions adjacent to dykes (e.g. Cullernose Point SS5 (Fig. 4.9), Grey Mares Rocks SS6 (Fig. 4.11), Beadnell SS7 (Fig. 4.13)). One possible explanation for this may be that the strike-

slip faults are unable to accommodate all of the imposed oblique extension, leading to strain partitioning with a residual component of (orthogonal) extensional strain developing in the wall rock regions immediately adjacent to active faults (Fig. 4.17a).

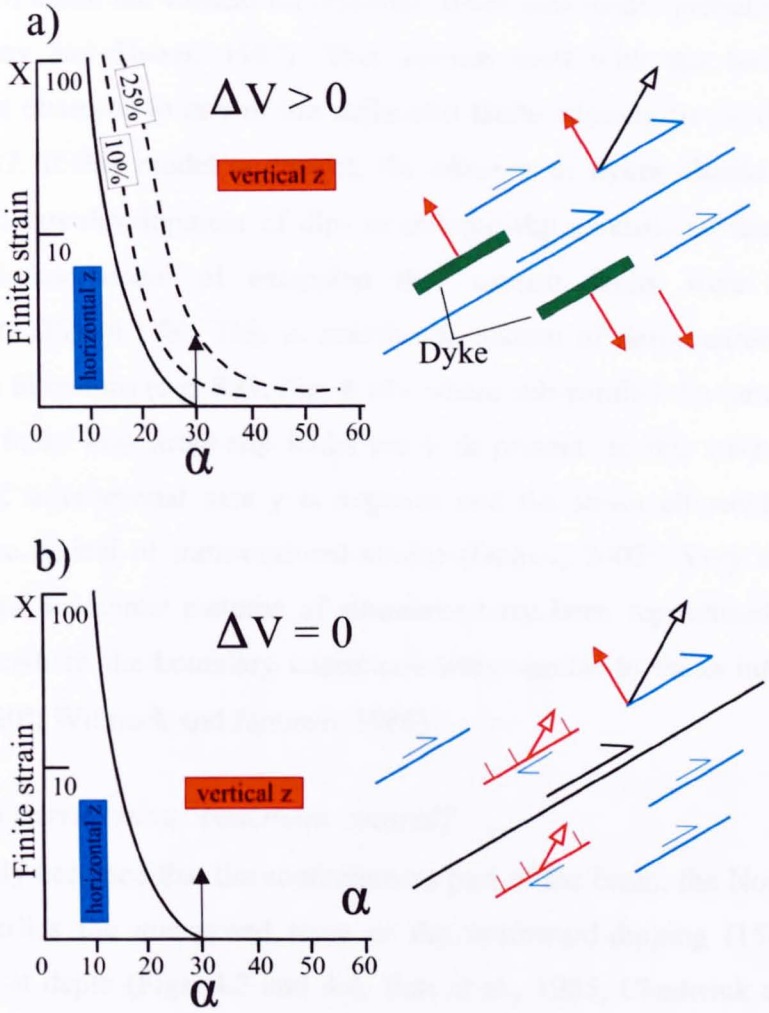

Figure 4.17: a) The fields of wrench-dominated transtension (horizontal z) and extension-dominated transtension (vertical z) plotted on a transport direction (α) vs finite horizontal extension strain axis (X) diagram. The dashed curves (from Teyssier and Tikoff, 1999) represent the effect of different amounts of volume increase during transtensional deformation. The sketch to the right shows the proposed structural model corresponding to the condition α = 30° plotted on the diagram (black arrow) when positive volume change is due to dyke/sill intrusion. b) Shows the same diagram as above, but plotted for a volume-constant transtensional deformation. The field of wrench-dominated transtension (horizontal z) is soon unstable with increasing amount of strain. The sketch to the right shows the plan-view structural model for the condition α = 30° plotted on the diagram (black arrow).

These regions would then conceivably be favoured sites for dyke emplacement. This in turn would lead to local volume increases which will lead to an expansion of

the field of the wrench-dominated transtensional strain, inhibiting the development of dip- or oblique-slip normal faults and potentially promoting a component of sub-horizontal E-W shortening, leading to the development of N-S folds, thrusts and stylolites (Fig. 4.17a). As dyke intrusion accommodates the orthogonal extensional component of strain the vertical infinitesimal strain axis would probably lie close to zero (Ramsey and Huber, 1987). This accords well with the lack of vertical displacement observed in any of the strike-slip faults adjacent to the dykes at SS4-SS5-SS6-SS7. If this model is correct, the *absence* of dykes should promote the contemporaneous development of dip- or oblique-slip extensional faults to relieve the residual component of extension that wrench faults were not able to accommodate (Fig. 4.17b). This is exactly the pattern of deformation observed at sites lacking intrusions (e.g. SS9, Fig. 4.14), where sub-parallel dip- and oblique-slip extensional faults and strike-slip faults are both present. In this case, the vertical, intermediate, infinitesimal axis y is negative and the strain ellipsoid will have a prolate shape typical of transtensional strains (Dewey, 2002). Very similar mixed geometric and kinematic patterns of structures have been reproduced in analogue experiments where the boundary conditions were similar to those inferred for the WDD ($\alpha < 30°$; Withjack and Jamison, 1986).

4.5.2 Strain partitioning: basement control?

It is widely accepted that the southernmost part of the basin, the Northumberland Trough, overlies the unexposed trace of the northward-dipping (15-25°) Iapetus Suture zone at depth (Figs. 4.3 and 4.4; Bott et al., 1985; Chadwick and Holliday, 1991). Despite some debate concerning exactly where the suture projects to the base of the post-Caledonian cover (e.g. see Soper et al., 1992), there is common agreement that the acoustically blank sequence observed in deep seismic reflection profiles within the basement overlying the suture corresponds to the southernmost part of the Southern Uplands accretionary prism (Bott et al., 1985; Beamish and Smythe, 1986). This means that most of the Northumberland Basin overlies Laurentian crust.

Chadwick and Holliday (1991) have suggested that the Dinantian bounding faults of both the Northumberland Trough and possibly the Tweed sub-basin may have reactivated northerly-dipping Caledonian thrust zones at depth, some of which link

into the Iapetus suture. A similar Caledonian basement control may have influenced the late Carboniferous deformation patterns. The ENE-WSW trend of the EDD-WDD boundaries, the dominant dextral strike-slip faults in the WDD and the trend of the Whin Sill complex dykes (Figs. 4.4, 4.9, 4.11a-b, 4.13a) all correspond well with the trends of basement structures exposed in nearby regions of the Southern Uplands. The latter rocks experienced significant amounts of orogen-parallel sinistral shear from the Late Llandovery to the Devonian and carry a very well-defined, moderately- to steeply-dipping ENE-WSW-trending fabric (e.g. see Holdsworth et al., 2002a & b). Reactivation of such a basement anisotropy during N-S or NE-SW extension would result in dextral transtensional bulk strains (Figs. 4.15-4.16).

The role of basement in controlling the *location* of the EDD and WDD is less clear. The WDD and trend of the associated en echelon dykes close to its northern and southern boundaries is clearly coincident with the position of the Cheviot Block (Fig. 4.4). The existence of this region as a relatively uplifted region during Dinantian rifting is likely to have been determined by the presence of the relatively buoyant Devonian Cheviot Granite at depth, a feature common to many of the uplifted horsts in the Carboniferous basins of Northern Britain (e.g. Leeder, 1982), including the Alston block immediately S of the Stublick-Ninety Fathom fault system (Fig. 4.3b). The partitioning of strike-slip deformation into the Carboniferous rocks overlying the Cheviot block may occur because the total thickness of basin fill is significantly reduced, making this region more susceptible to basement influence. More speculatively, it may be that the emplacement of the Cheviot granite – perhaps in a late Caledonian pull-apart – has in some way made the basement fabric in this basement block more prone to strike-slip reactivation.

4.5.3 Inversion vs strain partitioning in the Northumberland Basin

The most commonly accepted interpretation of the tectonic evolution of the Northumberland Basin involves the initiation of an extensional basin in the Dinantian, with a subsequent phase of late Carboniferous inversion followed very closely by a phase of extension continuing into the early Permian. The latter event is generally considered synchronous with intrusion of the Whin Sill complex (e.g. Leeder et al., 1989; Collier, 1989), although others suggest that intrusion may have overlapped the inversion event (e.g. Shiells, 1964, Robson, 1980, Johnson, 1995).

The late Carboniferous inversion is related, by almost all authors, to the far-field effects of the Variscan orogenic event in Southern Britain. The anomalous E-W orientation of shortening is generally attributed to the strike-slip jostling or lateral extrusion of basement-controlled fault bounded blocks in the Variscan foreland (e.g. Bower, 1990).

Our observations from the Northumberland Basin suggest an alternative and, from a regional late Carboniferous-early Permian tectonic viewpoint, much more straightforward interpretation. We propose that there was a single phase of prolonged (ca 15Ma) phase of dextral oblique extension in this part of Northern Britain (Fig 4.16). The differing and heterogeneous character of deformation observed across the basin results from a possibly basement-controlled partitioning of the regional transtension into geographically distinct domains of extension- and dextrally wrench-dominated strain. These contemporaneous strain fields can be integrated to give a bulk regional transport direction oriented about N-S, oblique to pre-existing NE-SW trending structures in the Laurentian basement underlying the Northumberland Basin (Fig. 4.16). The proposed tectonic setting fits well with the development of the tholeiitic Whin Sill complex during (oblique) lithospheric stretching, the effects of which are recognised all across NW Europe at this time (Neumann, 1994; Sundvoll and Larsen, 1994; Smythe et al., 1995; Ernst and Buchan, 1997, 2001; Timmerman, 2004). In the absence of any evidence for NNW-SSE shortening, our model also means that there is no need to invoke Variscan inversion in the Northumberland Basin, although it is very likely that the events described here were contemporaneous with orogenesis further to the south.

4.5.4 Implications for the Carboniferous of Northern Britain

The dextral transtensional structures of the Northumberland Basin – and particularly those of the WDD – are very similar in terms of their orientation and scale to those that occur widely in the Carboniferous and older rocks of the Midland Valley where a long history of dextral shearing is well known (e.g. Read, 1988; Read et al., 2003). The widespread development of conjugate strike-slip fault arrays that compartmentalise generally N-S-trending folds and thrusts and the synchronous occurrence of tholeiitic magmatism in both regions is particularly striking. The dominance of dextral strike-slip displacements along faults with a distinctly

Caledonian trend suggests that these basins are tectonically distinct from the other Carboniferous basins of Northern England, a feature almost certainly linked to the fact that they overlie Laurentian, as opposed to Avalonian, basement. On a broader scale, our findings have important implications for regional models of basin development and inversion, and how these events may be related to plate tectonic processes in Carboniferous-Permian times. The recent synthesis of Maynard et al. (1997) illustrates that tectonic models for this time period in Britain and NW Europe are becoming increasingly complex due to three inter-related factors:

1) the importance of basement fault reactivation in controlling local tectonic patterns and evolution (e.g. Corfield et al., 1996; Woodcock and Rickards, 2003);
2) the increasing recognition of the important role played by local and regional-scale strike-slip tectonics, partly – but not exclusively – due to reactivation of basement faults oriented obliquely to the regional plate tectonic vectors (e.g. Coward, 1990; Waters et al., 1994);
3) the recognition of numerous, often localised 'uplift events' and unconformities within the intra-Carboniferous sedimentary record (e.g. Maynard et al., 1997).

In all these models, *an explicit link is made between inversion/uplift events and compressional or transpressional tectonic episodes*. This inevitably leads to more complex regional tectonic models. Our model of strain partitioning during a single and possibly protracted phase of regional transtension removes this unnecessary and unrealistic link between tectonic complexity on local and regional scales, whilst still emphasising the important role of basement control on deformation patterns. It allows local 'inversion' events to occur while a region experiences extension on a lithospheric scale, which can lead to widespread synchronous tholeiitic magmatism as a result.

Our findings strongly suggest that existing models of late-Carboniferous-Permian inversion tectonics in the Variscan foreland of Northern Britain need to be reassessed, particularly in areas where the inferred shortening directions do not correspond well with the NNW-SSE orientation generally associated with Variscan collision (e.g. the Pennine Basin, for example; Waters et al., 1994).

4.5.5 Global implications of the present study

The recognition that strain partitioning leads to local structural complexity that is not necessarily of regional (e.g. plate-scale) significance is a recent theme that has received considerable attention in transpressional settings (e.g. Dewey et al., 1998; Holdsworth et al., 2002a; Jones et al., 2004; Clegg and Holdsworth, 2004). The equivalent importance of strain partitioning in transtension zones has received much less attention. Recent studies of tectonically active transtensional regimes have revealed the presence of structural domains characterised by different kinematic patterns and associated seismicity (e.g. Oldow, 2003). The domainal deformation patterns can be attributed directly to the obliquity between horizontal displacements measured using GPS velocity fields and pre-existing block-bounding faults in the crust. Oldow (2003) has demonstrated that the angular relationship between incremental horizontal strain axes and horizontal displacement deviates from the typical geometry of plane strain deformation in a way that would be expected during transtensional deformation (Figs. 4.2a, c and d, see also McCoss, 1984; Teyssier et al., 1995; Dewey et al., 1998; Dewey, 2002). In ancient terrains, the far-field regional transport direction is generally unknown, but our study of the Northumberland Basin demonstrates that it can be reconstructed from the partitioned components of strain recognised within contemporaneously active, kinematically-different and spatially distinct structural domains (e.g. Fig 4.16). These components can be calculated using the predictable geometric and kinematic relationships that exist between the orientations of the infinitesimal strain (stress) axes and the boundaries of the system in transpressional and transtensional systems (McCoss, 1984).

We suggest therefore that if the overall geometry, kinematics and spatial distribution of the structural domains in a basin display heterogeneous structural patterns and infinitesimal strain/stress inversions consistent with partitioned 3-D strain, then it is possible that the deformation was contemporaneous on a regional scale. Conversely tectonic events that are unrelated, and that occur at different times are much less likely to show consistent geometric and kinematic patterns. Our study illustrates that we cannot always reliably assume that infinitesimal strain or stress axes resolved in one part of a study area are parallel to regional transport directions, unless their relationship to the deformation patterns in adjacent crustal domains is

also considered. This can lead to misunderstandings concerning the regional meaning of the bulk strain and nature of the tectonic regime (Tikoff and Wojtal, 1999). Hence, the scale of observation is crucially important during crustal deformation.

Pulsed extension-inversion-extension models are commonly invoked for many basins of different ages in onshore and offshore environments from all around the world in extensional and strike-slip settings. Phases of compression or transpression are typically related in some way either to the far-field effects of some distant orogenic event of similar age or to geometric features of strike-slip faults (bends, offsets, etc) leading to local inversions. We suggest that these models need careful reappraisal to see whether strain partitioning into extension- and wrench-dominated transtensional deformation domains may provide an improved and more elegant explanation for the observed structural complexities. This may eventually help to simplify our increasing complex plate-tectonic models in ancient environments and lead to an improved understanding of basin dynamics that is central to hydrocarbon and other economic exploration activities in obliquely tectonic regimes.

5. THE PARTITIONING OF DEFORMATION AND FAULTING PATTERNS IN TRANSTENSIONAL PLATE MARGINS: IMPLICATIONS FROM THE ACTIVE DEAD SEA MARGIN

ABSTRACT

Most of active and ancient plate margins are studied and interpreted in terms of plane strain deformations. 2-D strain models rely on some key assumptions as: a) slip-vectors are parallel to plate motion vectors, b) major structures are the result of imposed regional stress. These two postulates may be correct for plane strain deformations, but they are not necessarily true in the case of 3-D strain.

Oblique extension leads to 3-D transtensional strain and is characterised by different styles of faulting compared to orthogonal rifting associated with plane strain deformation. Homogeneous transtension is rare in natural systems because pre-existing structures lying at an oblique angle to the opening vector often undergo reactivation leading to strain partitioning and the development of domainal strain patterns with complex heterogeneous fracture patterns.

A case of strain partitioning in an oblique margin is studied and discussed from the present-day active Dead Sea Transform (DST), NE Africa. The choice of an active area means that earthquakes focal mechanisms can be used to infer stress/strain fields in 3-D strain analysis. There is no ambiguity concerning the timing of deformation since these strains are –geologically speaking – contemporaneous.

3-D strain analysis suggests a slightly sinistral oblique (α = 5° - 10°) regional plate motions. A transtensional model is proposed for the DST based on the integration of geodetic, geological and a new analysis of seismological datasets. The only independent parameter, not affected by local geometry of the system, is the plate motion vector.

5.1 INTRODUCTION

For many years, most structural, tectonic and geodynamic models of extending zones have been implicitly or explicitly 2-D. This likely reflects the enduring influence of classical 2-D Andersonian faulting theory, with the additional convenience of being able to describe or analyse plane strain deformations using mathematically simple 2-D models and cross-sectional or plan view constructions. This approach is likely to be inadequate, however, where obliquely divergent or convergent plate motions give rise to 3-D transtensional or transpressional strains, respectively (Dewey, 1970; Woodcock, 1986; Tikoff and Teyssier, 1994; Teyssier et al., 1995; Dewey et al., 1998; Oldow, 2003).

The main consequences of transtensional and transpressional deformations are that complex relationships occur between the infinitesimal strain field (i.e. stress),

the observed finite strain and causative regional displacement (i.e. plate motion vector) (Sanderson and Marchini, 1984; Fossen and Tikoff, 1993; Dewey et al., 1998). Theoretical, analogue modelling and field-based studies of transtension (and transpression) zones have repeatedly demonstrated that the axes of infinitesimal strain (stress) are generally not coincident with far-field displacement vectors (e.g. see Withjack and Jamison, 1986; Tikoff and Wojtal, 1999; Ramani and Tikoff, 2002; Teyssier et al., 1995; Dewey, 2002; Oldow, 2003; Jones et al., 2004). The mismatch between the local infinitesimal strain/stress fields and the regional displacement is enhanced if the regional strain undergoes partitioning. In such circumstances, the regional displacement is split into secondary components of deformation depending on local boundary conditions (e.g. reactivation of pre-existing features lying at oblique angles to regional movements) and in general none of these secondary strain directions are parallel to the regional displacement. This has profound implications when 2-D strain/stress analysis is inappropriately applied to 3-D deformations.

The distribution of seismicity and the direct measurement of velocity fields reduces the uncertainty about the timing of deformation and orientation of the regional displacement in tectonically active areas. Nevertheless, most models of obliquely divergent boundaries rely on 2-D strain/stress analyses and often assume a parallelism between earthquakes slip vectors and plate motions. Plate boundary models based on geodetic measurements often only allow movement parallel or orthogonal to the boundary. These assumptions are inappropriate for 3-D deformations and they may lead to over-simplified models of a real geological system.

In order to test the potential and applicability of 3-D partitioned transtensional models to plate scale deformations, we choose to study the present-day seismically active Dead Sea Transform, NE Africa. Here there is evidence for regional transtension undergoing partitioning into kinematically distinct domains of contemporaneous deformation, but a comprehensive transtensional model has not yet been formulated.

5.2 3-D TRANSTENSIONAL INFINITESIMAL STRAIN AND STYLE OF FAULTING

5.2.1 Homogeneous Transtension

Homogeneous transtension can be modelled as the simultaneous and combined action of a wrench simple shear and pure shear extension resulting from an obliquely oriented divergent displacement relative to the deformation zone boundaries (Fig. 5.1a) (Sanderson and Marchini, 1984).

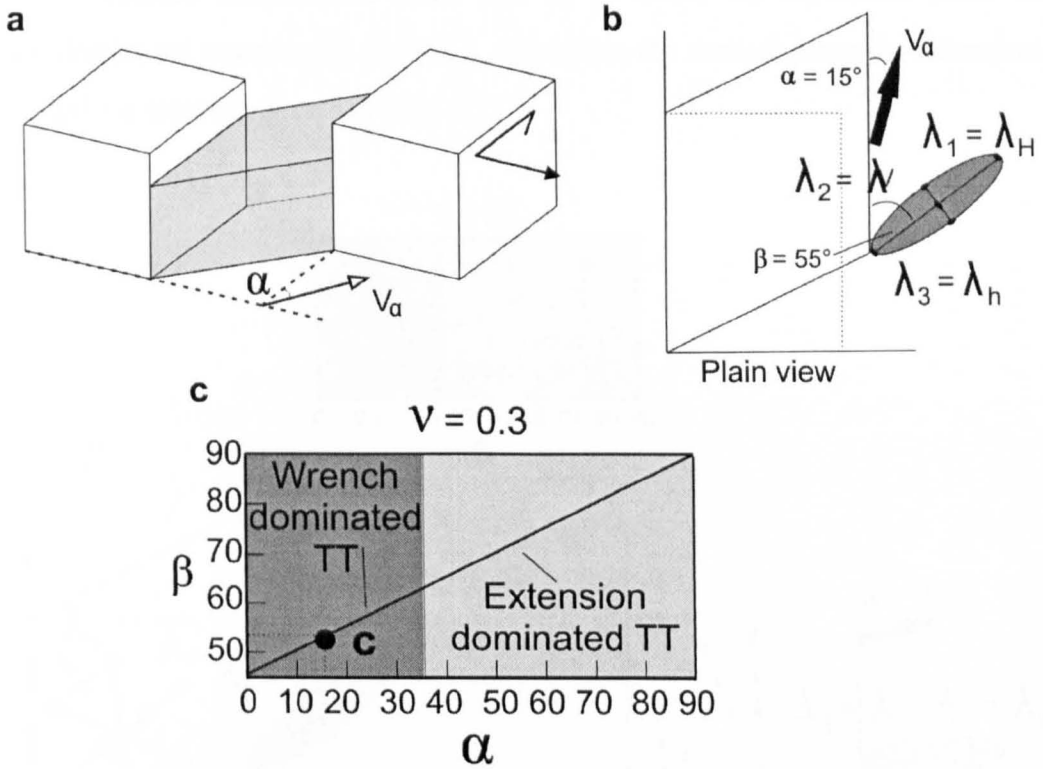

Figure 5.1: a) Homogeneous transtension arising from oblique divergence expressed by the angle α between the plate boundary and the displacement vector. b) Plan view of the previous figure for an arbitrary angle of divergence α = 15° between the imposed displacement vector V_α and the deformed zone boundary. The angle β between the infinitesimal maximum strain axis and the deformed zone boundary is also shown. c) α vs β diagram displaying the field of wrench- (dark grey) and extension-dominated (pale grey) infinitesimal transtensional strain.

The combination of these two plane strain end-member deformations results in a 3-D transtensional non-coaxial strain (Fossen and Tikoff, 1993). Predictable geometric relationships exist between the orientations of the deformation zone boundary and both the axis of maximum infinitesimal strain ($\lambda_1 \equiv \sigma_3$), expressed by

the angle β, and the far field transport direction V_α expressed by the angle α (Figs. 5.1a-b). Due to the non-coaxial nature of transtensional deformation, there is no coincidence between the orientation of the maximum infinitesimal axis λ_1 and the regional transport direction V_α, i.e. $\alpha \neq \beta$ (Fig. 5.1).

There are two states of infinitesimal transtensional strain, wrench- and extension-dominated, respectively, whose development depends on the value of the divergence angle α (Fig. 5.1c).

The maximum infinitesimal strain axis, λ_1, is always in the horizontal plane ($\lambda_1 = \lambda_H$), the minimum infinitesimal strain axis λ_3 is within the horizontal plane for wrench-dominated transtension ($\lambda_3 = \lambda_h$), and within the vertical plane for extension-dominated transtension ($\lambda_3 = \lambda_V$) (Fig. 5.2).

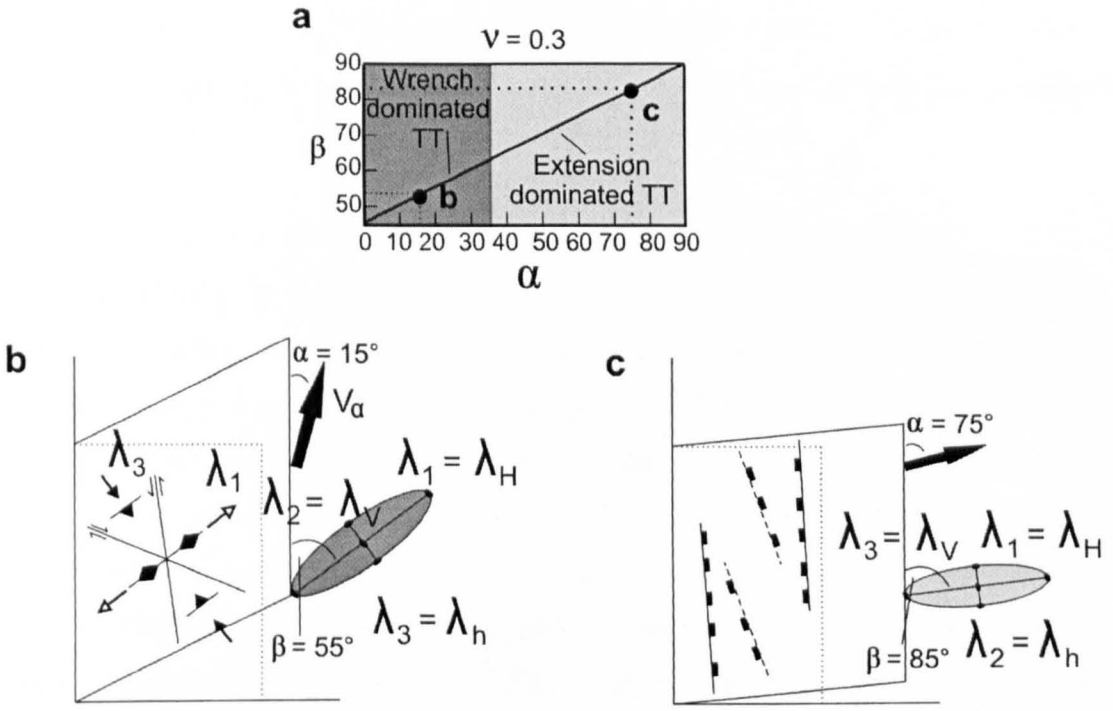

Figure 5.2: a) α vs β diagram where α and β are the angle between the boundary fault and the transport direction and the infinitesimal maximum extension axis, respectively. b) Wrench-dominated transtension (α = 15°). Style of faulting associated with slightly oblique sinistral shear. c) Extension-dominated transtension (α = 75°). Style of faulting associated with highly oblique sinistral shear.

Different styles and geometry of faulting, within the deformed zone, are predicted for wrench- and extension-dominated transtension (Figs. 5.2a-b-c; Withjack and Jamison, 1986; De Paola et al., 2005a-b). Wrench-dominated domains are

characterised by conjugate, often quadrimodal sets of strike-slip faults and by the development of open to tight, sub-horizontal folds and sub-parallel thrusts (Fig. 5.2b) that often link into adjacent strike-slip faults. Where folds develop, the trend of the axial traces and thrusts bisects the obtuse angle between the strike-slip fault arrays and lies at high angles to the deformation zone boundaries; these structures are often mistakenly related to phases of basin inversion (e.g. see De Paola et al., 2005b).

In distinct contrast, extension-dominated domains are typically characterised by a single bimodal to quadrimodal sets of dip-slip to oblique-slip normal faults trending at low angles to the deformation zone boundaries (Fig. 5.2c).

Experimental models investigating oblique divergence obtained a threshold angle $\alpha = 30°$ for the transition between wrench- and extension-dominated transtension (Withjack and Jamison, 1986; Ramani and Tikoff, 2002). A threshold value of $\alpha = 30°$ is similar to that calculated from strain modelling when using a Poisson's ratio ν value of 0.3 (giving $\alpha \approx 34°$) which corresponds to a mean value for most natural rocks (De Paola et al., 2005a).

5.2.2 Heterogeneous Transtension: the effects of strain partitioning

Idealised homogeneous transtensional strains are probably rare in natural systems, particularly when strain partitioning occurs due to reactivation of weak inherited structures lying at an oblique angle to regional displacement (Fig. 5.3a) (Tikoff and Teyssier, 1994; Jones and Tanner, 1995). Suitable pre-existing discontinuities could include lithological boundaries, faults and shear zones (Holdsworth et al., 1997). Reactivation of such structures may accommodate much of either the extensional or the wrench component, leaving a residual component of the remaining bulk strain to be accommodated within the surrounding country rocks (Figs. 5.3a-b) (Tikoff and Teyssier, 1994; Jones and Tanner, 1995; De Paola et al., 2005a-b). If the bulk strain undergoes total partitioning, i.e. the oblique regional displacement is split up into two components respectively parallel and orthogonal to the boundary shear zones and reactivated structures, then the bulk 3-D strain deformation is represented by two contemporaneous plane strain states (Figs. 5.3b-c).

Hence in examples with a high degree of partitioning, wrench-dominated transtension can occur even during weakly oblique regional divergence (regional angle α has a high value, Figs. 5.3b-c).

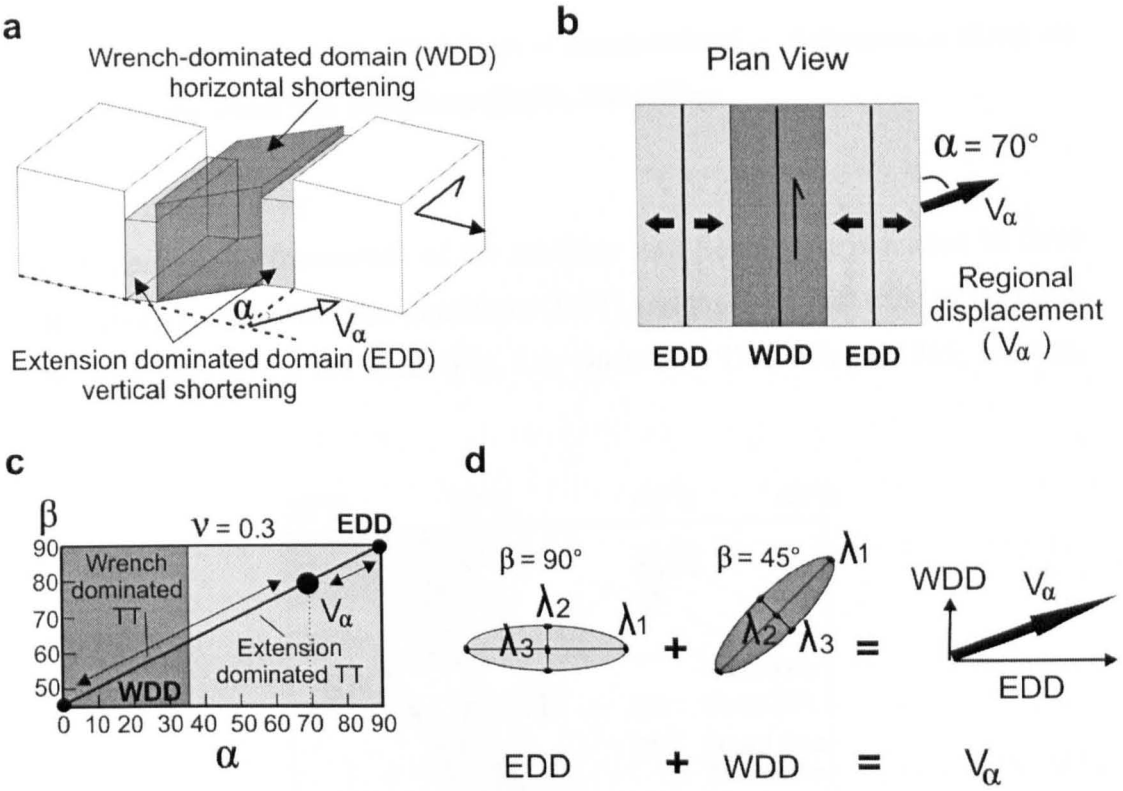

Figure 5.3: a-b) Partitioned transtension. The bulk displacement is partitioned into extension dominated domains (EDD) characterised by vertical shortening and into wrench dominated domains (WDD) characterised by horizontal shortening. c) Regional displacement (V_α) and partitioned components, within extension (EDD) and wrench (WDD) dominated domains, respectively, have been plotted on a α vs β diagram. d) Provided the ratio of boundary-parallel and boundary-normal displacement is known, the bulk displacement V_α can be reconstructed by integration of the two partitioned components accommodated within the EDD and WDD.

Thus partitioning of transtensional deformation can lead to the development of contemporaneous domains of crustal deformation (cf Figs. 5.2b-c) in which the strain may approximate a 2-D state of strain if partitioning is total (Fig. 5.3d). These situations are amenable to conventional palaeostress analysis, but may be mis-interpreted as being the result of different deformation events given the apparent mismatch in resolved infinitesimal strain/stress axis orientations within adjacent domains (Fig. 5.3). Thus, knowledge of both the appropriate boundary conditions and timing of deformation is essential in order to correctly define the regional tectonic framework responsible for the development of heterogeneous, but contemporaneous 3-D fault patterns.

5.3 THE DEAD SEA TRANSFORM, NE AFRICA

Here we examine the case of oblique – transtensional – deformation along an active margin, the Dead Sea Transform (DST), NE Africa.

5.3.1 Geological setting

The plate tectonic framework of the northern Red Sea region is related to three different margins: the Dead Sea Transform (DST) and the Suez Rift (SR) to the north and the Red Sea (RS) to the south (Fig. 5.4; Quennel, 1959; Wilson, 1965; Roberts, 1969).

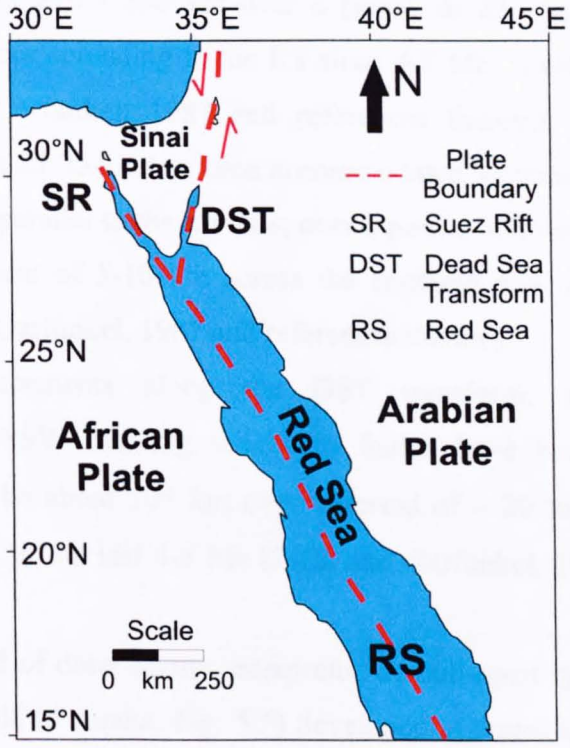

Figure 5.4: Location map of the Red Sea-Dead Sea region. The plate boundary configuration of the area is also shown.

Most authors view the northern region of the Red Sea as a triple junction between the African and Arabian plates and the Sinai micro-plate (Fig. 5.4). It is widely accepted that the DST corresponds to an active sinistral transform margin, more than 1000 km long, linking the Taurus-Zagros convergence zone in the north to the Red Sea rift in the south. Only its southern portion, which is about 450 km long, is considered here (Fig. 5.4).

The SR is an active extensional boundary whilst the RS represents a more mature accretional boundary since seafloor spreading has been recorded by magnetic anomalies in the last 4-5 Ma (Vine, 1966; Roeser, 1975). It has long been recognised that the structural pattern displayed in the exposed crust is inherited from pre-existing fabrics, mostly ~N-S trending, in the underlying Precambrian basement of the former Afro-Arabian macrocontinent (Colletta et al., 1988; Montenat et al. 1988; Bayer et al. 1988; Lyberis, 1988).

The opening in the RS was facilitated by the development of normal faults parallel to the trend of the rift, accommodating a total horizontal extensional displacement of about 270 - 290 km over a period of 25 Ma. The displacement associated with seafloor spreading in the RS since 4-5 Ma, is estimated to be about 75 km (Joffe and Garfunkel, 1987 and references therein). A total horizontal displacement of about 25-35 km has been accommodated by normal faults across the SR, with fault trends parallel to the rift axis, over a period of about 25 Ma. In the last 4-5 Ma, a displacement of 5-10 km across the southern end of the SR has been suggested (Joffe and Garfunkel, 1987 and references therein).

Left-lateral displacements along the DST transform, accommodated by approximately NNE-SSW trending strike-slip faults, have been estimated from geological offsets to be about 105 km over a period of ~ 20 to 25 Ma, and to be approximately 35 km in the last 4-5 Ma (Joffe and Garfunkel, 1987 and references therein).

A series of aligned of deep basins, interpreted as pull-apart type basins (e.g. the Dead Sea and the Gulf of Aqaba, Fig. 5.5) developed at zones of left overstepping between the most active sinistral strike-slip segments (Ben-Avraham et al., 1979a-b; Ben-Avraham and Garfunkel, 1986; Woodcock and Fischer, 1986; Reches, 1987).

Normal faults, sub-parallel to the strike-slip faults and not related to the pull-apart geometry, have been recognised adjacent to the most active sinistral strike-slip faults (Fig. 5.5; Ben-Avraham, 1985; Joffe and Garfunkel, 1987; Picard, 1987; Reches, 1987; Ben-Avraham and Zoback, 1992; Sagy et al., 2003). In particular, strain partitioning in the Dead Sea area has been reported since margin-parallel displacements occur along the N-S trending sinistral strike-slip faults at the same time as almost orthogonal displacements distributed in the surrounding areas (Garfunkel, 1981; Ben-Avraham and Zoback, 1992; Sagy et al., 2003).

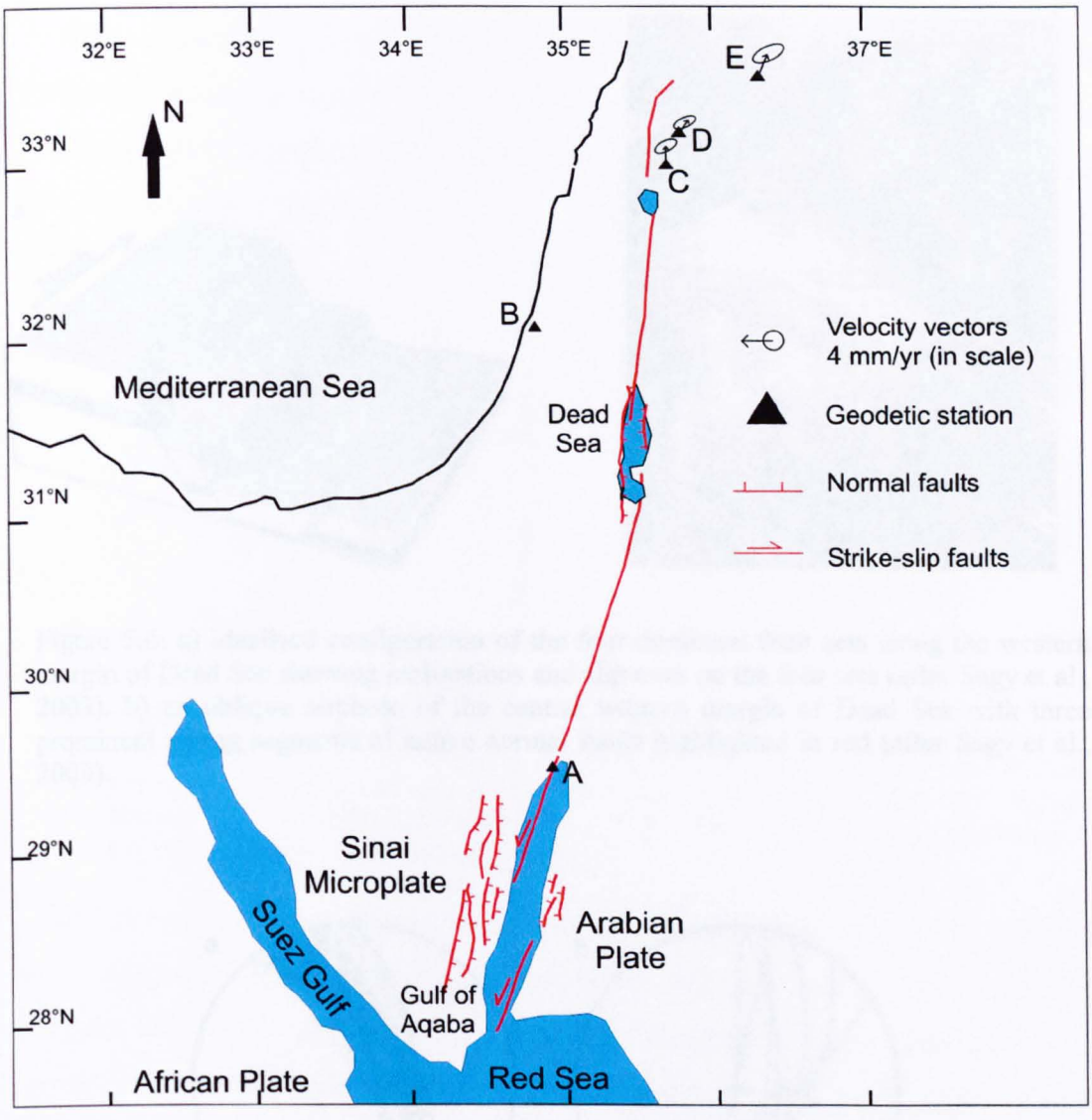

Figure 5.5: Schematic structural map of the Dead Sea region (geology from Picard, 1987; Lyberis, 1988, Sagy et al., 2003). Velocity of GPS stations with respect to SRF (Sinai Reference Frame) from Wdowinski et al. (2004).

3-D extensional strain, accommodated by quadrimodal faulting patterns, has been described in the western margin of the Dead Sea area (Fig 5.6; Sagy et al., 2003). These zigzag, orthorhombic faults have been interpreted as having formed in a 3-D strain field (Figs. 5.6 and 5.7). Sagy et al. (2003) used the faults and associated kinematics, as measured in the field (Fig. 5.7), to determine the 3-D strain state that best fits with the fault pattern.

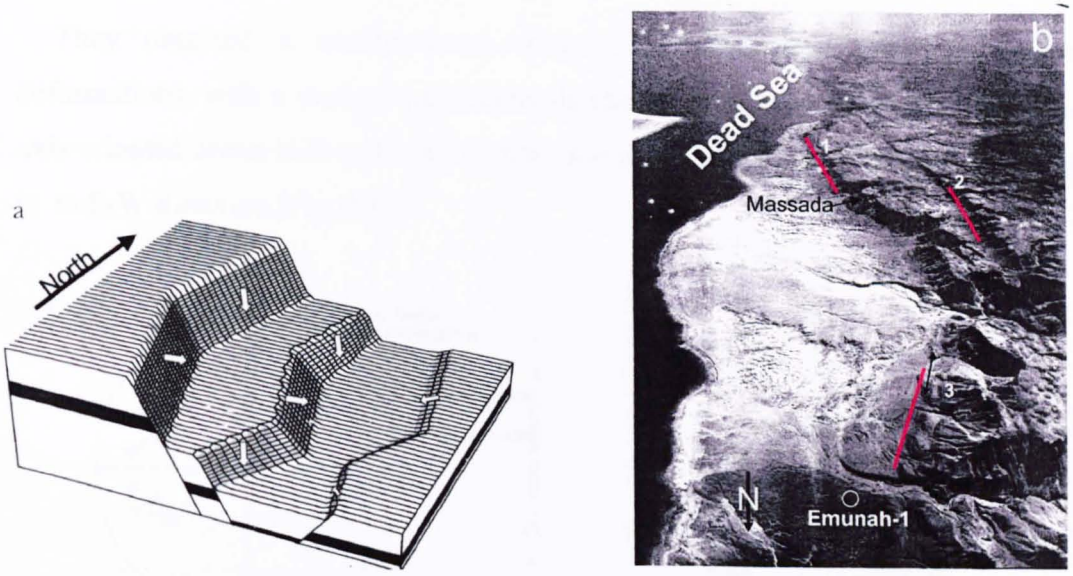

Figure 5.6: a) Idealised configuration of the four dominant fault sets along the western margin of Dead Sea showing inclinations and slip axes on the four sets (after Sagy et al., 2003). b) an oblique airphoto of the central western margin of Dead Sea with three prominent zigzag segments of active normal faults highlighted in red (after Sagy et al., 2003).

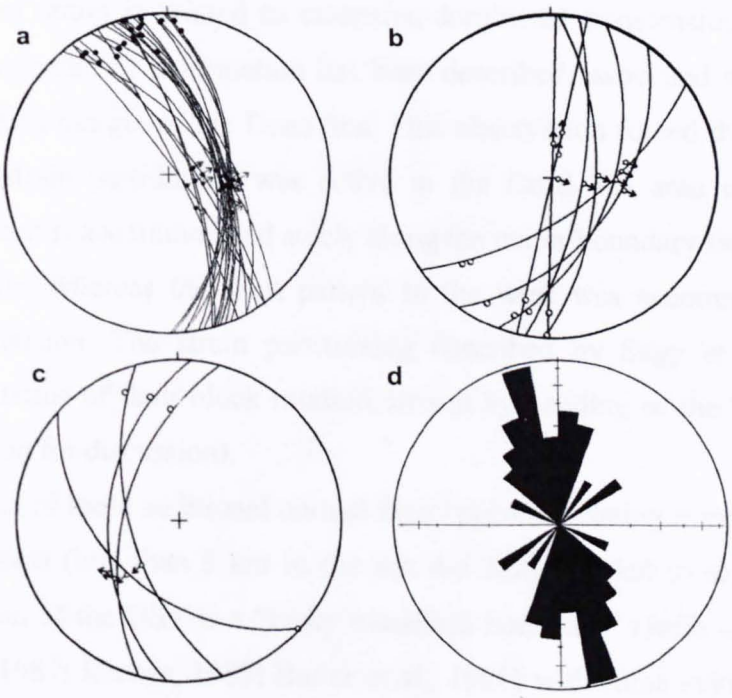

Figure 5.7: a-b-c) Directional data of large faults with slip axes measured in the field. Faults are divided into three sets; great circles on lower hemisphere, stereographic projection. d) rose diagram of faults trend. (After Sagy et al., 2003).

They obtained a constrictional strain field, consistent with transtensional deformations, with a vertical maximum shortening axis, an intermediate shortening axis oriented about N-S and a horizontal maximum extension axis oriented roughly in an E-W direction (Fig. 5.8).

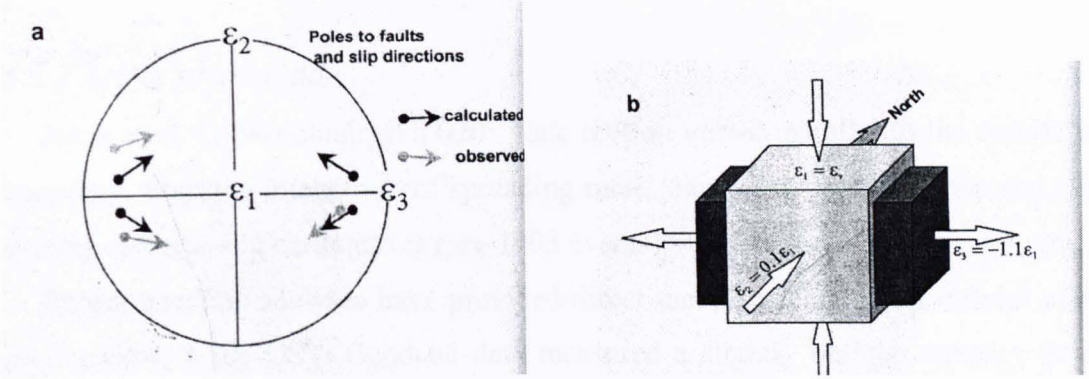

Figure 5.8: Best fit strain state for the measured normal faults of the western margin of the Dead Sea (after Sagy et al., 2003). a) Stereographic projection showing poles of mean sets and plunge directions of slip axes of field data and calculated sets. b) Schematic representation of the strain state calculated for the measured fault data according to Reches (1983) faulting model (see Chapter 2).

This state of strain is related to extension-dominated transtension. No sinistral strike-slip component of deformation has been described associated with structures along the western margin of the Dead Sea. This observation forced these authors to consider that strain partitioning was active in the Dead Sea area where sinistral strike-slip motion is accommodated solely along the major boundary faults within the Dead Sea basin, whereas the fault pattern to the west was accommodating only horizontal extension. The strain partitioning described by Sagy et al. (2003) is interpreted in terms of fault block rotation, driven by bending of the Sinai subplate (see later session for discussion).

The presence of these additional normal faults accommodating minor components of E-W extension (less than 5 km in the last 4-5 Ma), has led to suggest that the southern portion of the DST is a "leaky transform boundary" (Joffe and Garfunkel, 1987; Picard, 1987; Reches, 1987; Butler et al., 1998) with some evidence of strain partitioning (Garfunkel, 1981; Sagy et al, 2003).

Other outcrop-based studies have proposed more complex polyphase faulting histories along the DST, invoking different events related to continuous changes in the orientation and nature of the stress field, with regional plate-motion vectors

varying from N-S to E-W in the last 15-20 Ma (e.g. Lyberis, 1988; Montenat et al., 1988). This contrasts with what has been proposed in the Gulf of Aden further to the south, where the motion of the Arabian plate across the rift has been fairly constant at least over the last 10 Ma (Joffe and Garfunkel, 1987 and references therein; McQuarrie et al, 2003).

5.3.2 Active strain field

Jestin et al. (1994) obtained a 020° plate motion vector, parallel to the transform boundary, from the integration of spreading rates, transform fault azimuths and slip vectors of strike-slip earthquakes (pre-1993 events).

Recent geodetic analyses have provided direct measurements of the current plate motions across the DST. Geodetic data measured a slightly oblique velocity field, where an ~N-S margin-parallel component prevails over smaller extensional component acting at high angle to the boundary (Fig. 5.5, Pe'eri et al., 2002; Wdowinski et al. 2004). This extensional component has been estimated as 1.7 - 3.5 mm/yr by Pe'eri et al. (2002), whilst Wdowinski et al. (2004) suggest that E-W motions are present, but negligible within the estimated error. A locked fault model imposing a null velocity condition orthogonal to the boundary, i.e. plane strain wrench deformation, has been adopted to calculate the strain rates parallel to the DST as 2.6 ±1.1 mm/yr (Pe'eri et al., 2002) and 3.3 ±0.4 mm/yr (Wdowinski et al., 2004). The geodetically measured values are generally slow compared to the geologically derived strain-rates of 6 - 10 mm/yr (Joffe and Garfunkel, 1987), although the latter may be overestimated (see Pe'eri et al., 2002). They are slightly slower than rates estimated from neotectonic geologic, geomorphic and seismological data by Klinger et al. (2000) and Ginat et al. (1998) who obtained slip rates of 4 ± 2 mm/yr and 3 - 7.5 mm/yr, respectively.

The integration of geodetic and geological data leads to estimates of about 1mm/yr for the strain rate accommodated orthogonal to the boundary. This value is likely affected by measurement uncertainty, but still represents the best approximation possible from the available data. The component of movement parallel to the DST is subjected to more reliable calculated strain rates varying from 3 to 5 mm/yr. This implies that ratios between 5:1 and 3:1 are reasonable estimates

of the relative magnitudes of margin-parallel and orthogonal (oblique)-extensional displacement components.

5.3.3 Seismicity along the DST

Seismic records and focal mechanism solutions derived from earthquake events with magnitudes $4.5 < m_b < 6.5$ which have occurred in the DST region during the last 30 years are shown on Figure 5.9. (Harvard CMT catalogue, Foster and Jackson, 1998).

Seismic events have been filtered between those whose focal mechanisms match the condition $f_{clvd} \leq 0.17$, i.e. they approximate an almost pure double-couple source (Frohlich and Apperson, 1992; Foster and Jackson, 1998). These events are likely to accommodate most of the regional imposed strain since they reflect the kinematics and orientation of the main, regional-scale, geological structures of the area. The distribution of seismicity along the DST is mostly localised in areas adjacent to the deepest basins (Dead Sea and Gulf of Aqaba), where both extensional and transcurrent kinematics are recorded according by available focal mechanism solutions (Fig. 5.9).

N-S trending nodal planes, associated with extensional focal mechanisms, have been positively discriminated as potential rupture planes according to geological constraints (Fig. 5.9). NNE-trending nodal planes, associated with transcurrent focal mechanism solutions, have also been positively discriminated as rupture planes; these are parallel to the trend of the DST sinistral transform boundary (Fig. 5.9).

The slip vectors plotted for all events display two distinct clusters, horizontal N20° (strike-slip events) and N50°-N60° dipping (oblique extensional events), respectively (Fig. 5.10).

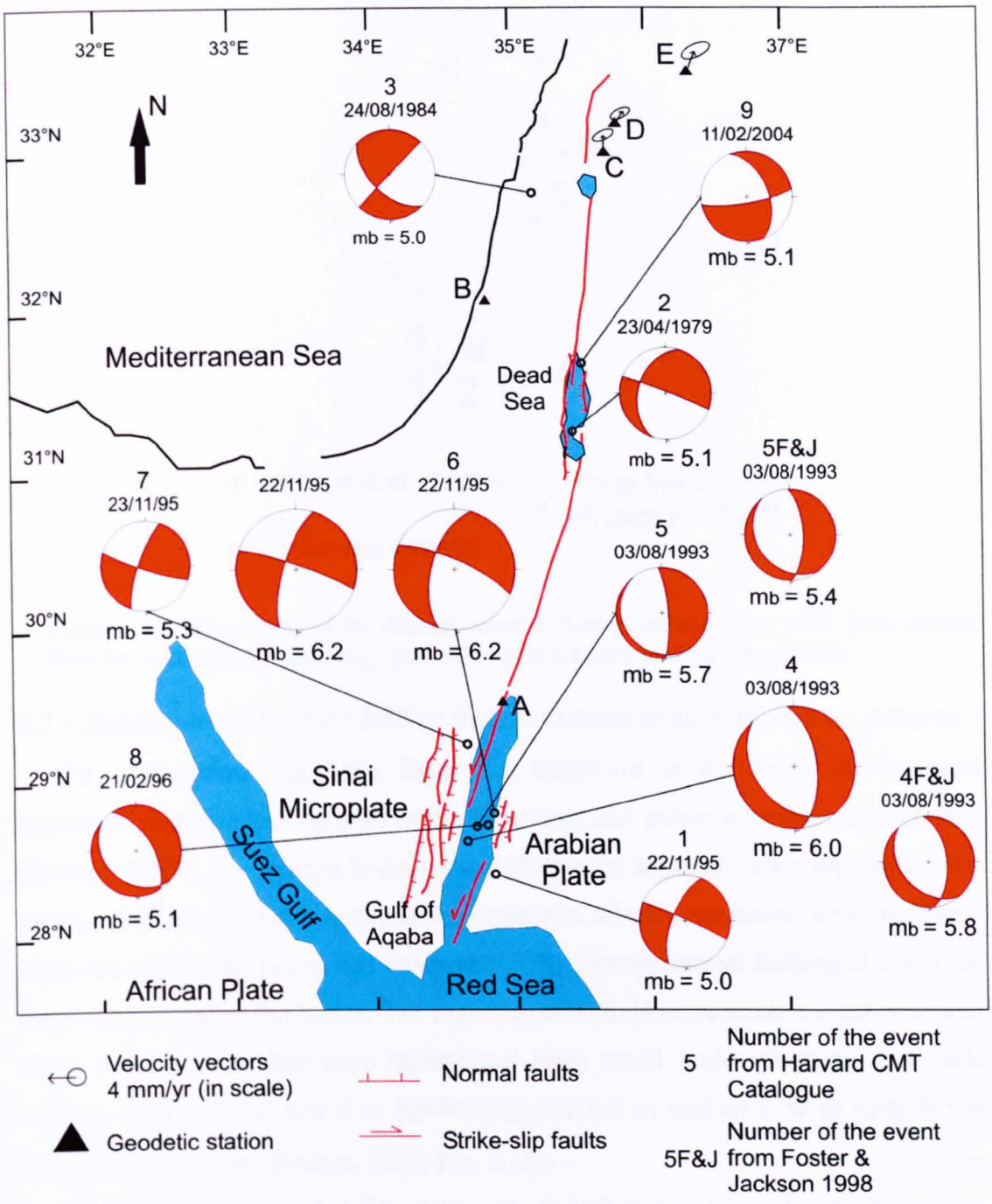

Figure 5.9: Schematic structural map of the Dead Sea region (geology from Picard, 1987; Lyberis, 1988, Sagy et al., 2003). Earthquakes focal mechanisms, magnitudes, data and event number from Harvard (www.seismology.harvard.edu) for the period 1976-2004 have been plotted on the map together with data from Foster and Jackson (1998). Harvard CMT solutions plotted here are almost pure double-couple source, i.e. $f_{CLVD} \leq 0.17$ (Frolich and Apperson, 1992; Foster and Jackson, 1998). Velocity of GPS stations with respect to SRF (Sinai Reference Frame) from Wdowinski et al. (2004).

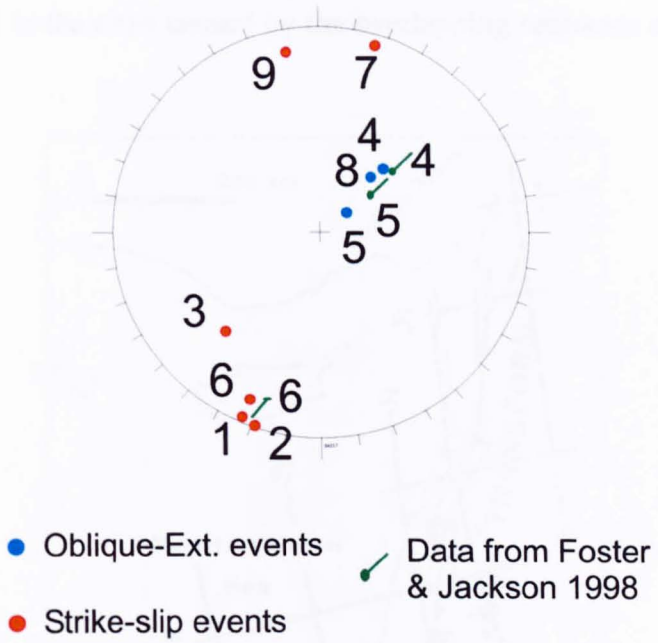

Figure 5.10: Slip vectors of the discriminated rupture plane along the DST. Data sources from Harvard (www.seismology.harvard.edu) and Foster and Jackson (1998).

5.3.4 Existing models of the DST margin and associated deformation patterns

The deformation along the Dead Sea transform is the result of dominant horizontal displacement parallel to the transform and minor extension normal to it (Reches, 1987). The margin is composed of straight segment strike-slip faults with zones of left overstepping between the segments, where deep basins develop. These areas are seismically active and characterised by intense normal faulting at either the centre or margins of the basins. The regional stress field responsible for deformations along the transform has been determined from small scale structures that yield curving trajectories of a N-S to NNW-SSE directed σ_1 and an E-W to ENE-WSW trending σ_3 (Eyal and Reches, 1983; Fig. 5.11).

Even though minor extension across the boundary has been always recognised, the plate boundary-structural models used to interpret the DST are plane strain, with the plate motion parallel to the boundary (although see Ben-Avraham and Zoback, 1992). In these models, the basins aligned along the DST (Fig. 5.5) are solely considered to be pull-apart basins, even though some differences with respect to "traditional" pull-apart basins have been noted. Quennel (1956) was probably the first to recognise the pull-apart basin or rhomb-shaped graben and proposed that the

Dead Sea is a void in the crust caused by the overlapping segments of the Dead Sea fault system.

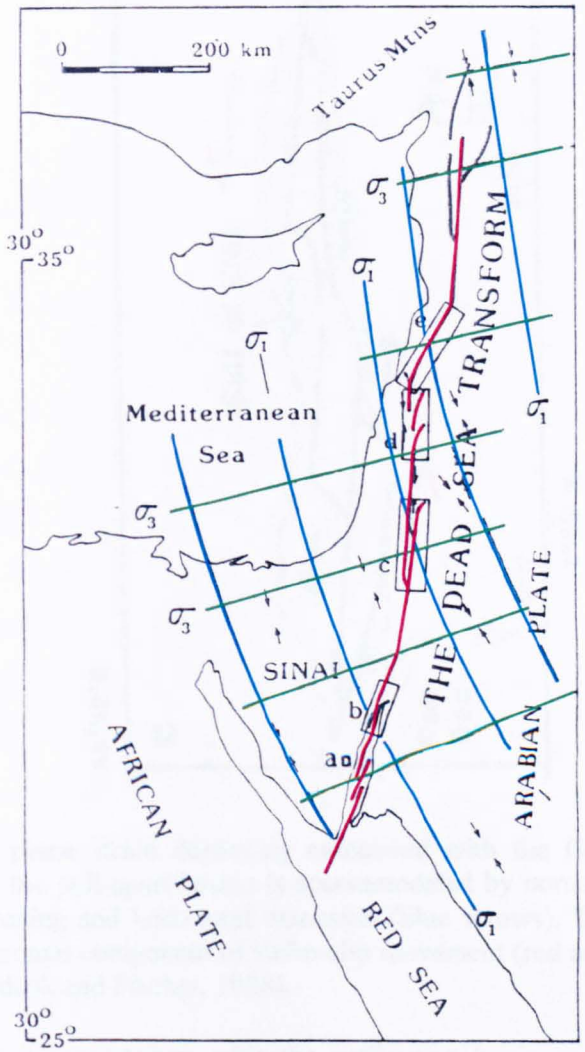

Figure 5.11: General view of the Dead Sea transform (red lines) and superimposed regional stress field. Small arrows indicate maximum compression directions. Blue lines are σ_1 trajectories and green lines are σ_3 trajectories according to small scale structures (after Eyal and Reches, 1983).

Woodcock and Fischer (1986) defined the Gulf of Aqaba as an extreme example of a pull-apart duplex. They classify the Gulf of Aqaba as a non-plane strain duplex structure, given the accentuated subsidence observed between the overlapping and bending strike-slip segments (Fig. 5.12). This generates a component of vertical shortening (thinning of the crust) and horizontal extension acting at the same time as strike-slip movements along the margin (Fig. 5.12; Woodcock and Fischer, 1986).

The regional wrench component and the local extensional component in this model are parallel (Fig. 5.12).

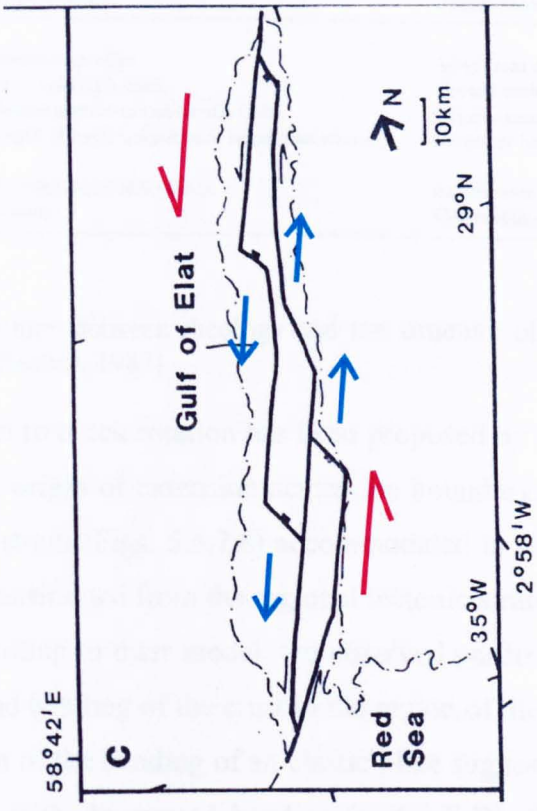

Figure 5.12: Non plane strain duplexing associated with the Gulf of Elat (Aqaba). Subsidence within the pull-apart basins is accommodated by normal faulting associated with vertical shortening and horizontal extension (blue arrows). The local extension is parallel to the horizontal component of strike-slip movement (red arrows) along the DST margin (after Woodcok and Fischer, 1986).

The first to note inconsistency with the pull-apart basin model in the Gulf of Aqaba (Fig. 5.5) were Eyal et al. (1985) who highlighted the mismatch between the calculated and actual value of extension measured parallel to the DST, i.e. along a transect at high angle to the normal faults bounding the pull-apart. According to their alternative model, the basins formed by the combined action of left lateral-slip and block rotation. Reches (1987) argued that the extension mismatch observed by Eyal et al. (1985) contradicts only a pull-apart basin model in the brittle crust, whereas in a partly ductile crust, the apparent mismatch may be explained. In particular, Reches (1987) propose a model where pull-apart basins in a ductile crust form fault patterns and length/displacement relationships that differ from their equivalents in the brittle crust as summarised in the following table:

Relationship between crustal rheology and the structure of pull-apart basins and push-up swells

Property	Brittle rheology	Ductile rheology
Fault bending		
(1) pull-apart basins	Toward each other	Away from each other
(2) push-up swells	Away from each other	Toward each other
Type of faulting	Oblique-normal and strike-slip faults	Oblique-reverse and strike-slip faults
Length/slip relations	Length of basin is equal to or larger than total slip	Length of basin has no simple relation to slip
Extension parallel to pull-apart basins	Extension equal to total slip	Extension is smaller than total slip
Style of deformation	Faulting	Continuous deformation and faulting

Figure 5.13: Relationships between rheology and the structure of pull-apart basins and push-up swells (after Reches, 1987).

An alternative model to block rotation has been proposed by Sagy et al. (2003) to explain the effects and origin of extension across the boundary. They observed that the 3-D transtensional strain (Figs. 5.6,7,8) accommodated in the western margin of the Dead Sea basin is partitioned from the regional tectonic strain that acts parallel to the DST margin. According to their model, the observed partitioning is the result of localised weakening and bending of the crust in the region of the Dead Sea pull-apart (Fig. 5.14). An analysis of the bending of an elastic plate suggests that it will deform into a "saddle" shape with downward bending in the E-W direction and upward bending in the N-S direction (Fig. 5.14b).

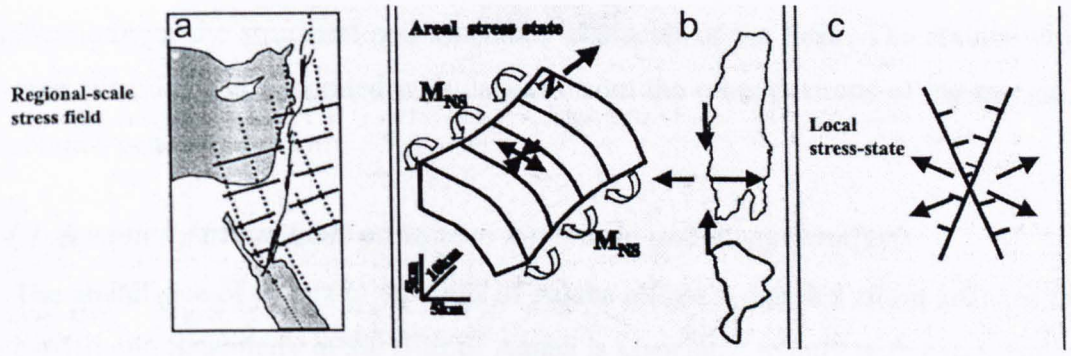

Figure 5.14: a) Dead Sea stress field according to Eyal and Reches (1983) and Reches (1987); continuous lines σ_3 trajectories; dashed lines σ_1 trajectories. b) A simplified model of plate-bending along the western margin of the Dead Sea under bending moment that leads to N-S shortening and E-W extension. This strain is consistent with the 3-D analysis of the zigzag faults (Figs. 5.6-7-8). c) The two axes of intermittent extension directions of the local stress field generated by flexing above normal faults. (after Sagy et al., 2003).

This generates extension in an E-W direction and shortening in both N-S and vertical directions. These orientations are in qualitatively in agreement with the strain state

calculated for the zigzag faults. According to Sagy et al. (2003), the profound weakening exerted by the normal fault networks led to further localisation of the pull-apart subsidence within this belt. At the same time, the strike-slip motion has continued exclusively along narrow subvertical segments of the DST margin.

5.4 AN ALTERNATIVE TRANSTENSIONAL PLATE BOUNDARY MODEL FOR THE DST

Most models proposed for about the DST are basically plane strain models. A component of extension acting orthogonal or at high angles to the margin is widely recognised and accepted, but few interpretations of the deformation pattern have considered this component. It has always been explained in terms of minor effects such as localised plate bending induced by subsidence in the pull-apart basin and/or rigid block rotation induced by simple shear along the main segments of the DST. According to all this models, the main control on the deformation patterns along the DST is imposed by the regional stress field that is coupled to a plate motion vector parallel to the plate boundary (Figs. 5.11 and 5.14a).

An alternative and new model of the DST is presented here and discussed using an integration of the available datasets, including seismological data. The study starts from the analysis of seismicity in the Gulf of Aqaba (Fig. 5.5 and Fig. 5.9) and its implications for the structural and kinematic character of the DST. The results will be then extended and integrated with datasets from the other portions of the margin, to obtain a general model.

5.4.1 Seismicity in the Gulf of Aqaba: kinematic and strain analysis

The abundance of events in the Gulf of Aqaba allows a detailed strain analysis to be carried out. Seismicity in the Gulf of Aqaba is associated mainly with two seismic swarms that occurred in 1993 and 1995 (Fig. 5.15).

Seismological data here are characterised by both extensional (events 2-3 in 1993 and event 6 in 1995; Fig. 5.15a) and transcurrent (events 1-4-5 in 1995; Fig. 5.15a) movements according to available reliable focal mechanisms (Frohlich and Apperson 1992; Foster and Jackson 1998). Thus the seismological data display two distinctly different, but broadly contemporaneous kinematic patterns: sinistral strike-slip (NNE trending planes) and slightly oblique, left-lateral, extensional (N-S planes) (Fig.

5.15a). This fits well with the observed clustering of slip vectors associated with the discriminated rupture planes into two distinct groups (~sub-horizontal /N20°E and ~60° /N55°E; Fig. 5.15b).

The stress tensor associated with the strike-slip focal mechanism solutions (Fig. 5.16a) yields an approximately vertical σ_2, a horizontal N65°E trending σ_3 and a subhorizontal N155°E σ_1 (Fig. 5.16a). Assuming that $\sigma_3 \cong \lambda_1$, this yields an angle β = 45°, from which the local component of displacement $V\alpha_1$ is calculated oriented parallel to the DST (e.g. α_1 = 0°), i.e. a 2-D wrench simple shear strain (Figs. 5.16a,c). The absolute trend of the wrench component accommodated by these faults is N20°E ($V\alpha_1$) (Fig. 5.16d).

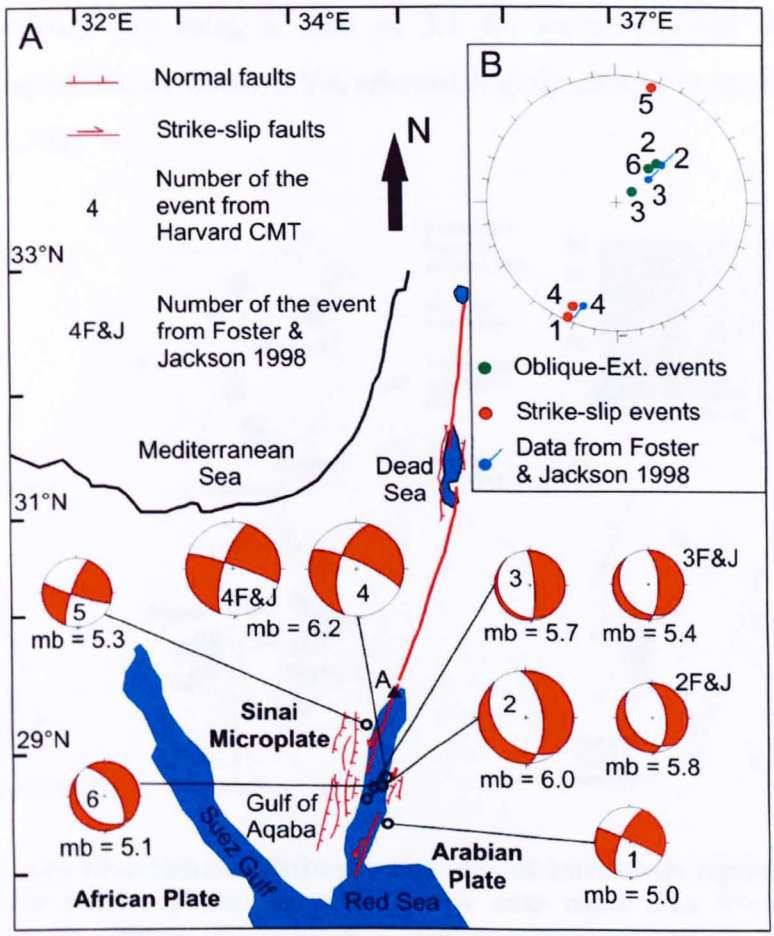

Figure 5.15: a) Schematic structural map of the Dead Sea region (modified from Picard, 1987; Sagy et al., 2003). Earthquakes focal mechanisms, magnitudes and event number from Harvard (www.seimsology.harvard.edu) for the period 1976-2004, in the Gulf of Aqaba, have been plotted on the map. b) Slip vectors of the discriminated rupture plane. Data sources from Harvard (www.seimsology.harvard.edu and Foster and Jackson, 1998).

The stress tensor associated with the oblique extensional focal mechanism solutions (Fig. 5.15) yields a subvertical σ_1 and a horizontal σ_3 trending N75°E (Fig. 5.16b). In this case, the direction of $\sigma_3 \cong \lambda_1$ gives an angle β of 75° suggesting that the local component of displacement is oriented at an angle $\alpha_2 = 60°$ (Figs. 5.16b-c). This is consistent with non-coaxial, extension-dominated transtensional strain. The absolute trend of the component of extension accommodated by these structures is N60°E ($V\alpha_2$) (Figs. 5.16c-d).

Figure 5.16d shows a plan-view reconstruction of the pull-apart structure in the Gulf of Aqaba based on seismic data. Both components of deformation, $V\alpha_1$ and $V\alpha_2$, need to be integrated in order to reconstruct the regional displacement ($V\alpha_r$) across the boundary. By using a ratio of 3:1 for margin-parallel and oblique extensional components, we obtain a $V\alpha_r$ oriented slightly oblique to the DST margin ($\alpha \approx 10°$; Fig. 5.16d).

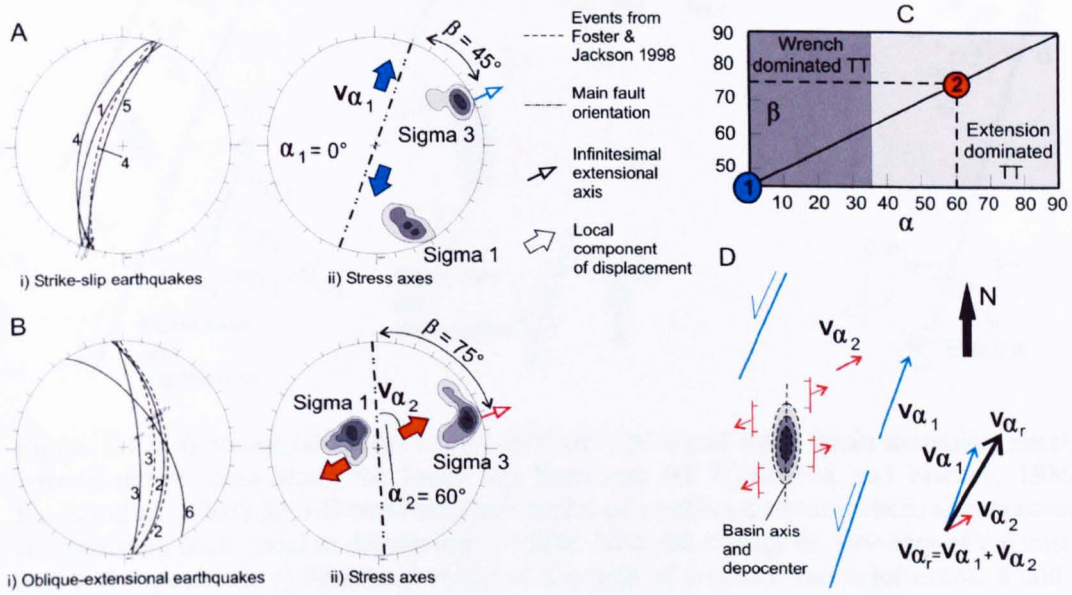

Figure 5.16: a-b) Discriminated strike-slip and oblique-extensional rupture planes and associated slip vectors plotted as great circles onto equal area lower emisphere projections. Event numbers of earthquakes plotted on Figure 5.15a are shown. The β angle has been measured between the $\sigma_3 \cong \lambda_1$ axes and the mean discriminated rupture planes orientation (dashed line). c) β values calculated after figures 5.16a-b have been plotted on the α vs β diagram to obtain the local components of displacement, $V\alpha_1$ and $V\alpha_2$, associated with earthquakes. d) Schematic structural model of the active Gulf of Aqaba along the Dead Sea transform.

The geometry and internal structure of the pull-apart basin in the Gulf of Aqaba (Figs. 5.15a and 5.16d) seems to be influenced by the extensional displacement component ($V\alpha_2$), since normal faults bounding the deep basins are clockwise rotated respect to a traditional pull-apart model (Woodcock and Fischer, 1986). As a result these faults and the associated elongate depocentres lie at a small angle to the boundary, compared to the high angle NW-SE-trend predicted using a classical pull-apart model for the Gulf of Aqaba (Figs. 5.17a-b, e.g. Woodcock and Fischer, 1988; Shamir et al., 2003).

The transtensional model also very accurately predicts the distribution and kinematics of aftershocks following the principal event (event 4, Fig. 5.15a) during the 8 month long 1995 seismic crisis (event 4; Figs. 5.15a and 5.17c).

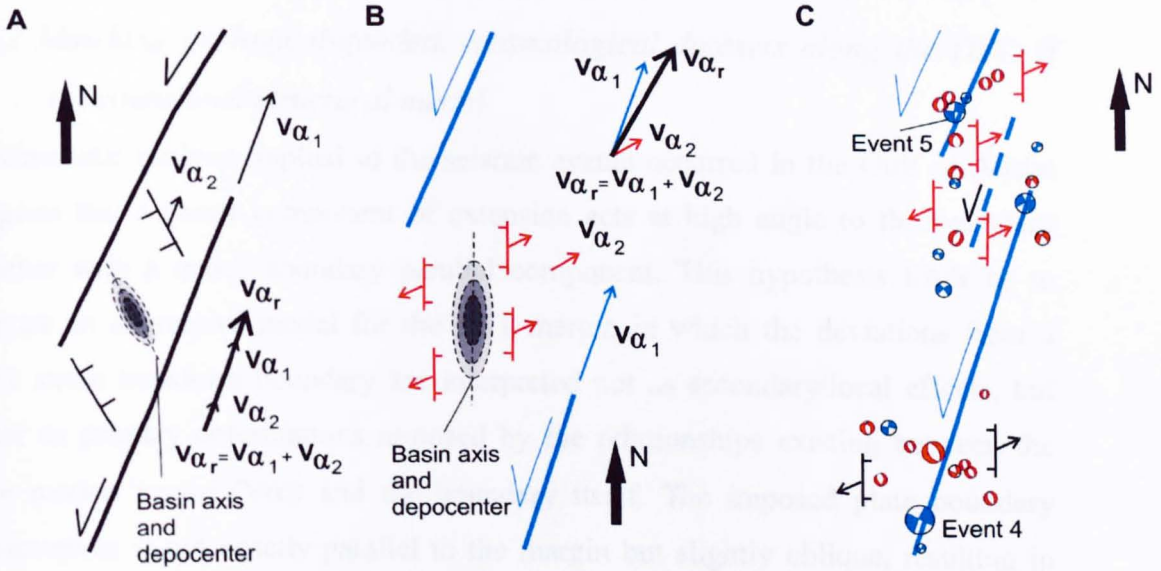

Figure 5.17: a) Structural model of the Gulf of Aqaba pull-apart basin assuming purely wrench deformation along the Dead Sea transform (cf Woodcock and Fischer, 1986; Shamir et al., 2003). b) 3-D transtensional model of a pull-apart basin where a component of extension, orthogonal to the margin is added. Note the change in geometry of the basin axis and depocentre. c) Structural model of the Gulf of Aqaba from major events 4 and 5 (see fig. 5.8a) and associated aftershocks of the 1995 seismic swarm (aftershocks from Shamir et al., 2003). The red dashed line is the fault not reactivated during the 1995 seismic crisis.

The main aftershock (event 5, Fig. 5.15a) did not occur on the next left-stepping segment of the fault system, where a higher stress Coulomb change was calculated, but onshore and further to the NW (Fig. 5.17c, Shamir et al., 2003).

The principal event (4) and the main aftershock (5) are linked by a series of small aftershocks with extensional focal mechanisms aligned along a N-S trend and similar

to the 1993 events, i.e. likely rupture planes trending N-S (Fig. 5.17c, Shamir et al., 2003). This suggests that strain partitioning has occurred during the 8 months duration of the 1995 seismic episode. Strain partitioning imposed by the regional strain and boundary geometry seems, in this case, to dominate over the stress Coulomb change. The process resembles the partitioning of the regional transtensional strain into the two displacement components $V\alpha_1$ and $V\alpha_2$, respectively parallel and oblique to the margin, but here they are sequentially released during major seismic crises (1993 and 1995). Normal faults causing the strain partitioning may be caused by the obliquity between regional imposed displacements and localised along pre-existing N-S trending fabrics in the underlying Precambrian basement (Lyberis, 1988).

5.4.2 Matching geological-geodetic-seismological datasets along the DST: a transtensional structural model

Kinematic analysis applied to the seismic events occurred in the Gulf of Aqaba suggests that a minor component of extension acts at high angle to the boundary together with a major boundary parallel component. This hypothesis leads us to propose an alternative model for the DST margin in which the deviations from a plane strain transform boundary are interpreted not as secondary/local effects, but rather as primary deformations imposed by the relationships existing between the plate motion vector ($V\alpha_r$) and the boundary itself. The imposed plate boundary displacement is not exactly parallel to the margin but slightly oblique, resulting in sinistral transtensional kinematics. Such component of oblique displacement has been detected and measured by geodetic measurements; is observed by analysis of normal faults localised along the margins of the most active areas and is inferred both by the geometry and seismicity of the pull-apart basins.

Most of the displacement is accommodated by margin-parallel strike-slip faults, whilst minor displacement components, at high angle to the boundary, are accommodated by normal to oblique-slip faults subparallel to the margin, often arranged in quadrimodal fault patterns. The same minor component of extension is accommodated within the pull-apart type basins whose geometry seems to be affected by regional transtensional strain.

The ratio between the absolute value of wrench and extensional components is not exactly known since there is still uncertainty about the values measured either from geodetic or geological studies. We have seen how the range of absolute values of the wrench component is approximately between 3 - 5 mm/yr whilst the extensional components is approximately between 1 - 2.5 mm/yr. This second range of strain rates is especially uncertain. The highest values have been measured by Pe'ri et al. (2002), but both geological and later geodetic measurements report lower values. A mean value of about 1 mm/yr seems consistent with a majority of the geological and geodetic data. These data suggest that the percentage strike-slip partitioning of the regional displacement along the boundary is between 75% and 85%. These data can be plotted on the diagram proposed by Teyssier et al. (1995) (cf Section 2.2.5 and Fig. 2.15), together with the values of the angle measured between the margin main trend and the maximum horizontal strain/stress axis associated with extensional structures and earthquakes.

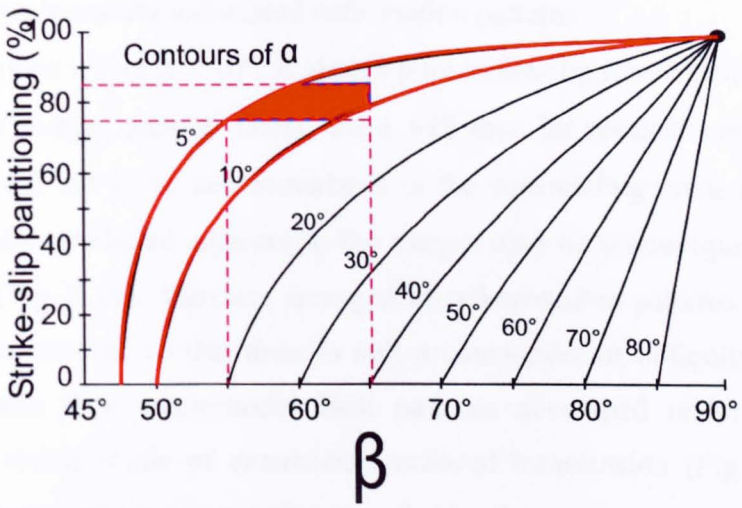

Figure 5.18: Plot showing contours of α on a graph of orientation of maximum horizontal infinitesimal strain axis (β) with respect to the plate margin and degree of strike-slip partitioning (cf 2.2.5). The vertical red dashed lines represent the mean values of β measured from earthquakes (55°) and field structures (65°), respectively. The horizontal red dashed lines are the percentage of strike-slip partitioning of the bulk displacement along margin parallel strike-slip faults as inferred from geological and geodetical data. The blue area represent the likely value of the angle α between the regional displacement ($V\alpha_r$) and the plate boundary. According to the plotted values, the angle α should range between 5° and 10°, i.e. the DST is a slightly transtensional boundary.

A mean value of the angle between the maximum horizontal stress/strain axis and the margin, trending N020°E, obtained from earthquake stress tensors is about 55°

(Fig. 5.16), (www.seimsology.harvard.edu) whilst from strain analysis applied to fault patterns, it is about 65° (Fig. 5.7 and 5.8; Sagy et al., 2003). By plotting together the values of the percentage of strike-slip partitioning and the angle between the maximum stress/infinitesimal strain axes and the plate margin, we calculate that the obliquity between the plate boundary and the regional displacement ($V\alpha_r$), expressed by the angle α, is 5° ÷ 10° (Fig. 5.18).

It appears therefore that the principal mechanism that determines the kinematic character of transtension along the DST is the obliquity between the plate motion vector and the plate margin. The condition of obliquity requires that the DST margin was a pre-existing feature able to localise and partition the bulk displacement. Reches (1987) suggests that the Dead Sea transform is localised along a rheological boundary that marks the suture between two different crusts, the weak Arabian crust to the east and the strong Sinai-Israel crust to the west. The reactivation of such an old, plate-scale feature, under oblique displacements, may have determined the partitioning of strain and the associated deformation patterns.

Under conditions where $\alpha = 10°$, if almost pure strike-slip movements ($V\alpha_1$) take place along the margin parallel faults, there will then be residual components of deformation ($V\alpha_2$) left to be accommodated in the surrounding areas (Figs. 5.19). The normal faults developed adjacent to the margin may be a consequence of such residual strain (Fig. 5.19). They are arranged in orthorhombic patterns because the partitioning was not total so that there is still a component of obliquity during the faulting processes. The quadrimodal fault patterns developed under 3-D strain conditions are characteristic of extension-dominated transtension (Fig. 5.19). The effects of the strain partitioning are also recorded by the geometries displayed in the pull-apart basins developed under 3-dimensional transtensional strain conditions along the DST (Fig. 5.17).

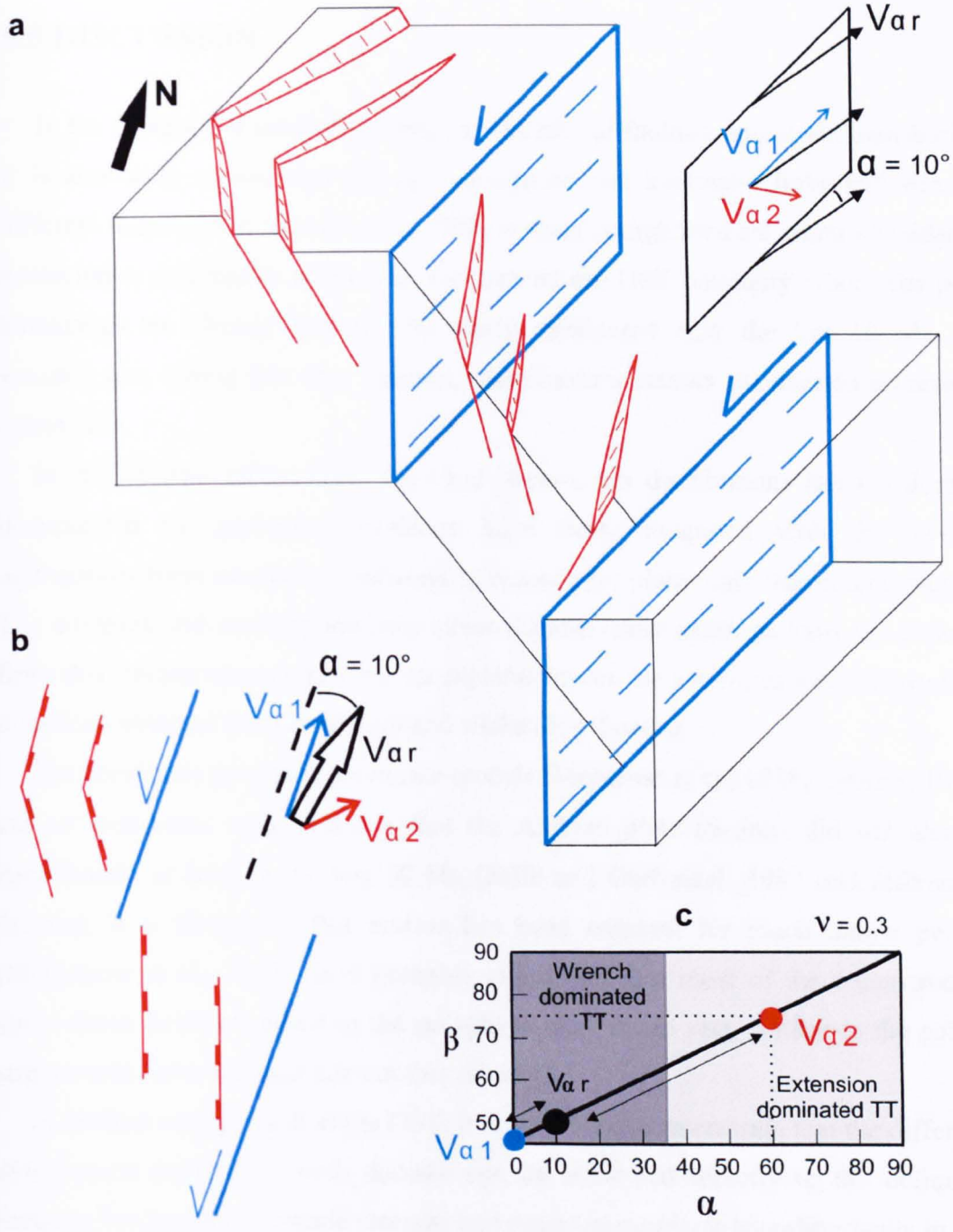

Figure 5.19: a) Transtensional structural model of the DST margin. The regional plate movement ($V\alpha_r$) is slightly oblique to the plate boundary ($\alpha \approx 10°$). This causes the partitioning of the bulk strain into a major, parallel margin component of displacement (blue arrows) and a minor, highly oblique component of displacement (red arrows). The extensional component of displacement is accommodated by oblique-extensional to normal faults localised in the regions surrounding the major segments of the DST. The normal faults bounding the pull-apart type basins developed between left overstepping segments of the DST. The pull-apart fault pattern is also influenced by the component of extension acting at high angle to the boundary. b) Plan view of the margin where the real trend of the structures has been reported. c) α vs β diagram where the two partitioned components acting along and across the DST, $V\alpha_1$ and $V\alpha_2$, respectively, are obtained from the partitioning of the regional displacement $V\alpha_r$.

5.5 DISCUSSION

In the presence of markedly domainal patterns of faulting and strain distribution, it is absolutely critical that the age constraints and kinematic links between the different domains are reconstructed. This is most straightforward when considering neotectonic, seismically active regions such as the DST boundary where the plate kinematics are already known. Our study considered only the last 10 Ma and assumes that during this time interval, plate motion vectors maintained a constant orientation.

In this analysis of the DST, the local stress-strain distributions in each domain documented by geological evidence have been integrated with the overall earthquakes focal mechanism datasets to reconstruct plate-scale movement vectors. The complex and contemporaneous stress-infinitessimal strain patterns we observe from this integration may provide an explanation for the heterogeneous palaeostress directions obtained from local fault and slickenline datasets.

The previously proposed polyphase models (Montenat et al., 1988; Lyberis, 1988) are not consistent with evidence that the Arabian plate motions did not change significantly at least in the last 10 Ma (Joffe and Garfunkel, 1987 and references therein); it is likely that this motion has been constant for much longer period (McQuarrie et al., 2003). It is probably significant that most of the reconstructed stress-strain fields proposed in the polyphase models are very similar to the active stress-strain fields reconstructed in this chapter.

In modern settings such as the DST, it is possible to demonstrate that the differing deformation patterns in each domain can be attributed directly to the obliquity between horizontal plate-scale motions and pre-existing block-bounding faults in the crust. The angular relationships between incremental horizontal stress/infinitesimal strain axes and horizontal displacement along the DST deviates from the typical geometry of plane strain deformation in a way that would be expected during transtensional deformation (Figs. 5.19; see also McCoss 1984, Dewey 2002 and Oldow 2003).

A transtensional model of the DST explains all the different observed deviations from a plane strain model of the boundary. The model elaborated seems consistent with the observation that zones of high subsidence, previously interpreted as pull-

aparts, cover about 70% of the total length of the margin (i.e. 300 km against 450 km). Pull-apart basins are typically developed at local bend, irregularities along a strike-slip fault, not along such a large part of the margin. Furthermore, along a plane strain transform margin, the pull-aparts should be accompanied by corresponding compressional push-ups. These structures are absent along the DST. Note however, that bends and irregularities may act as points of initial location for basin nucleation and development. Finally, if the fault patterns were associated with fault block rotations within a stress field, as shown in Figure 5.11, then fault pattern should display a fragmented character with many dextral antiriedel type-structures and different orientations of sets of blocks bounding faults as seen for example in the Basin and Range (Dewey, 2002; Oldow, 2003). This is not the case for the DST where a systematic pattern of structures is present, whose structural character is consistent with oblique extension. Nevertheless, block rotation may play an important role at small, local scale.

In conclusion, a 3-dimensional, partitioned transtensional model where the regional imposed displacement is the main parameter controlling the evolution of deformation, seems to best explain the existing datasets of the DST margin, including geodetic data and distribution and character of seismicity. In this context the fundamental assumptions that apply to plate boundaries deforming under plane strain conditions are not necessarily correct because:

a) Incremental (infinitesimal) strain axes are influenced by strain partitioning and oblique strains, so that they are likely not parallel and/or directly related to regional displacements.
b) Stress axes may not be representative of regional stress fields as their orientation and magnitude are likely controlled by local factors and partitioning of regional strain.
c) Slip vectors of main earthquakes are not necessarily parallel to plate motions since the distribution of seismicity is strongly influenced by partitioned components of the regional strain.

These considerations suggest that a different approach and methodology is required when studying plate margins developed and developing under oblique displacement conditions. This is the new approach attained in the present chapter.

6. DISCUSSION AND CONCLUSIONS

6.1 OBLIQUE DIVERGENCE: PROCESSES

Deformations associated with obliquely divergent displacements are geometrically and kinematically controlled by the angle α between the direction of divergence and the boundary faults orientation (cf Section 2.2). Even in the simplest case of homogeneous deformation this inevitably leads to a 3-D strain field and consequently, to complex and polymodal fault patterns, which may significantly deviate from the relatively simple Andersonian fault patterns developed under plane strain conditions (cf Sections 2.3 and 2.4).

The reactivation of major pre-existing structures, which often lie at an oblique angle to regional displacements, often leads to strain partitioning of the bulk strain and development of kinematically and spatially distinct, contemporaneous structural domains.

Lithological controls also play an additional important role on the development of fault patterns under 3-D transtensional strain fields.

6.1.1 3-D vs 2-D strain

Most structural, tectonic and geodynamic models are implicitly or explicitly based on the assumption of plane strain deformation. Plane strain deformation implies that:

- Deformation can be described in single 2-D cross-section or plan view
- Models are easily retrodeformed and palinspastically restored
- The mathematics is simpler
- There are few space problems, as the strain is generally more compatible
- Andersonian faulting models dominate

In contrast, 3-D deformations, cannot be fully described by single cross-sections since all of the three strain axes change length. Thus cross-sections parallel to a principal plane of strain, provide only partial information about the deformation associated with 3-D strain and may lead to underestimate the magnitude of strain or symmetry of the strain tensor and/or to misinterpret its kinematic significance.

This also means that 3-D strain models are not easily retrodeformable, and this is further complicated by the more complex fault geometries associated with transtensional deformations. The mathematics of transtensional deformations is not simple and many generalisations and assumptions are needed in order to apply this concept to real geological systems (e.g. Sanderson and Marchini, 1984; Fossen and Tikoff, 1993). These aspects tend to favour the elaboration of qualitative models of transtensional deformation and prevent quantitative analysis from being carried out in areas displaying extremely complicated fault patterns (but see Oldow, 2003; Dewey, 2002).

Strain incompatibility is one of the more controversial aspects of transtensional, and more generally 3-D strains. Dewey (2002) identified some major compatibility problems with block faulted patterns developed under transtensional strain. In particular, transtensional zones shorten almost parallel to their boundaries whilst wrenching alone cannot account for the vertical shortening. One solution to these problems is to develop fault patterns under 3-D transtensional strain that are orthorhombic but with oblique kinematics (cf Section 2.3.3, see also Reches, 1978 and 1983, Krantz, 1988 and 1989; Sagy et al., 2003). An alternative explanation (Dewey, 2002) is that wrench and normal fault systems develop synchronously and accommodate the horizontal and vertical shortening, respectively. Compatibility will dictate the kinematics, geometry, rotation, buckling and intersection relationship between the fault sets (Dewey, 2002). In these cases the main consequences are that the slip directions and stress patterns are mainly controlled by the infinitesimal 3-D transtensional strain which is controlled by the imposed bulk oblique divergence and by the compatibility requirements of the system. Block rotations may exert further controls on fault pattern development (Dewey, 2002). A third alternative (cf Section 2.2.5) is that pre-existing structures in suitable orientations undergo reactivation and partition the 3-D strain into a series of smaller domains in which the deformation lies closer to a 2-D plane-strain (De Paola et al., 2005b).

In general, faulting under 3-D strain field leads to the development of complex non-Andersonian fault patterns. 3-D fault patterns posses an higher symmetry and often, it is not easy to reconstruct the strain field associated with the faulting. The stress field associated with these type of deformations, are uncertain and subject to

perturbations that are difficult to predict and model (cf Section 2.4.3; Reches and Dieterich, 1983).

6.1.2 Lithological control on transtensional fault patterns

Homogeneous transtensional deformations have been previously modelled under the implicit assumption that rocks have the properties of an ideal incompressible material. If a Poisson's ratio $\nu = 0.5$, typical of an ideal incompressible material is used, it predicts that the switch between wrench- and extension-dominated transtension occurs at the critical value $\alpha_{crit} = 20°$. This implies that the critical angle α_{crit} for a geological system is an independent parameter.

In this thesis (and in De Paola et al., 2005a), infinitesimal transtensional strain modelling has been extended to different rock types, i.e. for different Poisson's ratios typical of each lithology. The assumption $\nu \neq 0.5$, implies that fault initiation under transtensional strain will be associated with a positive volume change, (i.e. uniaxial tension). The main effect obtained by including the real values of Poisson's ratio (for most rocks $\nu \approx 0.25$ - 0.3) is to widen the field of wrench-dominated transtension ($\alpha_{crit} \approx 33°$ - $38°$). The only exception to this occurs in quartz-rich lithologies (i.e. sandstones), which display very low values of the Poisson's ratio and consequently exhibit the highest values of critical angles, which in the case of 90% of quartz content, can reach 52°.

Sedimentary sequences with interbedded quartz-rich rock units, deformed under transtensional strain, may thus experience significantly heterogeneous strain states, leading to the development of spatially and kinematically heterogeneous fault patterns within immediately adjacent lithological layers. An example of this phenomenon has been observed in the hangingwall of the 90-Fathom Fault (interbedded quartz-rich sandstones and dolostones), NE England (cf Chapter 3 and De Paola et al., 2005a).

These findings have significant implications for structural models of fracture interconnectivity and fluid flow in hydrocarbon reservoirs. In the case of the 90-Fathom Fault, it is likely that based on multiple flow directions will occur along the intersections between the various fault sets formed under 3-D strain conditions. By recognising such complexity and incorporating it into permeability models of a

fractured reservoir, a more reliable and realistic prediction of fluid flows should be possible.

6.1.3 Reactivation and strain partitioning

Recent studies of tectonically active areas undergoing transtensional deformations have revealed the presence of structural domains characterized by different patterns of seismicity (e.g. Basin and Range and Sierra Nevada region, USA, in Dewey, 2002; Oldow, 2003). In these examples, it is evident that strain partitioning gives rise to fault patterns that are contemporaneous, but heterogeneous in terms of their geometry, kinematics and spatial distribution. The domainal fault patterns and associated seismicity seem to correspond well with the heterogeneous orientation of the velocity fields displayed by GPS measurements. In fact, geodetic data confirm the existence of multiple velocity fields, contemporaneously active within each deforming area. They can be interpreted as the result of strain partitioning arising from interaction between regional displacements and pre-existing regional structures such as faults, basement fabrics, etc. which form long-lived zones of weaknes. Active areas are particularly good natural laboratories in which to test strain partitioning models since the timing of deformation is unambiguous. In addition, the local displacement components can be directly measured with earthquakes providing a direct measure of infinitesimal strain/stress fields. The recognition of strain partitioning in ancient areas is more difficult as it may not be possible to unambiguously resolve the temporal relationships between the different fault sets in adjacent domains.

In the present study, it is shown that strain partitioning is likely to be very common in both ancient and modern examples of transtension zones, leading to local structural complexity that is not necessarily of regional (e.g. plate-scale) significance. In modern settings such as the DST, it is possible to demonstrate that the differing deformation patterns in each domain can be attributed directly to the obliquity between horizontal plate-scale motions and pre-existing block-bounding faults in the crust. The angular relationships between incremental horizontal stress/infinitesimal strain axes and horizontal displacement deviates from the typical geometry of plane strain deformation in a way that would be expected during transtensional deformation (see also McCoss, 1984; Dewey, 2002; Oldow, 2003). In ancient

terrains such as the Northumberland Basin, the far-field regional transport direction is generally unknown, but it can be reconstructed from the partitioned components of strain recognised within contemporaneously active, kinematically-different and spatially distinct structural domains. These components can be calculated using the predictable geometric and kinematic relationships that exist for transtension between the orientations of the infinitesimal strain (stress) axes and the deformation zone boundaries (McCoss, 1984). In the case of the Northumberland basin, the location and orientation of these boundaries is very strongly influenced by the presence of pre-existing structures in the crustal basement. Note that the contemporaneous nature of faulting in the different domains of the Northumberland basin was revealed in each domain by: a) the syn-tectonic intrusion of units of the Whin Sill complex and b) with mineralization episodes that are contemporaneous with faulting.

Major uncertainty exists about the absolute value of the partitioned components of ancient deformations. In most cases, the ratio between the partitioned components can be only approximately estimated from strain intensity in the adjacent domains. In such circumstances, rather than the plate motion vector, it is only possible to constrain an angular sector, that separates the end-member partitioned components, where the plate motion vector likely lies.

6.2 POLYPHASE DEFORMATION AND INVERSION: NOT SO COMMON AFTER ALL?

The recognition of contemporaneous deformation domains that partition 3-D non-coaxial transtensional strains on different scales allows significantly different interpretations to be made of crustal faulting patterns in obliquely divergent zones. Thus many existing models explained the late Carboniferous pattern of deformation in the Northumberland Basin in terms of polyphase deformation with pulses of extension and contraction/basin inversion events every few millions years (e.g. Leeder et al., 1989; Collier, 1989; Bower, 1990). The alternative basement-controlled partitioned transtensional model proposed in this thesis allows a more straightforward interpretation consistent with the regional N-S rifting recognised on a plate scale right across NW Europe at the end of the Carboniferous (cf Chapter 4).

In the presence of markedly domainal patterns of faulting and strain distribution, it is therefore absolutely critical that the age constraints and kinematic links between the different domains should always be tested before polyphase deformation is invoked. This is most straightforward when considering neotectonic, seismically active regions such as the DST boundary where the plate kinematics are already known. In our analysis of the DST, the local stress-strain distributions in each domain documented by geological evidence have been integrated with the overall earthquakes focal mechanism dataset to reconstruct plate-scale movement vectors. The complex and contemporaneous stress-infinitesimal strain patterns we observe from this integration may provide an explanation for the heterogeneous palaeostress directions obtained from local fault and slickenline datasets. These were previously interpreted as indicating a polyphase structural evolution (Montenat et al. 1988, Lyberis 1988), cf. previous interpretations of the Northumberland Basin. It is probably significant that most of the reconstructed stress-strain fields proposed in the polyphase models (Montenat et al. 1988, Lyberis 1988) are very similar to the active stress-strain fields reconstructed in this work.

Most basin evolution models and analyses assume an explicit link between inversion/uplift events and compressional or transpressional tectonic episodes. This inevitably leads to more complex regional tectonic models. The model presented in this thesis, for both case studies, of strain partitioning during a single and possibly protracted phase of regional transtension, removes this unnecessary and unrealistic link between tectonic complexity on local and regional scales, whilst still emphasising the important role of basement control on deformation patterns. The findings are in accord with the evidence that plate motions, as inferred for modern plate boundary, are often constant over long time periods, suggesting that heterogeneous fault patterns often are not caused by continuous changes in plate motion vectors.

6.3 STRESS vs STRAIN: WHAT CONTROLS KINEMATICS OF DEFORMATION AND GEOMETRY OF FAULTING?

The orientation and nature of the infinitesimal strain axes (i.e. stress axes), in the case of homogeneous transtension, are a function of the orientation of the far field

displacement vector relative to the boundary fault zone (angle α). Depending on the value of the angle of divergence α, the finite strain tensor may not show the same nature of the infinitesimal strain tensor (e.g. wrench-dominated transtension for $\alpha < 30°$). This implies that, even if unstable, infinitesimal strain fields are related to regional displacements whilst finite strains may not necessarily have a direct relationship with the far field displacements. As a consequence, finite strain axes should never be directly related to regional stress fields, and should never be assumed to be parallel to plate motions or regional displacements, unless 2-D plane strain can be proved (Dewey et al., 1998, Tikoff and Wojtal, 1999). Nevertheless infinitesimal strain axes (i.e. stress axes) are a powerful tool in the reconstruction of the far field displacement in ancient deformations provided the boundary conditions of the system are known and if 3-D strain analysis principles are applied.

In the case of strain partitioning, we cannot always reliably assume that infinitesimal strain or stress axes resolved in one part of a study area are parallel to regional transport directions, unless their relationship to the deformation patterns in adjacent crustal domains is also considered. Importantly, the fundamental assumptions that apply to plane strain deformations are not necessarily verified in the presence of partitioned 3-D transtensional strain since:

- Heterogeneously distributed strain velocity fields are not parallel to regional movements since they form in response to interactions between local factors, such as reactivation of pre-existing faults, and far field displacements.
- Stress/infinitesimal strain axes are not representative of regional stress/strain field. The regional strain field is obtained from the integration of all different partitioned components of displacement reconstructed from local strain fields.
- Slip vectors of main earthquakes and kinematics associated with main faults are not necessarily parallel to plate motions since the distributions of seismicity and fault reactivation may be themselves strongly influenced by partitioned components of regional strain.

If these aspects are not taken into consideration, they can lead to misunderstandings concerning the regional meaning of the bulk strain and nature of the tectonic regime (Dewey et al., 1998; Tikoff and Wojtal, 1999). Given the generally domainal

character of deformation and faulting in transtension zones, the scale of observation is crucially important.

In this study, it is demonstrated how the internal geometry and kinematics of the Northumberland Basin and DST margin is best explained by 3-D transtensional bulk strain. In both cases, however, the deformation is partitioned so that the regional plate motion is not parallel to the local displacement components accommodated by the fault systems within spatially distinct structural domains. The geometric analyses we have applied imply that the observed partitioning of the deformation is primarily controlled by the kinematic boundary conditions, i.e. the angular relationships between plate motion vectors, plate boundaries and pre-existing intraplate structures, and not by regional stress.

In conclusion, we note that the only parameter not affected by the orientation of pre-existing structures accommodating local deformation, seems to be the regional imposed displacement.

6.4 APPLICATIONS

The findings concerning the lithological controls on faulting patterns at the reservoir scale, are particularly significant when it is considered that they apply to lithologies such as quartz-rich sandstone that are very common reservoirs rock types. Faulting patterns developed under 3-D strain are more complex than plane strain "Andersonian" patterns, leading to highly compartmentalized reservoirs. Within sandstones these faults may well be deformation bands with a permeability that is 2-3 orders of magnitude lower than the surrounding undeformed rocks, which may account for low productivity that is observed in many sandstone reservoirs (Olsson et al., 2004 and references therein). Fault patterns developed under 3-D strain conditions also present preferential migration fluids paths in directions different to those suggested by conventional plane strain models.

The structure of an oblique rift basin varies considerably in three-dimensions and may have significant implications in terms of potential trap development. Oblique rift systems are associated with potential traps not found in other rifts. Examples include: footwall fault blocks bounded by normal faults on four sides (quadrimodal faulting); combined strike-slip and normal fault block traps; en echelon fault systems; folds created during the transtensional (constrictional) strain.

There are special reasons why oblique rift basins are favourable for hydrocarbon generation and accumulation, and reasons why they are not. Isolation from the open ocean system and anoxia are favoured by the typically low length to width ratios of oblique rift systems, which in turn favours the generation of source rocks during times that are not necessarily source-prone on a global scale (Mark Allen, pers. comm., 2004). Oblique rift fault systems often have to re-organise to accommodate the regional velocity field. Fault reorganizations lead to changes in drainage patterns that can use complex syn-rift stratigraphies. Unfortunately, short-lived, localised drainage systems do not favour the accumulation of large volumes of good quality reservoir sands. This can create possibilities for the generation and migration of hydrocarbons, but can also lead to small or breached traps and localised reservoirs.

APPENDICES*

Northumberland Basin Dataset

*Data plotted on equal area lower hemisphere projection

STRUCTURAL MAP OF THE NORTHUMBERLAND BASIN AND OUTCROPS LOCATION

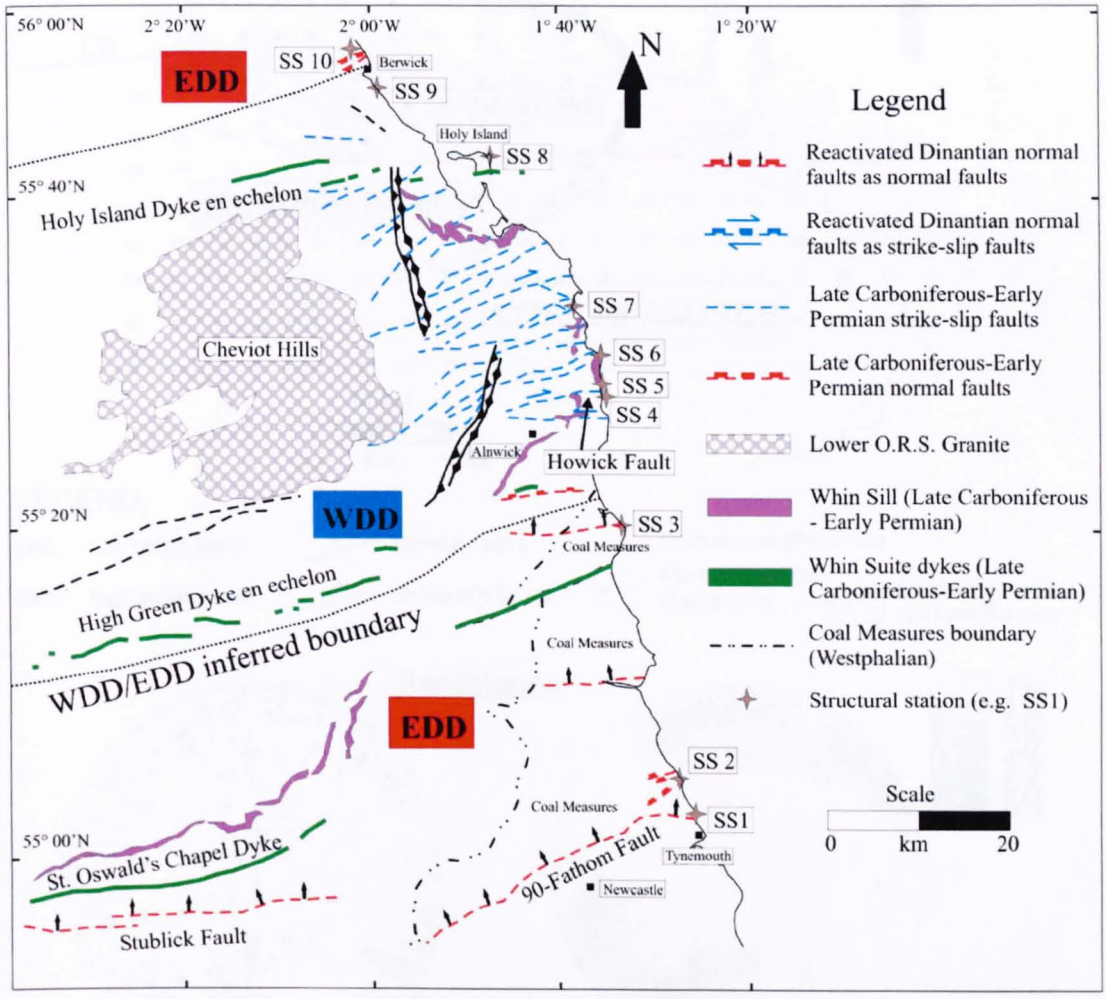

Ss1: CULLERCOATS

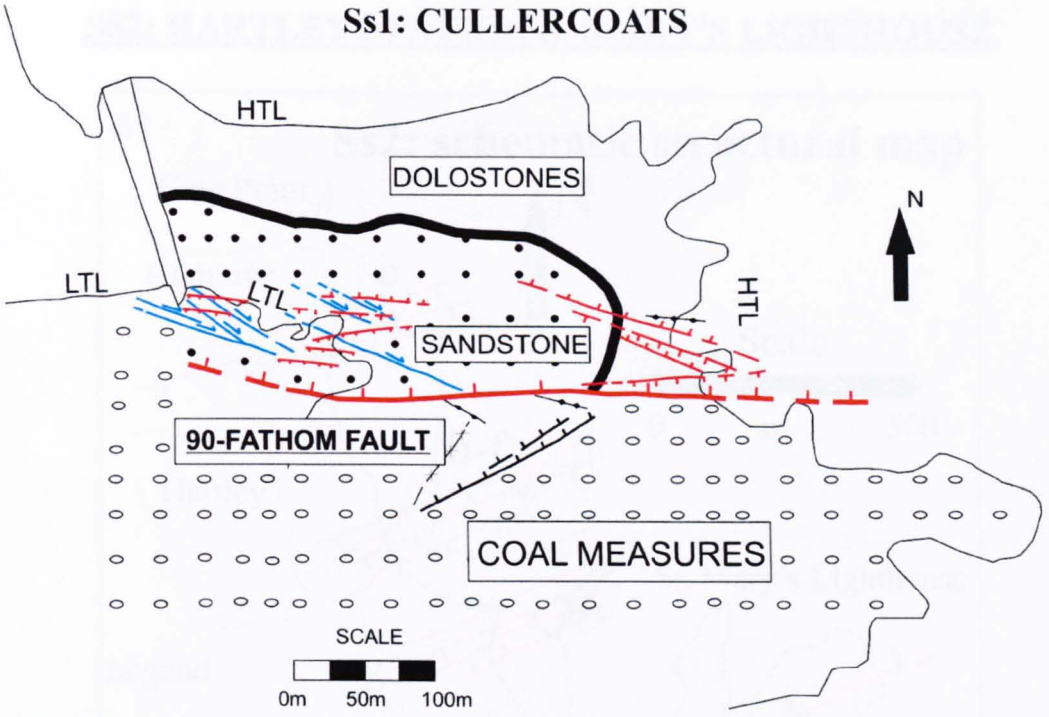

LEGEND

LWL low water level

HWL high water level

Normal faults

Strike-slip faults

Dolostones (Permian)

Permian Yellow Sandstone

Coal Measures (Carboniferous)

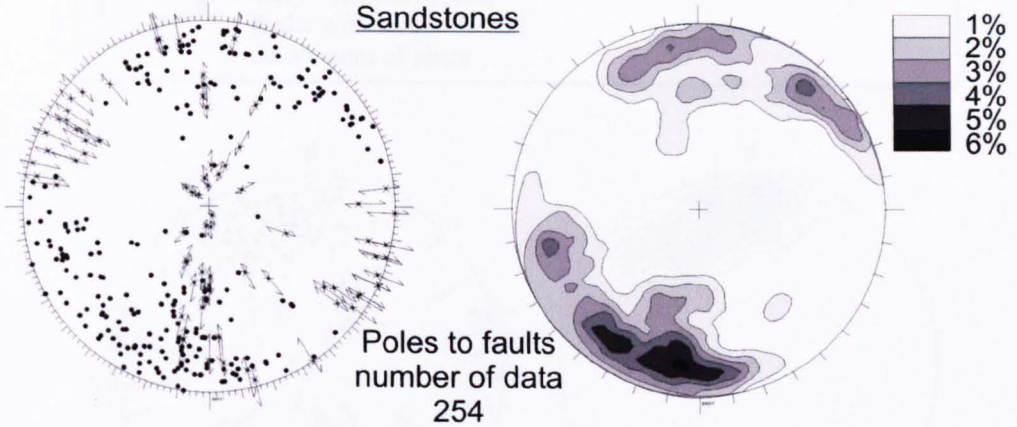

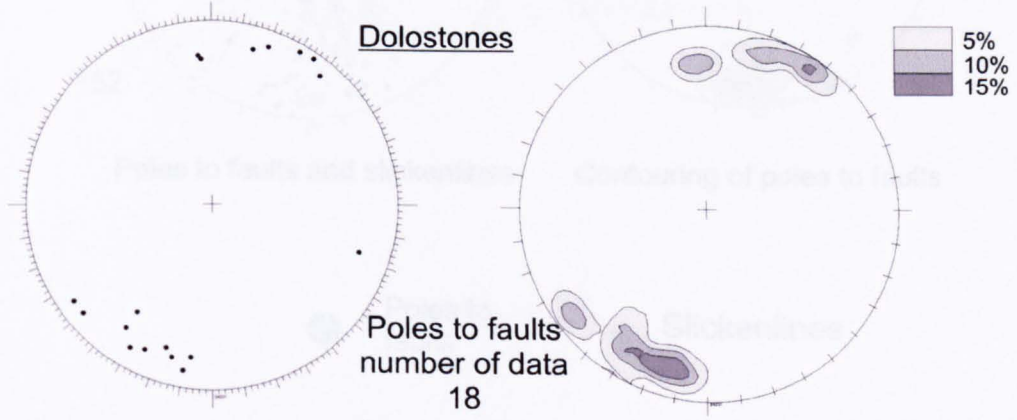

• Poles to faults

Slickenlines with sense of shear

SS2: HARTLEY STATION-S. MARY'S LIGHTHOUSE

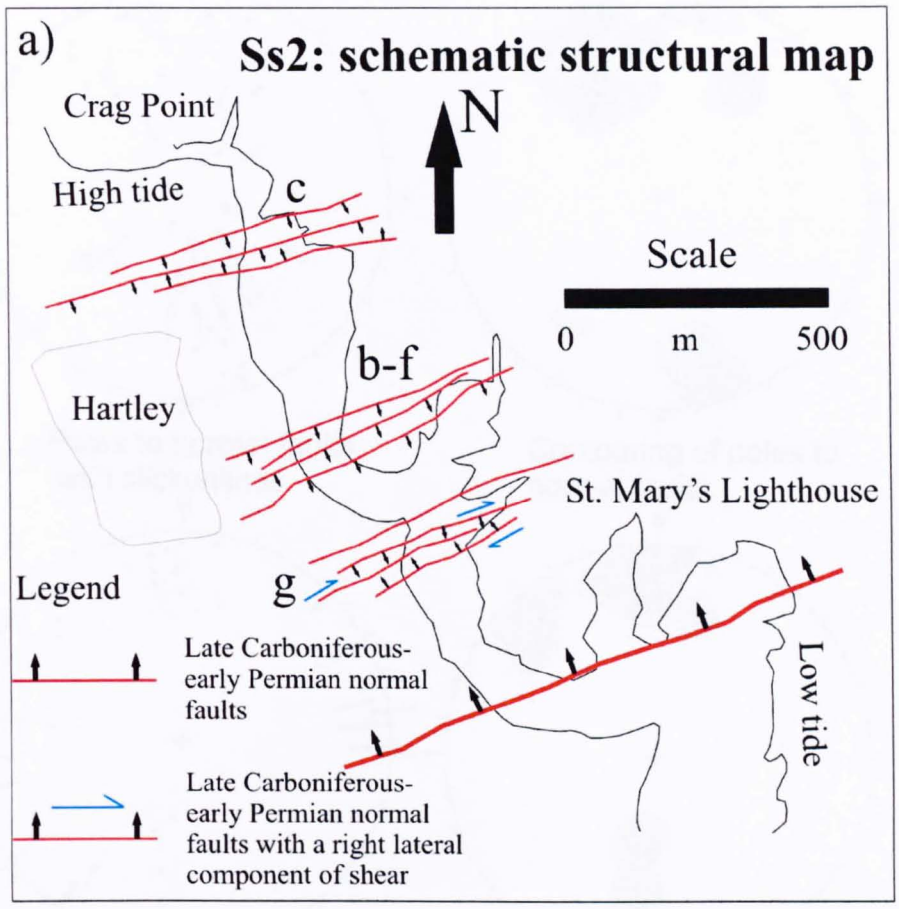

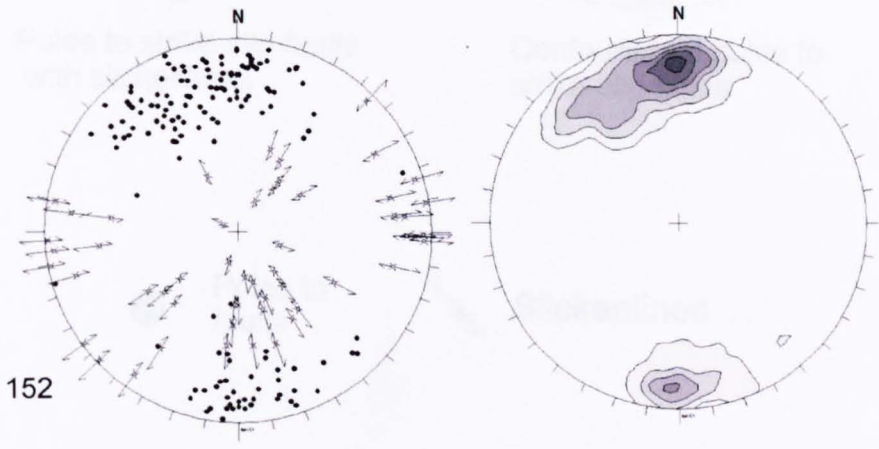

Poles to faults and slickenlines

Contouring of poles to faults

Poles to faults

Slickenlines

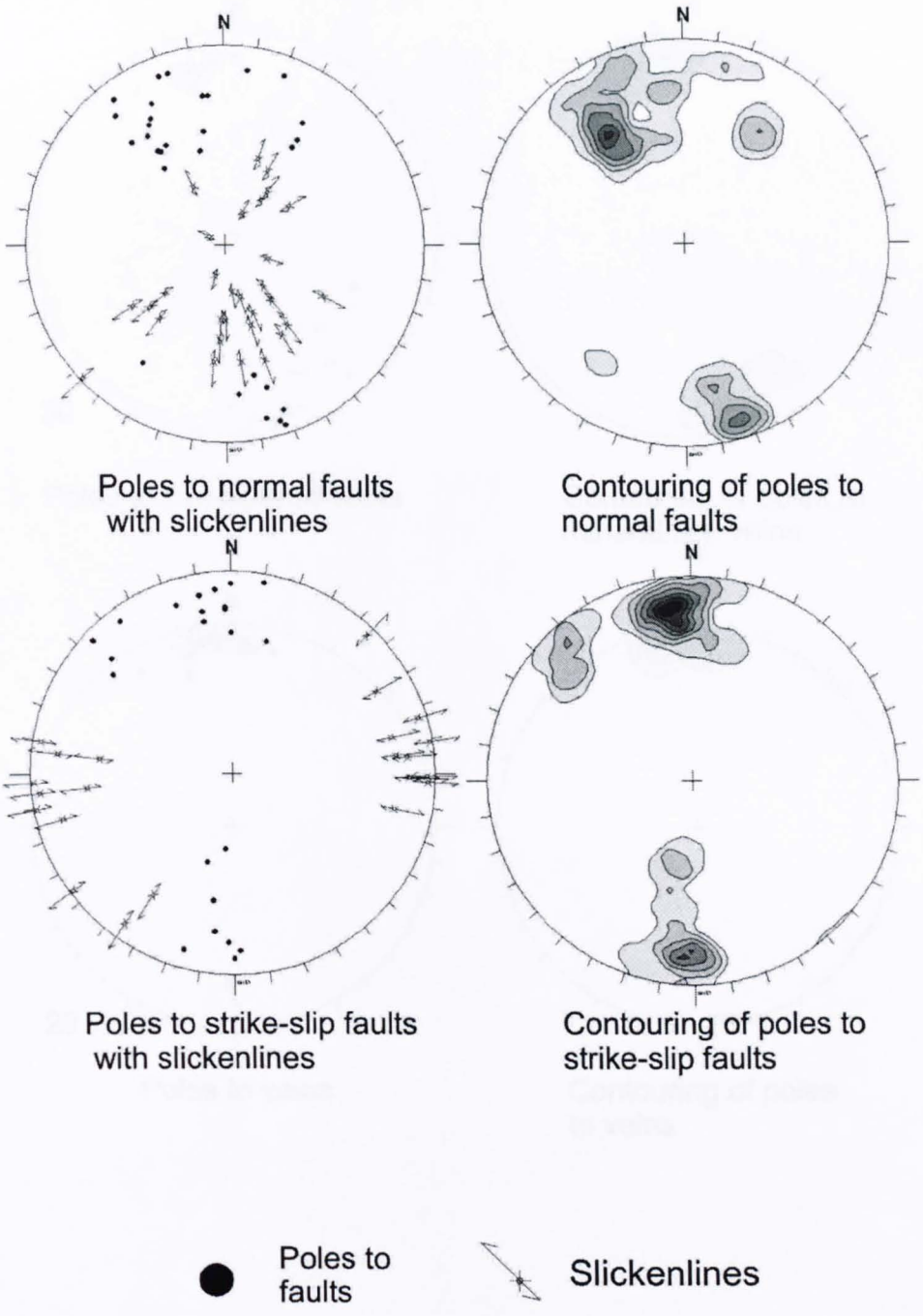
N
N
Poles to normal faults with slickenlines
Contouring of poles to normal faults
N
N
Poles to strike-slip faults with slickenlines
Contouring of poles to strike-slip faults
Poles to faults
Slickenlines

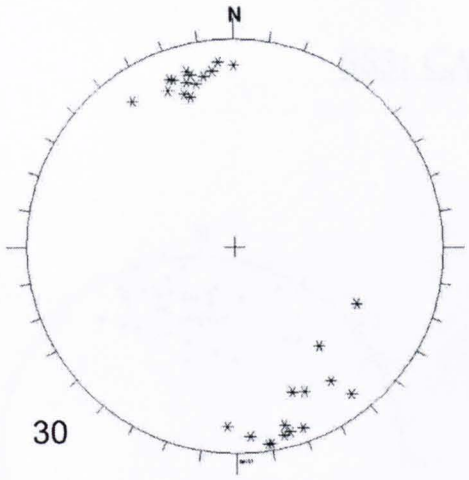

Poles to mineralized veins

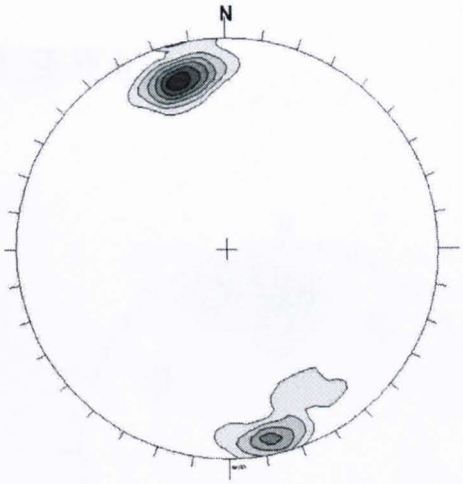

Contouring of poles to mineralized veins

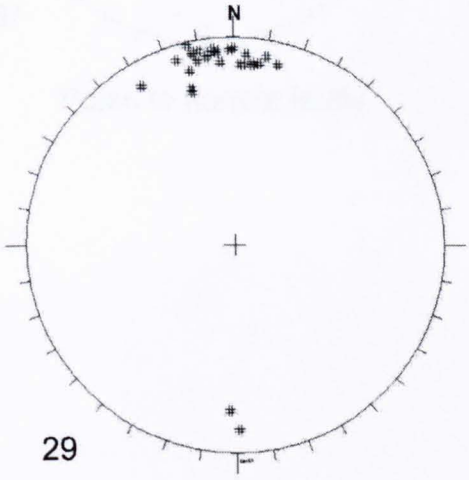

Poles to veins

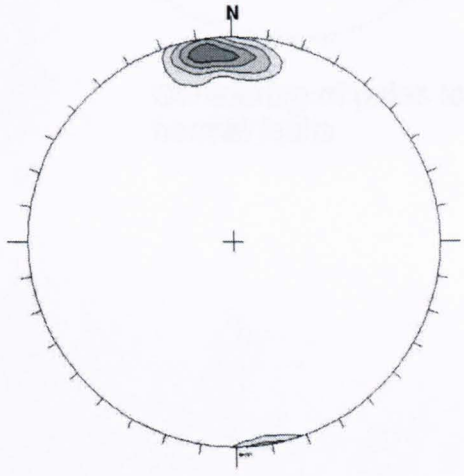

Contouring of poles to veins

SS3: CAUSEWAY

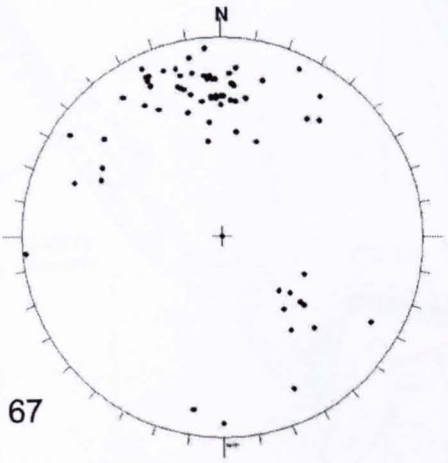

Poles to normal faults

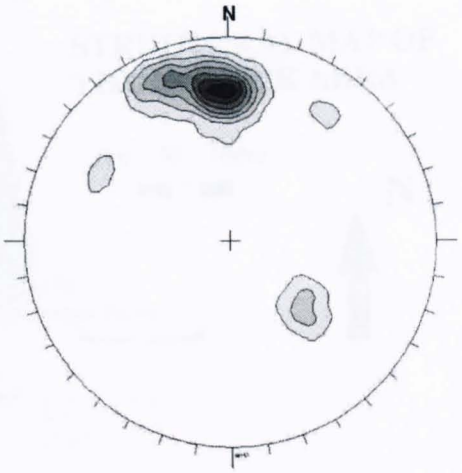

Contouring of poles to normal faults

SCHEMATIC STRUCTURAL MAP OF THE HOWICK AREA

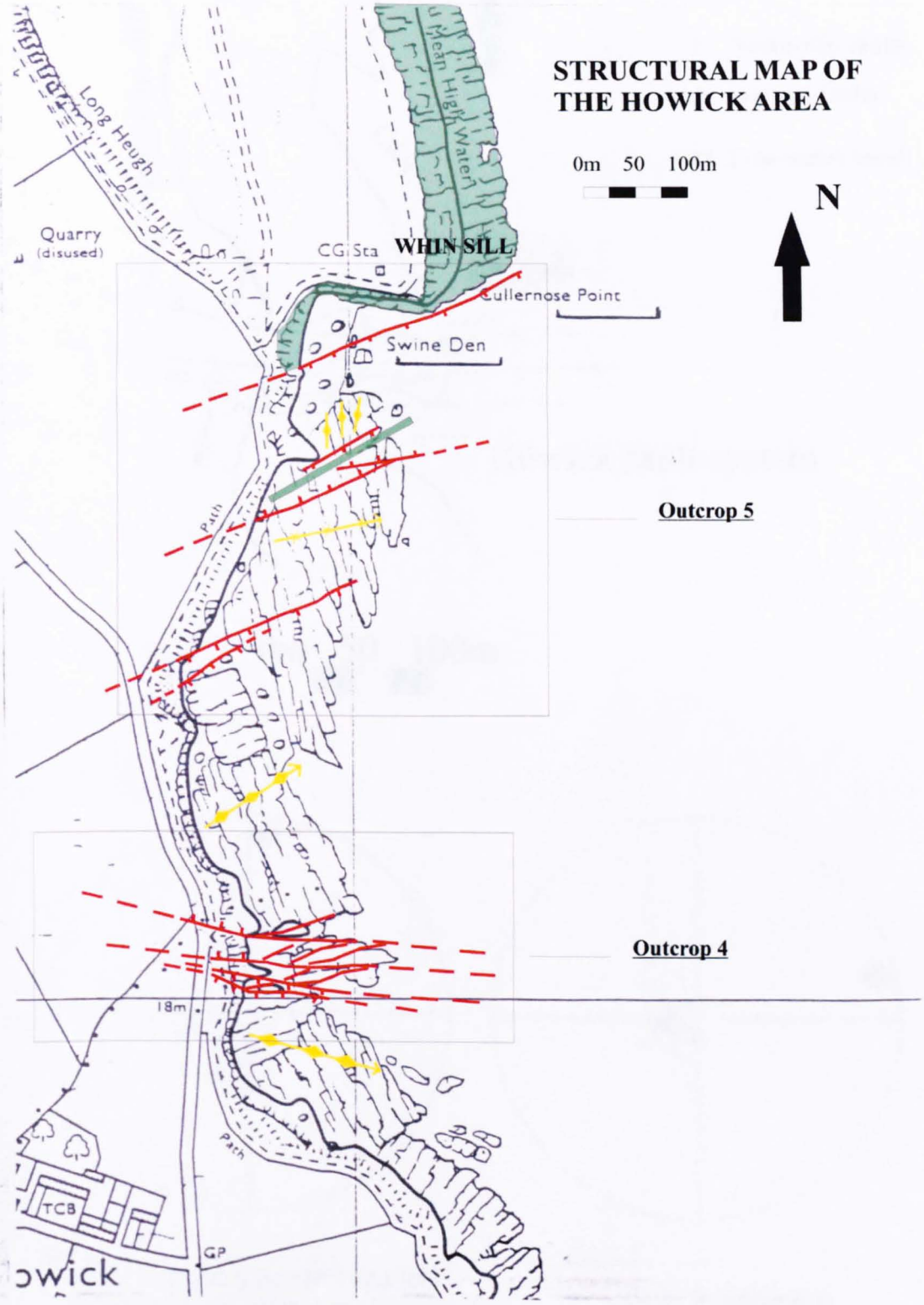

SS4: HOWICK

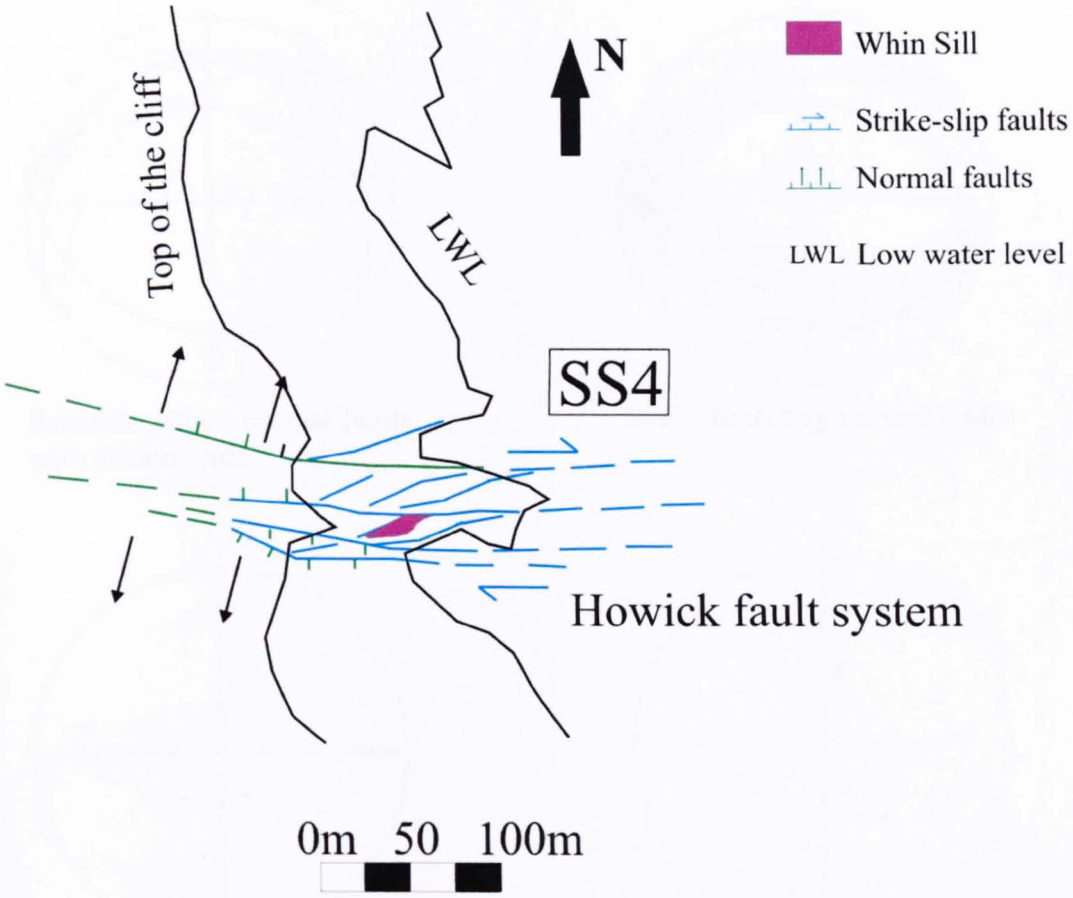

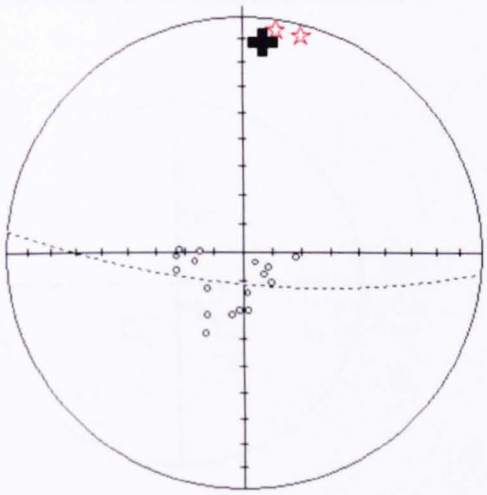

Poles to bedding (circles) and fold hinges (red stars) between reactivated synsedimentary normal faults

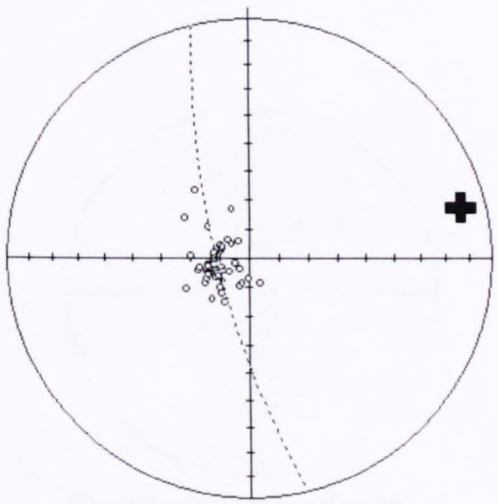

Poles to bedding in undeformed rocks

SYNSEDIMENTARY NORMAL FAULTS

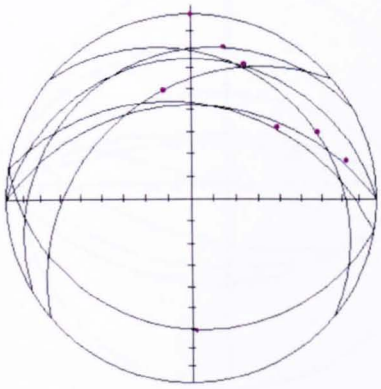

Synsedimentary normal faults with slickenlines

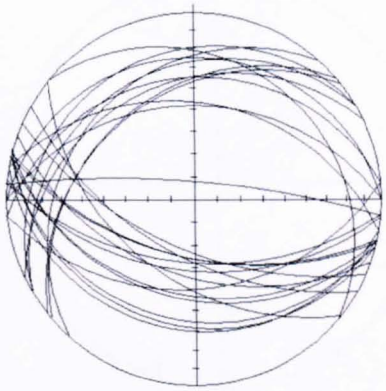

Synsedimentary normal faults

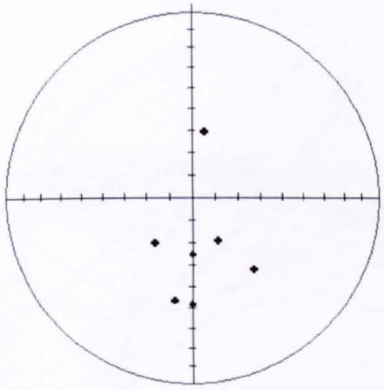

Poles to synsedimentary normal faults with slickenlines

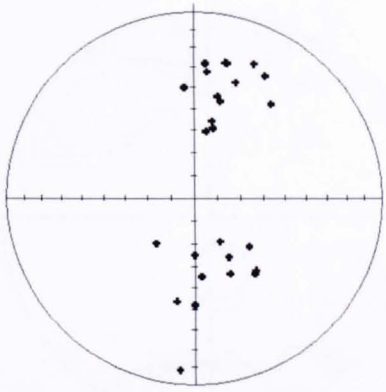

Poles to synsedimentary normal faults

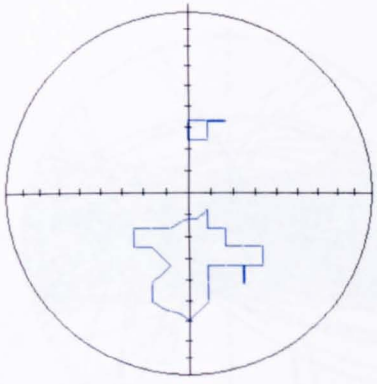

Contouring of poles to synsedimentary normal faults with slickenlines

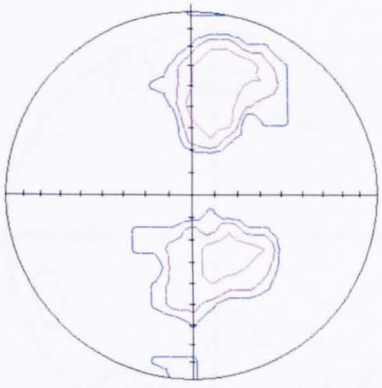

Contouring of poles to synsedimentary normal faults

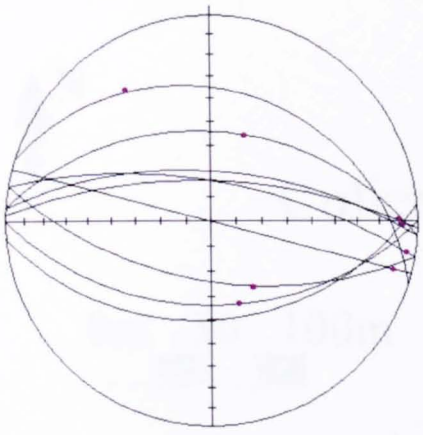

Principal reactivated strike-slip faults

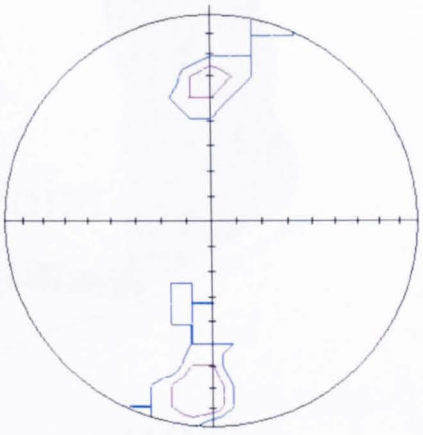

Contouring of poles to principal faults

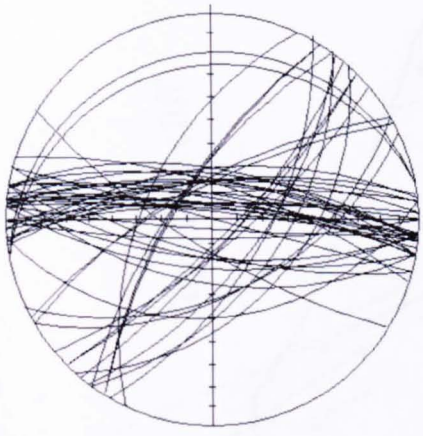

Shear planes between the principal faults

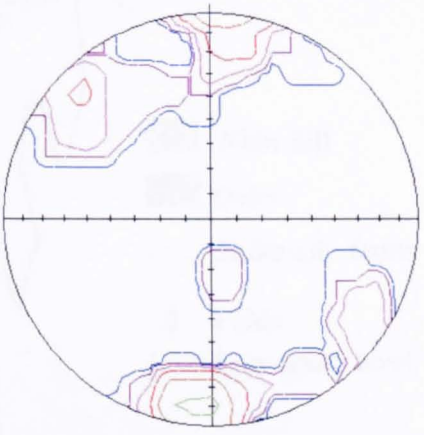

Contouring of poles to shear planes between the principal faults

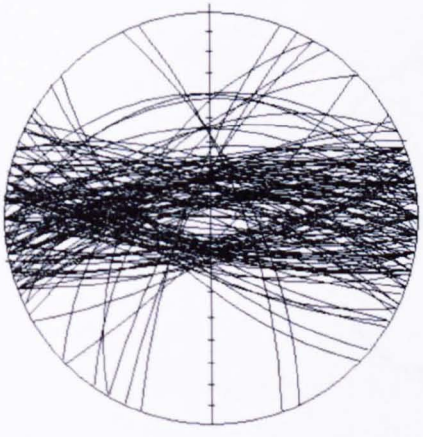

Veins

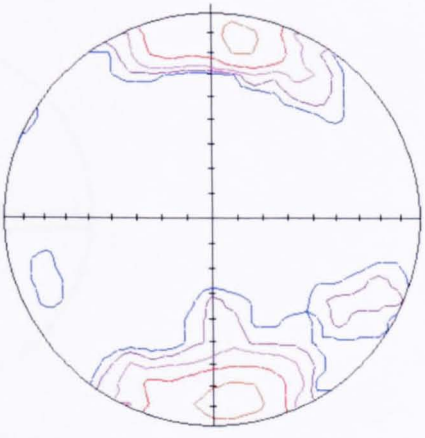

Contouring of poles to vein

SS5: CULLERNOSE POINT

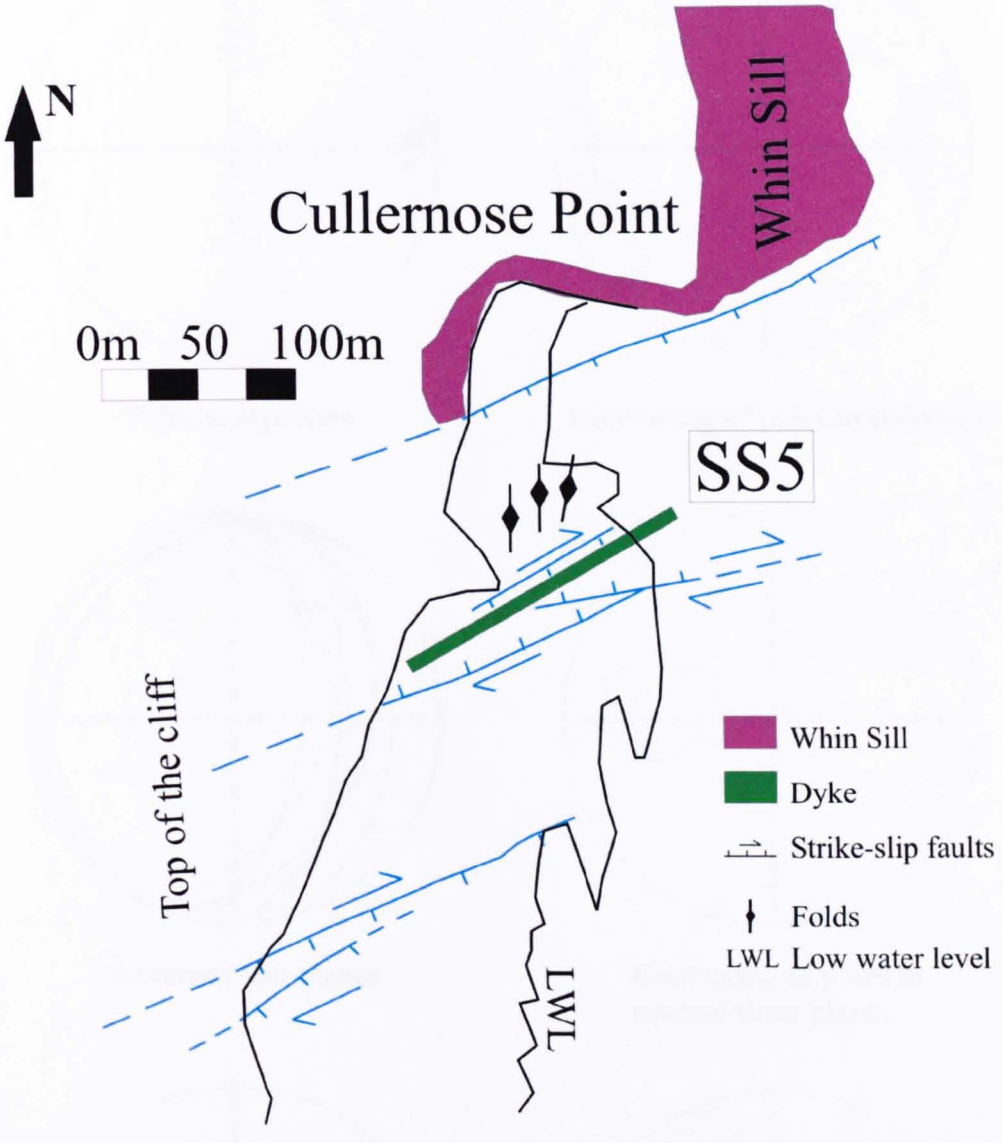

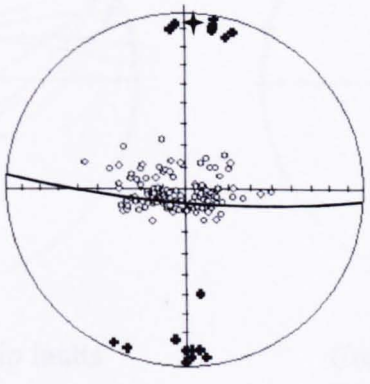

Poles to bedding (circles)
and fold hinges (crosses)

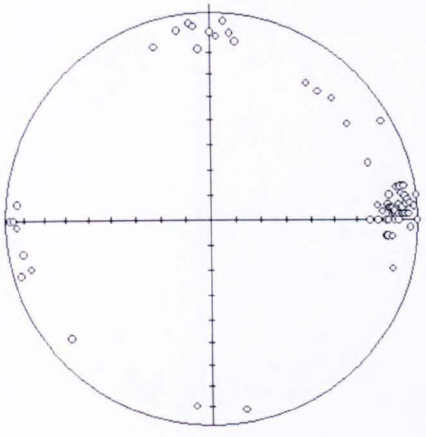

Poles to stylolites

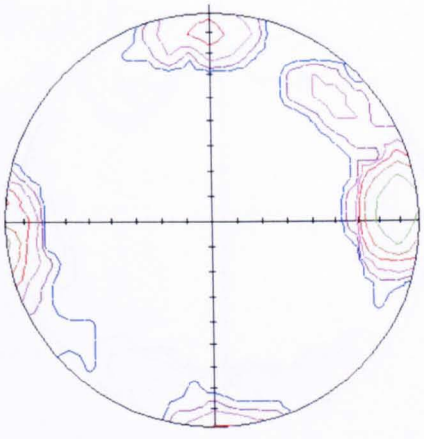

Contouring of poles to stylolites

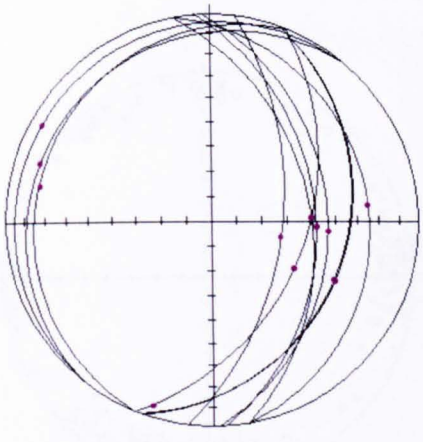

Reverse shear planes

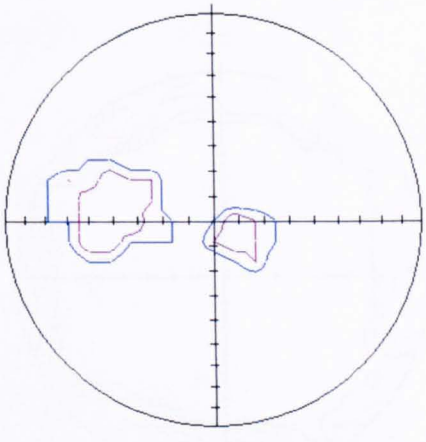

Contouring of poles to
reverse shear planes

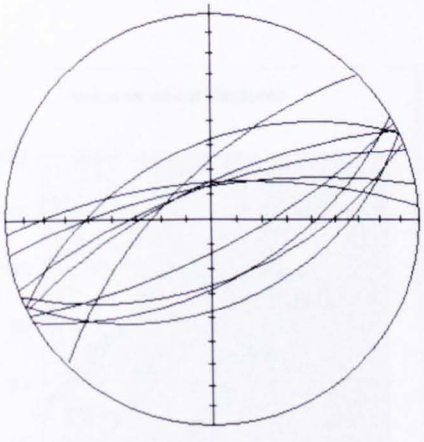

Principal strike-slip faults

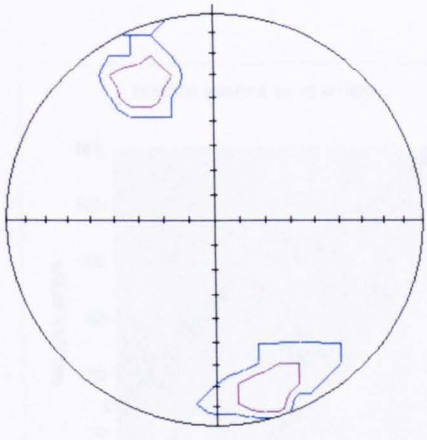

Contouring of poles to
principal strike-slip faults

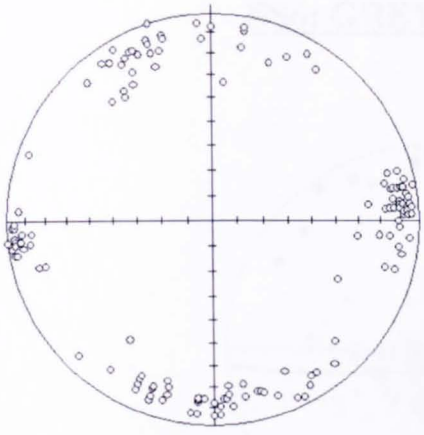

Poles to strike-slip shear planes

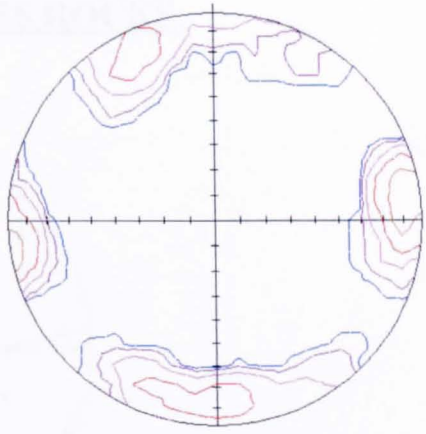

Contouring of poles to strike-slip shear planes

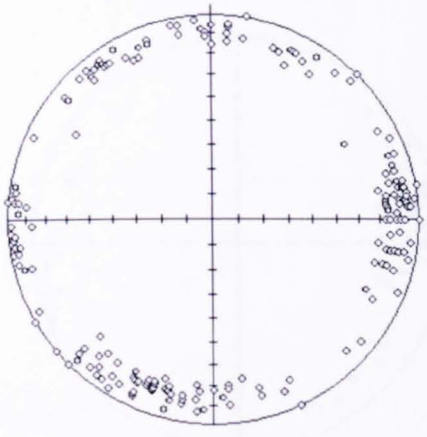

Poles to veins

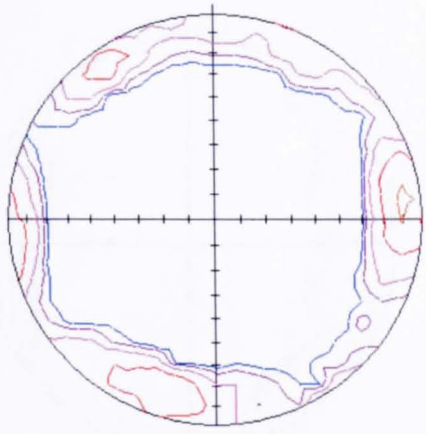

Contouring of poles to vein

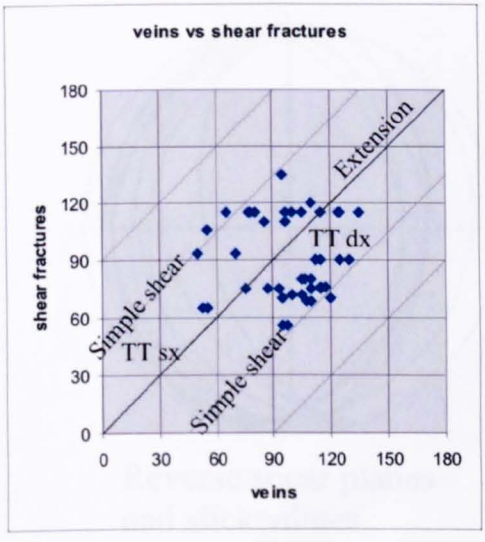

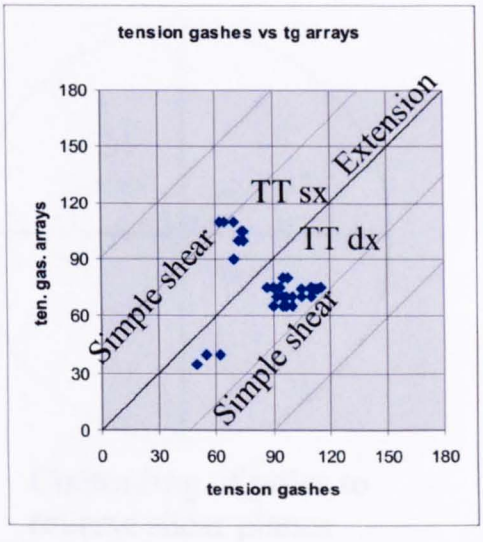

SS6: GREY MARES ROCKS

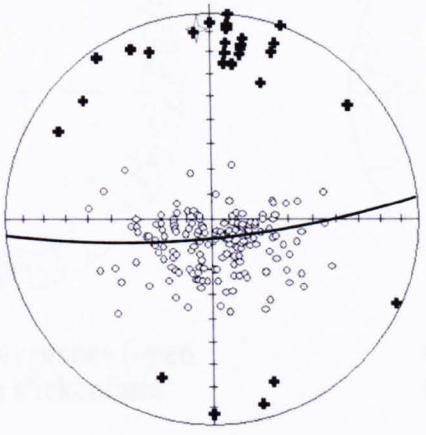

Poles to bedding(circles) and fold hinges (crosses)

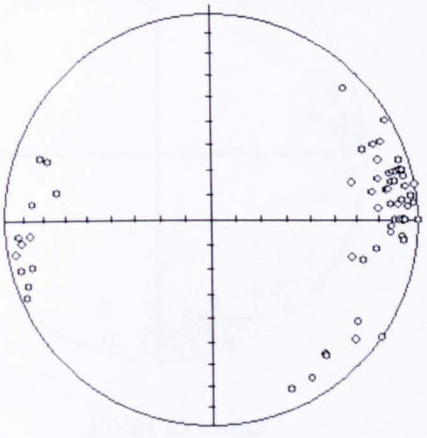

Poles to stylolites

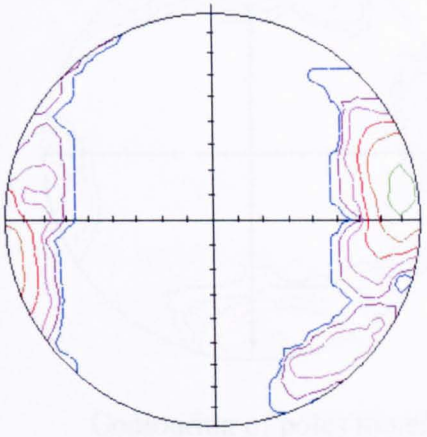

Contouring of poles to stylolites

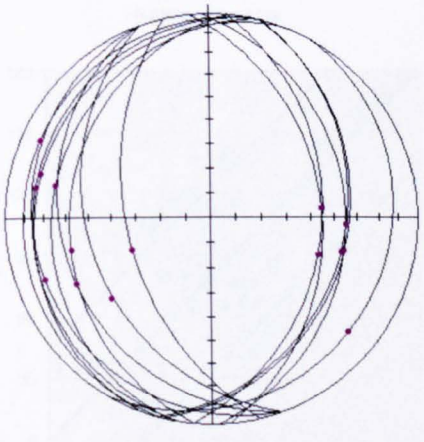

Reverse shear planes and slickenlines

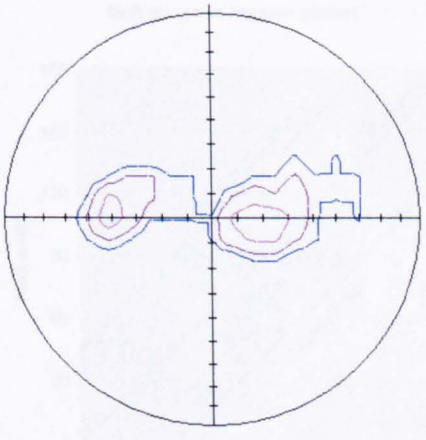

Contouring of poles to reverse shear planes

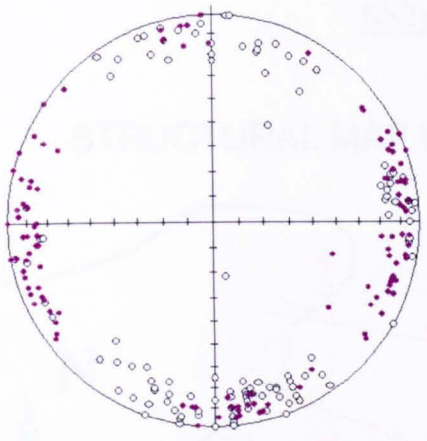

Poles to shear planes (open circles) with slickenlines

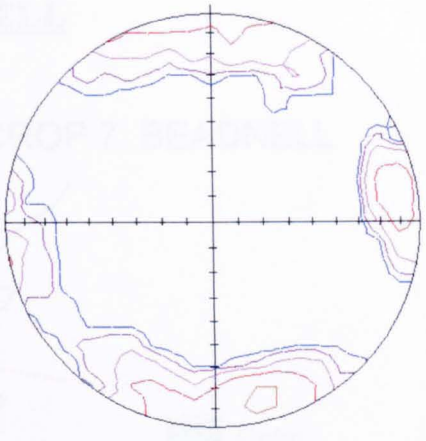

Contouring of poles to shear planes

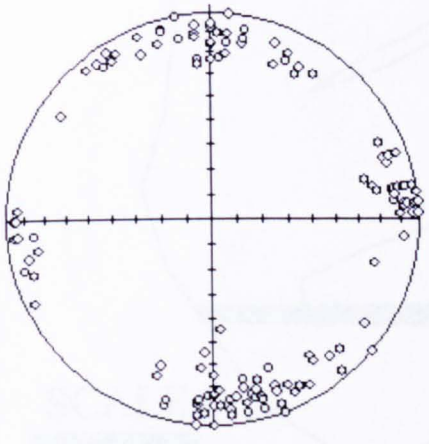

Poles to veins

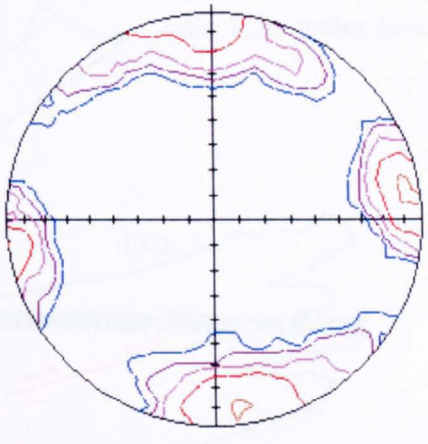

Contouring of poles to veins

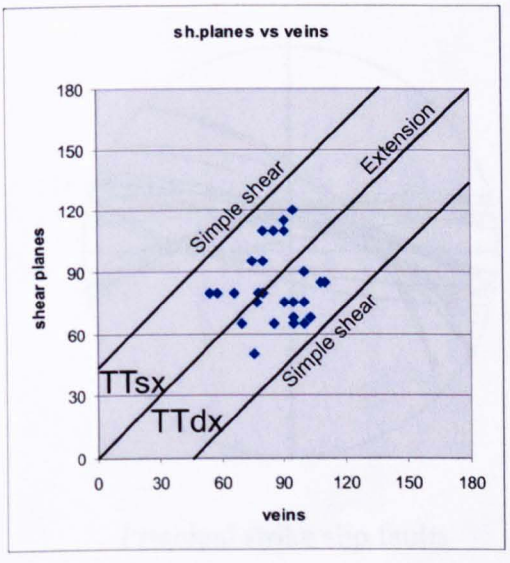

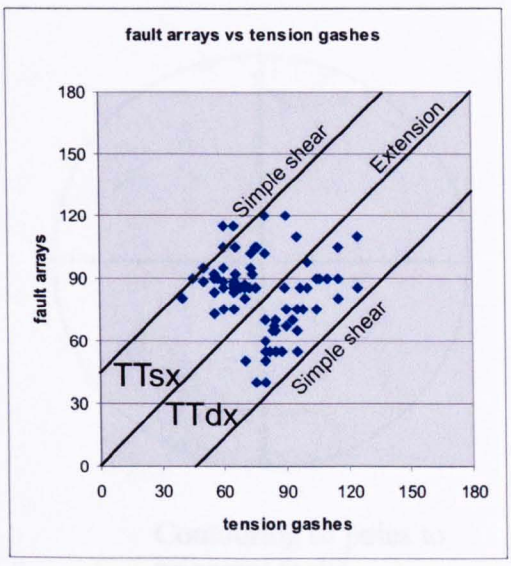

SS7: BEADNELL

STRUCTURAL MAP OF OUTCROP 7: BEADNELL

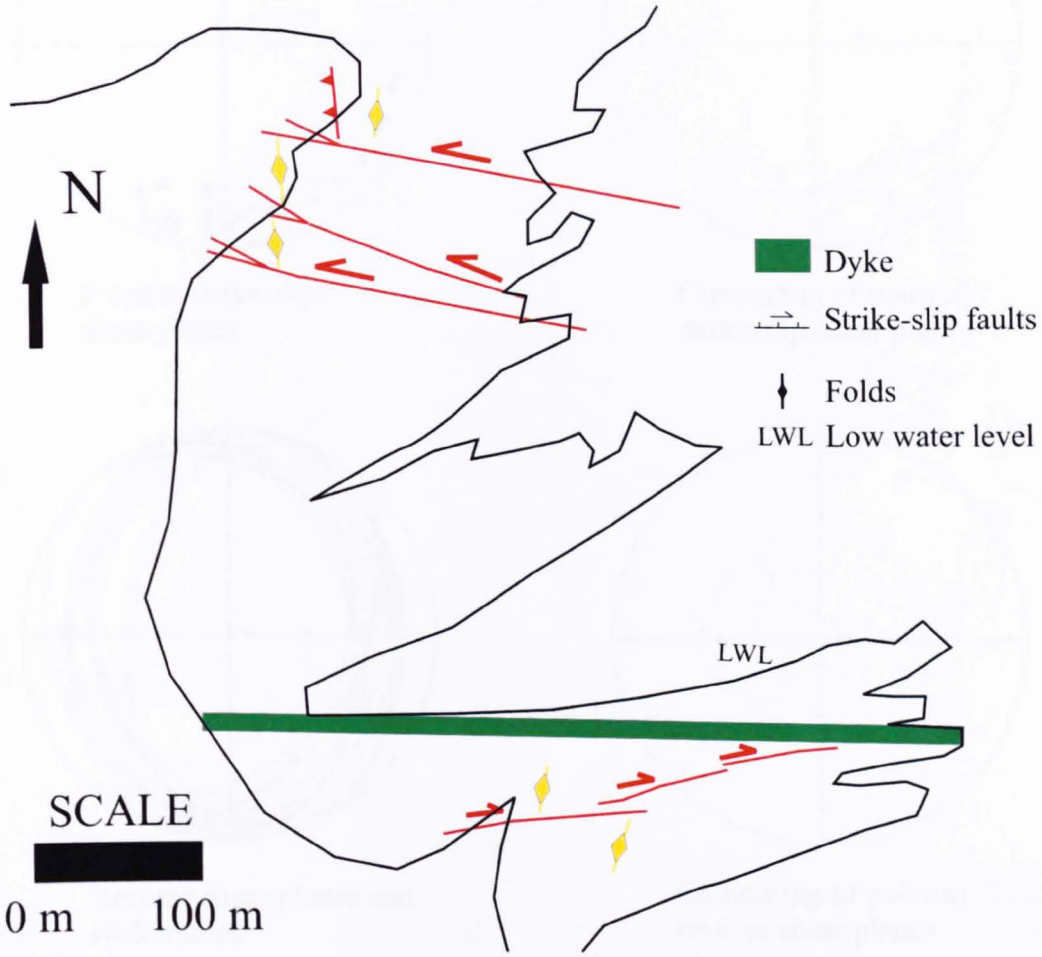

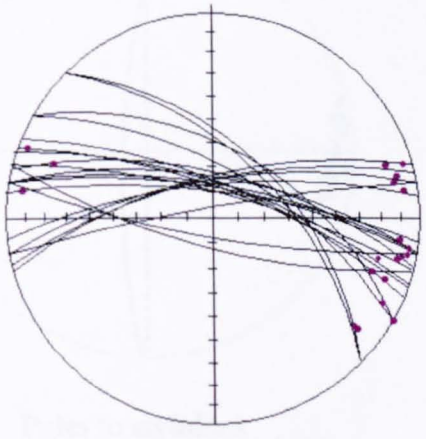

Principal strike slip faults

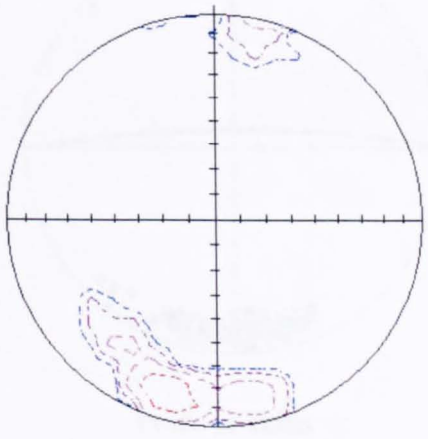

Contouring of poles to principal faults

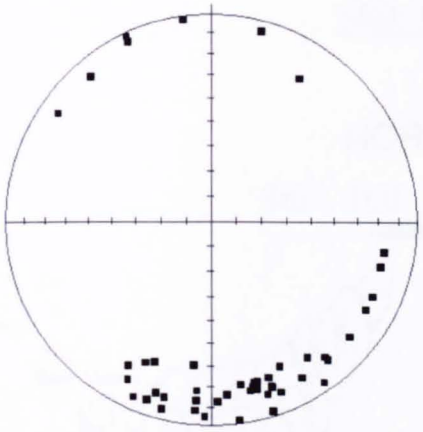

Poles to strike-slip shear planes

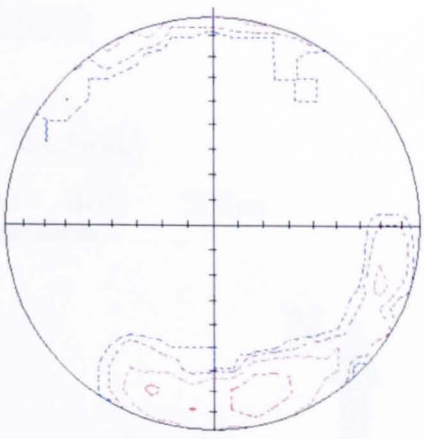

Contouring of poles to strike-slip shear planes

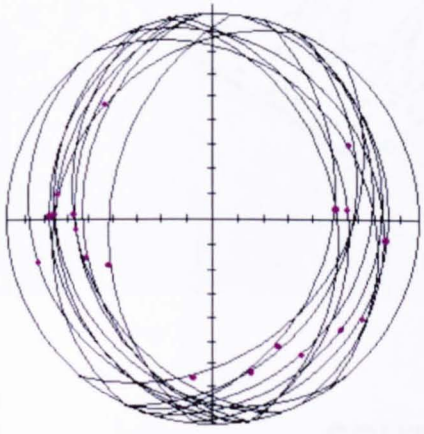

Reverse shear planes and slickenlines

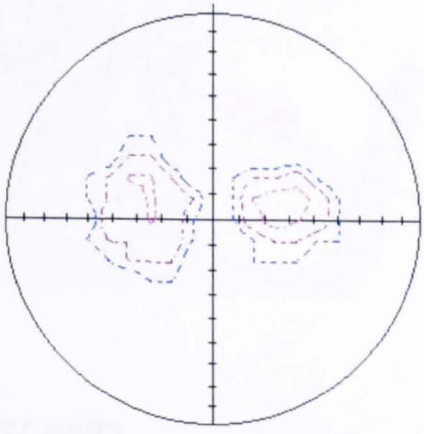

Contouring of poles to reverse shear planes

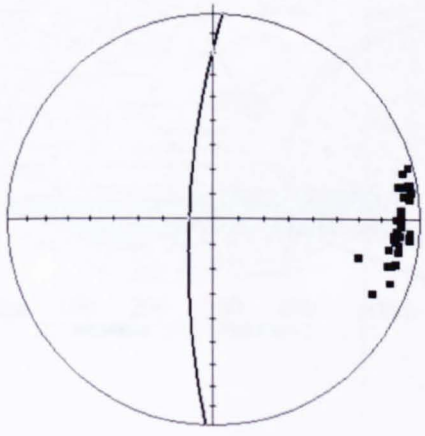

Poles to stylolites

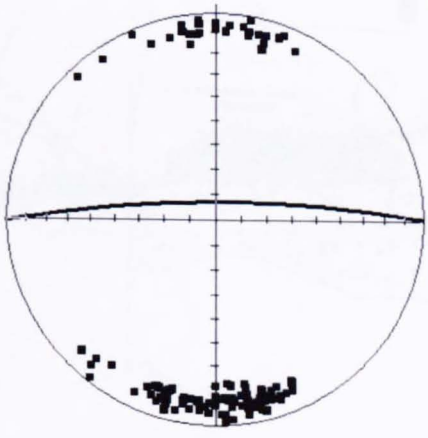

Poles to veins

SS8: HOLY ISLAND

NORTH HOLY ISLAND

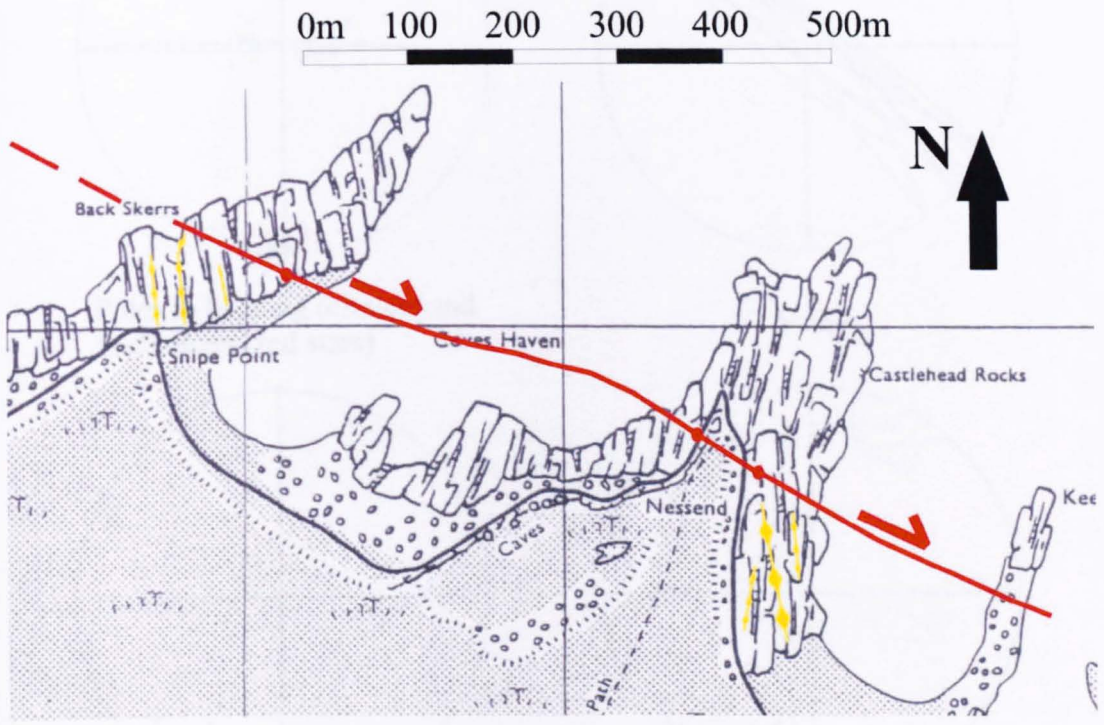

SOUTH HOLY ISLAND

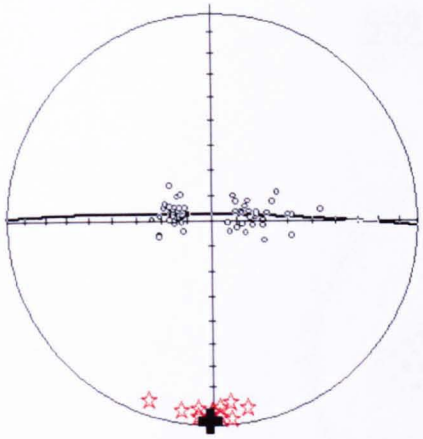

Poles to bedding (circles) and fold hinges (red stars)

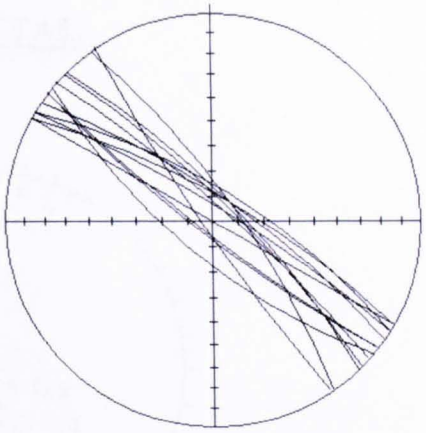

Veins

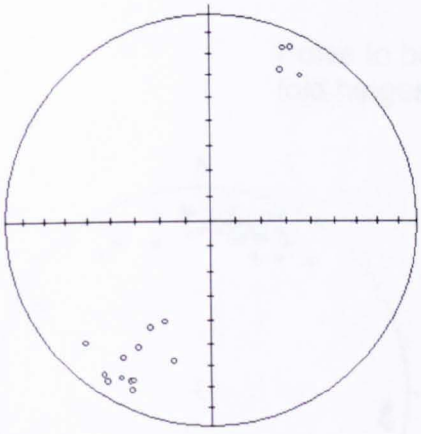

Poles to principal strike-slip faults F1

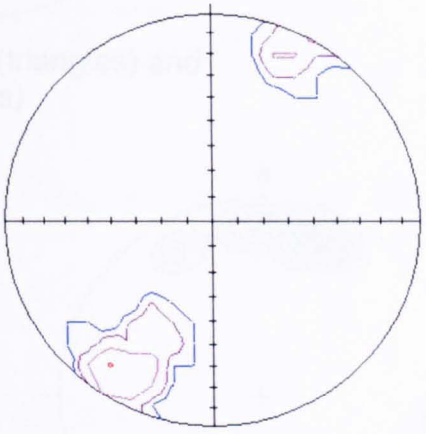

Contouring of poles to principal strike-slip faults

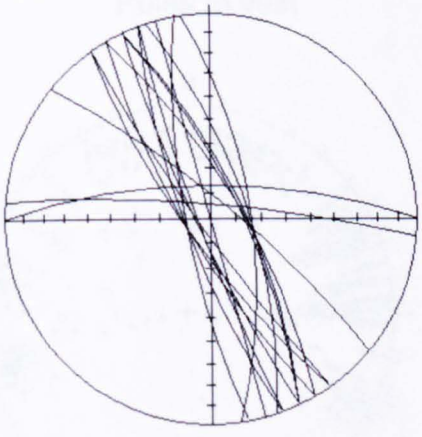

Strike-slip shear planes

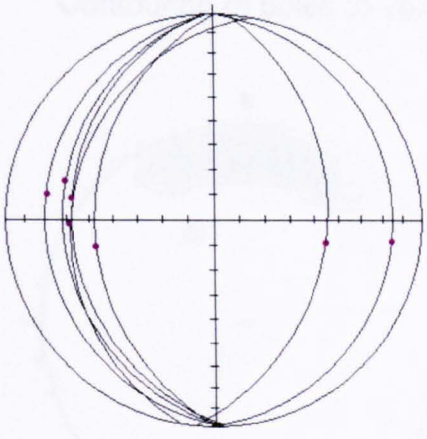

Reverse shear planes

SS9: SPITTAL

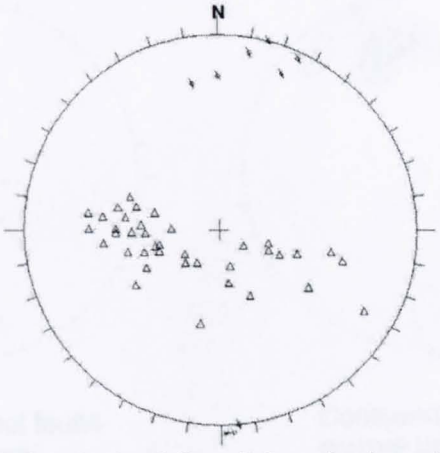

Poles to bedding (triangles) and fold hinges (circles)

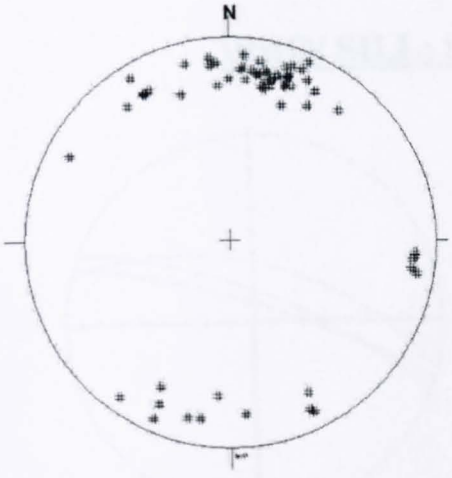

Poles to vein

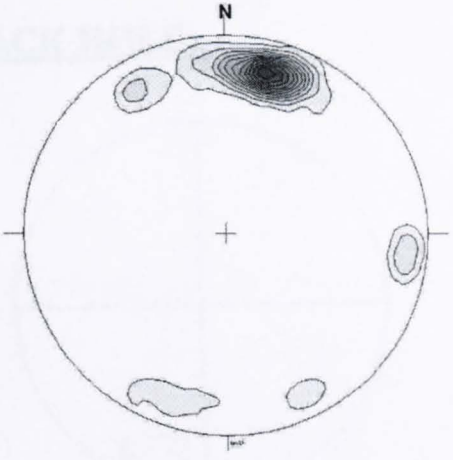

Contouring of poles to vein

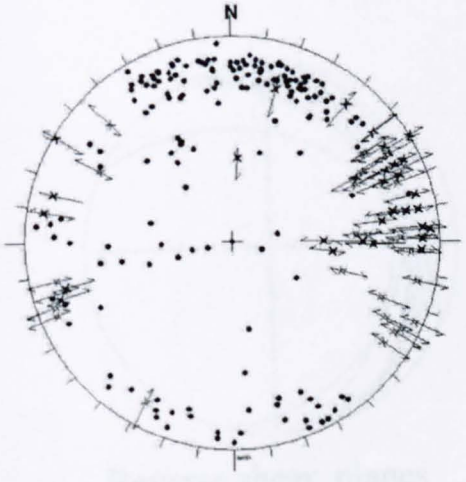

Poles to faults with slickenlines

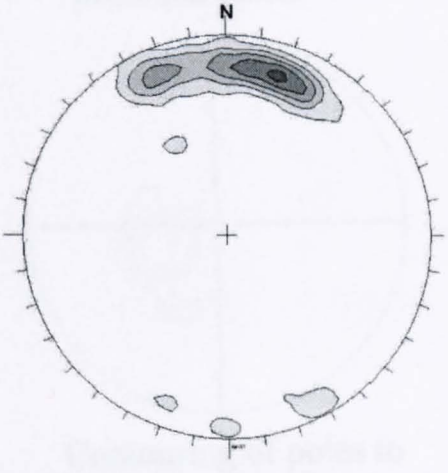

Contouring of poles to faults with slickenlines

SS10: BERWICK

Poles to normal faults and slickenlines

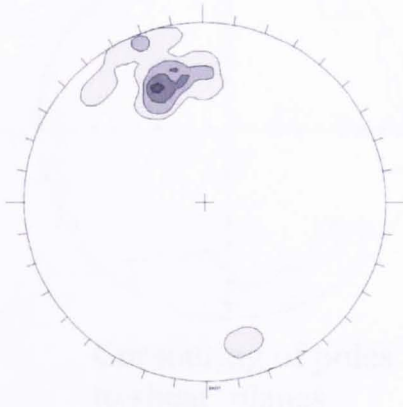

Contouring of poles to normal faults

WHIN SILL: SS5 (BLACK HOLE)

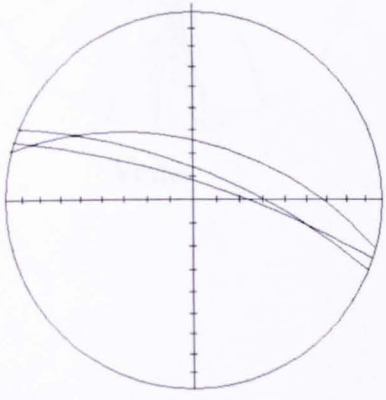

Principal strike-slip faults

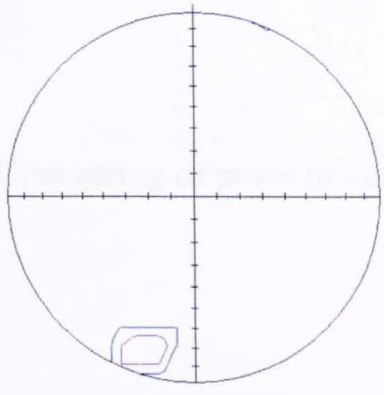

Contouring of poles to principal faults

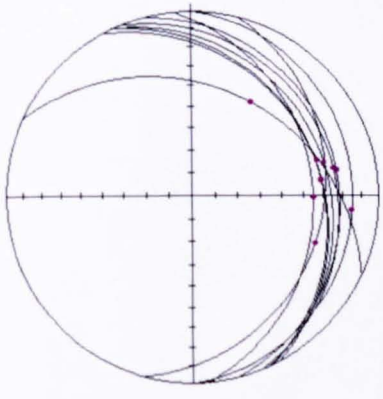

Reverse shear planes

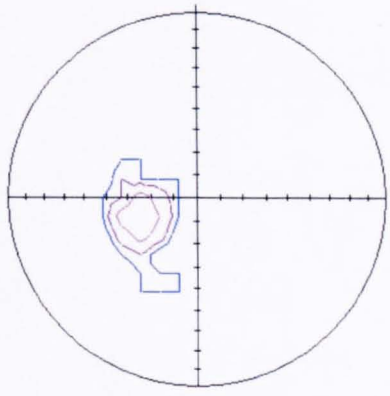

Contouring of poles to reverse shear planes

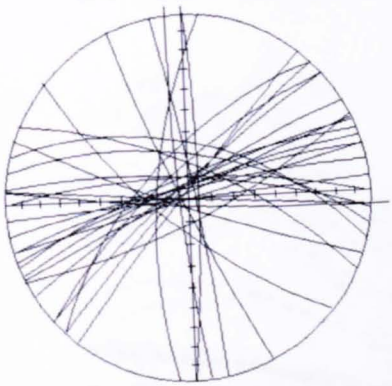

Strike-slip shear planes

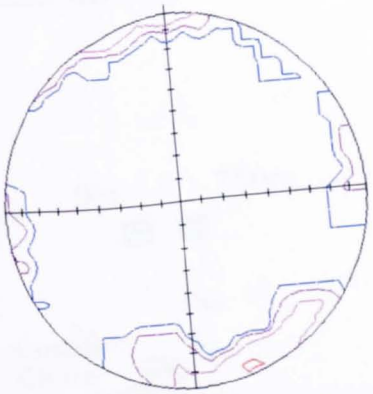

Contouring of poles to shear planes

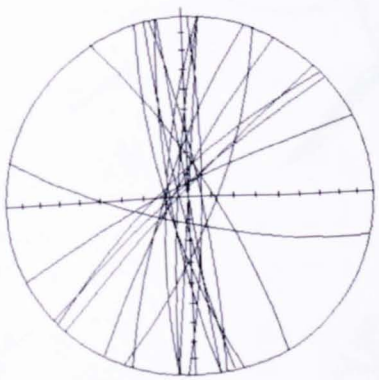

Veins

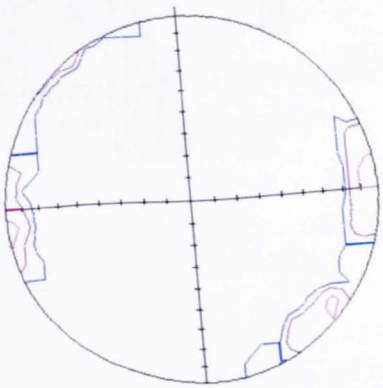

Contouring of poles to veins

WHIN SILL: SS6 (DUNSTANBURGH CASTLE)

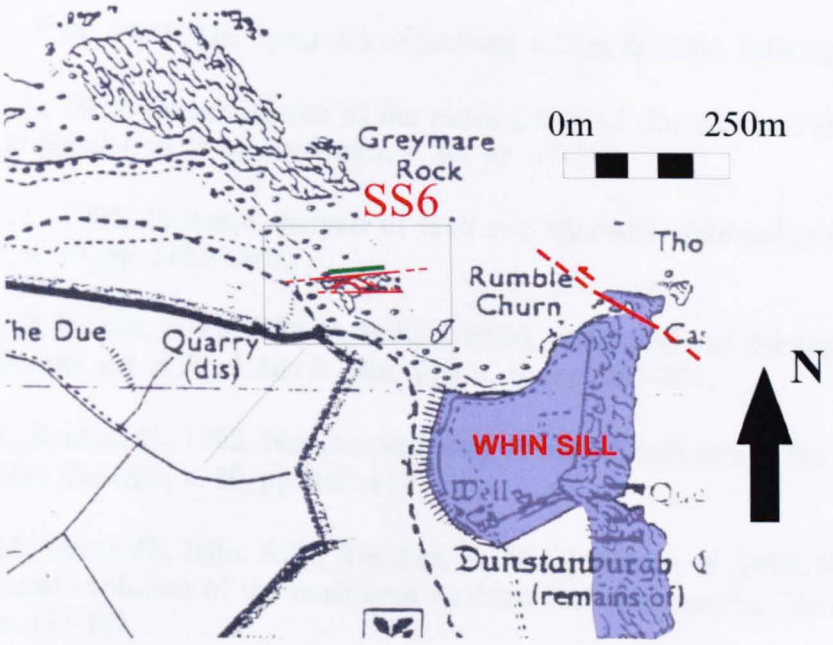

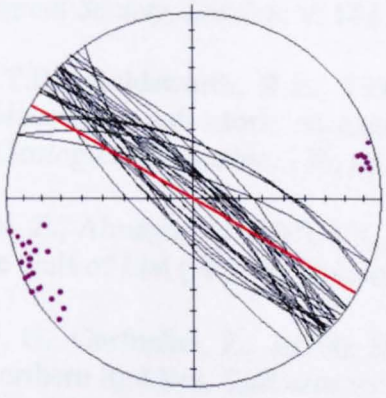

Shear zone in the Whin Sill with S(poles)-C (great circles) fabric

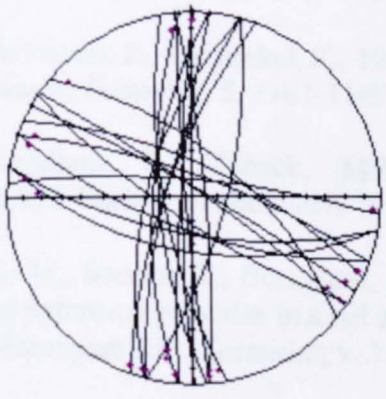

Shear planes + slickenlines

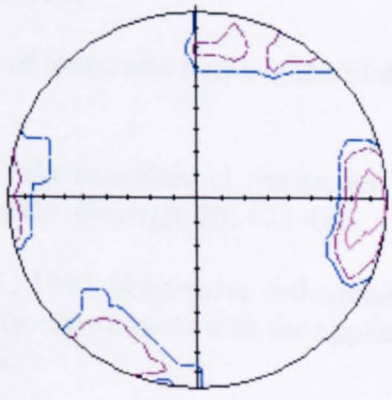

Contouring of poles to shear planes

REFERENCES CITED IN TEXT

Anderson, E.M., 1951. The dynamics of faulting. Oliver & Boyd, Edinburgh.

Angelier, J., 1979. Determination of the mean principal directions of stresses for a given fault population. *Tectonophysics*, v. 56, pp. 17-26.

Angelier, J., 1984. Tectonic analysis of fault slip data sets. *Journal of Geophysical Research*, v. 89, pp. 5835-5848.

Atkinson, R.H., Ko, H.Y., 1973. A fluid cushion, multiaxial cell for testing cubical rock specimens. *Int. J. Rock Mech. Min. Sci.*, v. 10, pp. 351-361.

Aydin, A., Reches, Z., 1982. Number and orientations of fault sets in the field and in experiments. *Geology*, v. 10, pp. 107-112.

Bayer, H.J., Hotzl, H., Jado, A.R., Roscher, B., Voggenreiter, W.,1988. Sedimentary and structural evolution of the northwest Arabian Red Sea margin, *Tectonophysics*, v. 153, pp. 137-151.

Beamish, D., Smythe, D.K., 1986. Geophysical images of the deep crust: the Iapetus suture. *Journal of the Geological Society, London,* v. 143, pp. 489-497.

Beamon, L.E., Anderson, T.B., Holdsworth, R.E., 1999. Using basement-hosted clastic dykes as syn-rift palaeostress indicators: an example from the basal Stoer Group, northeast Scotland. *Geological Magazine*, 136, pp. 301-310.

Ben-Avraham, Z., Garfunkel, Z., Almagor, G., Hall, J.K., 1979a. Continental break-up by a leaky transform: The Gulf of Elat (Aqaba), *Science*, 206, 214-216.

Ben-Avraham, Z., Almagor, G., Garfunkel, Z., 1979b. Sediments and structures of the Gulf of Elat (Aqaba) – northern Red Sea, *Sedimentary Geology*, 23, 239-267.

Ben-Avraham, Z., 1985. Structural framework of the Gulf of Elat (Aqaba) – northern Red Sea, *Journal of Geophysics Research*, 90, 703-726.

Ben-Avraham, Z., Garfunkel, Z., 1986. Character of transverse faults in the Elat pull-apart basin, *Tectonics*, 5, 1161-1169.

Ben-Avraham, Z., Zoback, M.D., 1992. Transform-Normal extension and asymmetric basins: an alternative to pull-apart models, *Geology*, 20, 423-426.

Bonini, M., Souriot, T., Boccaletti, M., Brun, J.P., 1997. Successive orthogonal and oblique extension episodes in a rift zone: laboratory experiments with the application to the Ethiopian Rift. *Tectonics*, v. 16, pp. 347-362.

Bott, M.H.P., 1959. The mechanics of oblique slip faulting. *Geological Magazine*, v. 46, pp. 109-117.

Bott, M.H.P., 1961. A gravity survey off the coast of north-east England. *Proc. Yorks. Geol. Soc.*, v. 33, pp. 1-20.

Bott, M.H.P., 1967. Geophysical investigations of the northern Pennine basement rocks. *Proc. Yorks. Geol. Soc.*, v. 36, pp. 139-168.

Bott, M.H.P., Swinburn, P.M., Long, R.E., 1984. Deep structure and origin of the Northumberland and Stainmore troughs. *Proc. Yorks. Geol. Soc.*, v. 44, pp. 479-495.

Bott, M.H.P., Long, R.E., Green, A.S.P., Lewis, A.H.J., Sinha, M.C., Stevenson, D.L., 1985. Crustal structure south of the Iapetus suture beneath northern England. *Nature*, v. 314, pp. 724-727.

Bower, S.L. 'Inversion tectonics in the Carboniferous basins of northern England: with special reference to Northumberland' (Leeds Univ. Ph.D. thesis, 1990).

Brace, W.F., 1964. Brittle fracture of rocks. In: State of stress in the earth's crust. In: J.W. Judd (Editor), Elsevier, Amsterdam, pp. 110-174.

Butler, R.W.H., Spencer, S., Griffiths, H.M., 1998. The structural response to evolving plate kinematics during transpression: evolution of the Lebanese restraining bend of the Dead Sea Transform, in: R.E Holdsworth, R.A. Strachan, J.F. Dewey, (ED.), Continental Transpressional and Transtensional Tectonics. *Special Publications, Geological Society, London*, v. 135, pp. 81-106.

Chadwick, R.A., Holliday, D.W., 1991. Deep crustal structure and Carboniferous basin development within the Iapetus convergence zone, northern England. *Journal of the Geological Society, London* v. 148, pp. 41-53.

Christensen, N.I., 1996. Poisson's ratio and crustal seismology. *Journal of Geophysical Research*, v. 101, pp. 3139-3156.

Clegg, P. and Holdsworth, R.E., 2005. Complex deformation due to strain partitioning in transpression zones: an example from the Leinster Terrane, SE Ireland. *Journal of the Geological Society, London*, v. 161, In Press.

Colletta, B., Le Quelec, P., Letouzey, J., Moretti, I., 1988. Longitudinal evolution of the Suez rift structure (Egypt), *Tectonophysics*, v. 153, pp. 221-233.

Collier, R.E., 1989. Tectonic evolution of the Northumberland Basin: the effects of renewed extension upon an inverted extensional basin. *Journal of the Geological Society, London*, v. 146, pp. 981-989.

Corfield, S.M., Gawthorpe, R.L., Gage, M., Fraser, A.J. Besley, B.M., 1996. Inversion tectonics of the Variscan foreland of the British Isles. *Journal of the Geological Society, London*, v. 153, pp. 17-32.

Coward, M.P., 1993. The effect of late Caledonian and Variscan contitnental escape tectonics on basement structure, Palaeozoic basin kinematics and subsequent Mesozoic basin development in NW Europe. In: Parker, J.R. (Eds.), Petroleum Geology of NW Europe: Proceedings of the 4th Conference. *Geological Society, London*, pp. 1095-1108.

De Paola, N., Holdsworth, R.E., McCaffrey, K.J.W., 2005a. The influence of lithology and pre-existing structures on reservoir-scale faulting patterns in transtensional rift zones. *Journal of the Geological Society, London*, In Press.

De Paola, N., Holdsworth, R.E., McCaffrey, K.J.W. & Barchi, M.R., 2005b. Partitioned transtension in the late Carboniferous of Northern Britain – a radical alternative to basin inversion models. *Journal of Structural Geology*, In Press.

Dewey, J.F., 1975. Finite plate evolution: some implications for the evolution of rock masses at plate margins. *American Journal of Science*, v. 275-A, pp. 260-284.

Dewey, J.F., Holdsworth, R.E., Strachan, R.A., 1998. Transpression and transtension zones. In: Holdsworth, R.E., Strachan R.A., Dewey J.F. (Ed.), Continental Transpressional and Transtensional Tectonics. *Geological Society, London, Special Publications* v. 135, pp. 1-14.

Dewey, J.F., 2002. Transtension in arcs and orogens. *International Geology Review*, v. 44, pp. 402-439.

Dewey, J.F., Strachan R.A., 2003. Changing Silurian-Devonian relative plate motion in the Caledonides: sinistral transpression to sinistral transtension. *Journal of the Geological Society, London*, v. 160, pp. 219-229.

Donath, F.A., 1962. Analysis of basin-range structure, South-central Oregon. *Geological Society of America Bulletin,* v. 73, pp. 1-16.

Dunham, A.C., Strasser-King, V.E.H., 1982. Late Carboniferous intrusions of northern Britain. In: Sutherland, D.S. (Eds.), Igneous Rocks of the British Isles. Wiley, Chischester, pp. 277-283.

Ernst, R.E., Buchan, K.L., 1997. Giant radiating dyke swarms: their use in identifying pre-Mesozoic large igneous provinces and mantle plumes. In Mahoney, J.J & Coffin, M.F. (Ed.), Large Igneous Provinces: Continental, Oceanic and Planetary Flood Volcanism. *American Geophysical Union, Geophysical Monograph* v. 100, pp. 297-333.

Ernst, R.E., Buchan, K.L., 2001. Large mafic magmatic events through time and links to mantle-plume heads. In: Ernst, R.E., Buchan, K.L. (Ed.), Mantle Plumes: their Identification Through Time. *Geological Society of America*, Special Papers v. 352, pp. 483-575.

Eyal, Y., Reches, Z., 1983. Tectonic analysis of the Dead Sea rift region since the Late-Cretaceous based on mesostructure. *Tectonics*, v. 2, pp. 167-185.

Eyal, Y., Eyal, M., Bartov, Y., Steinitz, G., Folkman, Y., 1985. The origin of the Bin Zreir rhomb-shaped graben. Eastern Sinai. *Tectonics*.

Fitch, F.J., Miller, J., 1967. The age of the Whin Sill. *Geological Journal*, v. 5, pp. 233-250.

Fossen, H., Tikoff, B., 1993. The deformation matrix for simultaneous simple shearing, pure shearing and volume change and its application to transpression/transtension tectonics. *Journal of Structural Geology*, v. 15, pp. 413-422.

Fossen, H., Tikoff, B., 1998. Extended models of transpression and transtension, and application to tectonic settings. In: HOLDSWORTH, R.E., STRACHAN R.A., DEWEY J.F., (Eds.). Continental Transpressional and Transtensional Tectonics. *Geological Society, London, Special Publications*, v. 135, pp. 15-33.

Foster, A.N., Jackson, J.A., 1998. Source parameters of large African earthquakes: implications for crustal rheology and regional kinematics, *Geophysical Journal International*, v. 134, pp. 422-448.

Francis, E.H., 1982. Magma and sediment- 1 Emplacement mechanism of late Carboniferous tholeiite sill in northern Britain. *Journal of the Geological Society, London*, v. 139, pp. 1-20.

Fraser, A.J., Nash, D.F., Steele, R.P., Ebdon, C.C., 1990. A regional assessment of the regional intra-Carboniferous play of northern England. In: Brooks, J. (Ed.), Classic Petroleum Provinces. *Geological Society, London, Special Publication*, v. 50, pp. 417-440.

Fraser, A.J., Gawthorpe, R.L., 2003. An Atlas of Carboniferous Basin Evolution in Northern England. *Geological Society, London, Memoir*, v. 28, pp. 79.

Frieman, M., Logan, J.M., 1973. Luder's band in experimentally deformed sandstone and limestone. *Geological Society of America Bulletin*, v. 84, pp. 1465-1476.

Frolich, C., Apperson, K.D., 1992. Earthquakes focal mechanisms, moment tensors, and the consistency of seismic activity near plate boundaries. *Tectonics*, v. 11, pp. 279-296.

Frost, D.V., Holliday, D.W., 1980. Geology of the country around Bellingham. *Memoirs of the Geological Survey, G. B.*

Garfunkel, Z., 1981. Internal structure of the Dead Sea leaky transform (rift) in relation to plate kinematics. *Tectonophysics*, v. 80, pp. 81-108.

Ginat, H., Enzel, T., Avni, Y., 1998. Translocated Plio-Pleistocene drainage system along the Arava fault of the Dead Sea transform. *Tectonophysics*, v. 284, pp. 151-160.

Harding, T.P., 1974. Petroleum traps associated with wrench faults. *American Association of Petroleum Geologists*, v. 58, pp. 1290-1304.

Harland, W.B., 1971. Tectonic transpression in Caledonian Spitzbergen. *Geological Magazine* v. 108, pp. 27-42.

Harvard CMT Catalogue, www.seismology.harvard.edu.

Hojem, J.P.M., Cook, N.G.W., 1969. the design and construction of a triaxial and polyaxial cell for testing rock specimens. *South Africa Mechanics Engineering*, v. 18, pp. 57-61.

Holdsworth, R.E., Butler, C.A. & Buick, I.S., 1997. The recognition of reactivation during continental deformation. *Journal of the Geological Society*, v. 154, pp. 73-78.

Holdsworth, R.E., Tavarnelli, E., Clegg, P., Pinheiro, R.V.L., Jones, R.R., McCaffrey, K.J.W., 2002a. Domainal defomation patterns and strain partitioning during transpression: an example from the Southern Uplands terrane, Scotland. *Journal of the Geological Society, London*, v. 159, pp. 401-415.

Holdsworth, R.E., Tavarnelli, E. & Clegg, P., 2002b. The nature and regional significance of structures in the Gala Group of the Southern Uplands terrane, Berwickshire, SE Scotland. *Geological Magazine*, v. 139, pp. 707-717.

Holmes, A., Harwood, H.F., 1928. The age and composition of the Whin Sill and the related dykes of the North of England. *Mineralogical Magazine*, v. 21, pp. 493-552.

Jaeger, J.C., 1964. Elasticity, fracture and flow with engineering and geological applications. Wiley, New York, N.Y., pp. 212.

Jestin, F., Huchon, P., Gaulier, J.M., 1994. The Somali plate and the East African rift system: present-day kinematics. *Geophysical Journal International*, v. 116, pp. 637-654.

Joffe, S., Garfunkel, Z., 1987. Plate kinematics of the circum Red Sea- a re-evaluation: *Tectonophysics*, v. 141, pp. 5-22.

Johnson, G.A.L., 1984. Subsidence and sedimentation in the Northumberland Trough. *Proceedings of the Yorkshire Geological Society*, v. 45, pp. 71-83.

Johnson, G.A.L., 1995. Robson's Geology of North East England. Tranactions of the Natural History Society of Northumbria, v. 56, pp. 226-391.

Johnson, G.A.L., Dunham, K.C., 2001. Emplacement of the Great Whin dolerite complex and the Little Whin Sill in relation to the structure of northern England. *Proceedings of the Yorkshire Geological Society*, v. 53, pp. 177-186.

Johnston, J.E. & Christensen, N.I., 1992. Shear wave reflectivity, anisotropies, Poisson's ratios and densities of a southern Appalachian Palaeozoic sedimentary sequence. *Tectonophysics*, v. 210, pp. 1-20.

Jones, R.R., Tanner, P.W.G., 1995. Strain partitioning in transpression zones. *Journal of Structural Geology*, v. 17, pp. 793-802.

Jones, R.R., Holdsworth, R.E. & Bailey, W., 1997. Lateral extrusion in transpression zones: the importance of boundary conditions. *Journal of Structural Geology*, v. 19, pp. 1201-1217.

Jones, R.R. & Holdsworth, R.E., 1998. Oblique simple shear in transpression zones. In: Holdsworth, R.E., Strachan R.A., Dewey J.F., (Eds.). Continental Transpressional and Transtensional Tectonics. *Geological Society, London, Special Publications*, v. 135, pp. 35-40.

Jones, R.R., Holdsworth, R.E., Clegg, P., McCaffrey, K.J.W, Tavarnelli, E., 2004. Inclined transpression. *Journal of Structural Geology*, v. 26, pp. 1531-1548.

Kelly, P.G., Sanderson, D.J., Peacock, D.C.P., 1998. Linkage and evolution of conjugate strike-slip fault zones in limestones of Somerset. *Journal of Structural Geology*, v. 20, pp. 1477-1493.and Northumbria.

Kimbell, G.S., Chadwick, R.A., Holliday, D.W., Werngren, O.C., 1989. The structure and evolution of the Northumberland Trough from new seismic reflection data and its bearing on modes of continental extension. *Journal of the Geological Society, London*, v. 146, pp. 775-787.

Kirschner, D.L., Teyssier, C., 1994. Orthorhombically arranged vein arrays. *Journal of Structural Geology*, v. 16, pp. 1129-1138.

Klinger, Y., Avouac, J.P., Abou Karaki, N., Dorbath, L., Bourles, D., Reyss, J.L., 2000. Slip rate on the Dead Sea transform fault in northern Araba valley (Jordan). *Geophysical Journal International*, v. 142, pp. 755-768.

Knott, S.D., Beach, A., Brockbank, P.J., Brown, J.L., McCallum, J.E. & Welbon, A.I., 1996. Spatial and mechanical controls on normal fault populations. *Journal of Structural Geology*, v. 18, pp. 359-372.

Krantz, R.W., 1988. Multiple fault sets and three-dimensional strain: theory and application. *Journal of Structural Geology*, v. 10, pp. 225-237.

Krantz, R.W., 1989. Orthorhombic fault patterns: the odd axis model and slip vector orientations. *Tectonics*, v. 8, pp. 483-495.

Leeder, M.R., 1982. Upper Palaeozoic basins of the British Isles-Caledinide inheritance versus Hercynian plate margin processes. *Journal of the Geological Society, London*, v. 139, pp. 479-491.

Leeder, M.R. & McMahon, A.H., 1988. Upper Carboniferous (Silesian) basin subsidence in northern Britain. In: Besly, B.M. & Kelling, G., (Eds.). Sedimentation in a synorogenic basin-the Upper carboniferous of northwest Europe. Blackie & Son Ltd, pp. 43-52.

Leeder, M.R., Fairhead, D., Lee, A., Stuart, G., Clemmey, H., Al-Haddeh, B. & Green, B., 1989. Sedimentary and tectonic evolution of the Northumberland Basin. *Proceedings of the Yorkshire Geological Society*, v. 47, pp. 207-223.

Lin, S., Jiang, D. & Williams, P.F., 1998. Transpression (or transtension) zones of triclinic symmetry: natural example and theoretical modelling. In: Holdsworth, R.E., Strachan R.A., Dewey J.F., (Eds.). Continental Transpressional and Transtensional Tectonics. *Geological Society, London, Special Publications*, v. 135, pp. 41-57.

Liss, D., Owens, W.H., Hutton,D.H.W., 2004. New palaeomagnetic results from the Whin Sill complex: evidence for a multiple intrusion event and revised virtual geomagnetic poles for the late Carboniferous for the British Isles. *Journal of the Geological Society, London* v. 161, pp. 1-12.

Lyberis, N., 1988. Tectonic evolution of the Gulf of Suez and Gulf of Aqaba. *Tectonophysics*, v. 153, pp. 209-220.

Maynard, J.R., Hofmann,W., Dunay, R.E., Bentham, P.N., Dean, K.P., Watson, I. 1997. The Carboniferous of Western Europe: the development of a petroleum system. *Petroleum Geosciences* 3, 97-116.

McClay, K.R., White, M., 1995. Analogue models of orthogonal and oblique rifting. *Marine and Petroleum Geology*, v. 12, pp. 137-151.

McCoss, A.M., 1986. Simple constructions for deformation in transpression/transtension zones. *Journal of Structural Geology*, v. 8, pp. 715-718.

McQuarrie, N., Stock, J.M., Verdel, C., Wernicke, B.P., 2003. Cenozoic evolution of Neotethys and implications for the causes of plate motions, Geophysical Research Letter, v. 30, No. 20.2036.

Michael, A.J., 1984. Determination of stress from slip data: faults and folds. *Journal of Geophysical Research,* v. 89, pp. 11517-11526.

Mogi, K., 1971. Fracture and flow of rocks under high triaxial compressions. *Tectonophysics*, v. 76, pp. 1255-1269.

Montenat, C., D'Estevous, P.O., Purser, B., Burollet, P.F., Jarrige, J.J., Orszag-Sperber, F., Philobbos, E., Plaziat, J.C., Prat, P., Richert, J.P., Roussel, N., Thiriet, J.P.,1988. Tectonic and sedimentary evolution of the Gulf of Suez and the northwestern Red Sea, *Tectonophysics*, v. 153, pp. 61-177.

Morley, C.K., 1999. How successful are analogue models in addressing the influence of pre-existing fabrics on rift structure? *Journal of Structural Geology*, v. 21, pp. 1267-1274.

Neumann, E.R., 1994. The Oslo Rift: P-T relations and lithospheric structure. *Tectonophysics*, v. 240, pp. 159-172.

Nieto-Samaniego, A.F., 1999. Stress, strain and fault patterns. *Journal of Structural Geology*, v. 21, pp. 1065-1070.

Nieto-Samaniego, A.F., Alaniz-Alvarez, S.A., 1995. Influence of the structural framework on the origin of multiple fault patterns. *Journal of Structural Geology*, v. 17, pp. 1571-1577.

Nieto-Samaniego, A.F., Alaniz-Alvarez, S.A., 1997. Origin and tectonic interpretation of multiple fault patterns. *Tectonophysics*, v. 270, pp. 197-206.

Oertel, G., 1965. The mechanism of faulting in clay experiments. *Tectonophysics*, v. 2, pp. 343-393.

Oldow, J.S., 2003. Active transtensional boundary zone between the western Great Basin and Sierra Nevada block, western U.S. Cordillera. *Geology*, v. 31, pp. 1033-1036.

Olsson, W.A., Lorenz, J.C. & Cooper, S.P., 2004. A mechanical model for multiply-oriented conjugate deformation bands. *Journal of Structural Geology*, v. 26, pp. 325-338.

Paterson, M.S., 1978. Experimental rock deformation – The brittle field. Springer, Berlin-Heidelberg, pp. 253.

Pe'eri, S., Wdowinski, S., Shtibelman, A., Bechor, N., Bock, Y., Nikolaidis, R., Domselaar, M. van, 2002. Current plate motion across the Dead Sea Fault from three years of continuous GPS monitoring. *Geophysical Research Letters*, v. 29, No.14, 10.29/2001GL013879.

Petroleum Exploration Society of Great Britain 2000. Structural framework of the North Sea and Atlantic Margin. Petroleum Exploration Society of Great Britain Map.

Picard, L., 1987. The Elat (Aqaba)-Dead Sea- Jordan subgraben system. *Tectonophysics*, v. 141, pp. 23-32.

Quennel, A.M., 1959. Tectonics of the Dead Sea Rift, International Geological Congress, 20th Mexico- Assoc. Serv. Geol. Afr., pp. 385-405.

Ramani, M.V., Tikoff, B., 2002. Physical models of transtensional folding. *Geology*, v. 30, pp. 523-526.

Ramsey, J.G., Huber, M.I., 1987. The techniques of modern structural geology. Volume 2: Folds and Fractures. Academic Press Inc. (London).

Read, W A., 1988. Controls on Silesian sedimentation in the Midland Valley of Scotland. In: Besly, B. M. & Kelling, G. (Ed.), Sedimentation in a synorogenic basin complex: the Upper Carboniferous of northwest Europe. Glasgow, Blackie & Son, pp. 222-241.

Read, W.A., Browne M.A.E., Stephenson D., Upton B.J.G., 2003. Carboniferous. In Trewin N.H. (Ed.), The Geology of Scotland. Fourth Edition. *The Geological Society, London* pp. 251-300.

Reches, Z., 1978. Analysis of faulting in three-dimensional strain field. *Tectonophysics*, v. 47, pp. 109-129.

Reches, Z., 1983. Faulting of rocks in three-dimensional strain field II. Theoretical analysis. *Tectonophysics*, v. 95, pp. 133-156.

Reches, Z., Dieterich, J., 1983. Faulting of rocks in three-dimensional strain field I. Failure of rocks in polyaxial, servo-control experiments. *Tectonophysics*, 95, pp. 111-132.

Reches, Z., 1987. Mechanical aspects of pull-apart basins and push-up swells with application to the Dead Sea Transform. *Tectonophysics*, v. 141, pp. 75-88.

Roberts, D.G., 1969.Structural evolution of the rift zones in the Middle East, *Nature*, v. 223, pp. 55-57.

Robin, P.Y.F. & Cruden, A.R., 1994. Strain and vorticity patterns in ideally ductile transpression zones. *Journal of Structural Geology*, v. 16, pp. 447-466.

Robson, D.A., 1980. The Geology of North East England. Special Publication of the natural History Society of Northumberland.

Roeser, H.A., 1975. A detailed magnetic survey of the southern Red Sea, Geol. Jahrb., v. D13, pp. 131-153.

Sagy, A., Reches, Z., Agnon, A., 2003. Hiearchic three-dimensional structure and slip partitioning in the western Dead sea pull-apart. *Tectonics*, v. 22 No.1, 10.1029/2001TC0013223.

Salvini, F., 2001. DAISY 2. The structural data integrated analyzer. Version 2.44b.

Sanderson, D.J., 1984. Structural variation across the northern margin of the Variscides in NW Europe. In: Hutton, D.H.W., Sanderson, D.J. (Ed.), Variscan

Tectonics of the North Atlantic Region. *Geological Society, London, Special Publication*, v. 14, pp. 149-166.

Sanderson, D.J., Marchini, W.R.D., 1984. Transpression. *Journal of Structural Geology*, v. 6, pp. 449-458.

Schreurs, G., Colletta, B., 1998. Analogue modelling of faulting in zones of continental transpression and transtension. In: Holdsworth, R.E., Strachan R.A., Dewey J.F. (Ed.), Continental Transpressional and Transtensional Tectonics. *Geological Society, London, Special Publications*, v. 135, pp. 59-79.

Serra, S., Nelson, R.A., 1988. Clay modelling of rift asymmetry and associated structures. *Tectonophysics*, v. 153, pp. 307-312.

Shiells, K.A.G., 1964. The geological structure of northeast Northumberland. *Transactions of the Royal Society of Edinburgh*, v. 65, pp. 449-484.

Sibson, R.H, 2000. Fluid involvement in normal faulting. *Journal of Geodynamics*, v. 29, pp. 469-499.

Smith, J.V., Durney, D.W., 1992. Experimental formation of brittle structural assemblages in oblique divergence. *Tectonophysics*, v. 216, pp. 235-253.

Smythe, D.K., Russel, M.J., Skuce, A.G., 1995. Intra-continental rifting inferred from the major late Carboniferous quartz-dolerite dyke swarm of NW Europe. *Scottish Journal of Geology*, v. 31, pp. 151-162.

Soper, N.J., England, R.W., Snyder, D.B., Ryan, P.D., 1992. The Iapetus suture zone in England, Scotland and eastern Ireland: a reconciliation of geological and deep seismic data. *Journal of the Geological Society*, v. 149, pp. 697-700.

Sundvoll, B., Larsen, B.T., 1994. Architecture and early evolution of the Oslo Rift. *Tectonophysics*, v. 240, pp. 173-189.

Teyssier, C., Tikoff, B., Markley, M., 1995. Oblique plate motion and continental tectonics. *Geology*, v. 23, pp. 447-450.

Teyssier, C., Tikoff, B., 1999. Fabric stability in oblique convergence and divergence. *Journal of Structural Geology*, v. 21, pp. 969-974.

Thompson, G.A., Burke, D.B., 1974. Regional geophysics of the Basin and Range Province. *Annu. Rev. Earth Planet. Sci.*, v. 2, pp. 213-238.

Tikoff, B., Teyssier, C., 1994. Strain modelling of displacement field partitioning in transpressional orogens. *Journal of Structural Geology*, v. 16, pp. 1575-1588.

Tikoff, B., Greene, D., 1997. Stretching lineations in transpressional shear zones: an example from the Sierra Nevada Batholith, California. *Journal of Structural Geology*, v. 19, p. 29-39.

Tikoff, B., Wojtal, S.F., 1999. Displacement control of geologic structures. *Journal of Structural Geology*, v. 21, pp. 959-967.

Timmerman, M.J., 2004. Timing, geodynamic setting and character of Permo-Carboniferous magmatism in the foreland of the Variscan Orogen, NW Europe. In: Wilson, M., Neumann, E.-R., Davis, G.R., Timmerman, M.J., Heeremans, Larsen, B.T. (Ed.), Permo-Carboniferous Magmatism and Rifting in Europe. *Geological Society, London, Special Publication*, v. 223, pp. 41-74.

Tron, V., Brun, J.P., 1991. Experiments on oblique rifting in brittle-ductile systems. *Tectonophysics*, v. 188, pp. 71-84.

Twiss, R.J., Moores, E.M., 1992. Structural Geology. W.H. Freeman & Co., New York, 532 pp.

Underhill, J.R., Woodcok, N.H., 1987. Faulting mechanisms in high-porosity sandstones; New Red Sandstone, Arran, Scotland. In: Jones, M.E., Preston, R.M.F. (eds), 1987, Deformation of Sediments and Sedimentary Rocks, *Geological Society Special Publication*, v. 29, pp. 91-105.

Vine, F.J., 1966. Spreading of ocean floor – new evidence, *Science*, v. 154, pp. 1405-1415.

Walsh, J.J, Watterson, J., Bailey, W.R., Childs, C., 1999. Fault relays, bends and branch lines. *Journal of Structural Geology*, v. 21, pp. 1019-1026.

Waters, C.N., Glover, B.W., Powell, J.H., 1994. Structural synthesis of S Staffordshire, UK: implications for the Variscan evolution of the Pennine Basin. *Journal of the Geological Society, London* v. 151, pp. 697-714.

Wdowinski, S., Bock, Y., Baer, G., Prawirodirdjo, L., Bechor, N., Naaman, S., Knafo, R., Forrai, Y., and Melzer, Y., 2004. GPS measurements of current crustal movements along the Dead Sea Fault. *Journal of Geophysical Research*, v. 109, B05403, 10.1029/2003JB002640.

Wilcox, R.E., Harding, T.P. & Seely, D.R., 1973. Basic wrench tectonics. *Bulletin American Association of Petroleum Geologists*, v. 57, pp. 74-96.

Wilson, J.T., 1965. A new class of faults and their bearing on continental drift, *Nature*, v. 207, pp. 343-347.

Withjack, M.O., Jamison, W.R., 1986. Deformation produced by oblique rifting. *Tectonophysics*, v. 126, pp. 99-124.

Woodcock, N.H., 1986. The role of strike-slip fault systems at plate boundaries. *Philosophical Transaction of the Royal Society of London*, v. A317, pp. 13-29.

Woodcock, N.H., Fischer, M., 1986. Strike-slip duplexes. *Journal of Structural Geology*, v. 8, pp. 725-735.

Woodcok, N.H., Underhill, J.R., 1987. Emplacement related fault patterns around the Northern Granite, Arran, Scotland. *Bulletin of Geological Society of America*, v. 98, pp. 515-527.

Woodcock, N.H. and Rickards, B., 2003. Transpressive duplex and flower structure: Dent Fault System, NW England. *Journal of Stuctural Geology*, v. 25, pp. 1981-1992.

Woodcock, N.H., Strachan, R.A., 2000. The Caledonian Orogeny: a multiple plate collision. In: Woodcock, N.H., Strachan, R.A. (Ed.), Geological History of Britain and Ireland. Blackwell Science, Oxford, pp. 187-206.

PLATE 3: DETAILED STRUCTURAL MAP OF CULLERNOSE POINT, NORTHUMBERLAND BASINSCALE 1:300

PLATE 1:GEOLOGICAL MAP OF NORTHUMBERLAND BASIN

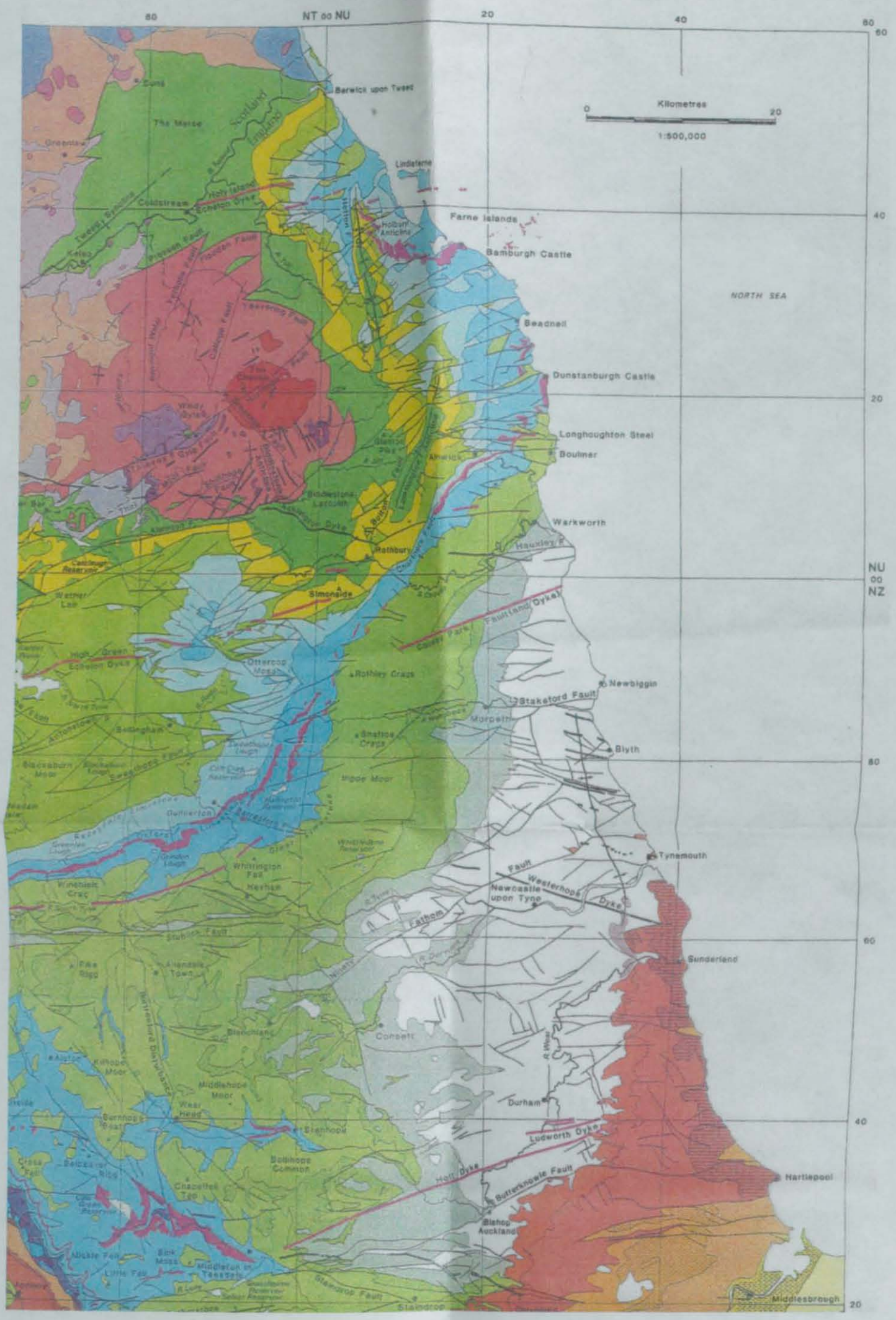

STRATIGRAPHICAL SUCCESSION

Cartography: Christine Cochrane

CARBONIFEROUS

		WEST OF PENNINES	PENNINES	EAST OF PENNINES
UPPER	Westphalian	Whitehaven Sandstone		Upper Coal Measures
		Coal Measures (undifferentiated)		Middle Coal Measures
				Lower Coal Measures
	Namurian	Upper Limestone Group	Longhoughton Grits Upper Limestone Group	Longhoughton Grits Upper Limestone Group
LOWER	Dinantian	Lower and Middle Limestone Groups	Lower and Middle Limestone Groups	Middle Limestone Group
		Basement Beds	Basement Beds	Lower Limestone Group
		Upper Border Group	SCOTLAND (Midland Valley)	Scremerston Coal Group
		Middle Border Group	Lower Limestone Group and Oil Shales	Fell Sandstone Group
		Lower Border Group	Calciferous Sandstone Group	Cementstone Group
				Conglomerates

OLD RED SANDSTONE (Devonian)

Upper
Lower

SILURIAN

SOUTHERN UPLANDS	LAKE DISTRICT
Wenlock–Ludlow	Ludlow
Llandovery	Wenlock–Llandovery

ORDOVICIAN

Llandello–Caradoc	Coniston Limestone–Ashgill
	Arenig–Llanvirn (Skiddaw Slates)

IGNEOUS ROCKS

	Extrusions	Minor Intrusions	
LOWER CARB.	Basalt	TERTIARY	Dykes
LOWER O.R.S.	Andesite	PERMO-CARB.	Whin Sill and Dykes
	Rhyolite	LOWER CARB.	Volcanic Vents etc.
	Pyroclast	LOWER O.R.S.	Dykes
ORDOVICIAN (Borrowdale Volcanic Series)	Pyroclast		Felsite
	Rhyolite	PRE-O.R.S.	Lake District
	Andesite	Major Intrusions	
	Basalt	LOWER O.R.S.	Granite/granophyre
		PRE-O.R.S.	Gabbro

Anticline
Syncline
Fault
Geological Boundary

GEOLOGICAL MAP of NORTH EAST ENGLAND

with the Scottish Borders and the Lake District

Based on a compilation carried out by K.R.Crossley in The University of Newcastle upon Tyne with later additions by G.A.L.Johnson and D.A.Robson

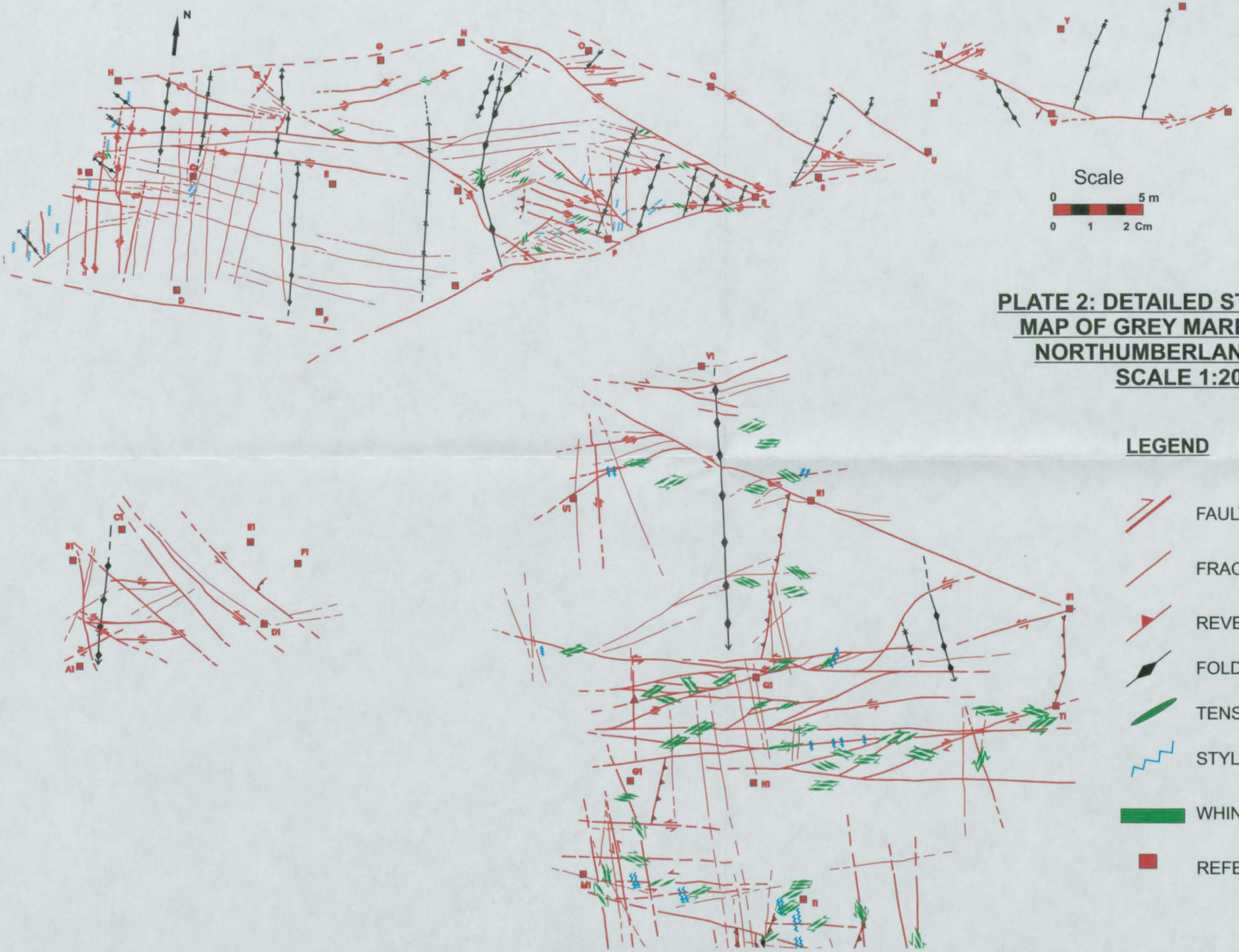

PLATE 2: DETAILED STRUCTURAL MAP OF GREY MARES ROCKS, NORTHUMBERLAND BASIN SCALE 1:200

LEGEND

- FAULTS
- FRACTURES
- REVERSE SHEARS
- FOLDS
- TENSION GASHES
- STYLOLITES
- WHIN SUITE DYKES
- REFERENCE POINTS